EXPERIMENTAL EVALUATION OF LOCAL BOND BEHAVIOUR OF DEFORMED REINFORCING BARS IN CONCRETE STRUCTURES

A THESIS

SUBMITTED TO THE UNIVERSITY OF CANTERBURY

IN PARTIAL FULFILMENT OF THE REQUIREMENTS

FOR THE DEGREE OF

MASTER OF ENGINEERING

Gareth J. Morris

June, 2015

Supervised by

Professor Des Bull

Associate Professor Brendon Bradley

DEPARTMENT OF CIVIL AND NATURAL RESOURCES ENGINEERING

UNIVERSITY OF CANTERBURY

CHRISTCHURCH, NEW ZEALAND

DISCLAIMER:

Any opinions, findings, conclusions or recommendations within this publication are those of the author and do not necessarily reflect the views of other people and organisations that have been associated or involved in undertaking this research.

THESIS ABSTRACT

This thesis addresses the topic of local bond behaviour in RC structures. The mechanism of bond refers to the composite action between deformed steel reinforcing bars and the surrounding concrete. Bond behaviour is an open research topic with a wide scope, particularly because bond it is such a fundamental concept to structural engineers. However, despite many bond-related research findings having wide applications, the primary contribution of this research is an experimental evaluation of the prominent features of local bond behaviour and the associated implications for the seismic performance of RC structures.

The findings presented in this thesis attempt to address some structural engineering recommendations made by the Canterbury Earthquakes Royal Commission following the 2010-2011 Canterbury (New Zealand) earthquake sequence. A chapter of this thesis discusses the structural behaviour of flexure-dominated RC wall structures with an insufficient quantity of longitudinal reinforcement, among other in situ conditions, that causes material damage to predominantly occur at a single crack plane. In this particular case, the extent of concrete damage and bond deterioration adjacent to the crack plane will influence the ductility capacity that is effectively provided by the reinforcing steel. As a consequence of these in situ conditions, some lightly reinforced wall buildings in Christchurch lost their structural integrity due to brittle fracture of the longitudinal reinforcement. With these concerning post-earthquake observations in mind, there is the underlying intention that this thesis presents experimental evidence of bond behaviour that allows structural engineers to re-assess their confidence levels for the ability of lightly reinforced concrete structures to achieve the life-safety seismic performance objective the ultimate limit state.

Three chapters of this thesis are devoted to the experimental work that was conducted as the main contribution of this research. Critical details of the experimental design, bond testing method and test programme are reported. The bond stress-slip relationship was studied through 75 bond pull-out tests. In order to measure the maximum local bond strength, all bond tests were carried out on deformed reinforcing bars that did not yield as the embedded bond length was relatively short. Bond test results have been presented in two separate chapters in which 48 monotonic bond tests and 27 cyclic bond tests are presented. Permutations of the experiments include the loading rate, cyclic loading history, concrete strength (25 to 70 MPa), concrete age, cover thickness, bar diameter (16 and 20 mm), embedded length, and position of the embedded bond region within the specimen (close or far away to the free surface).

The parametric study showed that the concrete strength significantly influences the maximum bond strength and that it is reasonable to normalise the bond stress by the square-root of the concrete compressive strength, $\sqrt{f'_c}$. The generalised monotonic bond behaviour is described within. An important

outcome of the research is that the measured bond strength and stiffness was higher than stated by the bond stress-slip relationship in the *fib* Model Code 2010. To account for these observed differences, an alternative model is proposed for the local monotonic bond stress-slip relationship.

Cyclic bond tests showed a significant proportion of the total bond degradation occurs after the loading cycle in the peak bond strength range, which is when bond slip has exceeded 0.5 mm. Subsequent loading to constant slip values showed a linear relationship between the amount of bond strength degradation and the log of the number of cycles that were applied. To a greater extent, the cyclic bond deterioration depends on the bond slip range, regardless of whether the applied load cycling is half- or fully-reversed. The observed bond deterioration and hysteretic energy dissipated during cyclic loading was found to agree reasonably well between these cyclic tests with different loading protocols. The cyclic bond deterioration was also found to be reasonably consistent exponential damage models found in the literature.

This research concluded that the deformed reinforcing bars used in NZ construction, embedded in moderate to high strength concrete, are able to develop high local bond stresses that are mobilised by a small amount of local bond slip. Although the relative rib geometry was not varied within this experimental programme, a general conclusion of this thesis is that deformed bars currently available in NZ have a relative rib bearing area that is comparatively higher than the test bars used in previous international research. From the parametric study it was found that the maximum monotonic bond strength is significant enhanced by dynamic loading rates.

Experimental evidence of high bond strength and initial bond stiffness generally suggests that only a small amount of local bond slip that can occur when the deformed test bar was subjected to large tension forces. Minimal bond slip and bond damage limits the effective yielding length that is available for the reinforcing steel to distribute inelastic material strains. Consequently, the potential for brittle fracture of the reinforcement may be a more problematic and widespread issue than is apparent to structural engineers. This research has provided information that improve the reliability of engineering predictions (with respect to ductility capacity) of maximum crack widths and the extent of bond deterioration that might occur in RC structures during seismic actions.

UNIVERSITY OF CANTERBURY
Te Whare Wānanga o Waitaha
CHRISTCHURCH NEW ZEALAND

Deputy Vice-Chancellor's Office
Postgraduate Office

Co-Authorship Form

This form is to accompany the submission of any thesis that contains research reported in co-authored work that has been published, accepted for publication, or submitted for publication. A copy of this form should be included for each co-authored work that is included in the thesis. Completed forms should be included at the front (after the thesis abstract) of each copy of the thesis submitted for examination and library deposit.

Please indicate the chapter/section/pages of this thesis that are extracted from co-authored work and provide details of the publication or submission from the extract comes:

Chapter 2:

Morris, G.J., Bull, D.K. and Bradley, B.A., (in press). "In situ conditions affecting the ductility capacity of lightly reinforced concrete wall structures in the Canterbury earthquake sequence", *Bulletin of the New Zealand Society of Earthquake Engineering*, submitted December 2014.

Chapter 5 and Chapter 6:

Morris, G.J., Bull, D.K. and Bradley, B.A., (2015). Monotonic and cyclic bond behaviour of deformed bars in reinforced concrete structures, C*onference proceedings of the New Zealand Society of Earthquake Engineering*, April 2015, Rotorua, New Zealand.

Please detail the nature and extent (%) of contribution by the candidate:

The candidate did all of the work included in the publications under our supervision.

Certification by Co-authors:

If there is more than one co-author then a single co-author can sign on behalf of all

The undersigned certifies that:

- The above statement correctly reflects the nature and extent of the Masters candidate's contribution to this co-authored work
- In cases where the candidate was the lead author of the co-authored work he or she wrote the text

Name: *Des Bull* Signature: *D.K. Bull* Date: *12/06/2015*

ACKNOWLEDGEMENTS

To my Professors; Des Bull, Brendon Bradley and Richard Fenwick – I am fortunate to have had access to your superior experience, skills and intelligence during a time when you have all been extremely active and dedicated with your respective contributions to the wider structural and earthquake engineering community. Thank you for providing me with firm technical and non-technical guidance during my University studies and in the early stages of my professional career. Being able to participate in discussions with each of you was the most rewarding aspect of my postgraduate studies.

The opportunity to undertake this research was made possible by the financial support from the University of Canterbury (UC) and the UC Quake Centre. Materials for the experiments were provided by Holcim cement and under the SAFER Concrete Technology project funded by Ministry of Business, Innovation and Employment (MBIE) via the Natural Hazards Research Platform. The Cement and Concrete Associate of New Zealand (CCANZ) are acknowledged for providing me with opportunities to become involved in the NZ concrete industry.

Thanks to Professor Mark Davidson and Professor Roger Nokes for the leadership you have shown to the Department of Civil and Natural Resources Engineering (CNRE) during and after Canterbury earthquake sequence. I observed that it can be difficult to demonstrate good leadership within the tertiary education system, especially amongst the academic mayhem. To the CNRE administrative staff, particularly Elizabeth Ackerman and Alan Jolliffe, thank you for your regular assistance. Thanks to the CNRE technical staff who provided valuable advice during the experimental phase of this research, particularly David MacPherson, Tim Perigo, Dr. Allan Scott, Stuart Toase and Alan Poynter.

For the many enthusiastic and motivating discussions, thanks to my postgraduate colleagues Jeff Tuck, Richard Malcolm, Harry Johnson, Mitchell Kemp, Maxim Millen, Audsley Jones, Sam McHattie, Varun Joshi, among others. Special thanks to Rich Malcolm, Alberto Cuevas and David Reynolds who helped review draft versions of some thesis chapters. Thanks to my flatmates for providing enjoyment on the occasions that I stepped out of the research environment.

To my grandparents Colin and Betty, I am fortunate to have had your support and interest during my studies. Colin, I'm especially grateful that your scientific interests were passed down to me. To my sister Leanne, I'm sorry I have not been able to visit you in Australia these past two years however I look forward to changing that. Lastly, to my parents John and Karen, I am forever grateful that you allowed me to 'steer my own cutter' from a young age. Your never ending faith and trust in me has been the greatest gift to my education and, in return, this thesis is rightfully dedicated to the both of you.

Gareth John Morris - 16th June 2015

"You can get help from teachers, but you are going to have to learn a lot by yourself, sitting alone in a room" ***- Dr Seuss (1904-1991).***

TABLE OF CONTENTS

LIST OF FIGURES

LIST OF TABLES

1 INTRODUCTION

1.1 MOTIVATION: CANTERBURY EARTHQUAKE SEQUENCE

The motivation for this research is the result of recent observations from the damaging 2010-2011 Canterbury earthquake sequence. Although damaging earthquakes generally have a major negative impact on society, post-earthquake reconnaissance is highly valuable for structural engineers to compare direct performance observations with the existing body of knowledge and to challenge assumptions that are used in conventional structural engineering practice.

The most significant structural damage was caused by the 22 February 2011 Christchurch earthquake, which was a moment magnitude M_w6.3 event with a source-to-site distance of less than 5 km from Christchurch's central business district (CBD). Relatively large-amplitude, short duration ground motions were recorded. For some vibration periods the spectral amplitude of the recorded motions exceeded the level of shaking that might have been expected to occur during a "maximum credible event" with a return period of 1/2500 years. Further discussion of the strong ground motions recorded during the 2011 Christchurch earthquake and the Canterbury earthquake sequence are presented in Bradley and Cubrinovski (2011) and Bradley *et al.* (2014).

Although the seismic demands from the 2011 Christchurch earthquake significantly exceeded the NZS1170.5:2004 design spectra, the performance of the majority of reinforced concrete (RC) commercial buildings was satisfactory with respect to the targeted performance criteria of maintaining "life safety". However, it is important to emphasize that the duration of strong ground shaking in the Christchurch CBD was approximately 10 seconds. Considering the damage observed and the apparent lack of ductility of some RC structures, it is conceivable that the number of building collapses would have been higher for a longer duration of strong ground shaking of similar amplitude. Figure 1-1 shows a sample of three RC buildings that sustained extensive structural damage and may be considered as incipient collapse. Unfortunately there were two catastrophic collapses of multi-storey RC buildings that contained several critical structural weaknesses. 18 people died following the collapse of the Pyne Gould Corporation (PGC) building and 115 people died following the collapse of the Canterbury Television (CTV) building.

(a) Fracture of vertical wall reinforcement in Gallery Apartments building.

(b) Beam elongation in Clarendon Tower led to corner column push out, fracture of topping slab reinforcement (cold drawn wire mesh) and partial loss of gravity support of precast double tee floor units.

(c) Compression buckling failure of north wall in the building at 123 Victoria Street. Inadequate restraint of core concrete due to lack of transverse reinforcement restraining main vertical and horizontal reinforcement.

Figure 1-1: Sample of reinforced concrete buildings that might have collapsed during shaking of a similar intensity of the 22 February 2011 Christchurch earthquake, but longer duration. (Pictures from Bull, 2012)

1.1.1 Canterbury Earthquakes Royal Commission (CERC)

The overall damage caused by the Canterbury earthquake sequence highlighted several issues for RC buildings. Some examples of these issues include: (i) inadequate detailing of reinforcement in beam-column joint zones for secondary frames; (ii) out-of-plane buckling of wall structures; (iii) fracture of vertical reinforcement in lightly reinforced wall structures; (iv) vulnerability of damaged precast floor diaphragms, and; (v) the collapse of stairs. Further discussion of the performance of Christchurch's representative building sample is found in the Canterbury Earthquakes Royal Commission report (CERC - Volume 2, 2012).

An emerging theme of the "lessons learnt" by the international structural engineering profession was that the observed performance of real RC structures was not consistent with long-held assumptions on structural behaviour used in conventional practice and based on decades of experimental testing on RC specimens. 189 recommended topics of further investigation were published by the Canterbury Earthquakes Royal Commission (CERC, 2012). Twelve recommendations are specifically aimed at improving the seismic performance of RC buildings and design implications for the New Zealand concrete structures standard, NZS3101:2006 (CERC, 2012). These recommendations refer to several topics that have been previously discussed in the literature with varying conclusions and, in many cases, no clear suggestions for the implications and outcomes for structural design practice.

Since the Canterbury earthquakes, the New Zealand research community has been particularly interested in the influence of the sequence and rate of loading on the behaviour of RC structures. The 22 February 2011 earthquake induced severe dynamic loading that is not typically replicated in the loading protocols that are adopted in structural tests performed in experimental programmes. Consequently, there is a lack of existing research in this particular area that can support structural design practice. Recommendations 40 and 41 of the CERC (2012) below were included as area of required research:

40. *"A comprehensive study into the existing literature on the influence of the rate of loading on the seismic performance of RC structures should be undertaken to address the inconsistencies in the published opinions, and to make appropriate recommendations for design."*
41. *"Research into the influence of the sequence of loading cycles on yield penetration of reinforcement into beam-column joints and the development zones of reinforcement is desirable."*

The scope of possible research associated with this recommendation is reasonably large. The underlying objective of recommendations 40 and 41 is to explain the apparent lack of ductility in lightly reinforced concrete walls by identifying what length of the reinforcing bar will yield under good bond conditions.

1.1.2 Research focus: bond behaviour in lightly reinforced concrete walls

Figure 1-2 schematically illustrates the case of a lightly reinforced wall that forms a single wide crack. The location of the crack is in the region of the construction joint, either at the fixed base of the wall or directly above the lapped splice region along the line at which the vertical starter bars from the foundation are terminated. In this case, the quantity of flexural tension reinforcement is relatively low and increased bar stresses due to strain hardening may be unable to contribute to the ductility capacity of the structural member. Instead, the lateral drift of the wall is primarily accommodated by the plastic elongation of the vertical reinforcement. This concerning damage mechanism in Figure 1-2 was recently observed in buildings such as the Gallery Apartments and PGC buildings (refer to Figure 1-1(a)). One possible notion for this mechanism is that high bond stresses between the vertical reinforcement and surrounding concrete was contributing factor to high strain concentrations that resulted in near or complete brittle fracture of the reinforcement. However, aside from the bond mechanics, there may have been several other possible factors, including the type of loading, in situ concrete strength and quantity of longitudinal reinforcement (Bull, 2012; Morris *et al.*, 2014, Lu *et al.*, 2014).

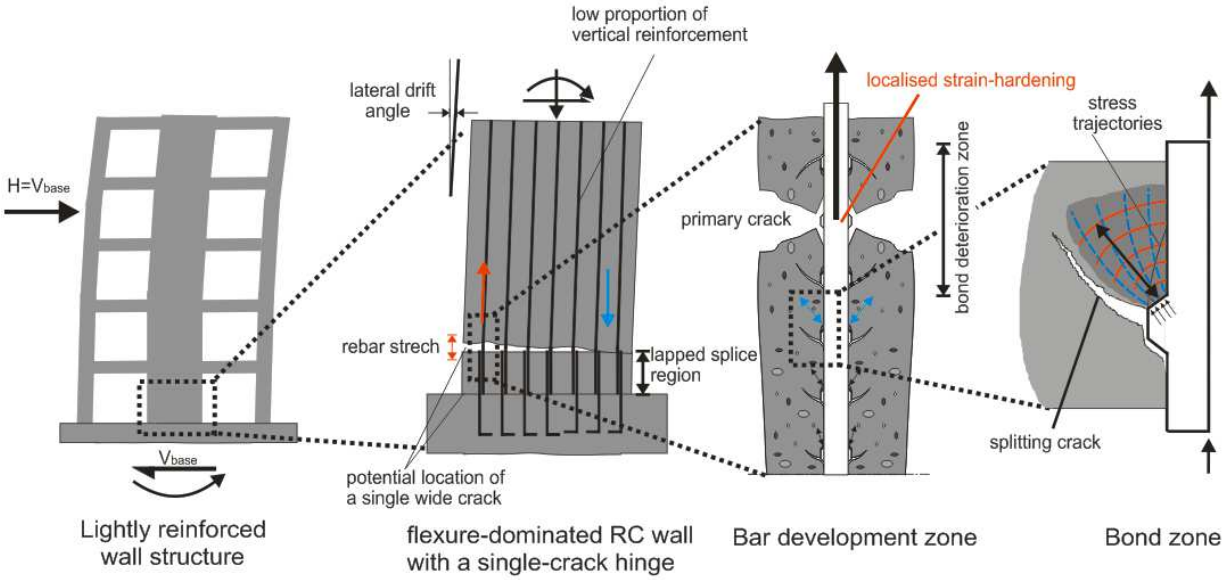

Figure 1-2: The deterioration of bond resistance in lightly reinforced concrete walls provides the only source of ductility if the wall forms a single crack (or few cracks) at the potential plastic hinge zones.

Practising structural engineers have been challenged on how to estimate the ductility capacity of RC wall buildings as there is a lack of clear practice guidance and therefore a range of approaches and assumptions are made. Destructive and non-destructive testing of reinforcing steel samples from the single crack plastic hinge zones (PHZs) of approximately 50 buildings have indicated that bar yielding was limited to 0.5 to 1.0 d_b (Hare *et al.*, 2012), which is significantly less than that allowed for by Priestley *et al.* (2007) and Paulay and Priestley (1992).

Previous studies by Shima *et al.* (1987), Mayer and Eligehausen (1998), and others found in ACI Committee 408 (1998) generally agree that the rotational capacity of plastic hinges is reduced if there is an excessively high tensile stress contribution of concrete between cracks which is enabled by the bond mechanism. There is a general consensus in the literature that the ductility of RC components is primarily influenced by the longitudinal reinforcement ratio and stress-strain relationship of the reinforcing steel. This conclusion is relevant for RC components that can form multiple cracks. However, when there is an insufficient quantity of longitudinal reinforcement, the ductility of a RC wall with a single crack PHZ will depend on the extent of bond deterioration that can occur near the crack plane.

The majority of previous research on bond in RC has focussed on the implications of the bond stress-slip relationship on the performance of beam-column joints in RC frames and bridges (Filippou *et al.*, 1983; Eligehausen *et al.*, 1983; Lowes, 1999). The structural conditions and state of stress in beam-column joints are complicated by the transient variation of axial loads, passive confinement pressures from the column reinforcement, and the propagation of cracks along the beam (and column) longitudinal bars towards the joint core area that reduces some of the bond condition.

Recent New Zealand research (Cuevas and Pampanin, 2015) on the residual capacity of ductile RC frames is also related to studying bond behaviour. Other recent research in New Zealand has been focussed on studying the significance of secondary crack formation on the ductility of lightly reinforced walls (Lu *et al.*, 2014). With respect to bond, the case of lightly reinforced walls is less complex in comparison to the conditions that may be accounted for in ductile beams or in beam-column joints. Some of these simplifications of the problem are listed below:

- Good bond conditions due to a large cover concrete thickness and between-bar spacing.
- Low quantities of longitudinal reinforcement and small to moderate bar sizes.
- Low shear stresses and shear displacements – not contributing any significant additional stresses to the concrete or to the reinforcement.
- No transverse pressures or longitudinal cracking in the vicinity of the embedded bond region.

Although this research is motivated by the brittle failure of lightly reinforced concrete walls, many aspects of bond behaviour described in this thesis will be widely applicable to all RC components.

1.2 RESEARCH OBJECTIVES

The previous section described the focus of this research. In order to address this focus, an experimental testing programme is undertaken and a large number of relevant test permutations are investigated to address the specific research objectives summarised below:

1. Examine why 'real' RC structures in the Christchurch CBD did not exhibit the extensive spread of plasticity previously observed in typical structural tests under laboratory conditions.
2. Determine the relevant outcomes from previous bond-related research, including a discussion of relevant outcomes that are not directly investigated in this particular experimental programme.
3. Obtain experimental measurements that provide insight into the bond stress-slip relationship under monotonic and cyclic loading, including parametric investigation of some test conditions in order to report on the likely influence of several variables on bond behaviour.
4. Present a rational interpretation of the bond behaviour of conventional NZ RC structural components observed in monotonic and cyclic bond tests and generalise this behaviour to present a constitutive relationship for the mean local bond stress-slip behaviour, and to compare with that stated in the Model Code 2010 (*fib*, 2012).

1.3 ORGANISATION OF THESIS

The thesis has been written as a collection of seven chapters. There is some minor repetition between the introductory sections to ensure that each chapter is read in the appropriate context. Each chapter contains a list of references from the relevant literature that was used.

The motivation, focus and objectives of this research have been described here in **CHAPTER 1**. Chapters 2, 3, 5, 6 will address each of the four research objectives. Chapter 4 is recommended reading to give some awareness of the experimental design and test set-up that was used.

CHAPTER 2 presents an observation-based comparison between the behaviour of RC specimens in previous experimental testing and the unexpected behaviour of some buildings during the 2010-2011 Canterbury earthquake sequence. The chapter describes some differences between typical "laboratory conditions" (test specimens under simulated seismic actions) in comparison to "field conditions" (real structures subjected to severe dynamic ground motions). In attempting to address Objective 1, this chapter discusses how the structural behaviour of RC structures is potentially influenced by the loading history; the in-place concrete strength, and; the quantity of longitudinal reinforcement. This chapter may be deemed to be optional reading as less attention has been given to the details of bond mechanics.

CHAPTER 3 focuses the remainder of the thesis on fundamentals of bond mechanics. Background description is given for the various roles of bond in ductile RC structures and the mechanism of bond resistance during monotonic and cyclic loading is illustrated. Objective 2 is addressed by summarising the available literature that extends over 100 years. The literature is examined to determine: (i) the important material properties and structural conditions that influence bond behaviour; (ii) how different test set-ups have been used to measure bond behaviour, and; (iii) what is the state-of-the-art information available for bond models in the Model Code 2010 (fib, 2012).

CHAPTER 4 contains the essential details of experimental programme. The chapter describes the test set-up, specimen design details and construction phases for 75 bond pull-out tests. An overview of the test permutations for monotonic and cyclic bond tests is presented in the form of written justification and a test matrix which is useful information prior to reading Chapters 5 and 6.

CHAPTER 5 presents the monotonic tests results for each series of the test programme in order to satisfy Objective 3. This chapter explains how the bond stress-slip relationship was evaluated from the test measurements. Observed failure modes are described and the generalised bond stress-slip behaviour is presented prior to independently discussing the results from each test series. To partly address Objective 4, a statistical interpretation of the monotonic test results is carried out to report the maximum bond strength, and a full bond stress-slip constitutive relationship is proposed to represent the mean monotonic bond behaviour.

CHAPTER 6 presents the cyclic test results, mainly for Series 4 and 7 of the test programme. Firstly, the chapter explains the basis for five different cyclic loading protocols that were selected. The observed failure modes are listed and cyclic stress-slip relationships are presented for each loading protocol. Interpretation of the test results studies the bond strength degradation and hysteretic energy dissipated during some of the cyclic bond tests. Objective 4 is satisfied by comparing the observed bond deterioration to the energy-based prediction model found in the Model Code 2010 (*fib*, 2012).

CHAPTER 7 is a stand-alone summary of the research presented within this thesis. The significant conclusions presented within the earlier chapters have been restated such that Chapter 7 can be read independently of the earlier chapters. Conclusions from the literature review (Chapter 3) and from the experimental research (Chapters 5 and 6) are listed, along with a list of technical advantages and disadvantages of the bond behaviour for deformed reinforcing bars embedded in concrete. Chapter 7 is not a key contribution of this research, however some linkages with other research are presented to suggest how the bond stress-slip behaviour may help structural engineers predict the width and spacing of cracks in RC structural components.

APPENDIX A outlines the properties of the deformed reinforcing bars and concrete that was used to construct the pull-out test specimens. **APPENDIX B** shows the calibration data for the 100 kN load cell that was used to measure the applied forces during bond testing.

APPENDIX C provides tabulated and photographic records of the failure modes and specimen damage that was observed. **APPENDIX D** presents additional test results that further support the typical bond behaviour described in Chapter 6. This appendix also contains results tables that compare the observed cyclic bond deterioration to the cumulative hysteretic energy dissipation.

1.4 REFERENCES

ACI Committee 408 (1998). Bond and development of reinforcement: A tribute to Peter Gergely, *Special Publication 180*. Farmington Hills, MI: ACI International. Leon, R. T: editor,

Bull, D. K. (2012). The performance of concrete structures in the Canterbury earthquakes: Lessons for concrete buildings, *Structural Engineers Association of California (SEAOC) Convention*, Santa Fe, NM.

Bradley, B. A. and Cubrinovski, M. (2011). Near-source strong ground motions observed in the 22 February 2011 Christchurch earthquake. Bulletin of the New Zealand Society of Earthquake Engineering, 44(4): 181-194.

Bradley, B. A., Quigley M. C., Van Dissen, R. J. and Litchfield, N. J. (2014). Ground motion and seismic source aspects of the Canterbury earthquake sequence. *Earthquake Spectra,* 30(1): 1-15.

Canterbury Earthquakes Royal Commission, CERC (2012). Final report: Volume 2, The performance of Christchurch CBD Buildings. http://canterbury.royalcommission.govt.nz/Final-Report---Volumes-1-2-and-3

Cuevas, A. and Pampanin, S. (2015). Effect of strain-rate and material characteristics on the seismic residual capacity of reinforced concrete plastic hinges: numerical investigation. Conference proceedings of the New Zealand Society of Earthquake Engineering, Rotorua.

Eligehausen, R., Popov, E.P., Bertero, V.V. (1983), Local bond stress-slip relationships of deformed bars under generalized excitations. *Report UCB/EERC-83/23*, Earthquake Engineering Research Centre, University of California, Berkeley.

Eligehausen, R., Ozbolt, J. and Mayer, U. (1998). Contribution of concrete between cracks at inelastic steel strains and conclusions for the optimisation of bond. *Symposium of the ACI Committee 408 – Bond and Development of Reinforcement* (edited by Leon, R). SP180-3: 45-80.

Fédération Internationale du Béton, fib. (2012), Model Code 2010 – First Complete Draft, Volume 1, Lausanne, Switzerland.

Filippou, F. C., Popov, E.P., Bertero, V.V. (1983), Effects of bond deterioration on hysteretic behaviour of reinforced concrete joints. *Report UCB/EERC-83/19*, Earthquake Engineering Research Centre, University of California, Berkeley.

Hare, H. J., Bull, D. K., Brown, B., Brunsdon, D. R., Jury, R., King, A., McCahon, I., Millar, P., Smith, P., and Stannard, M., (2012). Canterbury earthquake sequence: Detailed engineering evaluation of commercial buildings, *15 World Conference on Earthquake Engineering*, Lisbon.

Lowes, L.N. (1999). Finite element modelling of reinforced concrete bridge beam-column connections, *Doctor of Philosophy Thesis*, University of California, Berkeley, CA.

Lu, Y., Henry, R. S., and Ma, Q. T. (2014). Numerical modelling and testing of concrete walls with minimum vertical reinforcement. C*onference proceedings of the New Zealand Society of Earthquake Engineering*, Auckland.

Morris, G.J., Bull, D.K. and Bradley, B.A. (2014). Reviewing uncertainties in seismic experimentation following the unexpected performance of RC structures in the 2010-2011 Canterbury earthquakes. *Conference proceedings of the New Zealand Society of Earthquake Engineering,* Auckland.

NZSEE (2006). Assessment and improvement of the structural performance of buildings in earthquakes, *Recommendations of a study group of the New Zealand Society for Earthquake Engineering,* Wellington, New Zealand.

Paulay, T., and Priestley, M.J.N., (1992). Seismic design of reinforced concrete and masonry buildings. John Wiley & Son, Inc., New York, United States of America.

Priestley, M. J. N., Kowalsky, M. J., and Calvi, G. M. (2007). Displacement-based seismic design of structures, IUSS PRESS, Pavia, Italy.

Shima, H., Chou, L.L., and Okamura, H. (1987) Micro and macro models for bond in reinforced concrete. *Reprinted from Journal of the Faculty of Engineering*, The University of Tokyo, 39(2).

Standards New Zealand. (2004). Structural design actions, Part 5: Earthquake actions - New Zealand, NZS1170.5, Standards New Zealand: Wellington, New Zealand, 82.

Standards New Zealand. (2006). Concrete structures standard, NZS3101, Parts 1 & 2. Standards New Zealand: Wellington, New Zealand.

[This page is intentionally left blank]

2 IN SITU CONDITIONS AFFECTING THE DUCTILITY CAPACITY OF LIGHTLY REINFORCED CONCRETE WALL STRUCTURES IN THE CANTERBURY EARTHQUAKE SEQUENCE

Morris, G.J., Bull, D.K. and Bradley, B.A., (in press). "In situ conditions affecting the ductility capacity of lightly reinforced concrete wall structures in the Canterbury earthquake sequence", *Bulletin of the New Zealand Society of Earthquake Engineering*, submitted December 2014.

2.1 ABSTRACT

Following the 2010-2011 Christchurch earthquake sequence, the structural behaviour of some conventionally designed reinforced concrete (RC) structures was somewhat unexpected to practising structural engineers and researchers. Consequently, the Canterbury earthquakes demonstrated that there may be less confidence in the seismic performance of RC components than previously anticipated. In particular, lightly reinforced wall structures in the Christchurch central business district were observed to form undesirable crack patterns in the plastic hinge region, while yield penetration either side of cracks and into development zones was less than predicted using empirical expressions. This chapter provides an observation-based comparison between the behaviour of RC structural components in laboratory testing and the unexpected performance of some case study buildings in Christchurch that formed concentrated inelastic deformations. The unexpected behaviour and poor overall seismic performance of 'real' buildings (compared to the behaviour of laboratory test specimens) was due to the localization of peak inelastic strains, which is some cases led to: (i) significantly lower ductility capacity; (ii) less hysteretic energy dissipation; and (iii) the fracture of the longitudinal reinforcement. These observations have raised concerns about whether lightly reinforced wall structures can satisfy the performance objective of "Life Safety" at Ultimate Limit State (ULS). The significance of these issues and potential consequences has prompted a review of potential problems with the testing conditions and procedures that are commonly used in seismic experimentations on RC structures. This chapter attempts to revisit the principles of RC mechanics, in particular, the influence of loading history, concrete tensile strength, and the quantity of longitudinal reinforcement on the performance of real RC structures. Consideration of these issues in future research on the seismic performance of RC might improve the current confidence levels in newly designed conventional RC structures.

2.2 INTRODUCTION

The current understanding of the seismic performance of structural components is largely based on the outcomes and developments of previous research by methods of experimental testing and, in more recent times, numerical modelling techniques. As damaging earthquakes occur relatively infrequently, the information gained from examining the effects of damaging earthquakes provides a rare opportunity to assess whether the previous "laboratory-based understanding" provides a reasonable comparison to field observations.

The performance of some reinforced concrete (RC) buildings in the 2010-2011 Canterbury earthquake sequence was somewhat unexpected compared to previous structural tests performed in laboratories using typical seismic experimentation procedures (which is elaborated in detail later). Such observations have highlighted the need to reconsider the way in which structural tests are undertaken to make them representative of how 'real' RC structures might perform during severe earthquake-induced ground motions. Wider aspects of the performance of RC buildings in the Christchurch CBD have been documented by Kam *et al.* (2011), Bull (2012), the Canterbury Earthquakes Royal Commission (CERC, 2012), and Fenwick (2013), among others. In particular, the seismic performance of some RC wall structures was relatively poor.

This chapter examines several reasons for the lack of correlation between observations from previous laboratory testing and the damage states sustained by Christchurch buildings during the 2010-2011 Canterbury earthquake sequence. The reader should note that this lack of correlation may not necessarily be universal in all scenarios. Some of the aspects discussed in this chapter are considered to be 'in-situ field conditions' that may have been more pertinent overall factors in certain RC structures in Christchurch (or in New Zealand construction) that may be less relevant for other seismic regions of other structural types.

Firstly, the typical experimental behaviour of RC structural components is compared to post-earthquake observations in Christchurch buildings. While the first sections of this chapter are predominantly focussed on RC wall structures, the scope of the paper is intended to be relevant for all primary structural members that have been constructed in RC. Although the authors have attempted to distinguish important differences (between RC walls and RC beams, for example) within the paper, the final interpretation and application of the engineering concepts will depend somewhat on the reader' prior knowledge of the reader. Secondly, the effects of the nature and rate of loading, in-place concrete strength, and quantity of longitudinal reinforcement on the behaviour of RC components are discussed. These factors (the typical "experimental conditions") are further described in an attempt to explain the lack of correlation between laboratory and field observations. Lastly, considerations and challenges for future research and for structural engineering practice are outlined.

The key contribution of this chapter is the attempt to evaluate and utilize some of the outcomes found in wide ranging search of international literature. The contents of this chapter are intended to be a thought-provoking extension of the issues that were briefly discussed by Morris *et al.* (2014). Combinations of research and field observations have been included in the paper to in order to identify: (i) the inconsistencies in the current body of knowledge, and (ii) the implications for structural engineering practice in New Zealand (and perhaps internationally).

2.3 EXPERIMENTAL OBSERVATIONS VS. REALITY

2.3.1 Typical structural behaviour and spread of plasticity observed in experimental testing

Laboratory testing of RC components subjected to quasi-static loading protocols has historically exhibited the formation of a ductile plastic hinge zone (PHZ) adjacent to the fixed end region. Countless tests have shown the formation of diagonal flexure-shear crack patterns, examples of which are shown in Figure 2-1(a) for a RC beam and in Figure 2-1(b) for a RC wall. These fanned crack patterns progressively develop during simulated seismic loading and lead to the gradual spread of inelastic steel strains (i.e. the "spread of plasticity") from the critical section of maximum bending moment further into the component. Differences in the tensile strain capacity of the reinforcing steel and concrete mean that some bond slip must occur to accommodate this strain incompatibility. In general, this type of behaviour lengthens the PHZ, which is a significant requirement of ductile RC structure components that are designed to sustain multiple cycles of inelastic deformation. The longitudinal reinforcement will yield over a length equal to a combination of three segments due to: (i) yield penetration into anchorage zones; (ii) the relative increase in the maximum bending moment above the first yield moment due to strain hardening, and; (iii) extension due to tension shift as a result of diagonal flexure shear cracking (Fenwick and Dhakal, 2007b).

The "effective plastic hinge length*",* denoted L_p in Figure 2-1(c), is the length over which plastic curvature is assumed to be uniform for analytical purposes. L_p is strongly dependent on the slope of the bending moment (magnitude of shear) at the critical section, moment-shear M/V ratio, quantity of transverse reinforcement, and magnitude of axial load. The length of yielding, L_y, is referred to as the length of ductile detailing in the New Zealand concrete structures standard (referred to herein as NZS3101:2006), and is schematically shown on Figure 2-1(c) to be considerably longer than L_p. The extension of yielding along the member (the "spread of plasticity") also depends on the formation and spacing of flexural cracks, which is dependent on member geometry, tension force in the longitudinal reinforcement, and tensile strength of the surrounding concrete. The size of the flexural tension force is influenced by the quantity and the stress-strain relationship of the longitudinal reinforcement, particularly the maximum strain that can be sustained and the amount of strain hardening. If secondary cracks cannot form between primary

cracks, very high reinforcement strains are induced and limited ductility can be sustained before the reinforcement fails (Fenwick, 2013).

The spread of plasticity in real RC structures under seismic actions has long been expected to be consistent with experimental observations from laboratories around the world (e.g. Figure 2-1). Many of the assumptions for structural behaviour used in practice are based on the outcomes of the experimental studies described in the literature, such as Priestley and Park's (1984) extensive research on the seismic performance of RC bridge columns. For the purpose of preliminary design stages, or when using seismic assessment methods (such as NZSEE, 2006), the value of L_p is one of several simplifying assumptions made in lumped plasticity modelling approaches. This allows for an estimation of the overall structural ductility factor that reduces the force demands on a particular structural system. However, the structural ductility factor does not give a reliable indication of the deformation sustained in a potential PHZ (Fenwick and Dhakal, 2007a and 2007b).

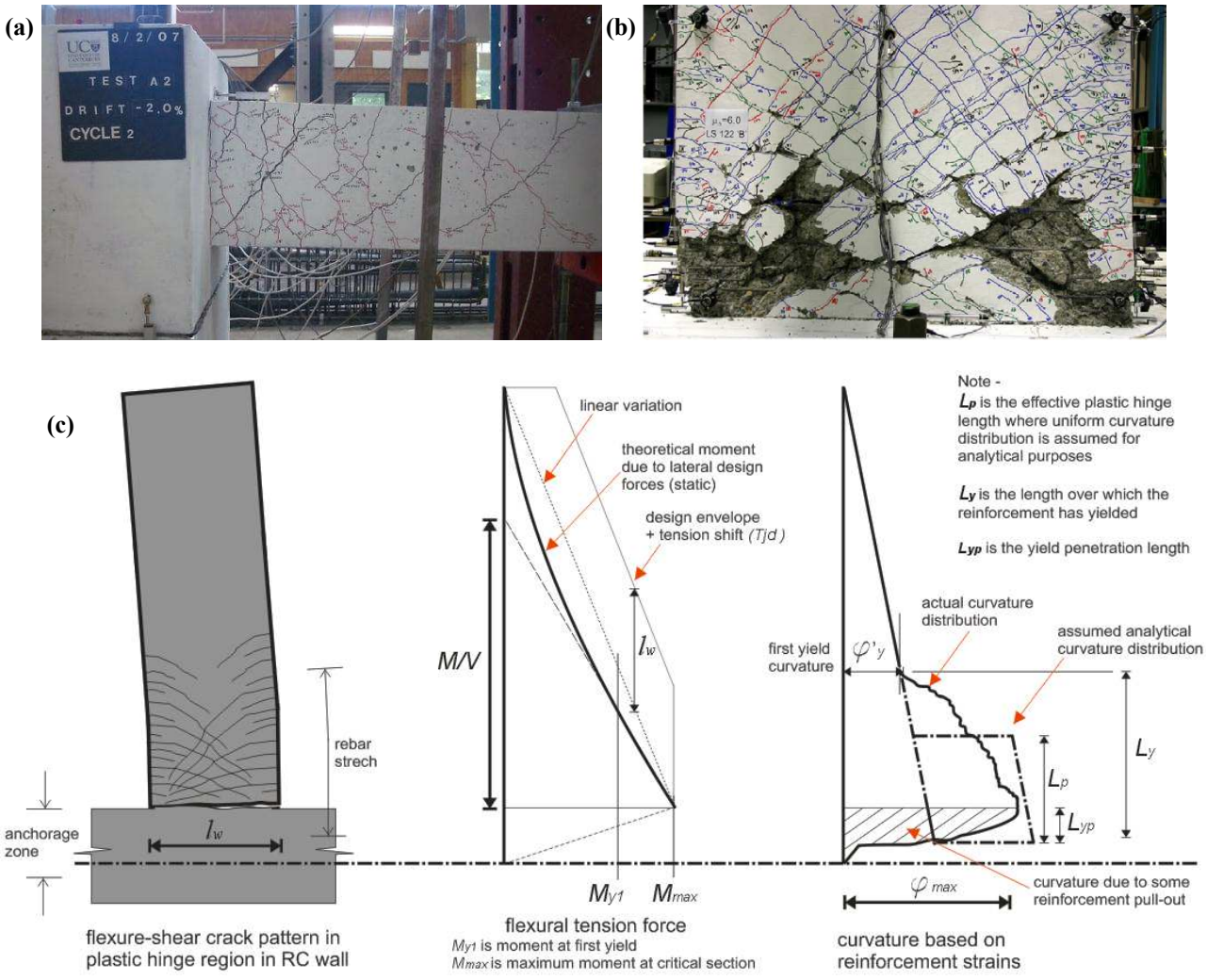

Figure 2-1: Distributed flexure-shear cracks observed in experimental testing: (a) RC beams tested by Walker (2007); (b) a U-shaped RC wall with boundary elements tested by Beyer *et al.* (2008). (c) Expected deformations in the PHZ of monolithic RC walls with distributed flexure-shear cracking.

NZS3101:2006 considers the value of L_p for the purposes of assessing section curvatures and determining the level of detailing required for potential PHZs. For RC beams, columns and walls, L_p is coupled with material strain limits (considered by maximum allowable curvatures stated in Table 2.4 of NZS3101:2006). Fenwick and Dhakal (2007b) used previous experimental data on RC beams, columns and walls to determine the allowable curvature values that corresponded to initially assumed values for L_p. For reversing plastic hinges in beams, columns or walls, L_p is taken as the smaller of half the section depth $0.5h$ or 0.2 times the *M/V* ratio, but not less than one quarter the section depth. In both research and practice there has long been a consistent agreement that using $L_p = 0.5h$ is a reasonable approximation (Paulay and Priestley, 1992). In NZS3101:2006, any error in the assumed values of L_p is removed when used with the corresponding material strain limits.

Suggestions for calculating L_p by Priestley *et al.* (2007) have been widely adopted in both research and in practice. Equation 2-1 is described as an "accurate" estimate compared to $L_p = 0.5h$, albeit a less conservative estimate with respect to ductility. Equations 2-1 to 2-3 were empirically derived from a database of experimentally measured section and member deformations such that curvature and displacement ductility relationships could be re-arranged and solved for L_p.

$$L_p = kL_c + L_{yp} \tag{2-1}$$

where:

$$k = 0.2\left(\frac{f_u}{f_y} - 1\right) \leq 0.08 \tag{2-2}$$

$$L_{yp} = 0.022 d_b f_y \tag{2-3}$$

where L_c is stated as the length from the critical section to the point of inflexion, f_u and f_y are the ultimate tensile strength and yield strength of the longitudinal reinforcement, d_b is the diameter of the longitudinal reinforcement, and L_{yp} is the yield penetration length. The factor k considers the slope of the bending moment at the critical section and hence the extension of yielding along the member due to strain hardening of the reinforcement, which appears reasonable.

In practice, the term L_c in Equation 2-1 is somewhat misleading for cantilevered walls in multi-storey buildings for two reasons. Firstly, simplified relationships between curvature and displacement ductility are based on an example of a cantilevered column with a point load applied at the top such that the column height is directly equal to L_c and the *M/V* ratio at the wall base (as shown in the central image of Figure 2-1). Secondly, some previous tests of RC walls used a concentrated load at the top of the scale-reduced specimens (again the component height is equal to the *M/V* ratio) and L_p was often expressed as a percentage of the specimen wall height. However, the force distribution for structural walls in real multi-storey buildings means the wall height is an inappropriate parameter to relate to the effective plastic hinge

length. The moment diagram in Figure 2-1(c) labels the *M/V* ratio as the appropriate length along the member that influences the spread of plasticity. This difference is recognised in Priestley *et al.* (2007) where L_p for cantilevered RC walls is estimated by Equation 2-4. The length, L_c, from Equation 2-1 is replaced by H_E, an effective height that should represent the M/V ratio for a structural wall.

$$L_p = kH_E + 0.1l_w + L_{yp} \quad 2\text{-}4$$

Equation 2-4 also includes an additional term of 10% of the section depth, $0.1l_w$, to account for greater tension shift occurring in walls compared to that in beams. For cracked RC components with combined flexure and axial loading, the axial load becomes inclined towards the compression zone such that a portion of the shear force is resisted through the concrete which therefore reduces the shear force V_s that is resisted by the transverse reinforcement (stirrups in beams/columns or horizontal reinforcement in walls). Considering the moment equilibrium for a free body of a diagonally cracked RC component, V_s provides some moment resistance however, as the axial loading increases and V_s reduces, the length of tension shift will increase. This influence of axial loading generally means the length of yielding will be longer in columns and walls than in beams.

Priestley and Park (1984) identified that some degree of bond deterioration will increase the length of the reinforcement that will yield as inelastic tensile strains penetrate some distance into the anchorage zones of the longitudinal reinforcement (e.g. beam-column joints and wall footings). As the anchorage zones of RC components are not fully rigid, the relative slip between the reinforcement and concrete (known as bond slip) near the critical section will contribute to the total inelastic deformation. The extent of yield penetration into, or through, a joint will depend on many factors, of which the number and amplitude of inelastic loading cycles will significantly influence bond deterioration.

There are many factors that influence the effective plastic hinge length that are not considered in Equations 2-1 to 2-4 which have been expressed in this form for ease and simplicity in design practice. Equation 2-3 suggests L_{yp} depends on the yield strength and nominal diameter of the reinforcement. It was previously suggested that the reinforcement may be expected to yield over a length of 6 times the bar diameter, i.e. $6d_b$ (Priestley and Park, 1984). More recently, Equation 2-3 suggests L_{yp} is equal to $6.6d_b$ for Grade 300 reinforcement and $11d_b$ for Grade 500 reinforcement. The following section of this chapter explains the significance of the true yield penetration length when this length of the reinforcement becomes the only available source of plastic deformation for components without extensive cracking and spread of plasticity along the member. Some previous structural tests on beam specimens used additional bars welded to the reinforcement passing through the anchorage zones in order to limit the extent of yield penetration (Liddell *et al.* 2000; Fenwick and Dhakal, 2007b; Walker, 2009). This technique has been employed to reduce the deformations attributed to anchorage slip to give conservative values of the plastic curvatures that are measured.

The simplified form of Equation 2-3 suggests that L_{yp} will be the same for identical reinforcement properties, irrespective of the mechanical properties of the surrounding concrete. Without presenting a detailed discussion of the mechanism of bond in this chapter, it is widely accepted that the strength of concrete (particularly the tensile strength) significantly influences the relationship between bond stress and bond slip (Eligehausen *et al.*, 1983). In recent decades there have been significant research developments in understanding bond behavior at inelastic reinforcement strains (Shima *et al.*, 1987; Bonacci, 1994; Mayer and Eligehausen, 1998; Lowes *et al.*, 2004; the Model Code 2010- *fib*, 2012; Soleymani Ashtiani *et al.*, 2013, among others). The literature suggests that the extent of yield penetration may be greater for lower grades of steel due to a greater reduction in bar diameter at large inelastic strain demands (known as the Poisson effect). The amount of relative bond slip near the crack plane will depend on the yield stress of the reinforcement if the strain demand is low. In contrast, if the strain demand is large then the local bond slip will depend on the length of the yield plateau and the strain hardening behaviour.

In both research and in practice, the understanding of the structural behaviour of RC and the published empirical expressions such as Equations 2-1 to 2-4 have largely emerged from research outcomes of laboratory-based experimental testing. Typical "experimental conditions" that may influence the structural behaviour include: (i) inelastic deformations measured during the application of a gradually increasing symmetric quasi-static loading protocol shown in Figure 2-4(a); (ii) test specimens containing relatively young concrete with compressive strengths ranging between 25 and 40 MPa, and; (iii) the use of moderate to high proportions of longitudinal reinforcement where there was no restriction of progressive cracking along the member.

2.3.2 Observed performance of real RC structures

Damage observations in the Christchurch CBD during the 2010-2011 Canterbury earthquake sequence demonstrated that some conventional RC wall structures developed regions of concentrated inelastic deformations that were markedly different than the distributed PHZs observed in experimental tests. When inelastic reinforcement strains are concentrated at a small number of large cracks the ductility capacity of the component is significantly reduced. Figure 2-2(d) illustrates the deformations in lightly reinforced walls developing a "single-crack-PHZ". The formation of the primary crack at the critical section reduces the tensile stress in the concrete over a reasonable height up the wall. The location where the next primary crack might form, denoted L_{pc} on Figure 2-2(d), is theoretically between one and two times the distance from the extreme tension fibre to the neutral axis at the initial crack (Dickson, 1986). At a distance of L_{pc} from the critical section, the flexural tension force might be less than the tensile strength of the surrounding concrete and the next potential crack cannot form. As a result, significant strain hardening of the reinforcement must occur at the critical section to increase the flexural tension force along the member and increase the possibility of developing the next potential primary crack.

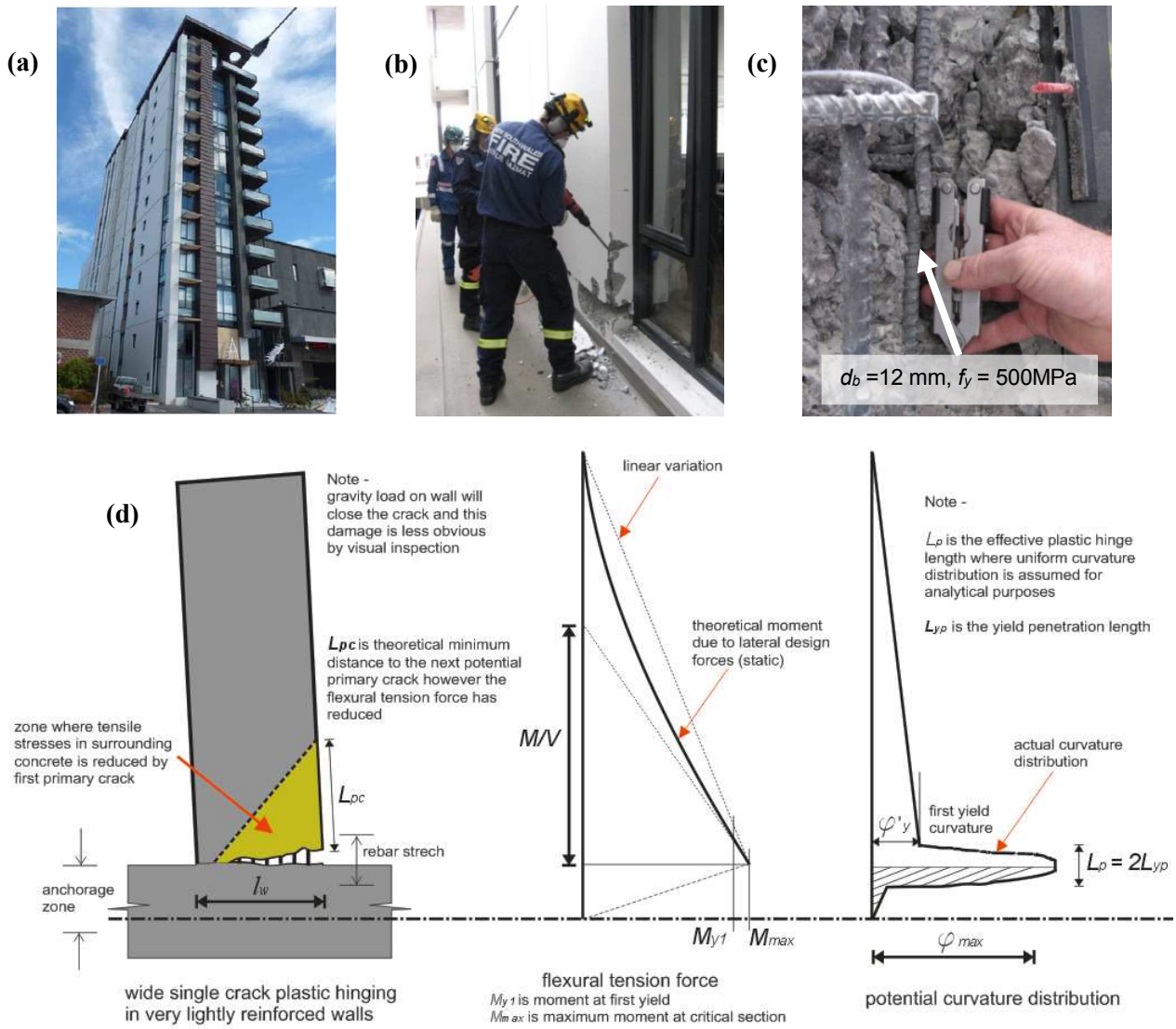

Figure 2-2: Illustration of frequently observed PHZ behaviour in the Canterbury earthquakes: (a) The Gallery Apartments RC wall building; (b) Urban Search and rescue (USAR) team removing cover concrete; (c) fractured vertical reinforcement (Bull, 2012); and (d) schematic illustration of deformations in the case of a single-crack-PHZ for monolithic RC walls.

This concentration of reinforcement strains significantly reduces the effective plastic hinge length that may be adopted for analytical purposes. Some buildings in this category exhibited much less available ductility than previously anticipated. Due to the lack of cracking along the member, the elongation of the reinforcing steel will depend on the magnitude of the steel strain and the true extent of yield penetration back into the surrounding concrete. RC walls with a single-crack-PHZ require significant bond deterioration adjacent to the crack in order to withstand the overall lateral deflection demands of the building. However, in cases where the vertical reinforcement had good bond conditions, and high bond stresses could be sustained, the extent of yield penetration might have been less than previous empirical suggestions such as Equation 2-3. The major consequence of this behavior is the high strain concentrations

and possible brittle failure of the vertical reinforcement. An example of this behaviour includes the Gallery Apartments building shown in Figure 2-2(a)-(c).

The vertical reinforcement in the critical wall of the Gallery Apartments contained two layers of HD12's (Grade 500, 12 mm bars) spaced at 420 mm. The rectangular section was 4300 mm in length and 325 mm thick. Initial assessments suggested the crack width during seismic excitation would have been on the range of 35 mm (Bull, 2012). At first visual inspection, the crack appeared to be relatively narrow and the damage to the building was not an obvious concern. However, in reality, the crack opened to a significant width as the wall deflected during seismic excitation, but closed as the wall re-centred itself under gravity load. Figure 2-2(b) shows the Urban Search and Rescue team from New South Wales who removed the cover concrete to find several bars had fractured along the length of the wall, as shown in Figure 2-2(c). The building's overall damage state may be described as being at near collapse. A potentially catastrophic failure might have been observed for longer duration of severe ground shaking of similar intensity. This example also highlights the care required in assessing a damaged building of this type.

The Pyne Gould Corporation (PGC) building is an example of a lightly reinforced wall building that catastrophically collapsed during the 22 February 2011 Christchurch earthquake, in which 18 people lost their lives (CERC, 2012). Due to the building being designed in the mid-1960s, it was originally categorised as a non-ductile RC structure. The postulated critical wall was 203 mm thick and contained a single layer of 16 mm vertical reinforcement spaced at 380 mm centres. There was a large cover concrete thickness of nearly $6d_b$ and the vertical reinforcement had good bond conditions which might have limited the extent of yield penetration that occurred. Elongation of the vertical reinforcement was limited to a short length and bar fracture is postulated to have occurred in the sequence of collapse. Further discussion of the building's seismic performance and potential collapse scenario is presented in the CERC report (2012).

The authors are aware of other lightly reinforced wall structures in Christchurch that formed concentrated regions of inelastic deformation during the Canterbury earthquake sequence (Kam *et al.*, 2011; CERC, 2012). Practising structural engineers throughout New Zealand will encounter existing buildings with RC walls designed to earlier standards (NZS3101:1995) that have a similar vulnerability. This does not mean to say, however, that similar issues may not exist for other structural members such as RC columns.

Some post-earthquake reports (Smith and Devine, 2012a and 2012b) describe examples of beams that formed apparent single-crack-PHZs as shown in Figure 2-3. The CERC report (2012) discusses beams containing sufficient longitudinal reinforcement such that secondary cracks were able to form; however crack widths were generally very narrow (less than 0.05 mm) and were not clearly visible. Bar yielding at secondary cracks can only occur if there is significant strain hardening at the nearby primary crack, meaning that appreciable strains must be induced and primary cracks need to be sufficiently wide (up to about 5 mm). This kind of behaviour is not overly concerning as it is consistent with what has been

observed in experimental tests on beams at a displacement ductility in the range of 2-3. Secondary cracks are somewhat easier to inspect during laboratory testing and all cracks are clearly marked on the test specimens during static loading.

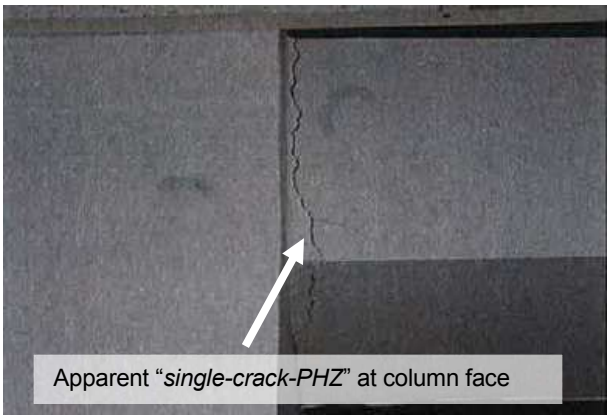

Figure 2-3: One example of localised damage observed in a RC frame building (Smith and Devine, 2012a).

In summary, damage states observed in post-earthquake field reconnaissance were not consistent with the spread of plasticity observed in previous experimental testing in the laboratory, thus highlighting the need to review and calibrate the current laboratory-based understanding for the behaviour of RC structures. Some of the typical seismic experimentation procedures and known laboratory conditions have potentially influenced the structural behaviour and long-held assumptions for RC that are used in research and in practice. Clear differences between conventional laboratory and field conditions include: (i) the type of dynamic loading from the 22 February 2011 Christchurch earthquake is significantly different to the typical quasi-static loading protocols often used in laboratory testing, and; (ii) real structures had significantly less cracking of the concrete, and hence the ductility of the reinforcement was not well utilised compared to laboratory test specimens. The following section discusses the influence of loading history on the behaviour of RC and the use of quasi-static testing. Later sections of this chapter discuss the significance of concrete tensile strength and quantity of longitudinal reinforcement on the restricted cracking and limited spread of plasticity in real structures.

2.4 INFLUENCE OF LOADING HISTORY

2.4.1 Underlying issues with seismic experimentation

For many laboratories conducting seismic experimentation, shake-table or pseudo-dynamic testing is constrained by resources and practicality (such as cost, available equipment, required computer software, support of laboratory technicians). To avoid these constraints, quasi-static cyclic loading is the most widely implemented method for structural tests (Leon and Deierlein, 1996). The results of quasi-static testing are assumed to provide a conservative lower bound for member strength capacity; however the

same cannot be said for ductility and energy dissipation. The technical disadvantages are that quasi-static testing cannot consider: (i) the influence of the loading rate on governing failure mode and; (ii) variations in moment-shear ratios and axial load that largely influence the deformation and strength capacities. The deformation and strength capacity depends on the cumulative damage due to the path-dependent behaviour of RC (Krawinkler, 2009). For components within a real structure, the amplitude, frequency and number of loading cycles (i.e. seismic demands) due to ground motion excitation depends on:

- The influence of earthquake source rupture, seismic wave propagation and local site response on the features of ground motion intensity measures: amplitude frequency content and duration.
- The configuration and relative strength of the component within the global system.
- The dynamic system properties such as stiffness, natural modes of vibration and characteristic inelastic response (ductility and hysteretic energy dissipation).

For several decades researchers have been aware of the need for generalised experimental loading protocols to reliably evaluate and compare the performance characteristics of structural components (Park, 1989). More recently, the popular notion of performance-based design has highlighted the importance of performance indicators such as deformation capacity to be used in design procedures and standards. Loading protocols are recognised as a source of epistemic uncertainty associated with evaluating performance indicators (or damage states) in the development of component fragility functions used for performance-based seismic assessment (Bradley, 2010).

2.4.2 Quasi-static loading protocols

Liddel *et al.* (2000) found differences in the ductility of RC components when subjected to varying quasi-static loading protocols used at different international research institutions. Loading protocols need to be reflective of the experimental objectives which may vary from determining potential failure modes to assessing the drift sensitivity of non-structural elements. FEMA-461 (2007) suggests quasi-static loading protocols should be generalised such that the sequence of displacement cycles are in order of increasing magnitude to ensure that component performance is not unique for specific ground motions and configurations, but for a range of potential displacement histories. Figure 2-4(a) and (b) shows typical loading protocols that have been widely used in experimental quasi-static testing of RC components that undergo strength and stiffness degradation in a gradual manner. Under this type of gradually increasing loading, crack propagation is more extensive which enables greater spread of plasticity and therefore significant levels of deformation capacity and hysteretic energy dissipation, while premature failure modes such as bar buckling or bar fracture are mitigated. It should be recognised that empirically-derived expressions for the effective plastic hinge length and estimates for the yield penetration length which are widely used in practice are based on outcomes of quasi-static testing using loading protocols such as that shown in Figure 2-4(a).

In contrast to typical quasi-static loading protocols, severe near-source ground motions from damaging earthquakes, such as the 1971 San Fernando (US), 1994 Northridge (US), 1995 Kobe (Japan) and 2011 Christchurch (NZ), can produce initially large amplitude, high frequency, and partially reversing loading histories without a number of initial small amplitude or gradually increasing loading cycles. FEMA-461 (2007) ignores the influence of near-source ground motions on the basis that these motions generate fewer response cycles and therefore are not likely to control the number and relative amplitudes of the loading excursions in a loading history. Krawinkler (2009) discussed various loading protocols used for multi-institutional testing programmes and standards, such as those shown in Figure 2-5(a) and (b) for steel and timber structures, respectively, with attempt to assess the seismic performance when subjected near-source ground motions with forward directivity. However, no common loading protocol specifically for RC structures has been widely discussed in the literature.

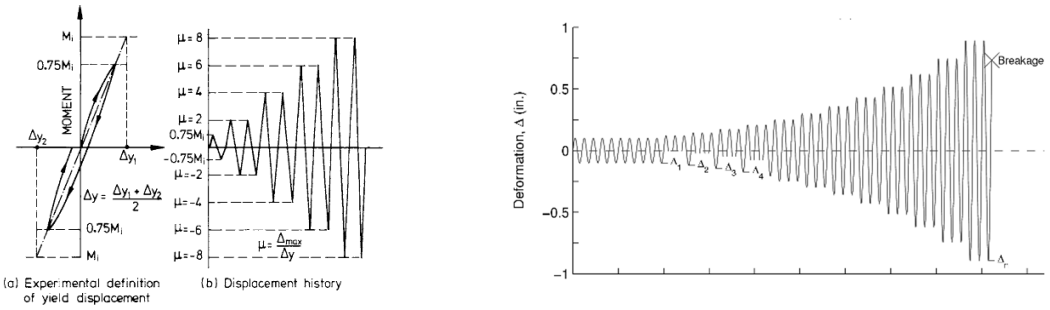

(a) Priestley and Park (1984) **(b)** Loading protocol stated in FEMA-461 (2007)

Figure 2-4: Typical examples of loading protocols for quasi-static cyclic testing.

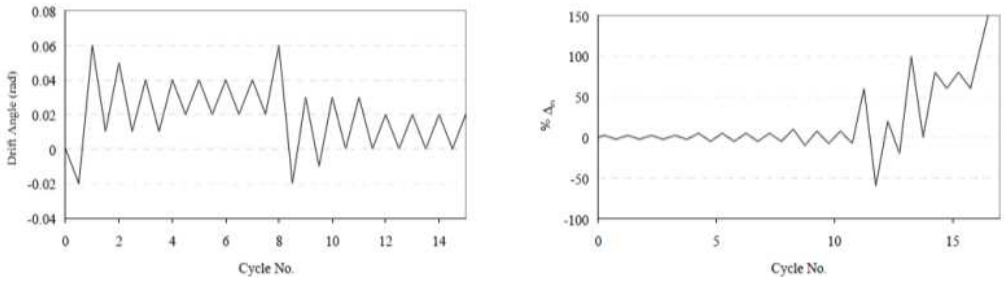

(a) **(b)**

Figure 2-5: "Near-source" loading protocols for (a) structural steel components, and (b) timber components (Krawinkler, 2009).

2.4.3 Loading rate

Despite the awareness that near-source events result in dynamic large amplitude ground motions, there are few consistent conclusions in the literature for the influence of loading rate on the seismic performance of RC components. Quasi-static loading potentially mitigates brittle failure modes that are otherwise realistic for real RC structures subjected to realistic seismic actions. Vos and Reinhardt (1982) found that deformed reinforcing bars have greater bond resistance when subject to faster loading rates and this enhancement for bond strength was more pronounced for lower quality concrete. As the concrete matrix becomes more uniform in high quality concrete, the relative micro-crack propagation is limited and less concrete degradation occurs. Chung and Shah (1989) investigated the effect of loading rate on small scale anchorage-bond and beam-column joint specimens and observed fracture of the reinforcement when subjected to faster loading rates.

Phan *et al.* (2007) and Choi *et al.* (2010) compared shake-table motions containing large asymmetric pulses to motions from "far-field" earthquakes when testing RC bridge columns containing relatively high quantities of longitudinal reinforcement (between 2.0-3.6%). There was no evidence of concentrated inelastic deformations, which is in agreement with CERC (2012); that the ductility of components with moderate or high reinforcement content is unlikely to be influenced by loading rates, however further investigations should be carried out for lightly reinforced components.

In the interest of producing realistic experimental outcomes, laboratory facilities within New Zealand could benefit from upgrading so that shake-table or pseudo-dynamic testing can be performed at a more appropriate geometric scale without being constrained by the speed at which loading is applied. However, conducting large scale experimental tests continues to be a relatively expensive task. Another approach might consider a combination of smaller experimental studies and detailed analytical modelling. The dynamic material response of reinforcing steel and concrete could be studied in experimental tests to determine the inputs in analytical models for predicting the behavior of RC structures. Alternatively, the influence of dynamic loading rates could be experimentally investigated at international research institutions with superior laboratory facilities (Bennett *et al.*, 2014).

2.5 IN-PLACE CONCRETE STRENGTH

2.5.1 Materials testing

Damage observations and materials testing from Christchurch CBD buildings indicate that the strength of concrete surrounding the reinforcement was notably higher than that specified in design. The CERC (2012) report describes the unexpected performance of several RC structures to be largely due to the reoccurring issue of higher-than-expected concrete strength. This section discusses some evidence of higher than expected concrete strength, the concrete tensile strength, some apparent factors that might enhance the concrete strength, and relevant considerations for future research.

From material testing of samples extracted from a number of Christchurch CBD buildings it was found that the in-place strength was significantly higher than expected (Holmes Solutions, 2011). The Gallery Apartments building (Figure 2) is an example where the specified 28 day compressive strength, $f'_{c,28\text{-days}}$, was 30 MPa, however, Holmes Solutions (2011) reported the cylinder compressive strength of two cores extracted from the critical walls were 46.5 MPa and 56.0 MPa, and non-destructive Schmidt hammer testing indicated a compressive strength in the range of 54-70 MPa. Two split cylinder tests measured the "indirect tensile strength" of 2.4 MPa and 3.4 MPa.

2.5.2 Concrete tensile strength

In practice the tensile strength of concrete is typically given greatest consideration at the serviceability limit state. Design codes typically state lower characteristic values for the tensile strength to provide some conservatism in calculating the strength capacity and deflection-induced cracking under serviceability loads. However, the earlier sections of this chapter highlighted that the performance of some structures at ultimate limit state (ULS) may be significantly influenced by the concrete tensile strength. It is widely accepted that high strength contributions from the concrete between the cracks (often referred to as "tension stiffening") will result in PHZs having a much lower rotation capacity. The tensile strength is also known to have a strong influence on bond behaviour (Eligehausen *et al.*, 1983). At ULS the concrete tensile strength may be a critical factor that restricts the available ductility of the reinforcement that is utilized due to: (i) secondary cracks are unable to develop; and (ii) limited bond deterioration near single-crack-PHZs. These issues suggest the need to carefully consider what the probable values of the tensile strength might be when a lightly reinforced structure is being assessed.

Figure 2-6(a) gives an indication of the relationship between the mean compressive strength and "direct tensile strength" f_{ct} by using the expressions shown in Equations 2-5 and 2-6. These expressions are from the Model Code 2010 (*fib*, 2012) and a proposed amendment to NZS 3101:2006, respectively. Figure 2-6 also shows upper and lower characteristic values which are taken as 1.32 and 0.68 times f_{ct} in the Model Code 2010 (and similarly in the commentary section of NZS3101:2006). The scatter in the concrete tensile strength represents the influence of several factors, including: the extent of cement hydration; member

geometry and differential shrinkage; the proportion, size and angularity of course aggregate; and segregation of constituent materials in casting. For higher grades of concrete (f_c' exceeding say 60-70 MPa) the relationship between direct tensile strength and compressive strength will vary from that suggested in Equations 2-5 and 2-6.

$$f_{ct} = 0.3(f'_c)^{\frac{2}{3}} \quad 2\text{-}5$$

$$f_{ct} = 0.55(f'_c)^{\frac{1}{2}} \quad 2\text{-}6$$

The aforementioned observations in some Christchurch buildings indicate that an upper characteristic value should be taken as the effective tensile strength for the purposes of assessing whether secondary crack formation can occur. Figure 2-6(b) qualitatively shows the relative differences between the three measurements of concrete tensile strength, in which it can be seen that:

- The indirect tensile strength is determined from splitting (or "Brazilian") tests which are easily performed on small cylinder specimens. There is typically a large amount of scatter in the results from performing a small number of splitting tests.
- The direct tensile strength, or uniaxial tensile strength, is seldom measured due to the difficulty in test set up and loading concrete specimens in direct uniaxial tension (Gopalaratnam and Shah, 1985). In most design codes the direct tensile strength is taken as 90% of the indirect tensile strength.
- The flexural tensile strength, or modulus of rupture (MoR), may be determined relatively easily from third-point loading of plain concrete prisms. These tests are not carried out on samples from buildings however as samples are typically extracted in the form of cylinders (hence splitting tests are most commonly used).

The relative difference between flexural and direct tensile strengths of plain concrete arises due to a combination of material and geometric non-linearity (Gopalaratnam and Shah, 1985; ACI Committee 446, 1992). This difference is described in the commentary section of NZS3101:2006 and recommended multipliers for this scale effect (Table C5.1, NZS3101:2006) are approximately identical to those determined using Equation 2-7 and 2-8 from the Model Code 2010 (*fib*, 2012) based on fracture mechanics for concrete structures.

$$\alpha_f = \frac{0.06h^{0.7}}{1 + 0.06h^{0.7}} \quad 2\text{-}7$$

$$f_{ct,fl} = \frac{f_{ct}}{\alpha_f} \quad 2\text{-}8$$

where h is the section depth and f_{ct} is the direct tensile strength which is often estimated from Equation 2-5, or from splitting tests.

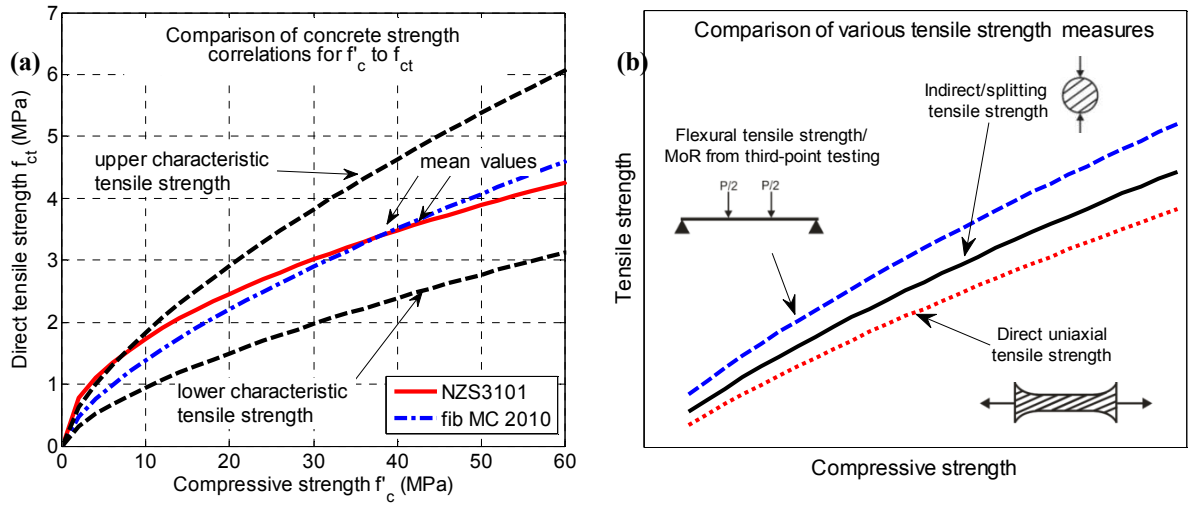

Figure 2-6: (a) Examples of some known correlations between the compressive and tensile strength of concrete; and (b) qualitative representation of the relative flexural, indirect and direct tensile strengths of concrete.

Assessments of secondary crack formation for the critical wall in the Gallery Apartments building are presented in Henry (2013) and Lu *et al.* (2014) using analytical modelling techniques. Henry (2013) estimated the flexural tensile strength using Equation 2-8, where f_{ct} was taken from Equation 2-5 based on the f_c' values reported by Holmes Solutions (2011). For typical wall sections, the difference between direct and flexural tensile strength values is minimal due to the relatively large section depth. Input values for the mean and upper characteristic flexural tensile strength of the concrete were taken as 4.3 MPa and 5.6 MPa, respectively. These values were determined using the Model Code 2010 expressions (*fib*, 2012) and both were considered as permutations in the analysis. The next section of this chapter briefly discusses the limited crack formation observed in the results from Henry (2013) and Lu *et al.* (2014).

Identifying that the compressive strength was appreciably higher than specified design values highlights the benefit in obtaining results from materials testing. Other approaches to assessing RC structures might depend on values of the compressive strength determined by non-destructive material testing. Variability in the results from all techniques for concrete materials testing should be considered appropriately, and potential reasons for the measured strength exceeding the specified design values are discussed in the following section.

2.5.3 Sources of apparent strength enhancement

For all concrete structures, the in-place strength will vary between different components due to the influence of casting direction and size effects. Construction methods used for placement, compaction and vibration (and potential re-vibration) of concrete also has some influence on strength. The direction of casting relative to the orientation of the structural component will influence the concrete's mechanical properties due to water gain (Fenwick and Sue, 1982). Due to segregation of the mix materials, concrete at the bottom of specimens is typically of higher strength than concrete in the middle, with lower strength concrete at the top. This notion suggests the concrete strength would have been higher at the base of some cast in-situ precast wall structures (cast in the vertical direction) where limited cracking was observed. For the future design of lightly reinforced components, Bull (2012) describes the need to consider concrete strength enhancements due to the following factors:

- Ready-mix suppliers targeting higher strength for quality assurance of the delivered concrete product.
- The ageing/maturing process resulting in a time-strength development.
- Dynamic strength enhancements when subjected to rapid loading rates (the implications of which were alluded to in an earlier section of this chapter).
- Precast fabricators using high strength and high early strength mixes to meet specification quickly to ensure speed of production.

Some flowable self-compacting concrete (SCC) mixes can result in high strengths that have not been anticipated by the design engineer. SESOC (2011) describes an example of a RC panel with a specified $f'_{c,28\ days}$ of 40 MPa, yet a self-compacting mix had a 7 day strength of 90 MPa. In another case example, a relatively modern RC building had precast wall panels with a 28 day strength of approximately 90 MPa such that the wall's internal actions were higher than might have been anticipated in design and subsequently contributed to failure of the foundations (Smith and Devine, 2012b).

Soleymani Ashtiani *et al.* (2014) recently performed quasi-static cyclic testing of four interior beam-column joint specimens containing high-strength SCC. At the time of testing, f'_c ranged between 100 and 120 MPa and the average indirect tensile strength was 7.2 MPa. The ratio of the longitudinal beam reinforcement was identical for all test specimens at 1.1%. Despite the high tensile strength of the concrete, the quantity of reinforcement and hence the tension force in the reinforcement was sufficient to progressively crack the concrete. Observations from these tests highlight that there were no restrictions on the formation of secondary cracking and thus the desired "spreading-PHZs" were able to form adjacent to the column faces.

2.5.4 "Laboratory" concrete vs. "real" in-place concrete

Some design expressions that are influenced by concrete strength (such as quantities of minimum reinforcement and development lengths) are derived from experimental work. While such expressions may account for some scatter by carrying out an appropriate number of tests, there may be some debate that the concrete used in the laboratory conditions may not reliably represent of the concrete used in real construction.

To reduce the time in undertaking experimental studies, concrete samples of RC specimens are typically tested at the milestone of 28 days after casting when the concrete is relatively young. The tensile strength in younger test specimens may be appreciably less than the in-place concrete in an existing structure of some age. Some experimental programmes might allow for 90 days of strength development to reduce the variability between specimens that are of slightly different maturity at the time of testing. A search of the literature or further experimental research is needed to investigate the rate at which concrete tensile strength develops. Research institutions and the New Zealand concrete industry should take careful consideration of the mix that is used in specimen construction and the age of concrete at the time of testing.

2.6 QUANTITY OF LONGITUDINAL REINFORCEMENT

To utilize the ductility of the reinforcement at ULS there needs to be sufficient tension force in the longitudinal reinforcement to progressively form cracks along the potential PHZ. The aim of code limitations for the minimum reinforcement quantity, ρ_{min}, is to prevent the formation of a single wide crack once the cracking moment of the section has been exceeded. To ensure a factor of safety against this undesired behaviour, the nominal moment capacity of a section with minimum reinforcement should be approximately 1.5-2.0 times the cracking moment (Paulay and Priestley, 1992). Henry (2013) further describes the background of the design expressions for the minimum reinforcement in RC beams and walls. The minimum reinforcement ratio stated in NZS3101:2006 for both walls and beams is given by:

$$\rho_n \geq \frac{\sqrt{f_c'}}{4f_y} \qquad 2\text{-}9$$

where f'_c is the specified 28 day strength (MPa) and ρ_n is the calculated total area of longitudinal reinforcement as a ratio of the area of the concrete section dimensions using the width of the web and the section depth, $b_w d$.

While Equation 2-9 appears to be identical for walls and beams, Henry (2013) describes a number of differences between each component that reduces the safety margin between the nominal and cracking moment capacity for wall sections. For example, the expression for walls is the total quantity of vertical

reinforcement that is distributed through the section, while for beams the expression represents only the quantity of reinforcement that is in tension, which is typically lumped in the flange regions.

An important difference between RC test specimens and components in real structures is that test specimens will typically contain moderate and high quantities of reinforcement. To minimize concrete volumes and specimen weight, the geometry of test specimens is often reduced in scale such that test specimens contain a higher proportion of reinforcement compared to real structures. Reducing the proportion of longitudinal reinforcement with specimen geometry is uncommon. This is based on a misconception that if there is good structural behavior for high values of ρ_n then there should also be good behavior at lower values.

2.6.1 RC walls

SESOC (2012) responded to the poor performance of lightly reinforced walls in the 2010-2011 Canterbury earthquakes with a proposed design recommendation for the minimum quantity and distribution of reinforcement for walls that are likely to yield. This interim design recommendation offered some improved confidence that newly designed walls can develop the desired flexure-shear crack patterns and achieve ductile behaviour at ULS. Equation 2-10 shows the SESOC (2012) expression was increased from the NZS3101:2006 minimum quantity of vertical reinforcement to account for the higher than expected concrete strength of up to 2.5 times the 28 day specified value:

$$\rho_l \geq \frac{\sqrt{2.5f_c'}}{4f_y} \rightarrow\rightarrow \rho_l \geq \frac{0.4\sqrt{f_c'}}{f_y} \qquad 2\text{-}10$$

Henry (2013) presents analytical moment-curvature and force-displacement results for the response of the critical wall in the Gallery Apartments building, for two cases: (i) using the as-built details with a reinforcement ratio of 0.160%; and (ii) approximately equal to the NZS3101:2006 minimum vertical reinforcement limits of 0.274%. In the first case, the damage shown in Figure 2-2(c) were in agreement with the bar fracture that was observed after the 22 February 2011 Christchurch earthquake. The results for the second case were found to be strongly dependent on larger magnitudes of axial loading to avoid sudden losses in strength after cracking and to sustain greater lateral deflections. Although the second case satisfied the NZS3101:2006 minimum reinforcement limit, Henry (2013) found the effective plastic hinge length was approximately half of the length that is typically assumed in practice. More detailed finite element analysis of this case example is presented in Sritharan *et al.* (2014) and Lu *et al.* (2014). For the as-built details, Figure 2-7(a) shows fracture of vertical reinforcement occurring at a lateral drift of 0.75%. No analytical evidence was presented for the SESOC (2012) recommendation in Equation 2-10. The University of Auckland is continuing to experimentally and analytically investigate the performance of lightly reinforced walls (Henry *et al.*, 2014).

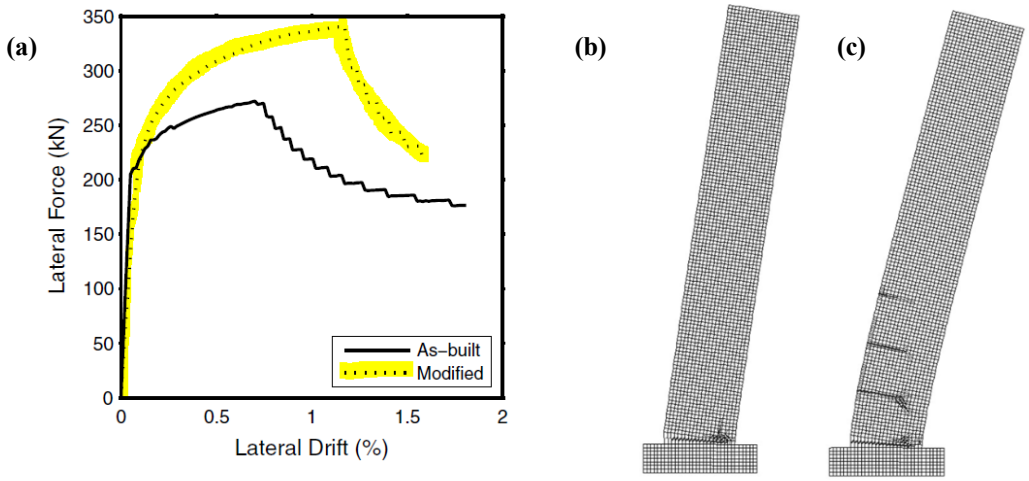

Figure 2-7: (a) Analytical predictions for the critical wall section in the Gallery Apartments building for: (b) the as-built details, and; (c) the wall containing the NZS3101:2006 minimum vertical reinforcement content (Sritharan *et al.*, 2014; Lu *et al.*, 2014)

Brief discussion of the distribution of vertical reinforcement in RC walls is included here for the sake of completeness. The majority of existing wall structures designed according to NZS3101:2006 (and earlier standards) typically comprises of uniformly distributed vertical reinforcement throughout the section. Following the Canterbury earthquakes, SESOC (2012) recommended that modern wall sections should contain greater quantities of reinforcement in the end regions (commonly referred to as boundary elements). The quantity and detailing of web reinforcement is also important for several reasons: (i) to prevent crushing of the concrete in the web; (ii) to prevent the web from forming a small number of wide cracks that may result in potential shear sliding; and (iii) to ensure that severe damage to the web region does not result in excessively large compression stresses and potential buckling of boundary elements (Sritharan *et al.*, 2014).

The design provisions for RC walls have undergone some revision in Amendment 3 of NZS3101:2006 to prevent some of the undesired structural behaviour that has been described in this chapter. Changes to the Standard have specified that end zones of walls must have a ratio of vertical reinforcement $\rho_{l,e}$ that is greater than Equation 2-11, twice the value that was previously considered as the minimum.

$$\rho_{l,e} \geq \frac{\sqrt{f_c'}}{2f_y} \qquad 2\text{-}11$$

The minimum reinforcement in the web region of the wall between recognised end zones must be greater than the ratio stated in Equation 2-9 and should also be greater than 0.3 times $\rho_{l,e}$. This second limit has been imposed to prevent the issues associated with shear strength and shear deformation as described earlier.

2.6.2 RC frames

Compared to walls, there are fewer structural and geometric conditions influencing the margin of safety between the nominal moment capacity of a typical beam section and the cracking moment capacity. Despite some apparent cases of "single-crack-PHZs" in RC beams (e.g. Figure 2-3) this was partly due to misinterpretation of this type of damage observation and is not overly concerning. Thus far, there has been no suggestion of revising the minimum reinforcement for beams, however further experimental investigations may address this issue in more detail.

To give some quantitative indication, a desktop study of the structural drawings for 21 RC frame buildings in the Christchurch CBD (within the post-1977 construction era) was conducted by the authors. The average reinforcement ratio in the ductile regions of beams within the lateral load resisting "seismic frames" was approximately 0.85 and 0.70 percent for top and bottom reinforcement, respectively. The study focused on beam elevations in the lower third of the frame height, though beams located in upper levels of high-rise buildings typically contain a lower proportion of reinforcement. Across New Zealand's existing building stock there will be some RC columns that have been designed to form ductile PHZs however insufficient vertical reinforcement or changes in cross-sectional dimensions could mean that single-crack-PHZs are more likely to form.

2.7 CONSIDERATIONS FOR FUTURE RESEARCH AND PRACTICE

The lack of correlation between the observations from previous structural tests and observations from buildings in Christchurch has highlighted some implications for the design and assessment of conventional RC structures. The following section briefly describes some other issues associated with the structural behaviour that was described earlier.

2.7.1 Flexural stiffness of RC components

One implication related to the limited cracking in some wall structures is that some assumptions for the effective stiffness of RC structures may be inappropriate. Design standards such as NZS3101 use multipliers of the gross-section properties that are based on extensive flexural cracking (Table C6.6, NZS3101:2006). Given that the extent of flexural cracking observed in some Christchurch buildings was much less than expected, the fundamental vibration period is likely to be less than what the structure was designed for and consequently the seismic forces may be higher than expected. Fenwick (2013) recommends that practising engineers compare the anticipated stiffness and strength degradation that is associated with the design actions from structural analysis.

2.7.2 Effective plastic hinge length

Practising engineers often make some lumped plasticity assumptions in using non-linear modelling techniques to predict the seismic response of a structure for the purposes of detailed seismic and damage assessments or in design stages. Coupled with the assumed value for the effective flexural stiffness, the assumed length for the effective plastic hinge, $L_{p,}$ is also important for structural analysis. Equations 2-1 and 2-4 presented some empirical expressions for L_p that engineers might adopt as the length of which plastic curvatures are assumed to be uniform. The seismic assessment guidelines in NZSEE (2006) state that half the effective section depth may be used for L_p, or taken "more accurately" and less conservatively by Equation 2-1 from Priestley *et al.* (2007). While these expressions might be adopted to evaluate the ductility of an existing structure, it is unclear whether the results from analysis are compared against allowable material strains that correspond to performance/damage states. In practice, estimates of ductility derived from nonlinear pushover or seismic response history analysis are commonly presented using other engineering demand parameters such as plastic hinge rotations and/or drift angles. The material strain limits can easily be overlooked if a blind value of L_p is assigned inappropriately and ductility may be over-estimated.

NZS3101:2006 assumes L_p for the purposes of assessing section curvatures and detailing requirements for potential plastic hinge zones. The value of L_p for RC beams, columns and walls is coupled with material strain limits (maximum allowable curvatures stated in Table 2.4 of NZS3101:2006). For reversing plastic hinges in beams, columns or walls the value of the effective plastic hinge length should be taken as the smaller of half the section depth or 0.2 times the *M/V* ratio, but not less than one quarter the section depth.

Since the Canterbury earthquakes there have been no recommendations to change the value of L_p that is used in non-linear modelling techniques. In the interim, L_p for lightly reinforced components could be taken as a variable parameter in the analysis input. Evaluations of the available ultimate deformation capacity of a system may input $0.5h$ as an upper-bound value for L_p. Considering the kind of damage observations discussed in some buildings in Christchurch, it may be more appropriate to run some permutations in the analysis with a lower-bound input value of L_p. The lower-bound will predict less available ductility, which may be foreseeable for the response of some RC components containing low quantities of longitudinal reinforcement.

2.7.3 Estimating the ductility in lightly reinforced components in practice: example

There will be cases where structural engineers have carried out post-earthquake seismic response predictions for damaged RC structures that formed single-crack-PHZs, as illustrated in Figure 2-2(d). In this case, the effective plastic hinge may be restricted to the true length of yield penetration that can occur

either side of the primary crack. Based on recent field observations, L_{yp} might be taken as 1-2d_b to provide a representative lower bound.

Davey and Blaikie (2005) provide an example where the ductility of a very lightly reinforced component was assessed based on a relatively simple and robust methodology as an alternative approach to that outlined in Priestley *et al.* (2007) for the yield penetration in RC components. In this particular case, a single-crack-PHZ was expected to form at the critical section of RC dam spillway piers (constructed in the 1960s). The longitudinal reinforcement comprised of 32 mm deformed reinforcing bars. The cracking moment and first yielding moment for the component was estimated to be 4600 kNm and 2100 kNm, respectively, thus leading to concerns about the significance of single-crack-PHZ behaviour on the fatigue behaviour of the reinforcement.

Davey and Blaikie (2005) implemented some existing models found in the literature to consider how the ductility of the component was influenced by: (i) the estimated low-cycle fatigue behaviour of the reinforcing bar; and (ii) the estimated maximum crack width based on an estimated amount of bond deterioration once the deformed bar has yielded. Several assumptions were made in order to use these models from existing literature. Based on some awareness of material properties of reinforcing steel that was available in New Zealand in the 1960s, Davey and Blaikie (2005) assumed ratio f_u/f_y of 1.50 was assumed. Materials testing of concrete core samples suggested that f_c' was 60 MPa. For this particular seismic assessment approach, the maximum bond strength was assumed to be $2.5\sqrt{f_c'}$. A cumulative damage indicator of bar strain was estimated using a relationship with the displacement history of the top of the modelled component from response history analysis.

Davey and Blaikie (2005) predicted the crack width due to plastic elongation of the reinforcement to be on the order of 10 mm when the inelastic strain range reached 5 percent. In the context of this chapter, the length of bar yielding is predicted to be the order of 200 mm, which corresponds to L_{yp} being about 3.0d_b. Overall, the outcomes of the modelling by Davey and Blaikie (2005) did not indicate that the reinforcement would fracture as the resultant cumulative damage parameter summed to 60 percent of the fatigue life (as predicted based on that particular steel fatigue model and based on response history analysis using only a single ground motion record).

In the model used by Davey and Blaikie (2005), the extent of crack widening due to plastic elongation of the reinforcement is heavily dependent on the ratio of f_u/f_y (sometimes denoted R_m/R_e, as in NZS 4671:2001). As shown earlier in this chapter, Equation 2-3 from Priestley *et al.* (2007) ignores the ratio of f_u/f_y, and instead suggests that L_{yp} is approximately equal to 6.6d_b for Grade 300 reinforcement, and 11d_b for Grade 500 reinforcement (using 5th percentile values of f_y). Overall, these resulting values of L_{yp} is a significant over-estimate compared to the calculations by Davey and Blaikie (2005) which used an alternative methodology with a more robust physical meaning. In the calculations shown here by the

authors of this chapter, Equation 2-3 vastly over-estimates L_{yp}. However, in this type of scenario of forming single-crack PHZs, accurate estimation of L_{yp} becomes vitally important for predicting seismic performance at the ultimate limit state.

2.7.4 Dynamic response of interacting structural systems

Although the response of individual components has long been studied in experimental testing in laboratories, the interaction between components and their influence on global system response may need further investigation. For instance, there are effects of interactions between floor slabs and beam elongation (NZS3101:2006) as axial restraint from floor slabs will increases the strength of adjacent components such as coupling beams in coupled wall systems and beams in moment resisting frames (Lau, 2007; Naish *et al*., 2009; CERC, 2012; Fenwick, 2013; Malcolm *et al*., 2014). The axial restraint provided by floor slabs may restrict the formation of diagonal cracks in the web of regular walls. These are some of the reasons that the spread of inelastic deformations in a system of interacting components is likely to deviate from the performance of an individual component. Relative differences in stiffness and the early onset of unexpected yielding can drastically influence the dynamic response and overall performance of a structural system. An example of this behaviour was the Clarendon Tower formerly at 78 Worcester Street, Christchurch (Fenwick, 2013).

The authors understand there are proposed investigations on the interaction of RC structural systems being undertaking in New Zealand (Bennett *et al*., 2014; Table 1). Full scale shake-table or pseudo-dynamic testing might offer further insight into the behaviour of interacting components; however this type of experimental work is somewhat constrained by the laboratory facilities available in New Zealand.

2.7.5 Assessing the residual capacity of RC structures

The issues described in this chapter also have implications for practitioners using seismic assessment methods (for damaged and un-damaged evaluations) which are largely based on the assumptions adopted in conventional design practice. Structural engineers have recently been challenged on the subject of evaluating the residual capacity of damaged RC buildings; an issue that also applies to well-designed structures that formed "spreading-PHZs" and performed with sufficient ductility. Uncertainties in the remaining life of the structure are partly due to: (i) the severity and number of strong ground motions in the Canterbury earthquake sequence and subsequent damage to the structure; and (ii) the uncertainty for the effectiveness and cost of structural repair techniques. Hundreds of RC buildings in Christchurch have subsequently been demolished after the Canterbury earthquake sequence.

In both research and in practice, the seismic performance and extent of structural damage is commonly expressed in terms of the peak values of non-cumulative damage indices or "demand metrics" (e.g. peak lateral drift) due to the simplistic nature of obtaining values for these metrics with physical meaning (Williams and Sexsmith, 1995). Cumulative demand metrics (e.g. energy-based measures) might provide

more reliable information for making post-earthquake decisions like seismic retrofit or demolition. Although cumulative metrics are more complicated to determine, they are more important for realistic seismic loading histories where the sequence of loading does not increase monotonically. The use of cumulative demand metrics does however require some calibration of damage model co-efficients (scale factors and exponents). In research these model co-efficients can be determined by using regression techniques based on experimental measurements. In practice however, model co-efficients are not well known as they cannot be determined with the same ease or reliability. Cumulative demand parameters are less comparable between different structural components with in-situ differences such as experimental boundary conditions, specimen geometry, reinforcing content, material properties and different loading protocols.

2.8 CONCLUSION

This chapter was motivated by the unexpected damage to some 'real' RC structures in the 2010-2011 Canterbury earthquakes. One of the main lessons learnt from these events was the concentration of inelastic deformations and brittle failure in some lightly reinforced wall structures which did not compare well to the fanned crack patterns and typical spread of plasticity observed in previous laboratory-based experimental testing. The damage to the critical wall in the Gallery Apartments building was described here as a particular example of concerning structural behaviour. This chapter focussed on differences between common experimental procedures and laboratory conditions and how those vary from the field conditions when a 'real' RC structure is subjected to severe earthquake-induced ground motions. Specific conditions discussed here included the applied loading history and loading rate, the concrete strength and the quantity of longitudinal reinforcement. Increased considerations and changes to structural engineering practice have been promoted by the lessons that have emerged from the Canterbury earthquake sequence. The issues and constraints that were imposed on previous experimental testing may be considered in future research topics to improve the confidence levels for the seismic performance of RC structures at the ultimate limit state.

The latter sections of this chapter described an example where practising structural engineers were challenged to estimate the ductility of a lightly reinforced structural component. The overall results from this example highlighted a major concern that two approaches in the existing literature would give vastly different results for the anticipated level of yield penetration in a single-crack-PHZ.

2.9 REFERENCES

ACI Committee 446 (1992). Fracture mechanics of concrete structures, Bazant Z. P – principal author and editor, Elsevier Applied Science, London, 1-140.

Beyer, K., Dazio, A., and Priestley, M.J.N. (2008). Quasi-static cyclic tests of two U-shaped reinforced concrete walls. *Journal of Earthquake Engineering*, 12:7, 1023-1053.

Bennett, A., Sharpe, R.D., and Stannard, M.C. (2014). Prioritising research into the seismic performance of reinforced concrete. C*onference proceedings of the New Zealand Society of Earthquake Engineering*, Auckland.

Bonacci, J.F. (1994a). Bar yield penetration in monotonically loaded anchorages. *Journal of Structural Engineering*, ASCE, 120(3), 965-986.

Bradley, B.A. (2010). Epistemic uncertainties in component fragility functions. *Earthquake Spectra*, 26(1), 41-62.

Bull, D.K. (2012). The performance of concrete structures in the Canterbury earthquakes: Lessons for concrete buildings, *Structural Engineers Association of California (SEAOC) Convention*, Santa Fe, NM.

Canterbury Earthquakes Royal Commission, CERC (2012). Final report: Volume 2, The performance of Christchurch CBD Buildings.

Choi, H., Saiidi, M.S., Somerville, P., and El-Azazy, S. (2010). Experimental study of reinforced concrete bridge columns subjected to near-fault ground motions. *ACI Structural Journal*, 107(1), 3-12.

Chung, L., and Shah, S.P. (1989). Effect of loading rate on anchorage bond and beam-column joints, ACI Structural Journal, 86(2), 132-142.

Davey, R.A., and Blaikie, E.L. (2005). On the flexural ductility of very lightly reinforced concrete sections, C*onference proceedings of the New Zealand Society of Earthquake Engineering*, Taupo.

Dickson, A.R. (1986). The response of reinforced concrete slabs to concentrated loading. *Report No. 408*, University of Auckland, New Zealand.

Eligehausen, R., Popov, E.P., Bertero, V.V. (1983), Local bond stress-slip relationships of deformed bars under generalized excitations. *Report UCB/EERC-83/23*, University of California, Berkeley.

Fédération Internationale du Béton, *fib*. (2012), Model Code 2010 - Final draft, Volume 2. *fib Bulletin* No. 66, Lausanne, Switzerland.

FEMA-461. (2007). Interim protocols for determining seismic performance characteristics of structural and non-structural components through laboratory testing. *Prepared by Applied Technology Council (ATC) for Federal Emergency Management Agency (FEMA)*, Redwood City, California.

Fenwick, R.C., and Sue, C.F.C (1982). The influence of water gain upon the tensile strength of concrete, Magazine of Concrete Research, 34(120): 139-145.

Fenwick, R.C. and Dhakal, R.P. (2007a) Material strains and relevance to seismic design. SESOC Journal, 20(1): 5-12.

Fenwick, R.C. and Dhakal, R.P. (2007b) Material strain limits for seismic design of concrete structures. SESOC Journal, 20(1): 14-28.

Fenwick, R.C. (2013). Aspects of the seismic performance of concrete buildings. *Conference proceedings of the New Zealand Concrete Society*, Queenstown, New Zealand.

Gopalaratnam, V.S. and Shah, S.P. (1985). Softening response of plain concrete in direct tension. *ACI Journal,* 82(3), 310-323.

Henry, R.S. (2013). Assessment of minimum vertical reinforcement limits for RC walls, *Bulletin of the New Zealand Society for Earthquake Engineering*. 46(2), 88-96.

Henry, R.S., Lu, Y., and Ingham, J.M. (2014). Experimental testing and modelling to address the performance of RC walls during the 2010/2011 Canterbury earthquakes. *Proceedings of the 10th National Conference in Earthquake Engineering*, Earthquake Engineering Research Institute, Anchorage, AK.

Holmes Solutions. (2011). Materials testing in buildings of interest: *Prepared for the Canterbury Earthquakes Royal Commission*, November 2011, Christchurch, New Zealand.

Kam, W.Y., Pampanin, S., and Elwood., K. (2011). Seismic performance of reinforced concrete buildings in the 22 February Christchurch (Lyttelton) earthquake. *Bulletin of the New Zealand Society for Earthquake Engineering*; 44(4): 239-278.

Krawinkler, H. (2009). Loading histories for cyclic tests in support of performance assessment of structural components. *The 3rd International Conference on Advances in Experimental Structural Engineering,* October 15-16, San Francisco, CA.

Lau, D.B.H. (2007). Influence of precast prestressed flooring on seismic performance of reinforced concrete perimeter frame buildings, *Doctor of Philosophy Thesis*, University of Auckland, New Zealand

Leon, R.T., and Deierlein, G.G. (1996). Considerations for the use of quasi-static testing. *Earthquake Spectra,* 12, 87-109.

Liddell, D., Ingham, J.M., and Davidson, B.J. (2000). Influence of loading history on ultimate displacement of concrete structures. *Report No. 597*, University of Auckland, Auckland, New Zealand.

Lowes, L.N., Moehle, J.P., and Govindjee, S. (2004). Concrete-steel bond model for use in finite element modelling of reinforced concrete structures, *ACI Structural Journal*, 101(4), 501-511.

Lu, Y., Henry, R.S., and Ma, Q.T. (2014). Numerical modelling and testing of concrete walls with minimum vertical reinforcement. C*onference proceedings of the New Zealand Society of Earthquake Engineering*, Auckland.

Malcolm, R.C., Bull, D.K., Henry, R.S., and Ingham, J.M. (2014). The effects of axial restraint in reinforced concrete coupling beams, *Proceedings of the New Zealand Concrete Industry Conference*, Taupo.

Mayer, U., and Eligehausen, R. (1998). Bond behaviour of ribbed bars at inelastic steel strains, *2nd International Ph.D. Symposium in Civil Engineering*, Budapest.

Morris, G.J., Bull, D.K. and Bradley, B.A. (2014). Reviewing uncertainties in seismic experimentation following the unexpected performance of RC structures in the 2010-2011 Canterbury earthquakes. C*onference proceedings of the New Zealand Society of Earthquake Engineering*, Auckland.

Naish, D., Fry, J.A., Klemencic, R., and Wallace, J. (2009). Experimental evaluation and analytical modeling of ACI 318-05/08 reinforced concrete coupling beams subjected to reversed cyclic loading. *UCLA/SGEL Report-2009/06*, University of California, Los Angeles.

NZSEE (2006). Assessment and improvement of the structural performance of buildings in earthquakes, *Recommendations of a study group of the New Zealand Society for Earthquake Engineering*.

Park, R. (1989). Evaluation of ductility of structures and structural assemblages from laboratory testing. *Bulletin of the New Zealand Society for Earthquake Engineering*. 22(3), 155-166.

Paulay, T., and Priestley, M.J.N. (1992). Seismic design of reinforced concrete and masonry buildings. John Wiley & Son, Inc., New York, United States of America.

Phan, V., Saiidi, M.S., Anderson, J., and Ghasemi, H. (2007). Near-fault ground motion effect on reinforced concrete bridge columns. *Journal of Structural Engineering*, ASCE, 133(7), 982-989.

Priestley, M.J.N., and Park, R. (1984). Strength and Ductility of bridge substructures. *RRU Bulletin 71*, National Roads Board, Wellington, New Zealand.

Priestley, M.J.N., Kowalsky, M.J., and Calvi, G.M. (2007). Displacement-based seismic design of structures, IUSS PRESS, Pavia, Italy.

SESOC. (2011). Preliminary observations from Christchurch earthquakes. *Prepared for the Canterbury Earthquakes Royal Commission.*

SESOC. (2012). Practice note - Design of conventional structural systems following Canterbury earthquakes. *Prepared for the Canterbury Earthquakes Royal Commission.*

Shima, H., Chou, L.L., and Okamura, H. (1987) Micro and macro models for bond in reinforced concrete. *Reprinted from Journal of the Faculty of Engineering*, The University of Tokyo, 39(2).

Smith, P.C., and Devine, J. (2012a). Independent assessment of earthquake performance of Craig's Investment Partners House – 90 Armagh Street, *Prepared for the Canterbury Earthquakes Royal Commission.*

Smith, P.C., and Devine, J. (2012b). Independent assessment of earthquake performance of Inland Revenue Department Building – 224 Cashell Street, *Prepared for the Canterbury Earthquakes Royal Commission.*

Soleymani Ashtiani, M., Dhakal, R.P., and Scott, A.N. (2013). Post-yield bond behaviour of deformed bars in high-strength self-compacting concrete, *Construction and Building Materials,* 44, 236-248.

Soleymani Ashtiani, M., Dhakal, R.P., and Scott, A.N. (2014). Seismic performance of high-strength self-compacting concrete in reinforced concrete beam-column joints, *Journal of Structural Engineering*, ASCE, 140(5), 04014002.

Sritharan, S., Beyer, K., Henry, R.S., Chai, Y.H., Kowalsky, M.J., and Bull, D.K (2014). Understanding poor seismic performance of concrete walls and design implications. *Earthquake Spectra,* 30(1), 307-334.

Standards New Zealand. (2006). Concrete structures standard, NZS3101, Parts 1 and 2. Standards New Zealand: Wellington, New Zealand.

Standards New Zealand. (1995). Concrete structures standard, NZS3101, Parts 1 and 2. Standards New Zealand: Wellington, New Zealand.

Standards New Zealand. (2001). Steel reinforcing materials standard, NZS4671. Standards New Zealand, Wellington, New Zealand.

Walker, A.F. (2007). Assessment of material strain limits for defining different forms of plastic hinge region in concrete structures. *Master of Engineering Thesis*, University of Canterbury, Christchurch, New Zealand.

Williams, M.S., and Sexsmith, R.G. (1995). Seismic damage indices for concrete structures: A state-of-the-art review, *Earthquake Spectra,* 11(2), 319-349.

Vos, E., and Reinhardt, H.W. (1982). Influence of loading rate on bond behaviour of reinforcing steel and prestressing strands, *Materials and Structures*. RILEM 15(85), 3-10.

[This page is intentionally left blank]

3 REVIEWING BOND MECHANICS IN RC STRUCTURES

3.1 INTRODUCTION: GENERAL REQUIREMENTS OF BOND IN DUCTILE RC STRUCTURES

3.1.1 Bond in different regions of RC components

In modern structural design practice it is inappropriate to use plain round bars for the longitudinal reinforcement in reinforced concrete (RC) structures in seismic regions, due to the relatively poor bond resistance under earthquake-induced cyclic loading of the structure. Bond in RC is referred to herein as the mechanical interaction between deformed reinforcing bars and the surrounding concrete that allows a gradual transfer of stresses between the two materials. Irrespective of the type of loading and required performance level, the strength and deformation capacity of RC components is fundamentally dependent on how effectively stresses are transferred between the reinforcement and the surrounding concrete (Park and Paulay, 1975).

The mechanism of bond has a various roles for the different regions of RC structures with different material and geometric properties and different structural conditions such as the state of stress induced by internal actions. Figure 3-1 illustrates a varying regions of a RC beam where the longitudinal reinforcement is subjected to relative differences in: (i) the axial and transverse bar forces induced by flexural and shear actions; (ii) transverse stresses caused by passive confinement at support reactions and by transverse reinforcement (such as stirrups), and; (iii) the extent of concrete cracking. Different regions within RC components have some characteristic bond related issues that are addressed differently in structural design.

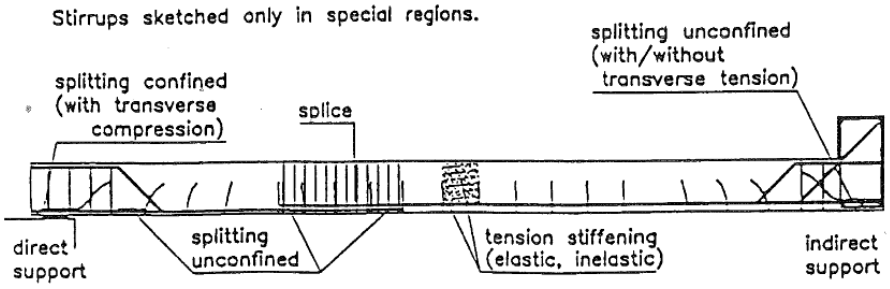

Figure 3-1: Diagram showing different regions of a RC beam (among other components) that has a range of bond related issues to design for (*fib*, 2000A).

3.1.2 Ductile regions of RC structures in seismic regions

Conventional modern RC structures (well-designed in post 1980s era) are designed and detailed to ensure that, in the event of severe earthquake-induced ground shaking, pre-determined regions of the structure can sustain multiple cycles of inelastic deformation where there is elongation of the reinforcement and the concrete is extensively cracked and crushed. The acceptance of material damage in specified regions of the structure is the fundamental principle of the ductile design approach introduced into structural engineering practice by John Hollings (1968a, 1968b). The inelastic deformation capacity (i.e. the amount of "ductility") allows for a reduction in the total seismic forces acting on the structure.

The ductile design philosophy and principles of "capacity design" of RC structures is widely understood and implemented in modern practice. This is due to the advancements in structural earthquake engineering made in the era of Professor Robert Park, Professor Tom Paulay and Professor Nigel Priestley who published valuable guidance for the seismic design and detailing of RC structures (Park and Paulay, 1975; Paulay and Priestley, 1992; Priestley *et al.* 1996).

The shaded regions of Figure 3-2 show the typical locations of the ductile regions (referred to herein as the potential plastic hinge zones, PPHZs) of various types of RC components. During severe seismic actions the developed plastic hinge zones (PHZs) are subjected to three components of deformations: (1) flexural deformation due to inelastic axial tensile strains mainly resisted by longitudinal reinforcement and compressive strains mainly resisted by concrete; (2) the rotation due to slip of the anchored reinforcing bars as some bond deterioration occurs (indicated by red arrows), and; (3) shear deformations. The structural behaviour of RC and factors that influence the spread of plasticity were described in Chapter 2.

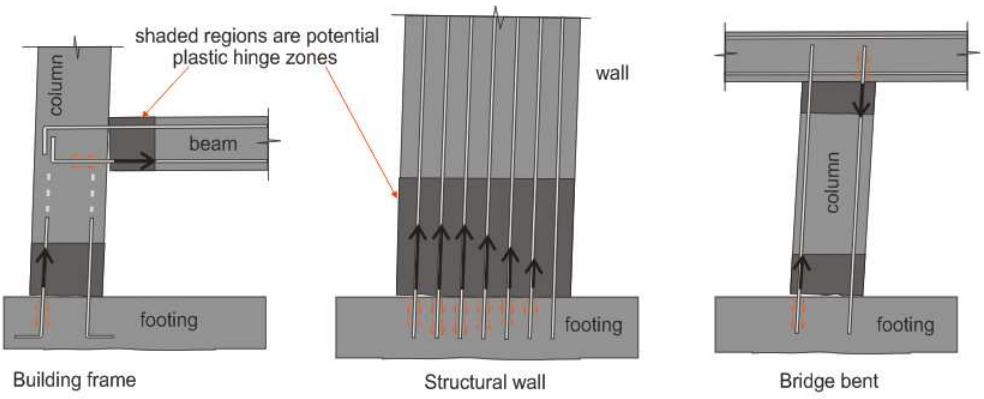

Figure 3-2: Schematic illustration of typical locations of RC structures which are designed and detailed to sustain inelastic deformations.

Modern design codes such as the New Zealand concrete structures standard (herein referred to as NZS3101:2006) have relatively strict detailing requirements to ensure that PPHZs can sustain a large number of reversing inelastic load cycles, such as those expected to occur during severe seismic actions.

Large flexural tension stresses are resisted by the longitudinal reinforcement which is designed to exceed the yield strength. For practical design and construction purposes the longitudinal reinforcement is often terminated inside construction joints adjacent to the PPHZ as illustrated in Figure 3-2. The joints act as anchorage zones for the longitudinal reinforcement which must have sufficient bond resistance when the bar is loaded in tension (and in compression, albeit less critical) to ensure there is adequate transfer of stresses between the reinforcement and the surrounding mass of concrete.

3.1.3 Definition of bond stress: simplified concept for design

Figure 3-3(a) illustrates the interface between the deformed bar and concrete. The first component of bond resistance is provided by some chemical adhesion (denoted by v_a) between the cement paste and bar surface; however this adhesion can be destroyed by small amounts of slip between the bar and the concrete. Further slip mobilizes the second component of bond resistance which is attributed to some friction between surface irregularities of the concrete and bar. Prior to using deformed bars, designers took preference in using plain round bars in a mildly rusty condition as the bars were more heavily pitted and had greater frictional resistance (Park and Paulay, 1975). For deformed bars, however, the majority of bond strength is developed by mechanical bearing (denoted by f_b) of concrete against the faces of transverse deformations (herein referred to as ribs) along the bar. The development of shear stresses in the concrete between the ribs is denoted by v_c in Figure 3-3(a). Further description of the mechanism of bond resistance is presented in Section 3.2.

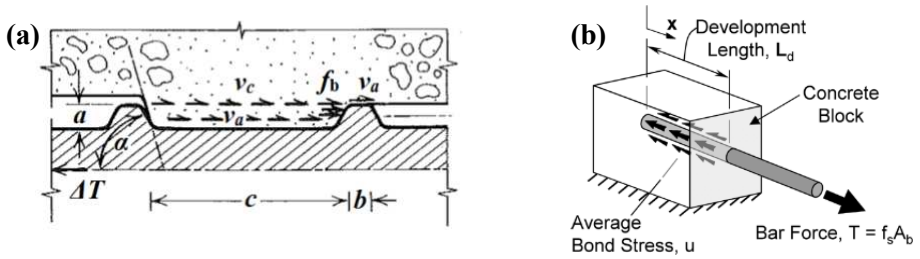

Figure 3-3: Diagrams showing bond resistance: (a) Actual components of bond resistance between two ribs of a deformed bar (Park and Paulay, 1975); (b) simplified approach of bond stress along the surface of the embedded bar (Thompson *et al.*, 2002).

In design practice it is impractical to evaluate each of the components of bond resistance at the micro-scale shown in Figure 3-3(a) when determining the available overall bond strength. Instead, some simplification is required to assess the average bond resistance of a larger segment of the embedded bar as illustrated in Figure 3-3(b). When there is sufficient bond stress τ (sometimes denoted as u) to maintain equilibrium of the bar under the design loads (in this case the bar yield or ultimate force) then the bar is "developed" and the embedment length necessary for anchorage of the fully stressed reinforcing bar is referred to as its "development length" (labeled L_d on Figure 3-3(b)).

The simplified bond concept makes use of a global model for a segment of the bar where the required embedment length L_d or maximum bond stress τ_{max} is determined by a simplified hand calculation. An

underlying assumption of this approach (for mathematical ease) is the assumption that the distribution of bond stress along the embedment length is uniform. Force equilibrium between the loads on the bar and the available bond resistance is shown by Equations 3-1 and 3-2 where the average bond stress is expressed in terms of the nominal bar diameter, d_b, the differential stress along the bars, Δf_s, and the length in which the reinforcing bar is embedded Δx or dx.

$$\Delta T = \frac{\pi {d_b}^2}{4} \Delta f_s = \tau \pi d_b dx \qquad 3\text{-}1$$

$$\therefore \tau(x) = \frac{1}{\pi d_b} \frac{\Delta T}{\Delta x} = \frac{d_b}{4} \frac{df_s}{dx} \qquad 3\text{-}2$$

The constitutive stress-strain relationship for reinforcing steel can be used to express bond stress as a function of the strain distribution (which varies with the position of the point *x* along the bar). If the steel remains in the elastic range, the bond stress may be determined according to Equation 3-3:

$$\tau(x) = \frac{E_s d_b}{4} \frac{d\varepsilon_s}{dx} \qquad 3\text{-}3$$

where E_s is Young's modulus for the reinforcing steel and ε_s is the steel strain.

The majority of previous experimental investigations into bond behaviour (e.g. Rehm and Eligehausen, 1979; Eligehausen *et al.*, 1983) have determined the ultimate bond stress for deformed reinforcing bars with short embedment lengths (3 to 5 d_b) such that the average bond stress is approximately equal to the local bond stress. Figure 3-4(a) illustrates that this assumption may be reasonable for a relatively short embedment length. However, to develop the reinforcing bar's yield or ultimate strength in the adjacent PHZ, the required embedment length of the bar is much longer. Figure 3-4(b) and (c) qualitatively illustrates that the bond stress distribution is highly non-uniform for longer embedment lengths and yielding of the reinforcing steel. Experimental measurements have shown that the local bond stress can be higher than twice the average bond stress (Mains, 1951).

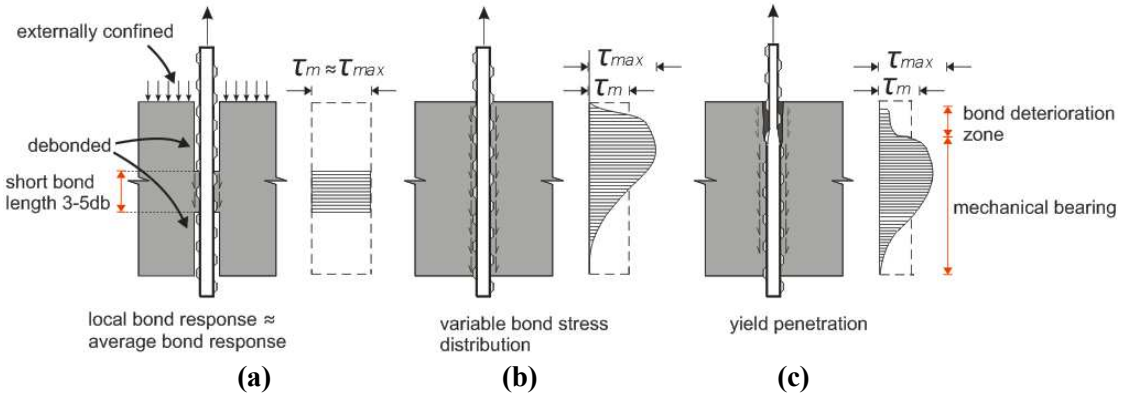

Figure 3-4: Qualitative illustrations showing: (a) Uniform bond stress along a short embedment length; actual bond stress distributions (b) without bond deterioration; (c) with bond deterioration.

3.1.4 Definition of bond slip

A shortfall of the simplified bond design concept is the lack of consideration of relative displacement between the deformed bar and concrete (herein referred to as "bond slip"). Accurate quantification of the overall deformation of a structure has become a significant requirement in recent decades due to the increased use of performance-based design objectives.

"Perfect bond" between the reinforcement and the concrete is a fundamental assumption of RC flexural theory, however, in reality there is some axial strain incompatibility which must be accommodated by some level of bond slip (see Figure 3-5). Bond slip of anchorages in some ductile RC test specimens has been found to contribute 40 to 50 percent of the total lateral deflection of a RC component (Eligehausen *et al.*, 1983; Saatcioglu and Ozcebe, 1989). If bond slip is not accounted for then the flexural stiffness of structural component s may be over-estimated and consequently the total deformations under seismic loading may be under predicted. Bond slip is typically considered in non-linear modelling techniques by defining some level of pinching in hysteretic relationships for RC sections or joint elements.

Bond slip is characterised by the difference in material strains at a point *x* along the bar:

$$\frac{ds}{dx} = \varepsilon_s(x) - \varepsilon_c(x) \qquad 3\text{-}4$$

where $\varepsilon_s(x)$ and $\varepsilon_c(x)$ are the material strains in the steel and the concrete at a particular point *x* along the embedded reinforcing bar.

at a particular position *x* the total bond slip is defined as:

$$s(x) = \left(\int_{x_0}^{x} \varepsilon_s dx - \int_{x_0}^{x} \varepsilon_c dx\right) + S_0 \qquad 3\text{-}5$$

where S_0 is global slip at the unloaded (free) end of the bar, and; the bracketed term refers to the local slip due to the integration of relative strains between the steel and concrete from the free end x_0 to the particular point *x*.

It is clear from Equations 3-3 and 5-2 that bond stress is a function of slip. If the constitutive stress-strain relationship of the steel and concrete is known (or simplified if in elastic range) then the integral of Equation 5-2 can be written in terms of bond stress $\tau(x)$ as shown below:

$$\frac{d^2s}{dx^2} = \frac{d\varepsilon_s(x)}{dx} - \frac{d\varepsilon_c(x)}{dx}$$
$$= \frac{1}{E_s}\frac{df_s(x)}{dx} - \frac{1}{E_c}\frac{df_c(x)}{dx} \qquad 3\text{-}6$$

by substituting Equation 3-2 into Equation 3-6;

$$= \frac{1}{E_s}\frac{4\tau(x)}{d_b} - \frac{1}{E_c}\frac{4\rho\tau(x)}{d_b} \qquad 3\text{-}7$$

where the reinforcement ratio and modular ratios can be substituted;

$$\rho = \frac{A_s}{A_c} \quad and \quad n = \frac{E_s}{E_c}$$

where A_s is the cross sectional area of the axially loaded reinforcing steel bar, A_c is the cross sectional area of the bond affected concrete E_c is Young's modulus for the concrete.

$$\therefore \frac{d^2s}{dx^2} = \frac{4}{E_s d_b}(1 + n\rho)\tau(x) \qquad 3\text{-}8$$

$$\tau(x) = \frac{E_s d_b}{4(1 + n\rho)}\frac{d^2s}{dx^2} \qquad 3\text{-}9$$

The second order differential equation shown in Equation 3-9 can be solved using the boundary conditions of force equilibrium (Equation 3-2), strain compatibility (Equation 3-4), the constitutive stress-strain relationship for the steel, and a constitutive relationship between bond stress and bond slip. A unique bond stress-slip-strain relationship was presented in Shima *et al.* (1987). Equation 3-10 summarises how the bond stress-slip-strain relationship is more commonly considered as a constitutive bond stress-slip relationship, which has been empirically derived from experimental testing (discussed later in Section 3.5).

$$\begin{aligned} \tau &= g\,(s, \varepsilon_s) \\ &= g\,\big(s, f(s)\big) \\ &= f(s) \end{aligned} \qquad 3\text{-}10$$

The position variable *x* is not shown in Equation 3-10 as previous experimental tests (Shima *et al.*, 1987; Viwathanatepa *et al.*, 1979) and finite element modelling (Fernandez Ruiz *et al.*, 2007) have shown the bond stress-slip relationship is independent of the position along an embedded reinforcing bar, unless the bond conditions drastically change (discussed later in 3.2.4).

3.1.5 Bond requirements for different performance criteria

Bond optimisation and trade-offs in the desired structural behaviour are inherent in modern design practice. Section 3.1.1 previously noted the varying bond behaviour that might occur in different regions of RC structures. Similarly, the targeted performance criteria and design requirements for serviceability limit state (SLS), ultimate limit state (ULS) and collapse prevention also requires differences in bond behaviour that are somewhat contradictory. Previous experimental research has recognised the trade-offs in achieving the desired level of structural performance at ULS that requires contrasting bond behaviour (Kimura and Jirsa, 1992; Patel *et al.*, 2014). These studies focussed mainly on using deformed bars where

the rib height and rib spacing was varied to see the influence of bond strength and bond slip (discussed further in Section 3.3.1).

At SLS, the bond mechanism should ensure that structural components have a high stiffness such that deflections under service loads are not excessive and there is some control of the width and spacing of cracks. In this case it is desirable to have relatively high tensile stress contributions from the concrete between the cracks (often referred to as "tension stiffening"). This structural behaviour can occur provided there is high bond strength and bond stiffness. In practice this requirement is generally satisfied by using deformed bars of a commercial standard and the rib geometry that complies with standard product specifications (such as the New Zealand Standard for steel reinforcing materials, NZS4671:2001).

At ULS, high bond strength and bond stiffness is required in anchorage and development zones and lapped splice zones of the reinforcement with the aim that small splitting (sometimes referred to as "bursting") forces are generated. Inside developed PHZs however, it is desirable to have some deterioration of the surrounding concrete as this helps in utilizing the ductility of the reinforcement and hence sufficient plastic rotation capacity. The deterioration of concrete resistance in a PHZ is due to: (i) the formation of a number of primary and secondary cracks, and; (ii) zones of bond deterioration at the cracks where the length of bar yielding can increase due to "yield penetration" (sometimes referred to as strain penetration). Figure 3-5 schematically illustrates the stresses carried by the reinforcing steel and the concrete from a cracked RC element within a developed PHZ.

Firstly, to promote the formation of secondary cracks, the bond mechanism is required to have a high bond strength and stiffness that effectively transfers tensile stresses in the reinforcement to the surrounding concrete. Figure 3-5 qualitatively shows the reinforcement will yield at the cracks and there is an increase in the average steel strain $\overline{\varepsilon_{sm}}$ (over a particular gauge length). When there is adequate bond between the cracks, the stresses in the reinforcing bar will be somewhat lower as the concrete will resist some of the flexural tension force. The rotation capacity of PHZs will increase as the ratio between $\overline{\varepsilon_{sm}}$ and the inelastic steel strain of the bare bar at the crack(s) ε_{sr} increases (Eligehausen *et al.*, 1998). Conversely, if secondary cracks cannot form there will be relatively large tension stiffening and the rotation capacity of PHZs will be much lower (a low value of $\overline{\varepsilon_{sm}}/\varepsilon_{sr}$ due to large concrete contribution). Much like the required bond behaviour at SLS, the deformed reinforcing bars of commercial standard will typically achieve high bond strength and stiffness. While the bond condition may provide good tensile stress transfer, there are certain conditions which may restrict the formation of secondary cracks due to (i) high concrete tensile strengths; (ii) low percentages of longitudinal reinforcement, and; (iii) limited strain hardening of the reinforcement (CERC, 2012).

Secondly, a bond deterioration zone must develop either side of the crack shown in Figure 3-5 to ensure the reinforcement can yield over a reasonable length. Under certain conditions where secondary cracks cannot develop, the total displacement ductility of the structural component depends on the magnitude of

inelastic steel strains that develop along the true length of yield penetration. For single crack PHZs to exhibit any level of ductility there must be a reduction of the bond resistance that extends a reasonable length outwards from crack centreline. It is desirable to develop a large bond deterioration zone such that the strains in the reinforcement can spread over a reasonable length, reducing the likelihood of premature fracture of the reinforcement.

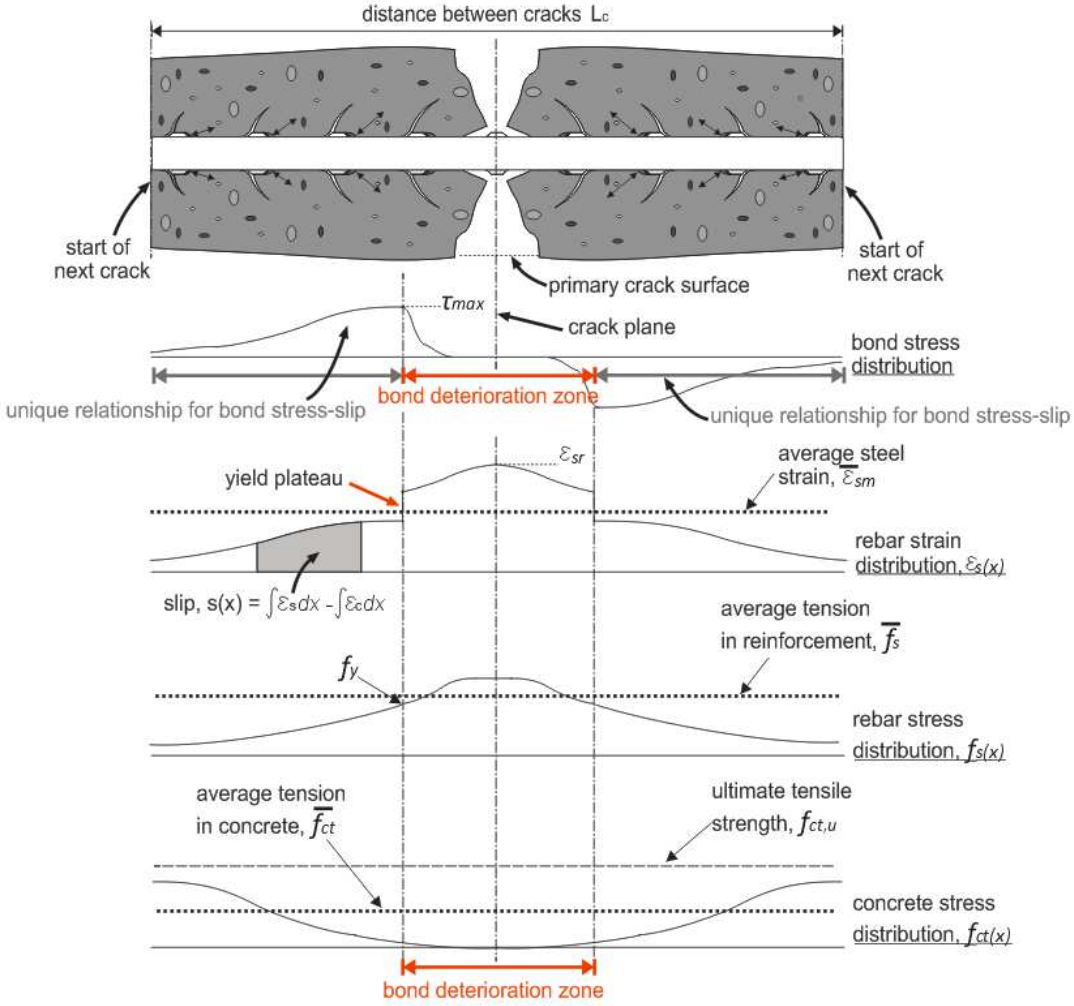

Figure 3-5: Qualitative illustration of how the stresses in the steel and concrete are distributed for a particular length of embedded reinforcement subjected to axial tension.

3.2 THE MECHANISM OF BOND

3.2.1 Behaviour at rib-to-concrete scale

Deformed reinforcing bars are primarily able to develop bond resistance by the mechanical bearing of the ribs against the surrounding concrete (labelled f_b on Figure 3-3). The longitudinal reinforcement in a RC element may be loaded in pure tension or flexure-induced tension which is predominantly resisted by the reinforcement. In a cracked RC element the reinforcing bars sustain large flexural tensile stresses and the corresponding tensile strains exceed the tensile strain capacity of the concrete. This strain incompatibility

is accommodated by bond slip (defined in Section 3.1.4) as there is axial displacement of the deformed bar relative to the concrete. Bond slip is the mobilisation of mechanical bearing and frictional resistance that enables bond stresses to be developed.

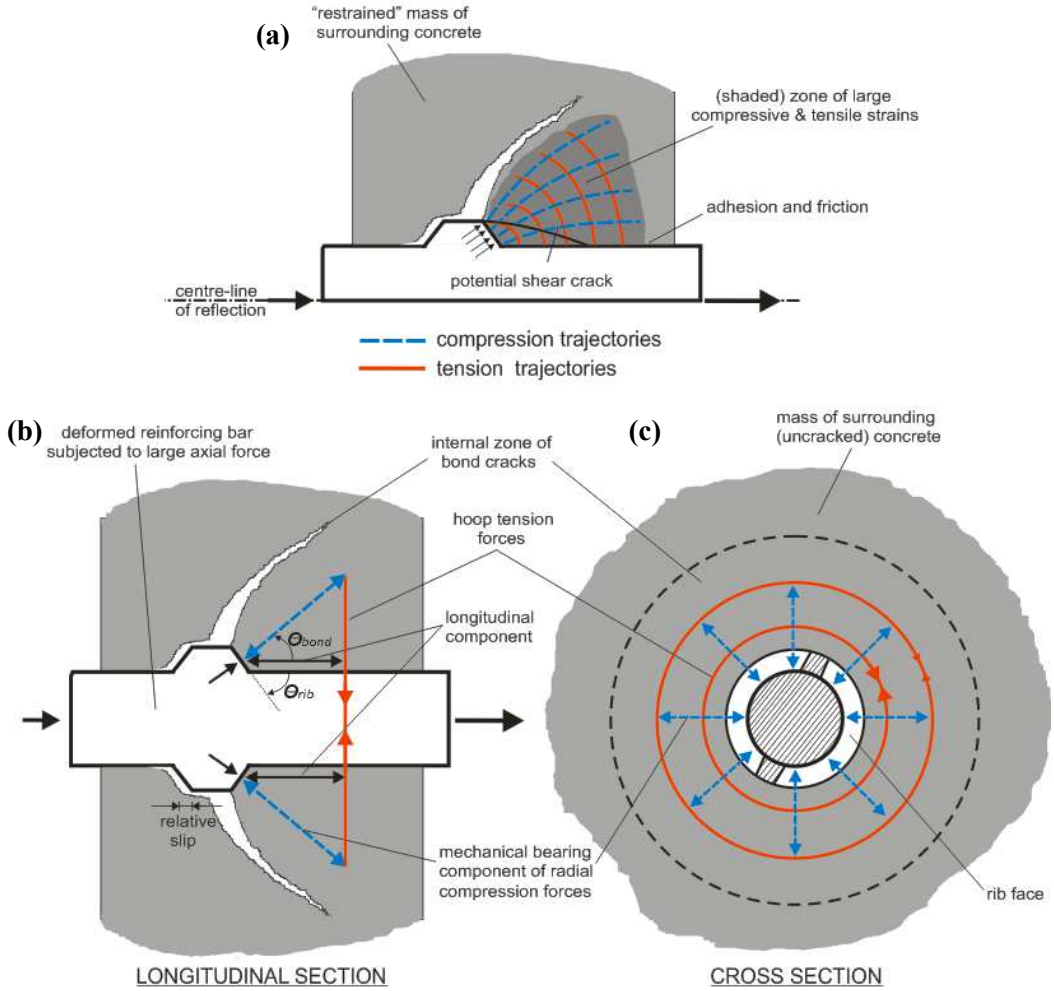

Figure 3-6: Schematic illustration of the mechanism of bond at the interface between ribs and the concrete.

Figure 3-6(a) schematically illustrates how the loaded deformed bar causes a field of intersecting compressive and tensile stress trajectories to develop in the concrete directly surrounding the rib. If the axial bar force is large then the bar must slip until large compressive stresses develop in the adjacent concrete. The concrete in the vicinity of the rib is confined by the surrounding concrete which allows local compressive stresses that are larger than measured values from compression tests on cylinder samples.

Local crushing of the concrete adjacent to the ribs will generate large compressive strains. Although the shaded concrete zone on Figure 3-6(a) is highly compressed and has a tendency to move, the surrounding volume of concrete is relatively massive and is effectively restrained, which means that large tensile stresses will also develop in the concrete in the vicinity of the rib. If the tensile stress exceeds the concrete tensile strength then internal bond cracks will develop from the top of the rib and extend at some angle. Internal bond cracks were traced by Goto (1971) using ink injection in RC prisms that were subjected to

direct axial tension. Figure 3-6(b) and (c) illustrates the development of "bond forces" that enable the bond mechanism to resist the axial bar forces as the horizontal component of radial bearing forces (compression struts) develops against the rib face. Local force equilibrium must be maintained by developing a series of hoop tension tie forces (i.e "strut-and-tie") that opposes the vertical component of the radial compression struts.

3.2.2 Monotonic bond behaviour

Figure 3-7(a) to (d) schematically illustrates the sequence of events for local bond behaviour under monotonic loading. The accompanying bond stress-slip curves for each state are qualitatively characterised by the points OABC. Bond behaviour in the pre-peak, peak- and post-peak range is influenced by several factors. The physical bond behaviour throughout each range of the monotonic envelop are described in the following sections and the most influential factors are briefly mentioned. Section 3.2.4 contains further discussion on factors influencing bond.

3.2.2.1 *Pre-peak bond behaviour*

Figure 3-7(a) illustrates at initially low levels of load, the "initial bond angle" $\theta_{bond,0}$ for deformed bars will project at an angle that is approximately normal to the rib face angle θ_{rib}. The contribution of chemical adhesion between the cement paste and bar surface is destroyed after a small amount of bond slip. Increasing the load from O to A is due to the mobilisation of frictional resistance and mechanical interlocking as the concrete directly in front of the rib is compressed to an extent that slip OA occurs. The initial slip OA will depend on the initial bond stiffness, which is mainly a function of the compressive stiffness of the concrete matrix (mainly cement paste), the extent of micro-cracking perhaps due to shrinkage, and on the rib geometry (rib face angle, rib height and rib spacing).

The deformed bars that are used in construction in seismic regions typically have the rib geometry (refer to Section 3.3.1.1) required to ensures a high initial bond stiffness. Minimal bond slip prior to reaching the maximum bond stress means the required bond behaviour and overall structural performance at SLS will be achieved.

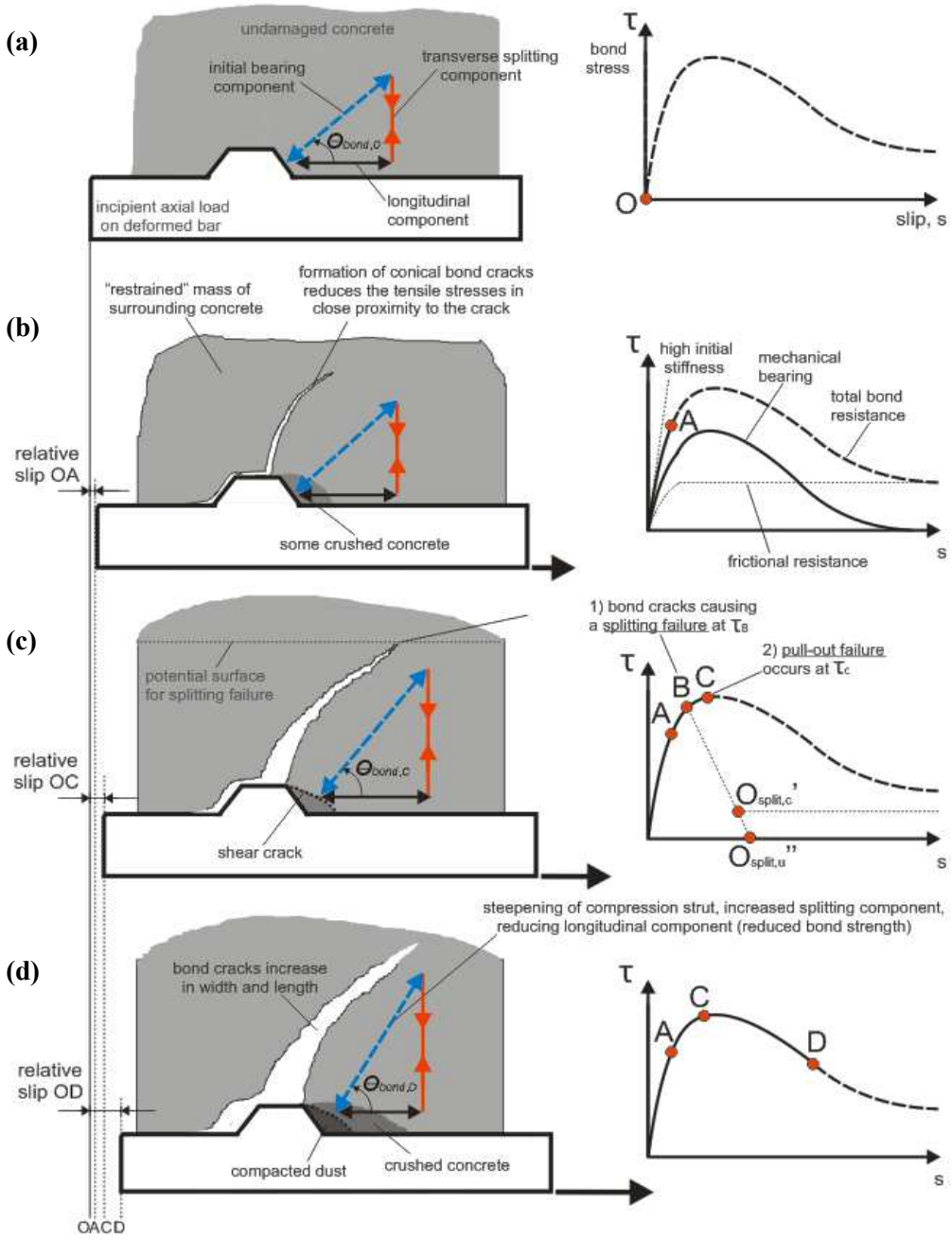

Figure 3-7: The mechanism of bond and qualitative bond stress-slip relationship at various damage states.

3.2.2.2 *Bond failure modes and peak behaviour*

Prior to reaching the maximum (or "peak") bond stress τ_{max} the localised crushing and internal bond cracking shown in Figure 3-7(b) causes the pre-peak stiffness to reduce. The transition between Figure 3-7(b) and (c) illustrates the propagation of internal bond cracks as the load is increased along path AB. The maximum bond stress will depend on the bond failure mode that occurs. Splitting failure can occur at lower bond stresses compared to the maximum stresses in a pull-out failure.

Splitting failure will occur at point B if splitting cracks extend through the cover concrete and the bond stress is suddenly reduced. The value of τ_{max} and negative post-peak stiffness depends on a combination of:

- the effective tensile strength of the concrete;
- the cover concrete thickness and spacing to parallel bars also subjected to high bond stresses;
- the presence and density of transverse reinforcement to confine the extension of splitting cracks. This is often referred to as confining steel used in bond test specimens;
- the amount of shear deformation of a cracked RC component that induces dowel forces on the deformed bar and further increases the tensile stresses in the concrete (Fenwick, 1966).

Figure 3-8(a) illustrates some possible splitting crack failures in a RC member. The largest radial length of the hoop tension stress field at failure will be the minimum of the face or side cover thickness, or half the clear spacing between two bars sustaining high bond stresses. Figure 3-8(b) illustrates how confining steel may intersect splitting cracks and resist a portion of the hoop tensile stresses. If a splitting failure develops and there is poor cover thickness and no confining steel then the post-peak bond stress will suddenly drop to zero along path B-$O_{split,u}$". If the cover concrete thickness is large and/or there are a moderate amount of stirrups near the bond region then some residual bond stresses can be resisted along the path B-$O_{split,c}$'.

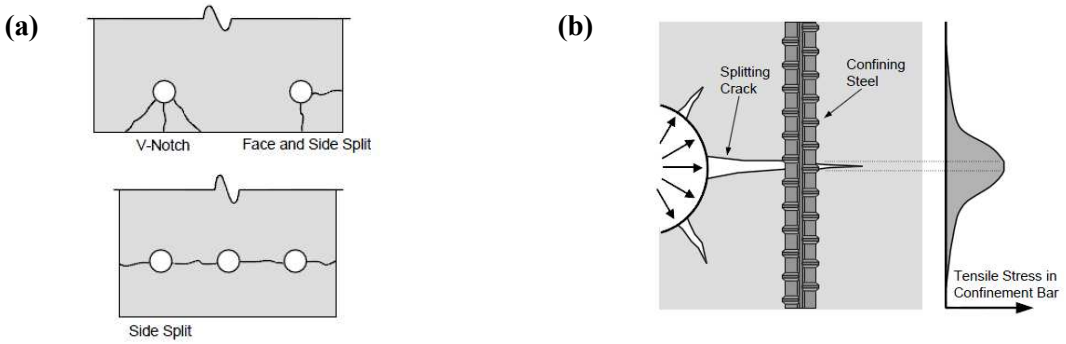

Figure 3-8: Possible splitting crack failures and resistance of bond-induced hoop tensile stresses by transverse reinforcement (Thompson *et al.*, 2002)

Pull-out failure will occur at point C on the monotonic envelop if splitting failure has been suppressed. Prior to reaching τ_{max} at point C, the compressive stresses in the concrete directly adjacent to the rib have exceeded the triaxial compressive strength and the formation of bond cracks means the local tensile stresses in the concrete have reduced. At this level of concrete damage the direction of the principle tensile and compressive stresses has rotated such that the shear stresses in the concrete "shear keys" between the ribs have increased. This behaviour is occurring along the path AC of in Figure 3-7(c) until τ_{max} occurs when a shear failure develops along the concrete key. Pull-out failures observed from previous bond tests have shown there is some plateau at the peak of the bond stress-slip curve until bond stresses reduce.

3.2.2.3 *Post-peak bond behaviour*

The formation of shear cracks and crushing of the concrete directly in front of the rib causes a wedge zone of compacted powder of cement and perhaps sand particles. The increased concrete damage causes the effective bond angle to increase between Figure 3-7(c) and Figure 3-7(d) at a rate that will reduce the longitudinal component of force that provides bond resistance, hence reducing the bond stress below the maximum.

The post-peak bond stress reduction will depend on the rate at which the mechanical resistance is destroyed. In turn this which will primarily depend on the length of the concrete key that is embedded between two ribs. If the ribs on the bar are closely spaced then there is a greater negative post-peak stiffness as compared to the post-peak stiffness when the ribs are spaced further apart. The residual bond stress is completely attributed to frictional resistance when bond slip exceeds the clear rib spacing.

3.2.3 Cyclic bond behaviour

The bond behaviour under cyclic loading is different to that under monotonic loading. Pull-out failure is more likely to occur during cyclic loading and the bond strength degradation depends on the maximum incremental slip that has previously been reached. Compared to the monotonic backbone, bond failure under cyclic loading can occur at lower bond stresses depending on: (i) the maximum incremental slip that has previously occurred, and (ii) the number of load cycles (ACI Committee 408, 1992). Bond behaviour under high-cycle fatigue (typical of periodic service loadings with lower amplitudes) is less detrimental to RC structures compared to the full or partial reversals of high-amplitude low-cycle fatigue that occurs during earthquake-induced seismic loading. Bond behaviour under high-cycle fatigue is not discussed further in this chapter, although some results from 308 pull-out bond tests are summarised in Rehm and Eligehausen (1979).

Figure 3-9 schematically illustrates the bond behaviour on the reversed loading cycle after undergoing some half cycles (or varying slip) in the previous direction. Figure 3-9(a) illustrates that if the first cycle(s) in the small slip range are less than the maximum bond stress then further slip in that direction will follow the monotonic backbone and stress degradation will be minimal.

Figure 3-9(b) illustrates a reduction in mechanical bearing and hence bond stress degradation which occurs due to significant crushing at both ends of the concrete between the ribs. On first loading in either direction the bond stress-slip curve is shown to be concave, whereas the re-loading branch illustrated in Figure 3-9(b) is shown to be convex until a point of inflexion at M when a higher slip value than previously loaded to means that that further mechanical bearing has been mobilised.

Figure 3-9(c) illustrates the behaviour when the slip increment Δs is almost as large as the clear rib spacing. The mechanical bearing resistance is almost completely destroyed and residual bond stresses due to some friction acting along the potential failure plane.

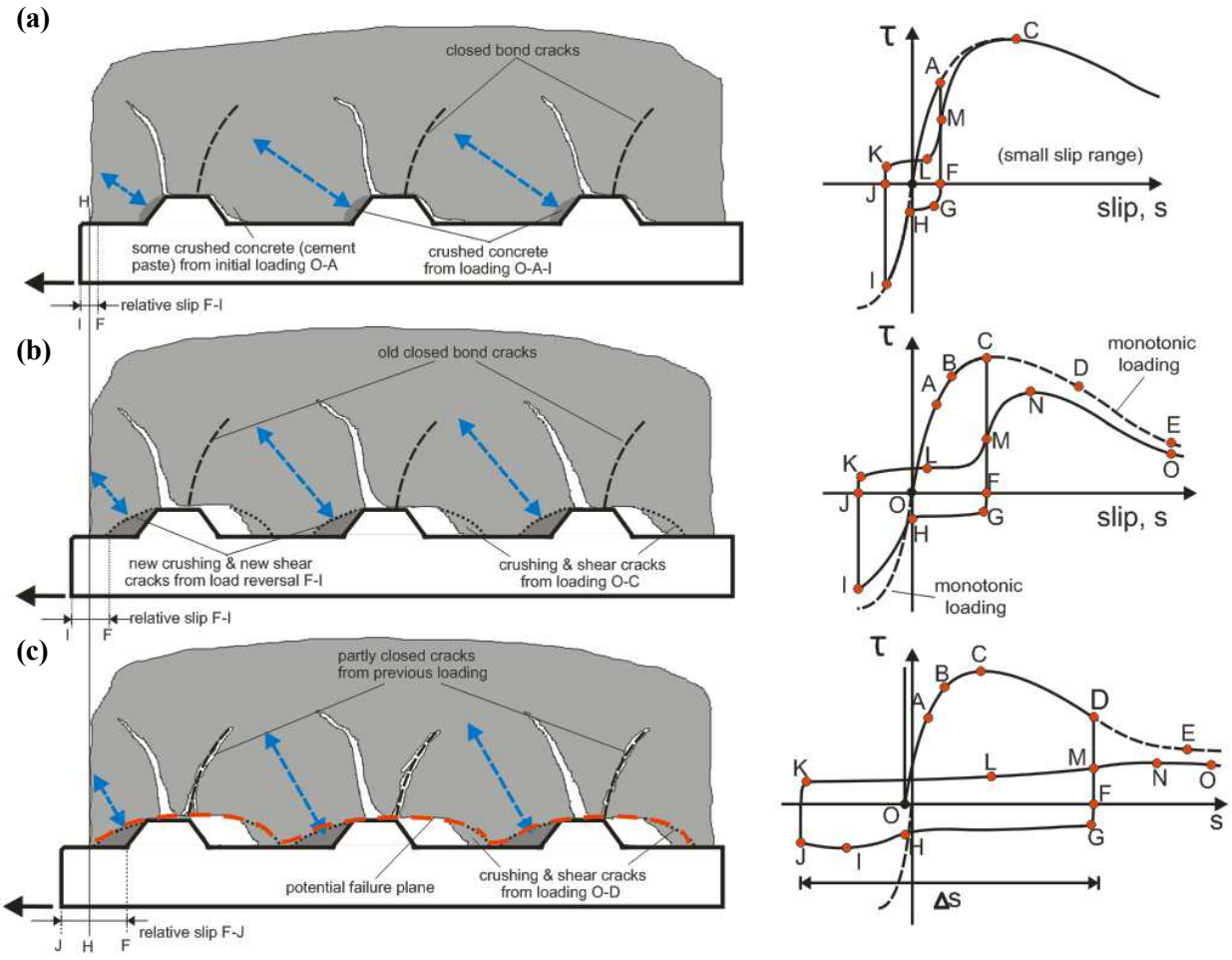

Figure 3-9: The mechanism of bond resistance and relative slip under reversed cyclic loading (not to scale, modified from Eligehausen *et al.*, 1983).

3.2.4 Cone break-out failure

Bond test specimens typically use a debonded length (about $5d_b$) from the loaded face to focus on bond in the confined region and avoid early failure due to cone break-out. Limited suggestions are made for bond behaviour in the vicinity of the crack plane where the concrete is unconfined. Hoop tensile stresses may propagate to the free surface/crack plane and a localised cone break-out failure may occur. Similar unconfined conditions exist at dry joints between precast concrete panels and for anchored bolts used in precast panels and footing connections into concrete floor slabs.

A cone break-out at the column face of a beam-column joint is shown in Figure 3-10(a) from experimental observations (Au, 2010). Figure 3-10(b) illustrates cone break-out during pull-out testing of a deformed bar embedded in large interior beam-column joint specimens. Viwathanatepa *et al.* (1979) generally found the concrete cone radius was about 115 mm and to a depth of 75 mm (a cone breakout angle of 30 to 35 degrees). The presence and arrangement of other reinforcement shown in Figure 3-10(b) will have influenced the geometry of the cone.

Results in Figure 3-10(c) and (d) shows that cone break-out occurred at much lower bond stresses than for the confined bond region. Eligehausen *et al.* (1983) approximated the bond response in unconfined regions of beam-column joints which a maximum bond stress of 5 MPa (at a bond slip of 0.3 mm) until cone break-out occurs, after which the bond stress suddenly reduces to 0 MPa at a slip of 1.0 mm.

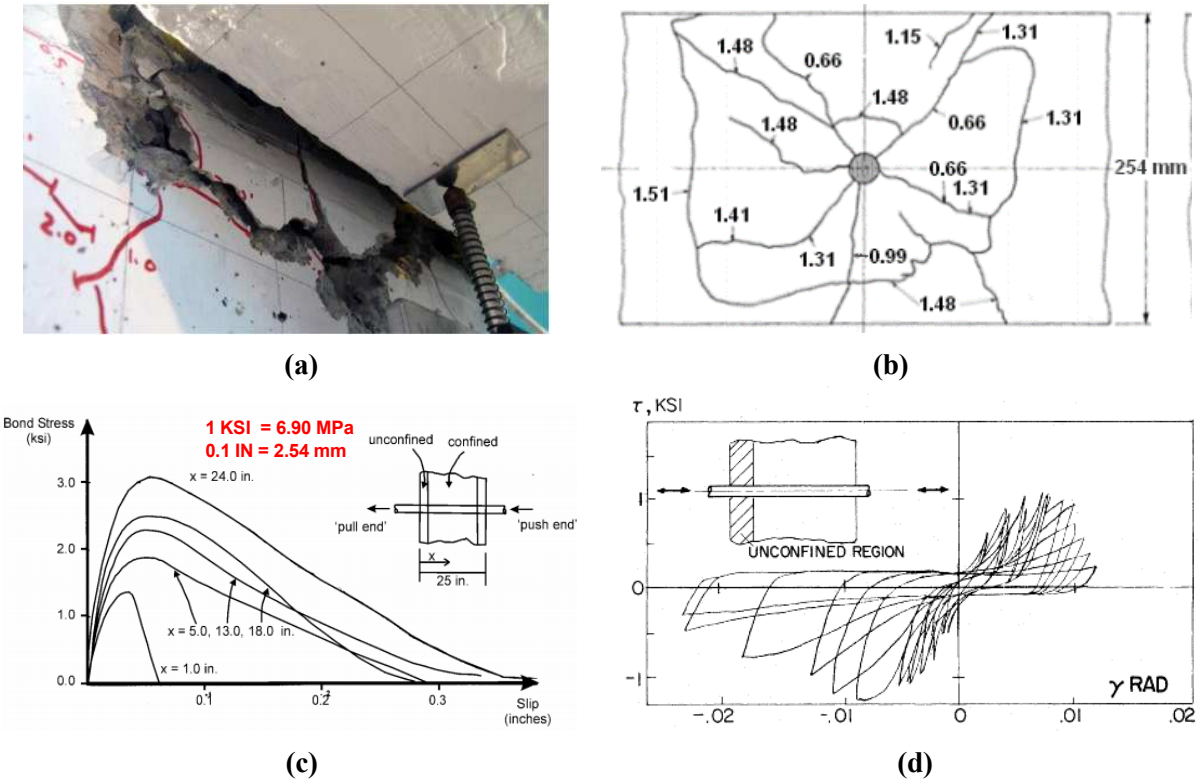

Figure 3-10: (a) Observed concrete break-out at the "loaded end" (b) schematic of crack pattern and cone break-out observed on loading face (Byrne, 2012; adapted from Viwathanatepa *et al.*, 1979). Local bond stress-slip results for the unconfined region under (c) monotonic loading and; (d) cyclic loading.

3.2.5 The bond deterioration zone

The literature generally agrees that the bond stress-slip relationship (discussed later in Section 3.5) is independent of the position x along the reinforcing bar, with the condition that a particular distance away from the crack plane is allowed for as a "bond deterioration zone" as shown in Figure 3-5. The length of the bond deterioration zone is physically related to and/or dependent on many factors, particularly the strain demand (average strain and at the crack, hence local slip), the spacing of cracks, cover concrete thickness, amount of shear deformation (among other factors discussed in Section 3.3 which also affect bond behaviour in confined regions).

Minor differences between the bond deterioration lengths stated by different researchers will largely be due to the accuracy of experimental measurements, variations in the testing conditions and modelling techniques and input parameters that are used or assumed. Measurements from cyclic bond tests by Viwathanatepa *et al.* (1979) suggested that 3 to $4d_b$ from the loaded end was a reasonable allowance for

early bond deterioration in the unconfined region. Further analytical work by Eligehausen *et al.* (1983) assumed that unconfined region extends $2d_b$ from the free surface then a transition zone exists between 2 and $5d_b$ from the free surface.

Maekawa, K., and Quereshi, J (1997) suggests there is zero bond resistance over a distance of $2.5d_b$ away from the crack plane, after which the bond stress linearly increases towards the maximum resistance at $5d_b$. High resolution finite element results from Saleem and Maekawa (2004) suggests the bond deterioration length may be between 3 and $4d_b$. *fib* (2000A) states that the bond stress-slip can be assumed to have a linear increase from zero resistance at the crack to the maximum bond resistance available at $5d_b$ from the crack. The Model Code 2010 takes the same approach but uses a distance of $2d_b$ from the crack however it is unclear whether there are any experimental tests results that support this distance. Fernandez Ruiz *et al.* (2007) presents results from finite element modelling showing that the bond stress-slip relationship is unique for short and long anchorage lengths up until a distance of three times the rib spacing, $3s_r$ from the crack plane.

3.3 FACTORS INFLUENCING BOND BEHAVIOUR

The bond stress-slip relationship depends on a myriad of factors or conditions that can be more easily considered as four overall categories: (i) the reinforcing steel properties; (ii) the concrete properties; (iii) the state of stress, and; (iv) the type of loading.

Early experimental research such as Abrams (1913) focussed on the effects of the first two categories with relative ease and this resulted in a widespread understanding that bond strength could be considered as a material property. Since the 1960s, an increase in bond related research has led to further awareness that bond behaviour is also a structural property with factors including member geometry and state of stress in the RC component. Some of these bond related deficiencies are significant enough to warrant consideration in design practice and codes such as NZS3101:2006.

This section presents findings from a search of the literature, however not every factor has been discussed. Listed below are some valuable publications with the complete references given in section 3.9.

- Eligehausen *et al.* (1983) – "Local bond stress-slip relationships of deformed bars under generalised excitations"
- ACI Committee 408 (1992, 2003) – "Bond and development of straight reinforcing bars in tension"
- ACI Committee 408 (1998) – Special Publication 180: "Bond and development of reinforcement: a tribute to Peter Gergely"
- *fib* (2000) – Bulletin 10: "Bond of reinforcement in concrete"
- *fib* (2012) – Part 1, referred to herein as the "Model Code 2010". Chapter 6: Interface Characteristics
- *fib* (2014) – Bulletin 72: "Bond and anchorage of embedded reinforcement."

3.3.1 Reinforcing steel properties

3.3.1.1 *Rib pattern and geometry of deformed bars*

The rib pattern and geometry of deformed bars includes angles of the rib face and rib inclination, height and crest width of the rib, clear spacing between ribs, and so on. Section A.1 of Appendix A presents a supplementary illustration of the deformed bar and measured dimensions for rib geometry.

Abrams (1913) published landmark research on the bond behaviour of plain round bars and many types of deformed and corrugated reinforcing bars. Among many findings, this study showed the bond strength was influenced by the ratio of bearing area (of the different ribs, lugs and indentations) to the bar surface area. Since Abrams (1913), the literature has consistently referred to the "relative rib area" which is a

combined geometric parameter that is the most important feature of the reinforcing steel that influences bond behaviour. ACI Committee 408 (2003) defines the ratio (denoted as R_r) of the bearing area to the shearing area as stated in Equation 3-11. The rib height h_r and the centre-to-centre rib spacing s_r are taken from raw measurements and any cross-sectional gaps that are not providing bond resistance are subtracted (these are often gaps caused by one or two longitudinal ribs).

$$R_r = \frac{projected\ rib\ area\ normal\ to\ bar\ axis}{nominal\ bar\ perimeter \times centre \cdot centre\ rib\ spacing} \approx \frac{h_r}{s_r}\left(1 - \frac{\sum gaps}{\pi d_b}\right) \qquad 3\text{-}11$$

For ribbed bars with a diameter between 10 and 40 mm the minimum relative rib area permitted by NZS4671:2001 is stated as 0.056. Similar standard requirements for rib geometry also exist in ASTM A615 "*Standard specification for deformed and plain billet-steel bars for concrete reinforcement*". The average rib spacing must not exceed $0.7d_b$ and the rib height must be greater than 0.04 to 0.05 times d_b (depending on d_b) which corresponds to a minimum relative rib area of 0.057. The requirements in the Japan Industrial Standard (JIS G3112) are recognised as being approximately the same as those laid out in NZS4671:2001 and ASTM A615 (Kimura and Jirsa, 1992).

Figure 3-11(a) shows some test results from Eligehausen *et al.* (1983) where curves (2) and (3) illustrate two bars of identical diameter that have different relative rib areas. The results show differences in bond behaviour in the pre-peak and peak range. Curve (2) reaches the maximum bond strength at a slip of 1 mm while curve (3) with a lower relative rib area develops the maximum bond strength at a larger slip of about 2 mm. The relative rib area influences the initial bond stiffness and the curvature of the ascending branch towards the peak. Lower bond stresses are shown for curve (4) which may be due to a large relative rib area, along with potential effects of the larger bar diameter.

Kimura and Jirsa (1992) studied the effect of the rib height, rib spacing and rib face angle more closely by using specially machined test bars with the same nominal core diameter of 36 mm. Figure 3-11(b) shows the extent of the test matrix from Kimura and Jirsa (1992). Bond pull-out tests were completed on specimens with an embedded length of 150 mm. Test results from Kimura and Jirsa (1992) showed that increasing the relating rib area from 0.075 to 0.20 had a positive influence on the bond strength and stiffness. If the relative rib area is too large, however, then the magnitude of the shear stresses along the plane of the concrete key (denoted v_c in Figure 3-3(a)) will be large. A more sudden bond failure may occur at lower total bond stresses without any micro-cracking crushing of the concrete that is typical when the stress transfer between the bar and the concrete is most effective. This notion agrees with the results from Kimura and Jirsa (1992) and the work of other Japanese researchers who observed the bond strength stiffness either became constant or decreased for relative rib areas higher than 0.20. The literature makes

a consistent conclusion that deformed bars with relative rib areas higher than 0.20 should not be used as the bond behaviour is less desirable.

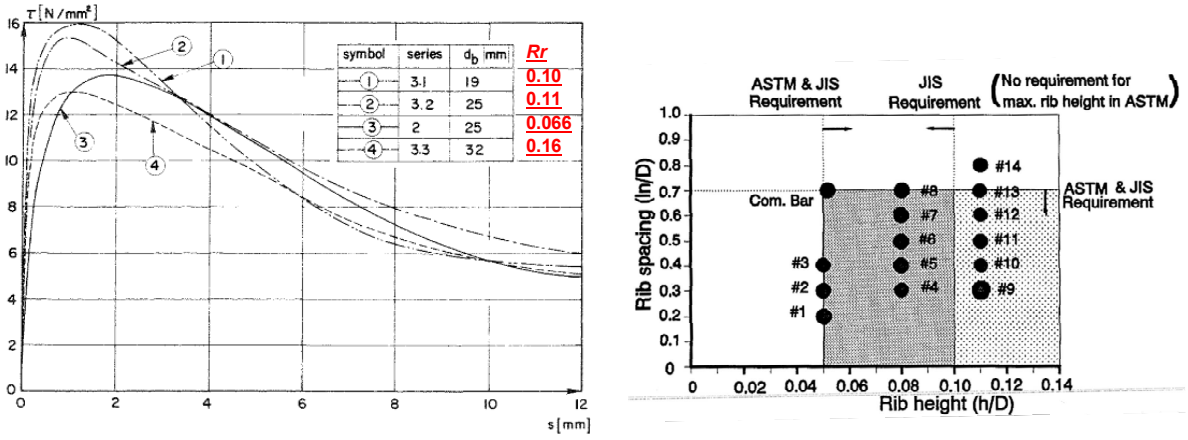

(a) **(b)**

Figure 3-11: (a) Bond behaviour for different deformed bar geometry (Eligehausen *et al.*, 1983). (b) Kimura and Jirsa's (1992) test matrix for 35.8 mm reinforcing bars varying rib height and rib spacing.

Patel *et al.* (2014) conducted bond tests on pull-out specimens and direct tension tests of RC prisms specimens using 12 mm deformed bars. The standard test bar had a rib height and spacing of 1.2 and 8.5 mm (R_r = 0.14) and two sets of specially machined bars with (i) double rib spacing, and; (ii) half the rib height (R_r = 0.07). The load-slip curves were very similar for both cases of R_r = 0.07 and the maximum resistance was about 60 percent of that for the standard bar.

The clear rib spacing (hence length of concrete shear key) clearly influences the bond stress-slip relationship. Once the bar has slipped through a distance equal to the clear rib spacing then mechanical bearing resistance is lost as the concrete key is completely destroyed and the residual bond stresses are due to frictional resistance. Considering the schematic shown in Figure 3-9(c), reversed cyclic loading means that bearing resistance is completely lost once the incremental slip value has exceeded the clear rib spacing.

NZS4671:2001 requires that the rib face angle must be greater than 45 degrees and the root of the ribs are slightly curved near the core to prevent steel stress concentrations. A smaller rib face angle, say 30 degrees, results in less crushing of the concrete and hence less mechanical bearing develops in the small slip range. This notion is supported by the test results in Kimura and Jirsa (1992). An increased rib face angle above 45 degrees will be less influential as this change is somewhat neutralised by crushing of the concrete wedge, meaning the maximum bond stress depends more on the effective bond angle (labelled $\theta_{bond,C}$ on Figure 3-9(c)). This notion is supported by a number of previous bond tests by Skorobogatov and Edwards (1979) who found the maximum bond strength of 16 mm bars did not vary when the rib face angle was either 48 or 58 degrees. Kimura and Jirsa (1992) also found that the bond stress-slip relationships were almost identical when the rib face angle was 45 and 60 degrees.

3.3.1.2 *Bar diameter*

Standard bar sizes generally have different relative rib areas (defined previously in Section 3.3.1.1). The literature generally suggests there is slightly higher bond strength for deformed bars of a smaller diameter; however it is unclear whether differences in bond behaviour are attributed solely to the bar diameter or whether there is some additional influence from different relative rib areas. In New Zealand design and construction practice the common bar sizes for longitudinal reinforcement are typically ranges 20, 25 and 32 mm bars for RC beams and 40 mm bars may also be used for RC columns. Existing RC wall structures in New Zealand have been constructed using 12, 16 and 20 mm bars for the vertical reinforcement.

After obtaining the test results shown in Figure 3-11(a), Eligehausen *et al.* (1983) proposed that the bond strength of 19 mm bars may be 10 percent higher than 25 mm bars, and for 32 mm bars the bond strength may be about 10 percent less. The paper by Lowes *et al.* (2004) considers a bond strength multiplier Γ_4 as a function of bar diameter based on the test results of Viwathanatepa *et al.* (1979) and Eligehausen *et al.* (1983). Lowes *et al.* (2004) allows for the bond strength to be higher when the nominal diameter is less than 19 mm ($\Gamma_4 = 1.09$) and lower when the diameter is greater than 32 mm ($\Gamma_4 = 0.91$) and interpolation is used for 20 to 32mm bars.

Maekawa *et al.* (2003) suggests bar diameter has a significant effect on bond and must be considered by those conducting experimental testing on scaled-down RC specimens. If the bar diameter is not scaled to the same proportion, it is possible that bond slip in experimental testing has a larger contribution to the total deformation of the specimen in comparison with real RC structures. Maekawa *et al.* (2003) recommends the contribution of bond slip to total deflection should be investigated separately. This notion may be reasonable, depending on the bond behaviour of different bar sizes, though the magnitude of the steel stresses and strains are also particularly relevant and must also be considered.

The need for large diameter bars becomes more common in large structural components and systems that are designed to keep the material stresses in the elastic range. Such cases might include nuclear power plants and foundation systems for bridges, tanks and buildings, where bar diameters are often 32 mm and larger. When bond slip of large bars occurs, large strains are mobilised in the surrounding concrete. If nearby transverse reinforcement is present then large stresses can be resisted as the relative confinement of the concrete is large. Investigations on bond behaviour of large bar sizes are not discussed further here but may be found in Murcia-Delso *et al.* (2013) and Jirsa and Kimura (1992).

3.3.1.3 *Steel stress-strain behaviour*

The influence of the steel stress-strain behaviour on bond will depend on a combination of the material properties and the state of stress. The literature contains some particularly interesting and valuable conclusions about the influence of inelastic steel strains. Typical medium and large scale experimental tests on ductile RC components and sub-assemblages will result in large variations in bond strength due

to yielding of the reinforcing steel. In contrast, the majority of previous bond tests were set up to ensure the steel remained in the elastic range. There have been some, although fewer, studies that closely investigate the bond when the steel is in the inelastic range.

It is intuitive from the effect of Poisson's ratio that the local bond strength decreases due to bar diameter contraction, or "necking", in the inelastic range when axial tensile strains are large. Once the reinforcing steel has yielded and "softening" occurs, the Poisson's ratio v_s may be substantially greater than 0.3 which is only true when the material response remains elastic. The value of v_s in the post-yield range may be as high as 0.5 for mild reinforcing steel (Park, 1987). Figure 3-12(a) schematically illustrates the bar diameter reduction resulting in a reduced effective rib height and overall reduction in bond resistance.

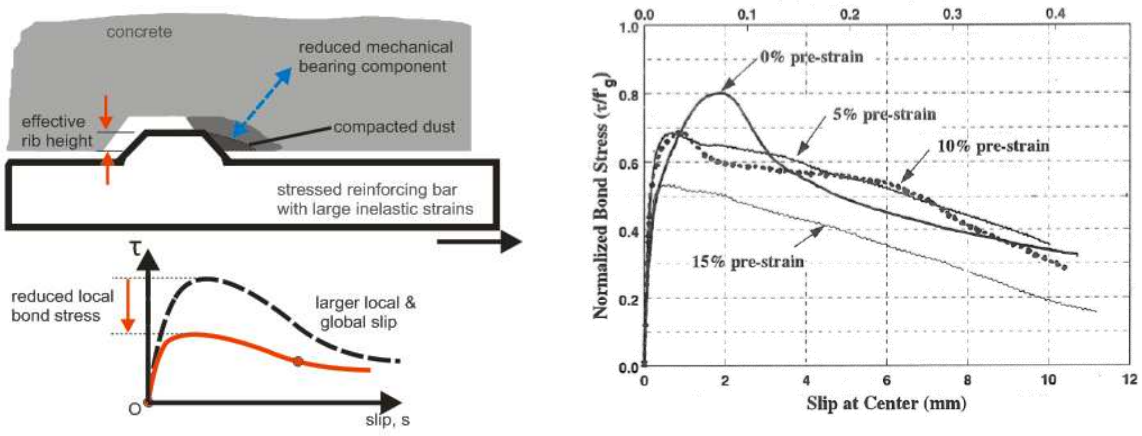

(a) **(b)**

Figure 3-12: (a) Schematic illustration of the reduction in effective rib height and hence reduced bond resistance at large inelastic strains; (b) Bond test results for pre-yielded reinforcing bars (Raynor, 2002).

Viwathanatepa *et al.* (1979) was one of the first to note there is also superior bond response due to dilation of the reinforcing bar under large compressive strains. This is partly illustrated by the "pushed end region" of Figure 3-10(c). Soleymani Ashtiani (2013) measured the bar diameter reduction in monotonic bond pull-out tests where the deformed test bars were subjected to very large axial strains. The diameter reduction was stated to be 9.1 percent for Grade 300 steel (with axial strains of about 20 percent at the loaded end) and 5.6 percent for Grade 500 steel (average axial strains on the order of 14 percent). At the maximum demands imposed during these tests the Poisson's ratio may be 0.5 and 0.4 for the respective steel grades.

Raynor (2002) carried out monotonic bond tests on reinforcing bars subjected to different levels of tensile pre-strain. Figure 3-12(b) illustrates there is similar reduction in bond stress for bars subjected to an axial pre-strain of 5 and 10 percent, whilst bond strength is further reduced at 15 percent pre-strain. This notion has some implications for the residual capacity of ductile RC structures. The similarity of the results for 5 and 10 percent pre-strain may suggest that, for this particular steel, the Poisson's ratio is constant over

this strain range where strain-hardening still occurs, whilst a higher ratio is valid at 15 percent axial strain near the maximum steel stress.

Shima *et al.* (1987) tested the bond stress and slip distribution of yielding bar anchorages as function of the measured steel strain distribution (defined in Equation 3-3). Monotonic tension testing of long anchorage specimens and RC concrete prisms was carried out to study the influence of steel stress-strain relationship and reinforcement ratio on the composite behaviour of reinforcing steel and concrete in tension. The reinforcement strain measurements and deduced bond stress distributions from long anchorage specimens are shown in Figure 3-13.

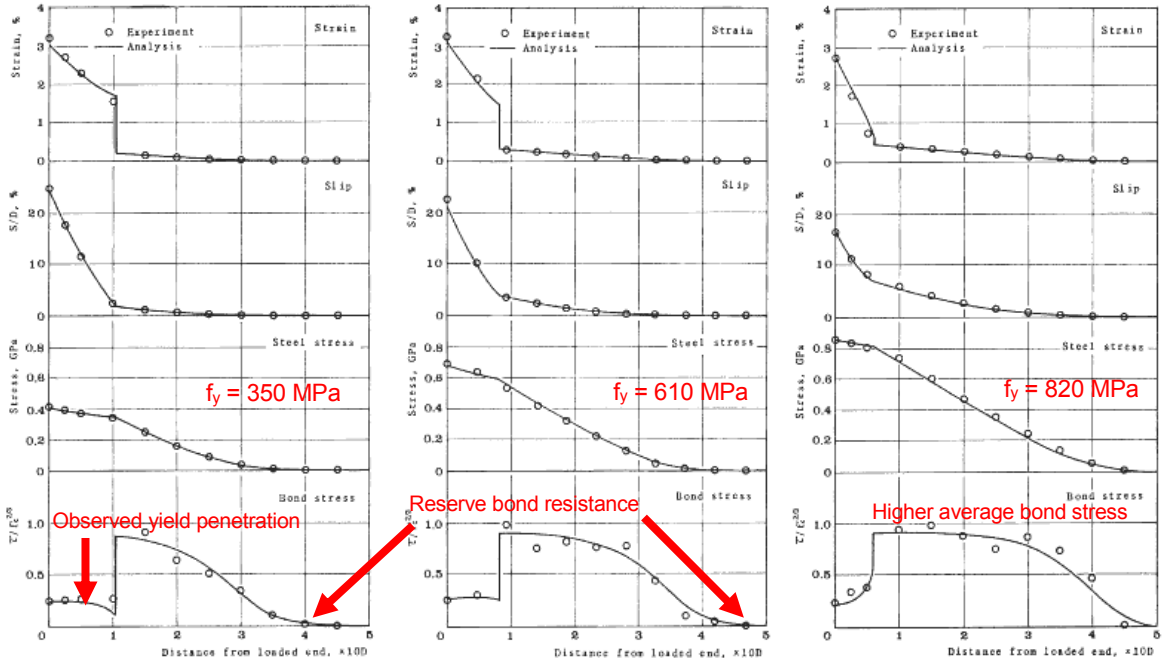

Figure 3-13: Test measurements showing distributions of reinforcing strains and inferred values of slip, reinforcing stress and bond stress (annotations on Figures from Shima *et al.*, 1987).

Significant bond deterioration is shown near the loaded end where the strain demand is large. Figure 3-13(a) shows the length of yield penetration was greater for "softer" steels with a lower yield strength. Figure 3-13(b) and (c) shows that higher grades of steel would result in less yield penetration from the loaded end, however the average bond stress along the entire embedment length increases as the steel strength increases. The larger axial force demands from the higher steel grades were found to be accommodated by engaging the ribs further along the embedment length and hence bond stresses are developed over a greater total length. Shima *et al.* (1987) concluded that the loss of bond strength was found to depend on the post-yield stiffness of the reinforcing steel (providing the anchorages were long enough to provide reserve bond resistance). Since the findings of Shima *et al.* (1987), there is an improved awareness that the bond stress-slip-strain relationship can be studied when the reinforcing bars are in the inelastic range.

> *"…it is recommended that absolute statements about performance of long anchorages with yielding reinforcement be derived from, and restricted to, specific structural conditions, which must be carefully modelled in the specimen form."* – Bonacci (1994b).

Bonacci (1994b) found the post-yield softening of the steel significantly reduced the "rate" of force transfer from an anchored bar when there are increasing steel strains at the loaded end. The overall performance of the anchorage becomes a trade-off between the average behaviour along the entire anchorage length and the behaviour over a particular length of the anchorage near the loaded end that is influenced by the steel strain demand. Bonacci (1994a) discusses some performance-based design considerations for anchorages in RC frames to ensure that steel strain demands can be met and excessive anchorage slip can be limited. The maximum steel strains were 0.025 and a critical bond slip of 4 mm was considered in these studies dedicated to the performance RC frames.

The experimental data from Shima *et al.* (1987) and Viwathanatepa (1979), among others, has been used to develop a bond-model parameter Ω_y that accounts for the effect of inelastic steel strains on the bond stress-slip relationship. Figure 3-14(a) illustrates the model proposed by Lowes *et al.* (2004) which significantly modifies the "elastic relationship" for inelastic strains of 0.01 (tension) and -0.01 (compression). The expressions found in Lowes *et al.* (2004) for determining Ω_y depend only on the yield strain of the steel.

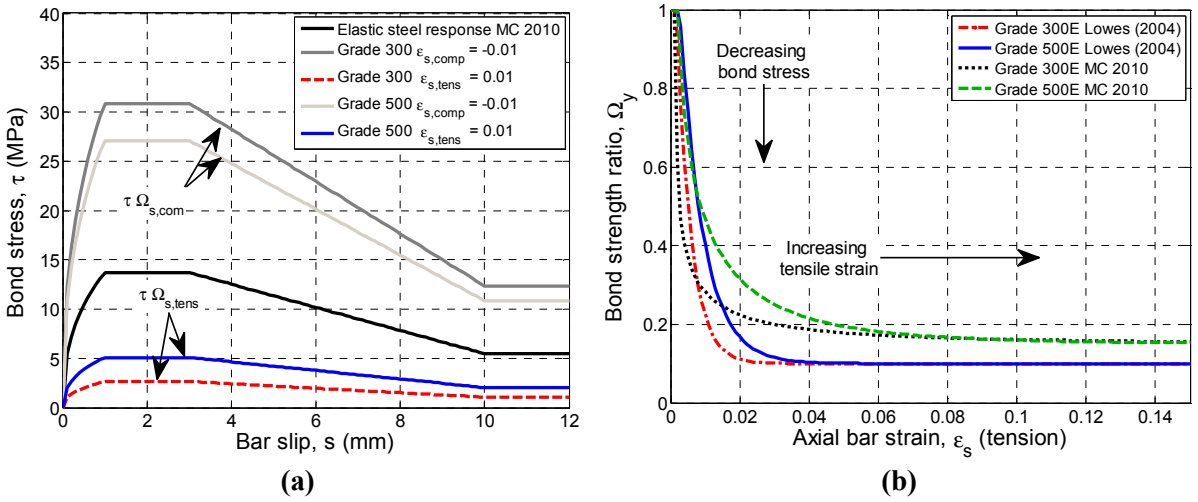

Figure 3-14: Plots showing the influence of inelastic steel strains on bond strength: (a) the modified bond stress-slip relationship proposed by Lowes *et al.* (2004). (b) The bond strength ratio proposed by Lowes *et al.* (2004) and in the Mode Code 2010 (*fib*, 2012).

The Model Code 2010 presents the same type of parameter $\Omega_{y,MC2010}$ shown in Equation 3-12 which makes greater consideration of the steel post-yield behaviour. Using average stress-strain properties of Grade 300E and Grade 500E steel used in New Zealand, the approximate values of $\Omega_{y,MC2010}$ are compared to the values of $\Omega_{y,Lowes(2004)}$ in Figure 3-14(b) as the tensile strain increases. The reduction on bond stress in the Mode Code 2010 is shown to be less than that suggested by Lowes *et al.* (2004),

which was likely derived using less experimental data. It is unclear which additional experimental data was used to derive Equation 3-12 and there is no supplementary discussion about this empirical parameter in *fib* (2014).

$$\Omega_{y,MC2010} = \begin{cases} 1.0 & \text{for } \varepsilon < \varepsilon_y \\ 1.0 - 0.85(1 - \exp(-5a^b)) & \text{for } \varepsilon > \varepsilon_y \end{cases} \quad 3\text{-}12$$

where:

$$a = \frac{\varepsilon_s - \varepsilon_{sy}}{\varepsilon_{su} - \varepsilon_{sy}} \quad and \quad b = \left[2 - \frac{f_{su}}{f_{sy}}\right]^2$$

Direct tension tests on concrete prism specimens have been performed by some researchers (Shima *et al.*, 1987; Mayer and Eligehausen, 1998; Patel *et al.*, 2014) to study the effect of inelastic bar strains at the slightly larger scale compared to bond pull-out tests. The concrete prism typically contains a single reinforcing bar to represent a RC element within a larger ductile RC component. Primary cracks are either initiated by pre-notching the concrete or the cracks are naturally formed, after which the formation of secondary cracks and the elongation of the reinforcement (locally and globally) is of particular interest. The most important indicator of ductile behaviour is the ratio of the local strain measured at a primary crack ε_{sr} to the average strain $\overline{\varepsilon_{sm}}$ over the gauge length of the specimen. It is important to realise, however, that observations and results from these types prism tests may be of limited value if the specimen cracking behaviour is influenced by incorrect boundary conditions of the testing set-up which, unfortunately, leads to an unrealistic first crack formation (such as the tests presented in Huffadine *et al.*, 2015).

In the Mayer and Eligehausen (1998) study, strain gauges were placed in grooves that were formed in the longitudinal ribs of the deformed bar in an attempt to mitigate any compromise of the undisturbed bond condition. Figure 3-15(a) presents an example of the steel strain distribution of a 2000 mm long prism with a concrete strength of 30 MPa and reinforcement ratio of 0.5 percent. Eligehausen, Ozbolt and Mayer discuss their research in further detail in Paper SP180-3 in ACI Committee 408 (1998). Figure 3-15(b) illustrates the ratio of the post-yield steel stress to the yield stress f_t/f_y has a significant effect on the overall ductility of the RC prism. The steel's post-yield stiffness provides a useful indicator of whether the ductility of the reinforcement can be utilized most effectively without developing severely large local strains at the crack.

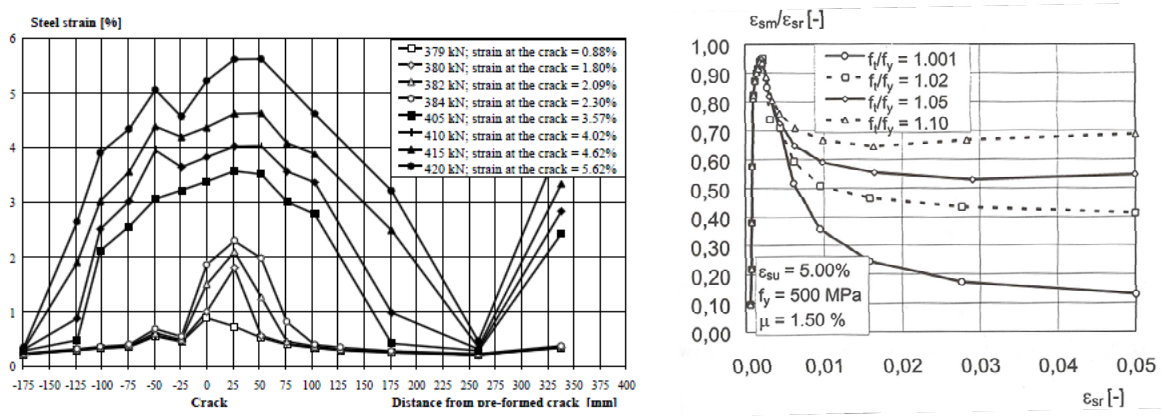

(a) **(b)**

Figure 3-15: (a) Reinforcing steel strain measurements for increasing axial load (Mayer and Eligehausen, 1998); (b) experimental results showing influence of f_u/f_y on the overall ductility of the RC prisms (SP180-3: ACI Committee 408, 1998).

For a common grade of reinforcing steel that exhibits a large amount of strain-hardening (f_u/f_y greater than 1.20), the ductility of the RC prism can generally described at different levels of strain at the crack:

- Once the steel reaches first yield at a primary crack then the ratio $\overline{\varepsilon_{sm}}/\varepsilon_{sr}$ reduces very suddenly as the total elongation of the specimen is due only to the localised inelastic strain at the cracks.
- The smallest value of $\overline{\varepsilon_{sm}}/\varepsilon_{sr}$ occurs at the onset of strain-hardening at the crack (ε_{sr} $\approx$ 0.015-0.020).
- The value of $\overline{\varepsilon_{sm}}/\varepsilon_{sr}$ increases in proportion with the increase of ε_{sr} once appreciable strain-hardening can occur at the crack.
- Once the steel stress tends towards the ultimate value f_u the relationship between $\overline{\varepsilon_{sm}}/\varepsilon_{sr}$ and ε_{sr} reaches a plateau. This ratio decreases once the ultimate strain is exceeded, until fracture occurs.

Mayer and Eligehausen (1998) also showed at strains exceeding 0.05 that the $\overline{\varepsilon_{sm}}/\varepsilon_{sr}$ was equal to 0.4 when the reinforcement ratio was 0.5 percent and compared to $\overline{\varepsilon_{sm}}/\varepsilon_{sr}$ was equal to 0.7 when the reinforcement ratio was 1.5 percent. The studies by Shima *et al.* (1987), Bonacci (1994b) and Mayer and Eligehausen (1998) concluded that the behaviour of the specimens was significantly affected by the reinforcement ratio, the ductility of the reinforcement and the increase in steel stresses due to strain-hardening (i.e. post-yield hardening stiffness).

With these conclusions in mind, the stress-strain characteristic of reinforcing steel that is available in other countries will have some comparative differences with the conventional reinforcing steel used in New Zealand. Figure 3-16 illustrates some examples of stress-strain behaviour obtained from direct tension tests on Grade 300 and 500 steel samples. The average stress-strain behaviour of the Grade 300 steel was taken from over 200 samples from Pacific Steel samples in a study by Davies-Colley *et al.*, (2015), whilst the behaviour of the Grade 500 steel is based on direct tension test results by the author (as a later part of

this research programme). Both steel grades exhibit significant strain hardening which is a favourable characteristic in terms of the formation of secondary cracks such that the ductility is improved. The f_u/f_y ratio for Grade 500E reinforcing steel is on the order of 1.25, which is somewhat less than the Grade 300E steel where the mean ratio f_u/f_y is on the order of 1.43 (Davies-Colley *et al.*, 2015).

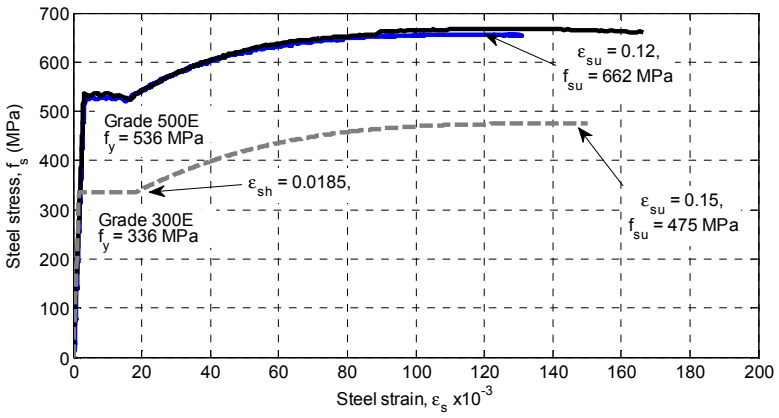

Figure 3-16: Stress-strain behaviour of Grade 300E and Grade 500E reinforcing steel samples from direct tension tests.

3.3.2 Surrounding concrete properties

It is intuitive from the discussion in Section 3.2.1 that concrete strength significantly influences bond behaviour, particularly the bond stiffness and maximum bond strength. Chapter 2 discussed some reasons for high in-place concrete strength in real structures and the implications this may have on structural behaviour. Concrete is a highly variable material and the mechanical properties (stiffness, compressive and tensile strength) is influenced by a large number of factors. The most important factor in construction practice is the quality of workmanship that is most involved in concrete mixing, placing and curing. Additional awareness and care is needed when the supplied concrete is substantially stronger than what is specified in design, particularly when using precast concrete elements. Putting the "human element" and aside, the following sections discuss aspects of the surrounding concrete that are deemed to be most relevant.

3.3.2.1 *Mix properties*

The mechanical properties of the concrete will fundamentally depend on the quantity and type of binder and the quantity, size, porosity and angularity of the aggregates used. The hardened concrete properties may also depend on the location within New Zealand from which the types of aggregates were sourced (Mackechnie, 2003). This influence of aggregate size may be relevant for the splitting failure mode, but is expected to be less relevant for pull-out failure because there is only cement paste and perhaps some sand particles harden at the interface between the ribs of the deformed bar. Design codes typically require that the anchorage or development length is increased by 1.3 times to account for the relatively lower

tensile and shear strength of lightweight concrete that has reduced bond strength. The effects of fresh properties of concrete and mix materials (such as lightweight concrete) on bond strength are included in the ACI Committee 408 (2003) report but are not discussed further here.

3.3.2.2 *Casting direction and setting in the fresh state*

During casting, vibration and initial setting of the fresh concrete there is some segregation of the mix materials. Figure 3-17(a) schematically illustrates the consolidation of relatively heavy aggregates towards the bottom while bleed water and air voids rise to the top surface. In all cases the initial bond stiffness is influenced by the quality of the cement paste in front of the rib, the presence of bleed lenses and air voids, and how effectively the aggregates are distributed in proximity to the rib faces. The orientation of the bar with respect to the casting direction may result in differential bond conditions around the embedded ribs of the deformed bar. Vibration and re-vibration of the concrete will also have some effect on the bond condition.

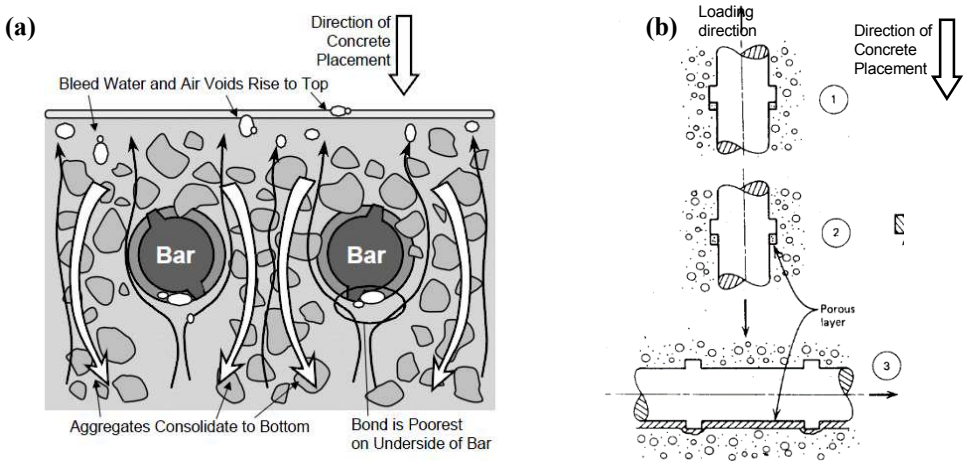

Figure 3-17: Schematic illustrations showing the influence of bar position and casting direction on the bond condition (a) from Thompson *et al.* (2002), and; (b) from Park and Paulay (1975).

The first segment in Figure 3-17(b) is an example where the bar is loaded against the casting direction and the bond stiffness will greater compared to when loaded in the opposite direction (shown by the second bar segment). When the bar axis is perpendicular to the casting direction there will be relatively spongey layer along the underside of bar due to the trapping of bleed lenses and air voids which may result in an uneven distribution of bond stresses around the bar (Fenwick, 1982). The "top-bar effect" is widely recognised in design practice and codes, accepting the reduced bond strength for the top layers of reinforcement due to segregated mix materials when a thick layer of fresh concrete is placed beneath the bar.

3.3.2.3 *Concrete strength and stiffness*

The compressive stiffness of the concrete (defined by the elastic modulus E_c) also has some effect on the pre-peak bond stiffness, although to a much lesser extent compared to the variation of concrete strength. The positive effect of higher concrete strengths was shown in early bond tests by Abrams (1913) and more recently by Vos and Reinhardt (1982) and Eligehausen *et al.* (1983).

The literature generally states the maximum bond strength is proportional to the square-root of the cylinder compressive strength $\sqrt{f'_c}$ for conventional structural concretes (f'_c < 60 MPa) which is supported by the normalised test results in Eligehausen *et al.* (1983). This notion seems reasonable given that bond stresses will induce a combination of axial and shear stresses in the concrete. The theory of Mohr's circle suggests that the principle tensile stress and maximum shear stress of the concrete can be expressed as a square-root function of the axial compressive strength, although at the bond region a pure concrete shear failure cannot occur due to the large bearing stresses.

The Model Code 2010 (*fib*, 2012) considers that the bond strength is proportional to f'_c to the power of 1/2. Anchorage and development length expressions in NZS3101:2006 use the power of 1/2 whilst Eurocode 2 (2005) suggests the power of 2/3 and ACI Committee 408 (2003) suggests the power of 1/4. A recent study by Soleymani Ashtiani (2013) investigated bond behaviour where high strength self-compacting concrete (100 to 110 MPa) developed bond stresses between 30 and 40 MPa prior to fracturing the reinforcing steel.

3.3.2.4 *Concrete age and construction era*

The mechanical properties of concrete within an existing structure will be influenced by the "concrete age" (the amount of time after casting) and the particular construction era (the Portland cement blend). Short term concrete strength development (up to 90 days) is well understood from experimental testing on plain concrete samples and by the generalization of Abrams law. Previous bond tests were usually completed around 28 days after the specimens were cast or closer to 90 days to reduce the between-specimen variability (Kivell, 2011; Soleymani, 2013). It is important to recognise the long-term strength development of concrete for the purpose of assessing the concrete strength and bond behaviour within an existing structure that may vary in age.

Some test results are available for the static strength of concrete samples of up to 50 years old (Withey, 1961; Washa, 1975). Figure 3-18(a) illustrates tensile test results from Withey (1961) for samples that were made in 1910 and cured in three different conditions. This study also found the compressive strength continued to increase between 10 and 50 years. Results reported by Washa and Wendt (1975) showed that the tensile strength was approximately 1.20 and 1.25 times the 28 day strength (4.7 MPa) at 10 and 25 years after casting respectively, whilst after 50 years the strength ratio decreased to 1.15. The literature agrees that aged concrete is stronger but more brittle than young concrete.

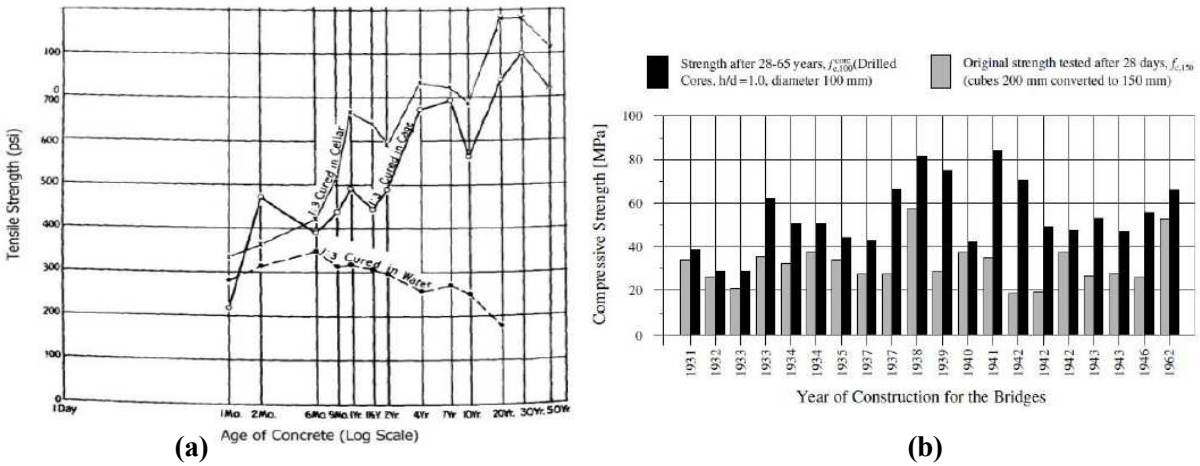

(a) **(b)**

Figure 3-18: Static test results on the effects of concrete maturity: (a) Tensile strength of concrete over 50 years (Withey, 1961); (b) Compressive strength results from concrete samples taken from existing bridges in Sweden (Thun *et al.*, 2001)

Levtchitch *et al.* (2004) presented a study on the static and dynamic behaviour of concrete of up to 30 years old and attempted to reproduce the mix properties and curing conditions so a comparable "young concrete" could be tested at 28 days. The results showed that older concrete had a greater stiffness than young concrete even if the compressive strength was not increased. Other interesting findings include that the ratio of dynamic tensile-compressive strength of old concrete is two times lower than for young concrete. The ability to reliably reproduce a mix for young concrete is very difficult so these results and comparisons to old concrete samples are rather questionable.

Figure 3-18(b) presents the results from Thun *et al.* (2001) on a study of 20 existing bridges in Sweden that were constructed between 1931 and 1962. The 28 day samples that were originally prepared during casting are compared to cores samples that were extracted between 1990 and 1994 to show a noticeable strength increase. Extracted samples from eight railway tunnels constructed between 1965 and 1980 had compression strengths between 60 and 85 MPa, which is potentially 40 and 90 percent greater, respectively, than the 28 day strength that was specified. Strength increases of this magnitude are often neglected in practice but potentially warrant further consideration. It should be noted that different blends of Portland cement have been used in the last 100 years where the main differences are the fineness and the content of di-calcium silicate (C_2S) and tri-calcium silicate (C_3S). Modern construction practice has benefitted from an increase in C_3S (Thun *et al.*, 2001) which means concrete can develop high early-age strength. Reductions in C_2S content have perhaps reduced the amount of strength development at late age, or in some cases low values of C_2S have resulted in strength reductions between 10 and 25 years old (Washa and Wendt, 1975). A relatively large proportion of C_2S might explain the long term strength development observed by Withey (1961) and Thun *et al.* (2001).

3.3.2.5 *Cover thickness*

The relative amount of concrete surrounding the deformed bar will depend on the cover thickness and the condition of the member once cracking has developed. At the bar interface the concrete is in a passively confined state as the total concrete mass is effectively restrained. Increased cover thicknesses and embedded bond regions away from crack surfaces will have good bond conditions.

The occurrence of bond splitting failure (described Section 3.2.2.2) depends on the thickness of cover concrete and the spacing between other highly stressed reinforcing bars. The hoop tensile stresses shown in Figure 3-6 will decrease linearly with radial distance away from the interface. Bond test specimens are often designed with a relatively massive concrete volume with large cover thickness with the aim of suppressing splitting failure to achieve a pull-out failure.

NZS3101:2006 considers the cover thickness for more refined calculation of the development length of deformed bars. Cover thickness is also considered in bond stress-slip expressions in the Model Code 2010 (*fib*, 2012) when the occurrence of splitting failure is anticipated. In a lightly reinforced concrete wall the vertical reinforcement may be spaced at 300 to 400 mm centres and are either doubly reinforced (two layers) with reasonable cover or singly reinforced such that the clear cover may be greater than 90 mm thick. Thick cover concrete and large between-bar spacing therefore means the bond conditions are very good for developing large bond stresses.

3.3.3 State of stress

3.3.3.1 *Transverse reinforcement*

Figure 3-8(b) showed how the presence of transverse reinforcing, or "confining steel", will delay the onset of splitting failure. Byrne (2012) found that anchored beam bars could sustain larger bond stresses when the quantity of vertical reinforcement in the beam column joint was increased (more vertical column bars and stirrups in the joint). The concrete core has greater confinement due to vertical bars effectively 'clamping' the development zone (Eligehausen *et al.*, 1983; ACI Committee 408, 1992; *fib*, 2000; Byrne, 2012). If a splitting failure might occur, the density and configuration of transverse reinforcement around the deformed bar is considered within the bond stress expressions in the Model Code 2010.

3.3.3.2 *Influence of transverse stresses*

Considering the bond mechanism described in Section 3.2.1, hoop tensile stresses develop in the concrete surrounding the bar. If transverse compressive (confining) stresses act perpendicular to the bar axis, within the vicinity of the bond zone, this will reduce the prorogation of bond cracks and bond failure will be delayed and the bond strength will be enhanced. The extent of this influence will depend on the magnitude of confining stresses and the concrete compressive strength. An example of confining stresses affected bond is shown at the direct support in Figure 3-1. In a beam-column joint, for example, the longitudinal

beam bars have greater bond stresses due to transverse stresses caused by axial compression loads in the column.

Test results from Eligehausen *et al.* (1983) showed that increasing transverse compressive stresses had a positive influence on bond strength. A plateau is eventually reached where larger transverse/radial compressive stresses no longer enhances the relative bond strength. The bond-models suggested in Lowes *et al.* (2004) and the Model Code 2010 (*fib*, 2012) include a modifying parameter that accounts for the effect of confining stresses as illustrated in Figure 3-19(b).

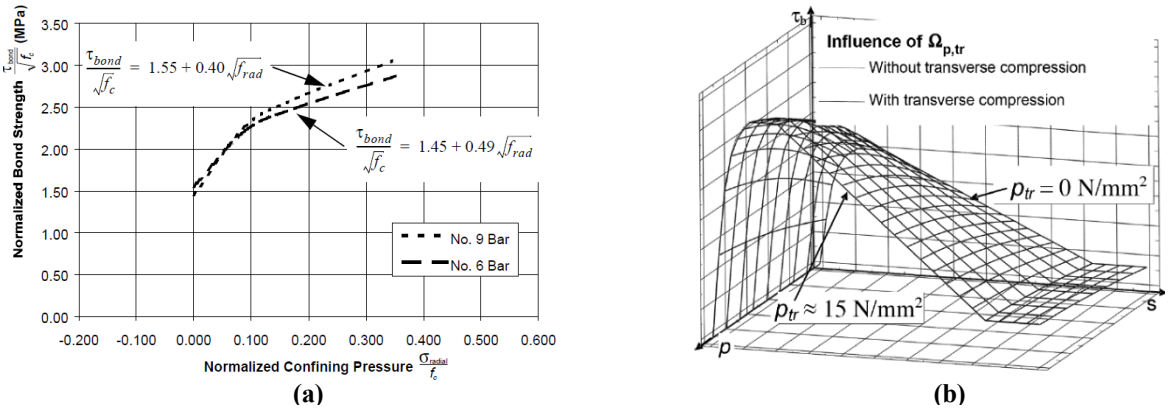

Figure 3-19: Enhanced bond stress-slip relationship due to transverse stresses (a) empirical relationship from in Lowes (1999); (b) bond modifier in the Model Code 2010(*fib*, 2012).

Transverse tensile stresses may also reduce bond strength. For example, the formation of plastic hinges in transverse beams at a two-way beam column joint will reduce the joint confining stresses and therefore reduces the bond strength for longitudinal beam bars.

3.3.3.3 *The influence of longitudinal cracking*

The presence of tensile stresses transverse to the bar axis may reduce the bond strength. In some RC components there may be instances where longitudinal cracks form parallel to the bar axis which, depending on the crack width, may result in a reduction in the bond strength (Mahrenholtz, 2012). Large flexural deformations may result in longitudinal cracks forming along the reinforcement anchored into column footings and along the beam bars in beam-column joints as illustrated in Figure 3-34(a). If there are large shear stresses acting on the component then dowel cracking might develop as shown by Figure 3-20(b) and bond strength in this vicinity may be further reduced.

Considering the interior beam-column joint, the flexural tension corners typically form longitudinal cracks along the beam bars which act as a crack initiator in the joint zone. Under seismic actions the opening and closing of this crack will influence the bond condition. If the column bars yield in tension this crack width increases such that the concrete and bar ribs might disengage to some extent, hence reducing the bond resistance. Mahrenholtz (2012) considered this longitudinal cracking in experimental studies on bond behaviour as a physical basis for design considerations to permit reducing the development length required

for straight anchorages at column-foundation connections. The minimum development lengths stated in design codes are generally conservative as these expressions are typically derived from experimental tests where this longitudinal cracking can occur.

3.3.3.4 *Combined axial and transverse (shear) deformation*

The influence of shear deformation on the bond deterioration zone is described briefly here for the sake of completeness. Some RC components may be subjected to large shear stresses and shear displacements that will influence the extent of bond deterioration near a transverse crack greater than about 2 mm (once aggregate interlock is lost). Maekawa and Qureshi (1997) and Maekawa *et al.* (2003) focussed their research on the influence of coupled deformation from axial pullout and transverse dowel action at the bond deterioration zone, as schematically illustrated by Figure 3-20(a). At the crack plane, localised yielding occurs due to additional bending of the deformed bar which results in a reduced axial stiffness and mean yield strength of the reinforcement. If there is a lack of confining pressure and minimal restraint from the transverse reinforcement then large dowel forces mean that larger bond slip will occur. Figure 3-20(b) from Fenwick (1966) illustrates the development of dowel cracks that will also reduce the bond resistance by some amount which is expected to depend on the amount of steel providing dowel action, the density of stirrups supporting the longitudinal bars, and the tensile rupture strength of the concrete.

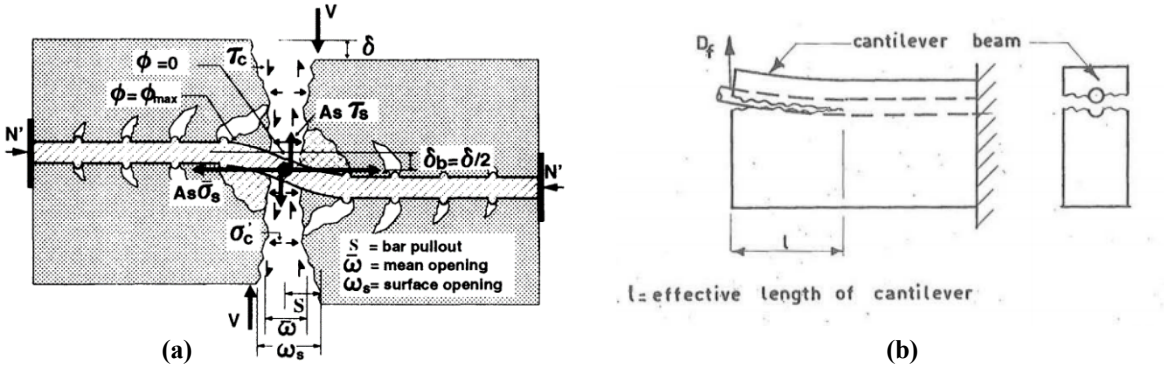

Figure 3-20: Schematic illustrations of transverse dowel action on the axially loaded reinforcing bar: (a) from Maekawa and Qureshi (1997); (b) from Fenwick (1966).

3.3.4 Type of loading

The influence of loading history and loading rate on the seismic performance of RC structures was previously discussed in Chapter 2. Tests on structural components (e.g. Goodsir, 1985) have shown that relatively steep strain gradients (hence large local bond stresses) may develop on the first loading cycle that is of significant amplitude, whilst strain gradients are reduced in subsequent loading cycles as damage sustained results in a redistribution of bond stresses. The remainder of the discussion presented below focuses on specific studies into the effects of loading history and loading rate on bond behaviour.

3.3.4.1 *Loading history*

Deterioration of the bond mechanism during cyclic loading was described in Section 3.2.3. Previous experimental investigations on cyclic bond behaviour have typically used test specimens with short embedment lengths (2 to $5d_b$). The report by ACI Committee 408 (1992) gives some references to cyclic bond behaviour. Aside from the study by Eligehausen *et al.* (1983), few consider the cyclic bond stress-slip response under low-cycle high-amplitude loading protocols that might be more realistic for structures subjected to earthquake-induced seismic loading. Balazs (1991) completed a cyclic bond study for relatively low-amplitude high-cycle bond behaviour where the maximum slip demand was ± 0.25 mm which means a significant amount of mechanical bearing resistance could be mobilised beyond this slip range.

Experimental tests by Hawkins *et al.* (1982) and Eligehausen *et al.* (1983) define the cyclic bond response under more appropriate loading histories for bond behaviour under severe seismic actions. It is intuitive from earlier discussion in Section 3.2.3 that full cyclic load reversals result in more significant strength and stiffness degradation compared to the same number of cycles under unidirectional loading. This was shown in test results of Hawkins *et al.* (1982) shown in Figure 3-22(a) and Figure 3-22(b)

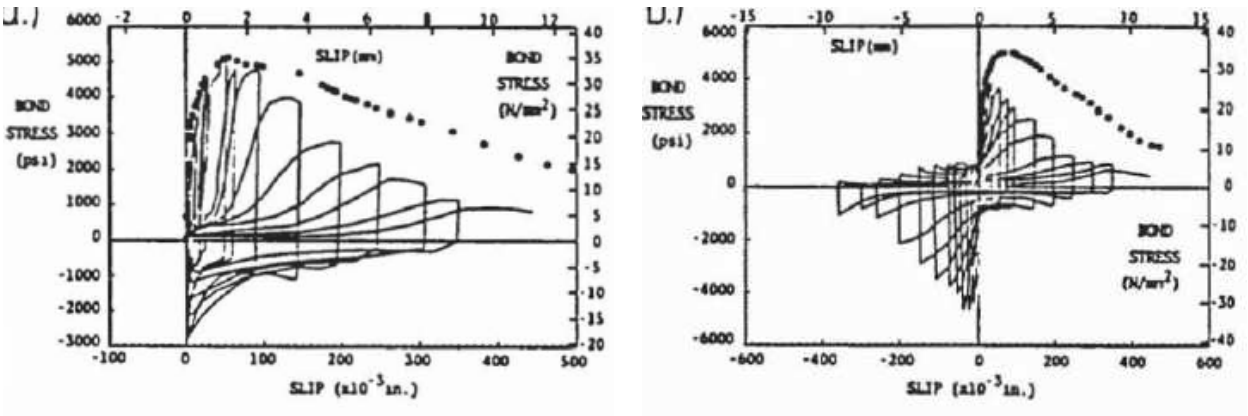

(a) **(b)**

Figure 3-21: Previous cyclic bond test results: (a) unidirectional cyclic and (b) fully reversed cyclic loading Hawkins et al. (1982).

Eligehausen *et al.* (1983) varied the loading history to different slip amplitudes as shown in Figure 3-22(a) and Figure 3-22(b) as the extent of bond degradation is primarily influenced by the peak slip from either previous loading direction. Figure 3-22(a) illustrates that if the peak bond stress is less than 70 to 80 percent of the monotonic bond strength during the first load cycle then the bond response on load reversal and larger slip values is not significantly degraded for up to ten repeated cycles. In contrast, Figure 3-22(b) shows that exceeding the ultimate monotonic bond strength on the first half cycle results in significant strength degradation during subsequent load reversals. Eligehausen *et al.* (1983) showed the influence of the number of load cycles on bond deterioration was of moderate severity compared to the influence of

peak slip amplitudes. Eligehausen *et al.* (1983) found that the majority of bond strength and stiffness degradation was observed in the first five loading cycles to constant slip values of 1.0 mm or greater.

Other experimental research with cyclic loading is found in the literature (Viwathanatepa *et al.*, 1979; Kivell, 2011; Murcia-Delso *et al.*, 2013; Soleymani Ashtiani, 2013). These studies generally use slip-controlled loading protocols where the slip amplitude is constant as in Figure 3-22(c), or gradually increasing fully symmetric load cycles such as in Figure 3-22(d). This type of loading is often adopted as the most severe case that a deformed bar may be subjected to however it is somewhat unrealistic of the structural behaviour that physically occurs in some RC components. Cyclic bond behaviour of deformed bars in grouted ducts (for precast joints) was experimentally studied Raynor *et al.*, (2002) who used a non-symmetric loading protocol as illustrated in Figure 3-22(e).

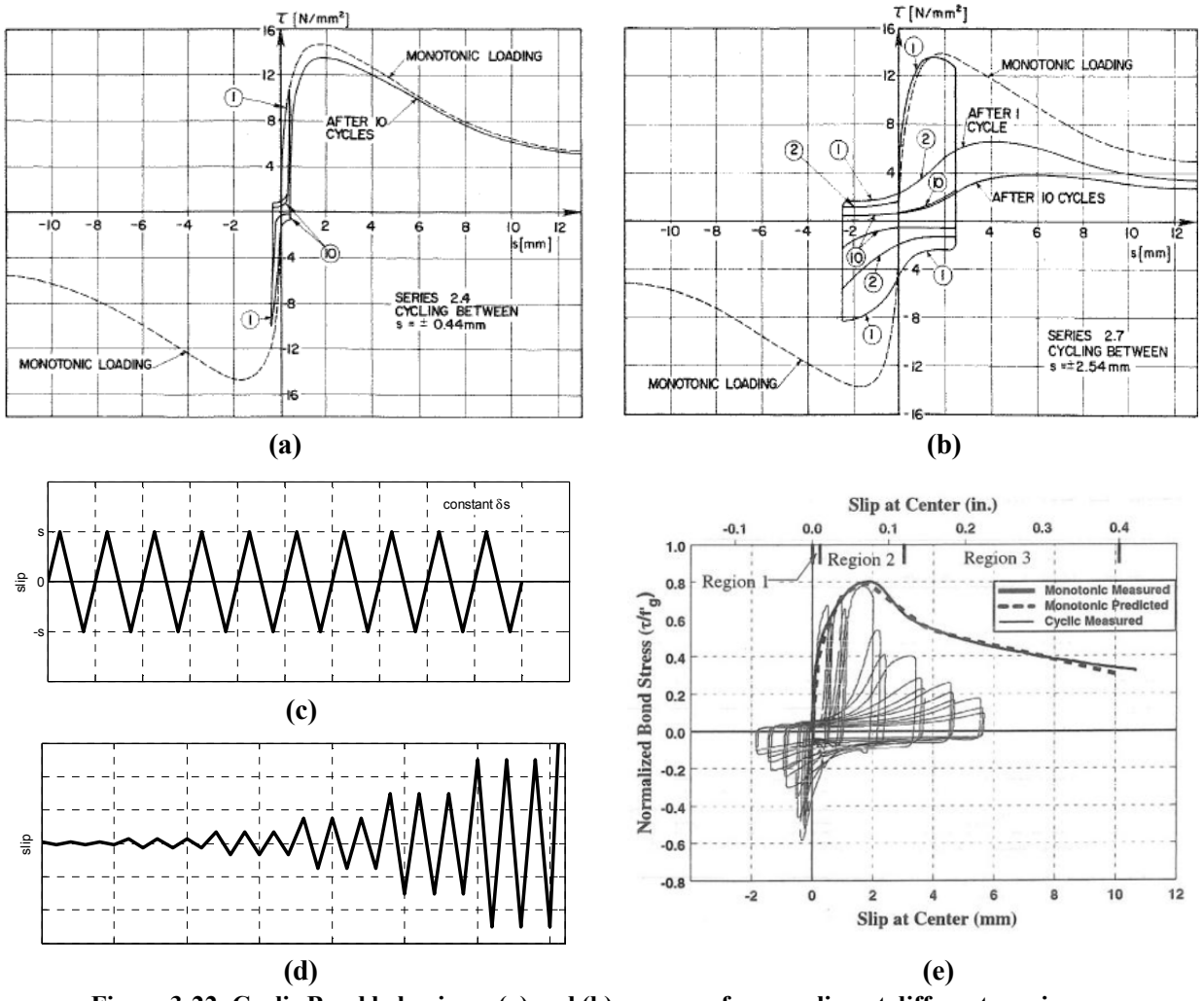

Figure 3-22: Cyclic Bond behaviour: (a) and (b) response from cycling at different maximum slips. (Eligehausen *et al.* 1983); (c) and (d) qualitative illustration of typical slip controlled cyclic loading protocols; (g) non-symmetric cyclic bond behaviour from tests by Raynor *et al.* (2002).

3.3.4.2 *Loading rate*

The influence of loading rate is highly important considering that earthquake-induced ground motions produce dynamic seismic actions that can have varying effects on the behaviour of RC structures. There are concerns that the apparent concrete strength increase during dynamic loading rates may result in undesired brittle failure of components (e.g. fracture of the reinforcement). This subject was described previously in Chapter 2 with reference to the Christchurch earthquake event on 22 February 2011.

Monotonic bond pull-out tests by Vos and Reinhardt (1982) found that deformed reinforcing bars have greater bond resistance when subjected to faster loading rates. Figure 3-24(a) shows for a 23 MPa concrete (cube strength) that the enhancement in bond strength at the fastest applied loading rate was about 60 percent greater, compared to the quasi-static loading. The bond strength at the highest loading rate was increased by 30 percent for a 45 MPa concrete and by 8 percent for a 55 MPa concrete as shown in Figure 3-24(b). The initial bond stiffness for all concrete strengths was increased. Results from this study show the loading rate does not significantly influence bond behaviour of plain round bars or prestressing strands. This finding suggests that frictional resistance is independent of loading rate; however the mechanical bearing resistance is largely influenced by loading rate.

> *"In the case of deformed bars the bond zone near a crack in concrete is shorter as the load is applied more rapidly… cracks will open less at the same steel stress in the crack if the load is caused by impact rather than by static action*" - Vos and Reinhardt (1982).

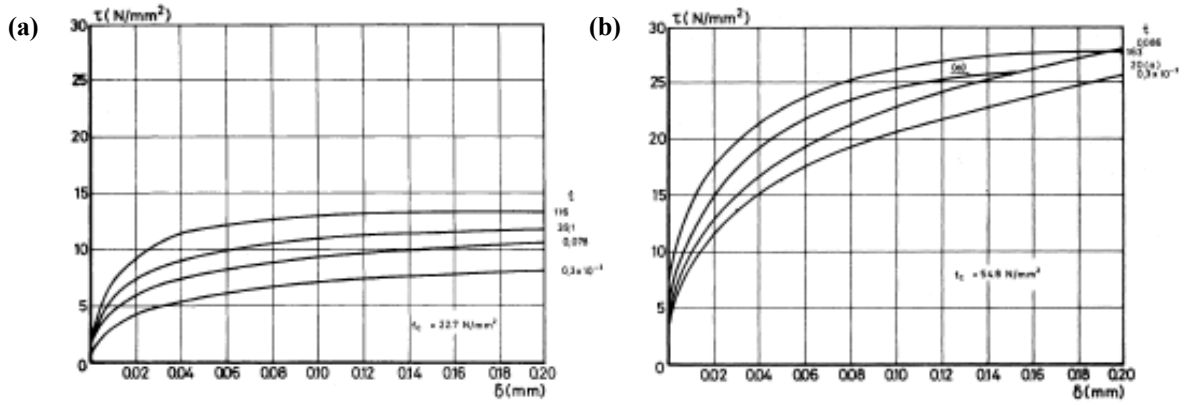

Figure 3-23: Observed bond stress-slip for (a) lower strength concrete, f'_c = 23 MPa; and (b) higher strength concrete, f'_c = 55 MPa (Vos and Reinhardt, 1982).

Eligehausen *et al.* (1983) did some tests studying loading rate with an applied maximum of 170 mm slip/min and results showed the maximum bond strength was 15 percent higher compared to tests at a loading rate of 1.7 mm/min.

Chung and Shah (1989) tested 12 ductile RC beam specimens under displacement controlled loading rates between 0.0025 to 2.0 Hz. Specimens subjected to slower loading rates showed a larger number of distributed cracks compared to the behaviour under fast loading rates. An array of internally mounted strain gauges in the anchorage region to measure the strain distribution. Faster loading resulted in a steeper

strain gradient near the loaded end, compared to a more gradual strain distribution along the anchorage under slower loading. Takeda (1984) also measured steeper strain gradients and hence more concentrated bond stress distributions under faster loading rates. Chung and Shah (1989) suggest that enhanced concrete strength, and hence greater bond strength, was the likely reason for localization of steel strains under faster loading rates. Faster loading of beam-column joint specimens resulted in fracture of the reinforcement at a lower displacement demand compared to the more ductile specimen behaviour under slower loading rates.

An assessment of a bond dynamic influence factor is presented by Michal and Keuser (2014) who summarises some studies on loading rate dating back to the 1960s. Figure 3-24 illustrates the experimental results that were studied, as well as some suggested trend lines for loading rate and the dynamic influence factor to be applied to the maximum bond strength. Michal and Keuser (2014) developed a bond model that accounts for increased localised bond strength near the loaded end of a longer anchorage, meaning that less bond stress distribution occurs under faster loading. No discussion of the modelling results is provided, however the results in Michal and Keuser (2014) suggest that bond strength enhancement for bar diameter of 20 mm further from the loaded end would have less dynamic influence compared to a 10 mm bar.

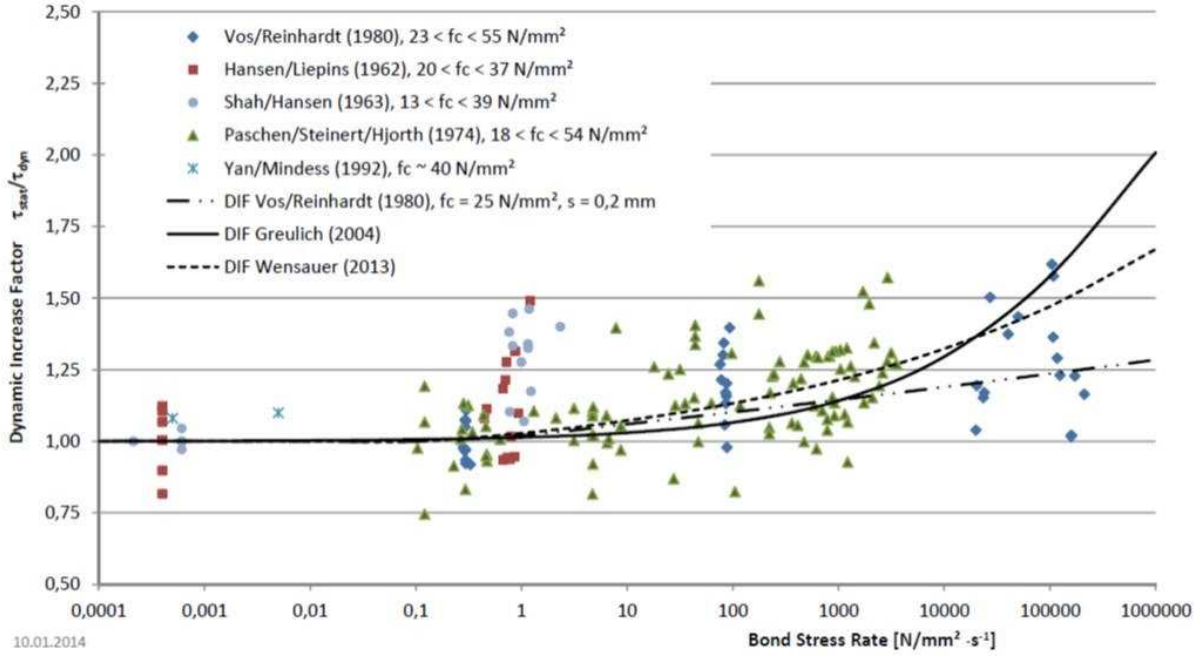

Figure 3-24: Previous results comparing bond strength and bond stress rate (Michal and Keuser, 2014).

Loading rate can be expressed in using a variety of metrics. Mahin and Bertero (1972) suggested the maximum steel strain rate, $\dot{\varepsilon}_s$ during dynamic seismic actions may range significant between 0.001 and 0.25 per second. As described in this section, other researchers have discussed loading rate based on bond slip rates (Eligehausen *et al.*, 1983) and bond stress rates (Vos and Reinhardt, 1982; Michal and Keuser,

2014). Lowes (1999) estimated the bond slip rate for an anchored reinforcing bar that had reached yield by using simplified expression shown in Equation 3-13.

$$\dot{s} = \frac{E_{sh}}{E_{bond}} \frac{d_b}{4\Delta x} \dot{\varepsilon}_s \qquad 3\text{-}13$$

where:

E_{sh} = post yield stiffness of the reinforcing steel

E_{bond} = secant stiffness of the bond stress-slip curve [Lowes (1999) assumed 20 MPa/mm slip]

d_b = nominal bar diameter

Δx = considered bar embedment length [Lowes (1999) considered a full anchorage length of $40d_b$]

$\dot{\varepsilon}_s$ = maximum steel strain rate as yielding occurs [Lowes (1999) assumed 0.03/sec].

Estimates by Lowes (1999) give a maximum bond slip rate of about 0.08 mm/sec and the associated bond stress rate may be around 1.6 MPa/sec. These loading rates are somewhat lower than considered by Eligehausen *et al.* (1983) and others as shown in Figure 3-24. Simplified calculations (discussed later in Chapter 6) suggest that, for the vertical reinforcement in the critical wall of the Gallery Apartments building, the maximum slip rate may be on the order of 2 to 5 mm/sec.

3.4 TEST SET-UPS AND MEASURED BOND BEHAVIOUR

3.4.1 Evaluation of bond behaviour from test results

Sections 3.1.3 and 3.1.4 described how the distribution of bond stresses and slip is defined in terms of the stresses and strains in the reinforcing steel and surrounding concrete and how the distribution (or average values) of bond stress and bond slip may be obtained. The bond strength that is measured in any type of bond test will be an average bond stress that is developed by the applied pull-out force along the embedded surface area (Park and Paulay, 1975). Bond behaviour reported from experimental research will be significantly influenced by the conditions under which the measurements were obtained. Relevant reports and bulletins by the ACI Committee 408 (1992, 2003) and *fib* (2000A, 2000B, and 2012) emphasize that the particular test set-up, loading arrangements and specimen particulars will influence the test measurements.

> "*Therefore test results must be treated with caution since they are representative for a specific set of conditions…"* (*fib,* 200A).

Chosen test arrangements and measurements need to reflect the particular bond-related information that is sought by each researcher. Section 3.1 described the different roles and performance requirements of bond within the different regions of RC structures. It is clear that a variety of testing approaches must exist in order to assess each particular aspect. As an example, the structural performance of splice region shown

in Figure 3-1 may be assessed by performing tests that study the stress transfer between the concrete and two lapped reinforcing bars. Different researchers are unlikely to investigate the same aspects of bond behaviour using the same experimental procedures and test arrangements due to the practicality of using the available resources and equipment (such as hydraulic actuators and testing machines).

Experimental measurements by Mains (1951) found the maximum local bond stress can be greater than twice the average stress that is usually reported for longer embedment lengths and is conservatively adopted in design standards. On one hand the average bond behaviour provides more useful information for the performance the longitudinal reinforcement in a beam under service loading and for the performance of anchorage zones, whilst on the other hand high local bond stresses and bond slip is the focus of this research. Local bond behaviour is most commonly assessed using pull-out specimens, and less commonly assessed using beam specimens, where a short embedment length is provided to ensure the average behaviour is approximately similar to the local behaviour as schematically illustrated in Figure 3-4(a). Pull-out tests and beam tests are described in the following sections. Experimental difficulties in determining the distribution of bond stress and slip from strain measurements are also presented.

3.4.2 Pull-out tests

Pull-out tests have been long been used (e.g. Abrams, 1913; Rehm and Eligehausen, 1979; Mahrenholtz, 2012) as the predominated bond test set-up due to the ease of constructing a large number of test specimens where a range of parameters can be isolated between different tests. It should be noted that the results from pull-out tests (particularly Eligehausen *et al.*, 1983) have been referred to in valuable documents such as Paulay and Priestley (1992) and the Model Codes (1993; 2010).

Figure 3-25(a) is a set of specimen details specified in RILEM/CEB-FIP (1982) for measuring bond. A simplified loading arrangement is schematically illustrated in Figure 3-25(b) for monotonic pull-out tests. Pull-out specimens are typically designed to meet some geometry requirements of specifications such as RC6 of RILEM/CEB-FIP (1982) for the embedded bond length, unbonded lengths, and the clear cover thickness; all of which are usually expressed in terms of the test bar diameter, d_b. The embedded length may be relatively long (for anchorage tests), or relatively short (3 to $5d_b$ for local bond tests).

Figure 3-4 illustrated the effect of the embedded length on the distribution of bond stresses. An un-bonded length (typically 3 to $5d_b$) is used to ensure there is a confined embedded region away from the free surface to mitigate failure by cone break out. The specimens may be square or circular in shape and the outer dimensions are usually taken as about 10 or $11d_b$ to ensure the splitting failure mode is suppressed and instead a pull-out failure can occur. This requirement for the cover concrete means that the total weight of the specimens increases and lifted by hand may become difficult. Figure 3-25(c) illustrates how many researchers (e.g. Kimura and Jirsa, 1992; Kivell, 2011; Patel *et al.*, 2014) have placed spiralled hoops as

transverse reinforcement around the deformed test bar to provide some resistance to splitting failure. This reduces the total concrete volume in the specimen so that handling by one person is made possible.

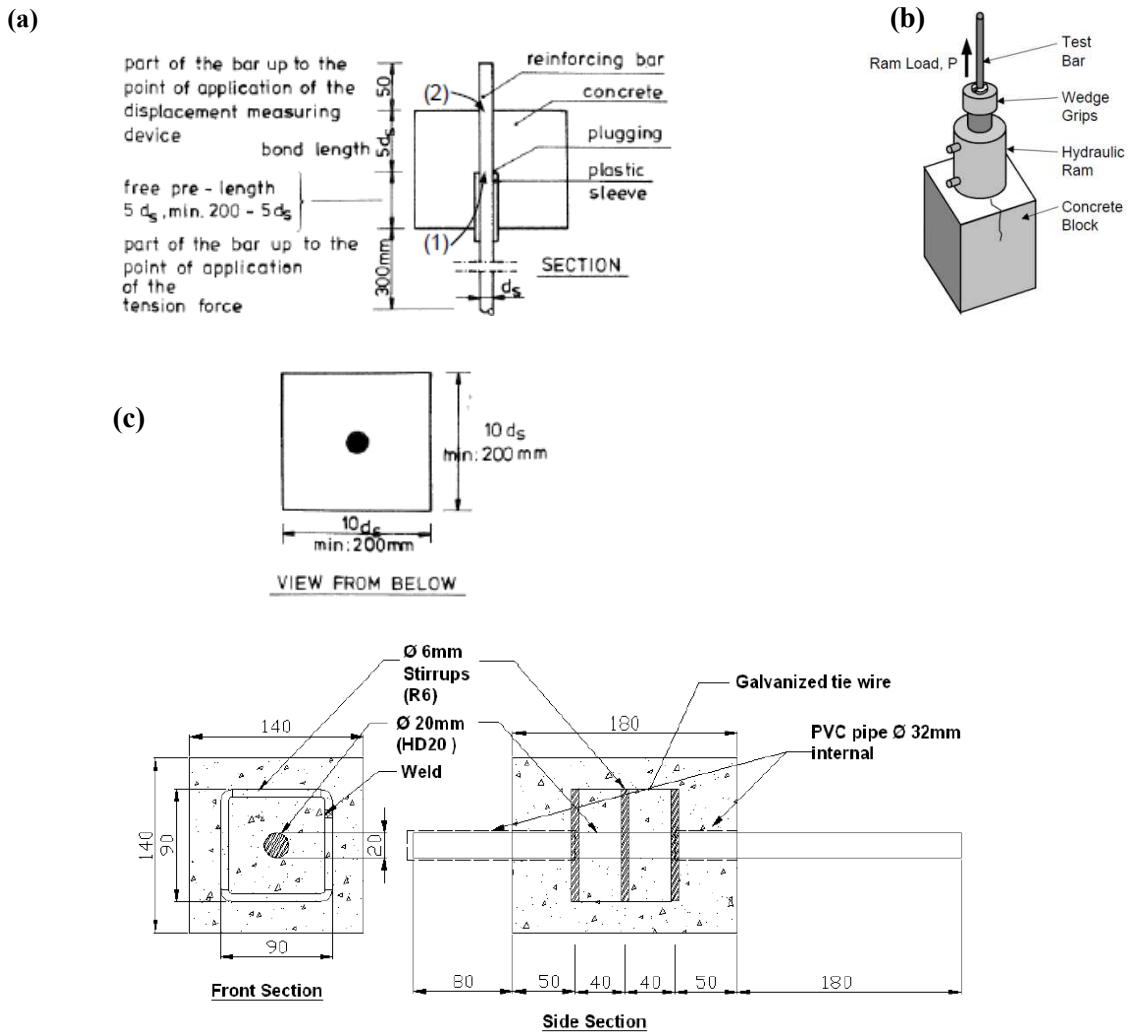

Figure 3-25: (a) Schematic illustration of the specimen details, (RILEM/CEB-FIP, 1982); (b) simplified loading arrangement (right, Thomspon, 2002) for the recommended set-up for monotonic bond pull-out tests; (c) drawings of pull-out specimens by Kivell (2011).

ETAG 001 (2006) specifies an unconfined and confined loading arrangement that may be used for assessing anchorage resistance. The unconfined set-up illustrated in Figure 3-26(a) requires that the loading reaction forces are spaced at some distance (a function of the embedment length) away to ensure the bond zone is unconfined and a natural concrete cone failure can occur at the free surface. Spacing of reaction plates often means that unconfined pull-out tests become less favourable as the specimen and loading frame can become relatively large. For this reason, the confined set-up shown in Figure 3-26(b) was developed to promote bar pull-out for long anchorages and short embedment lengths. In the latter case, ETAG 001 (2006) specifies that the reactions of the loading frame are applied near the axis of the bar through a hole in a bearing reaction plate that is 1.5 to 2.0d_b in diameter.

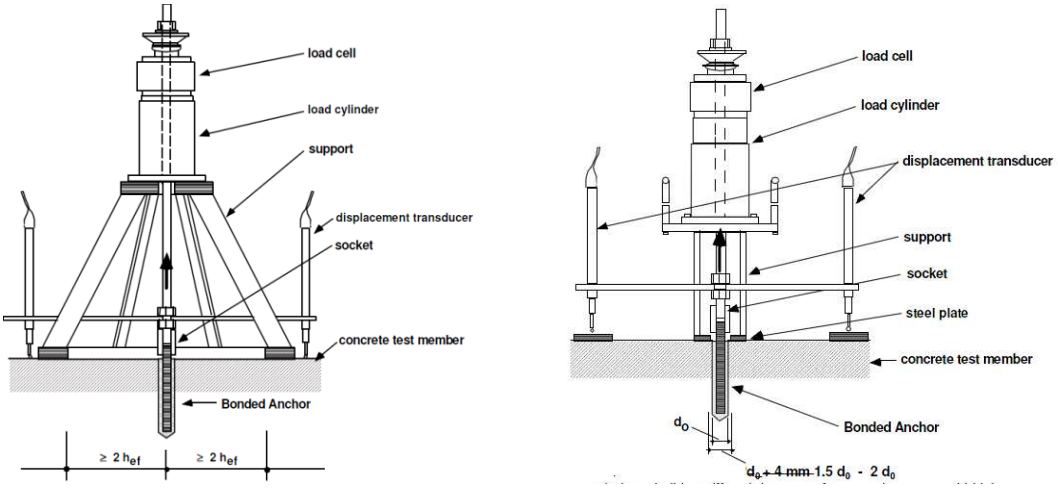

(a) **(b)**

Figure 3-26: Test set up specified in ETAG 001 (2006) – Part 5 for: (a) unconfined and; (b) confined.

Cyclic pull-out tests can be used whilst maintaining simple specimen details, but some modifications to the loading arrangement may be required. Figure 3-25(c) illustrates the specimen details from Kivell (2011) as an example. Test set-ups used to assess cyclic bond behaviour can be found in Eligehausen *et al.*, (1983), Balazs (1991), and Murcia-Delso *et al.*, (2013). Mahrenholtz (2012) modified the confined set-up specified in ETAG 001 (2006) such that the external pull-out force was applied and a separate actuator was used to apply a cyclic load in the direction transverse to the test bar. This was done in order to simulate crack opening and closing that might occur along the longitudinal reinforcement in the footing of RC columns.

3.4.3 Beam tests

One limitation of the confined pull-out set-up is that the reaction plate(s) bearing against the concrete will induce compressive stresses in the concrete, however the test bar is loaded in the opposite direction, such that the state of stress is unrealistic compared with the flexural tension side of a real RC structural component. This issue can be avoided by more complex specimen details and loading arrangements as illustrated in Figure 3-27(a) from the beam test that was specified in RILEM/CEB-FIP (1982) for assessing bond under monotonic loading. The "test bar" is embedded within a region inside two separate concrete blocks that deform rigidly under a centre point loading at a hinge in the mid-span. The length of the separate blocks is usually much greater than the required embedded length, which may be taken as 5 or $10d_b$ (RILEM/CEB-FIP, 1982; Soleymani Ashtiani, 2013). Past the unbonded lengths shown in Figure 3-27(a) the effective loaded ends are at points (1) and therefore the unloaded ends are at the points labelled (2).

The RILEM beam test shown in Figure 3-27(a) required some modifications to be used for assessing cyclic bond behaviour. Figure 3-27(b) is a photograph of the cyclic beam bending set-up used by

Soleymani Ashtiani (2013). Although the beam test may provide a more realistic state of stress within the specimen, this approach introduces additional complexities in the specimen design and loading arrangement that often restricts the total number of tests that can completed. For instance, Soleymani Ashtiani (2013) encountered the issue of the test bar buckling between the separate concrete blocks. As such, the cyclic loading protocol used in these tests was somewhat constrained by a need to limit the loading cycles that may prematurely fracture of test bar.

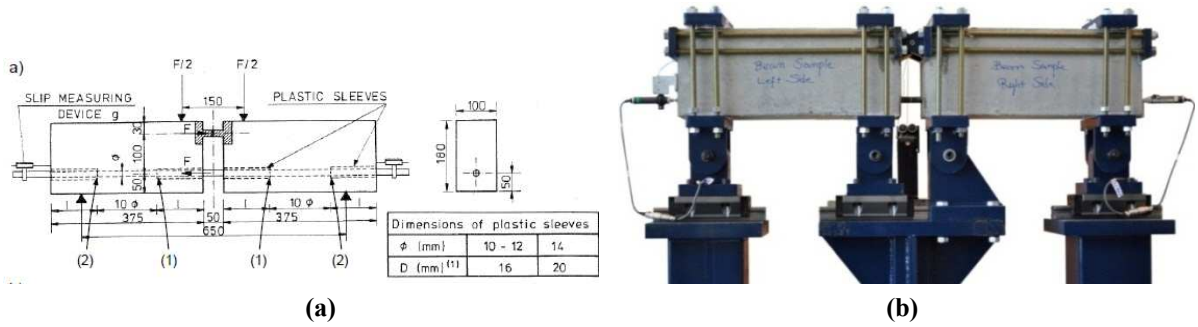

Figure 3-27: Details of the beam bending test specimens used to assess bond behaviour: (a) RILEM (1982) specimen for monotonic bond testing; (b) the modified RILEM beam specimen and test set-up used by Soleymani Ashtiani (2013) for cyclic loading.

Figure 3-28(a) illustrates the beam-end test (sometimes referred to as "semi-beam tests"); another standardised test method is that is specified in ASTM A944 (2010). This test set up resembles a combination of the pull-out test and the beam test. The specimen has a direct compression corner that is some distance away from the axis of the loaded test bar. This type of set-up is still relatively complex and modifications are required such that cycling loading can be applied.

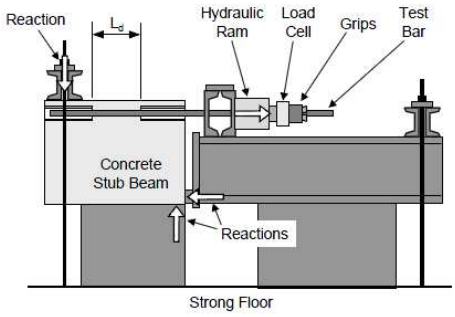

Figure 3-28: Example of a typical beam-end test stated in ASTM 944 (2010) (from Thompson *et al.*, 2002).

3.4.4 Deriving bond stresses from strain measurements

The bond stress distribution in a RC component or sub-assemblages may be obtained based on the strain distribution along the reinforcement. This approach might allow researchers to measure the large variations in bond stress in larger scale experimental tests when the reinforcing steel has yielded. The method of bond stress calculation is such that slip is determined from integrating reinforcing strains along the embedment length, and the corresponding bar stress is determined from the constitutive stress-strain

relationship. Bond stress is then determined using the definition of Equation 3-2 by the difference in bar stress between two strain gages.

Major limitations of deriving the bond stress distribution in this manner are due to the reliability of strain measurements and the potential for compounding errors. The instrumentation used by Shima *et al.* (1987) included strain gauges (and associated wiring) that were mounted to the bar surface, so the local bond condition around the bar perimeter was somewhat compromised. Conventional installation of strain gauges requires that ribs of the deformed bar are removed over a length of about 50 mm to improve the attachment of the gauge to the bar surface. After the gauge is glued onto the bar it is then covered by a layer of mastic tape. This is mostly problematic for those looking to obtain a relatively continuous distribution of strain measurements as the bond stress transfer is reduced. The other practical issue associated with using strain gauges to measure bond behaviour is that the wires to the strain gauges are damaged once bond slip increases and the measurement from the gauges is lost.

Some researchers were able to measure the strain distribution using electric-resistance strain gauges that were mounted in an interior duct through the centre of the reinforcing bars (Scott and Gill, 1987; Chung and Shah, 1989; Scott, 1996; Kankam, 1997). This conceptually simple technique was first introduced by Mains (1951). Firstly, two solid reinforcing bars are milled into two sections that may be rejoined such that the nominal diameter is unchanged. The size of the grooves (forming the duct) and the subsequent reduction in cross sectional area will depend on the number of gauges and wires required. The primary disadvantage of this approach is the increased labour in manufacturing the test bars. The gauges should be located as near to the bar centroid as possible to mitigate any local bar bending (Mains, 1951).

Improved strain measurement technology such as optical fibre strain gauges may be less disruptive to the bond conditions and reliable strain measurements may be obtained however this approach is very expensive.

3.4.5 Maximum bond strength from previous tests

This particular research is interested is the maximum "local" bond strength τ_{max} measured in previous bond tests on specimens with short embedment lengths (2 to $5d_b$) such that the uniform bond stress idealisation of Figure 3-4(a) is appropriate. Test results reporting the maximum applied load or maximum bond strength on longer embedment lengths (greater than $5d_b$) are typically reporting an average bond strength that is less than the local bond strength. Table 3-1 contains a sample of the maximum bond strength τ_{max} observed in previous experimental tests which are predominantly from pull-out tests. A relatively generalised version of the results is presented here for an appropriate range of reinforcing bar sizes (12 to 25 mm) and concrete strengths, with the exception of Soleymani Ashtiani (2013). Yielding of the reinforcing bar was observed in some of these tests (Viwathanatepa *et al.* 1979; Soleymani Ashtiani, 2013) which would have reduced the value of τ_{max} compared to an elastic bar.

The literature contains many other results for the maximum bond strength that are omitted from Table 3-1 as the test conditions and specimen particulars these were derived from are considered to be inappropriate for this research (Kimura and Jirsa, 1992; Walker *et al.*, 1997; Raynor *et al.*, 2002; Murcia-Delso *et al.*, 2013; Soleymani Ashtiani, 2013; Patel et *al.*, 2014). Other test results (e.g. Mahrenholtz, 2012) have not been included in Table 3-1 due to an insufficient number of repeated tests for a set of constant parameters. A fundamental assumption of the values presented for τ_{max} is that they can be normalised by $\sqrt{f'_c}$ for the purpose of comparing values between tests. Eligehausen *et al.* (1983) showed normalised test results obtained from different concrete strengths allows for very similar monotonic bond stress-slip relationships.

Another desktop study of the literature by Byrne (2012) found that the maximum bond strength under good bond conditions can reliably be taken as $2.5\sqrt{f'_c}$. Experimental results from Byrne (2012) found a higher τ_{max} of 2.7 to 3 times $\sqrt{f'_c}$ could be adopted for a particular beam-column joint anchorage detail for highly stressed beams reinforcement.

Table 3-1: General results for the maximum "local" bond strength in experimental tests

Study	Test type	Concrete strength, f'_c	Embedment length, l_e	Maximum bond strength, τ_{max}
Viwathanatepa *et al.* (1979)[1]	long anchorage pull-out	30 MPa	-	15 MPa ($2.7\sqrt{f'_c}$)
Hawkins *et al.* (1982)	pull-out	45 MPa	$2d_b$	34 MPa ($5.0\sqrt{f'_c}$)[1]
Vos and Reinhardt (1982)[2]	pull-out[3]	20 MPa[4] 35 MPa[4] 45 MPa[4]	$3d_b$	8 MPa ($1.7\sqrt{f'_c}$) 17 MPa ($2.9\sqrt{f'_c}$) 25 MPa ($3.7\sqrt{f'_c}$)
Eligehausen *et al.* (1983).	pull-out	30 and 55 MPa	$5d_b$	14 and 19 MPa ($2.6\sqrt{f'_c}$)
Fang *et al.* (2006)[2]	pull-out	22-43 MPa	$4d_b$	22 MPa ($2.9\sqrt{f'_c}$)
Kivell *et al.* (2011)[2]	pull-out	65 MPa	$4d_b$	32 MPa ($4.0\sqrt{f'_c}$)
Araujo *et al.* (2013)	pull-out	60 MPa	$5d_b$	20 MPa ($2.6\sqrt{f'_c}$)

Notes:
[1] Deduced from strain gauge measurements along a 635mm anchored reinforcing bar
[2] Results from typical materials and test conditions (e.g. no dynamic loading/corrosion/steel-fibres)
[3] Bond stress at 0.2 mm end slip; not tested/reported to failure in Vos and Reinhardt (1982)
[4] Approximate values from cube strengths

Table 3-1 shows there is appreciable scatter in the values of τ_{max} which will largely be due two reasons:

1. Inherent variability between test results on nominally identical specimens using the same set-up;
2. Combined inaccuracies and variations in determining test results using different test set-ups, measurement techniques and specimen particulars.

The first point can be understood by appreciating the scatter between test results from Eligehausen *et al.* (1983) shown in Figure 3-29(a) from a series of specimens that were cast from the same batch of concrete. Figure 3-29(b) shows some additional scatter arising due to different concrete batches although the concrete quality was well controlled with f'_c between 28 and 31 MPa. In construction practice the variation in the concrete quality will be significantly greater and this should be recognised when considering the probable bond strength.

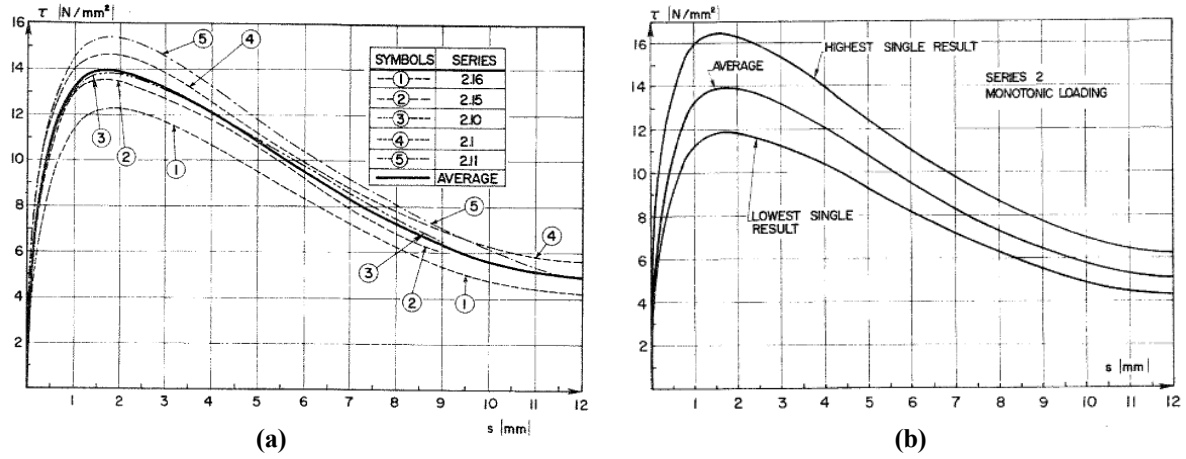

Figure 3-29: (a) Monotonic bond stress-slip relationship for nominally identical specimens, and (b) Scatter of bond stress-slip relationship from Tests (Eligehausen *et al.*, 1983).

An example of second point is briefly suggested here due to the difficulty in assessing and explaining the variations between studies. Table 3-1 shows the lowest value of τ_{max} is about 2.6 times $\sqrt{f'_c}$ while a substantially large value of $5.0\sqrt{f'_c}$ was found by Hawkins *et al.* (1982). Such high bond strength may be due to the shortest bond length of $2d_b$. Raynor *et al.* (2002) used test specimens comprising of deformed bars inside grouted ducts with an embedment length $2d_b$. In that study the measured cube strength of the grout was only 45 MPa yet a significant τ_{max} of 38 MPa was found. Lowes (1999) suggests a short embedment length of the loaded bar may mean the demand in the nearby concrete is relatively lower such that less damage occurs and an apparently higher strength is measured. This notion suggests an appropriate embedded length should be greater than $2d_b$ to ensure that the local bond strength is not excessively high.

3.5 CONSTITUTIVE RELATIONSHIPS FOR BOND BEHAVIOUR

3.5.1 Model Code 2010 monotonic bond stress-slip relationship

Section 3.1.4 discussed how bond stress is typically considered to have a unique relationship with bond slip that is largely independent of the position along the bar, with the exception of when the bond region within a particular bond deterioration zone near the crack plane or loaded end (refer to Section 3.2.4). Those who wish to undertake analytical modelling of bond behaviour must utilize a constitutive bond stress-slip relationship in order to solve the differential equation of bond (Equation 3-9). A variety of bond stress-slip relationships have been empirically derived from test results, such as those listed in Section 3.4.5. The need to have a bond stress-slip relationship that is reasonably generalised and simple is due to the variations between bond tests that have been performed and the scatter of test results.

Figure 3-30(a) illustrates the generalised monotonic bond stress-slip relationship in Model Code 2010 for splitting or pull-out failure. The bond response is only valid when the reinforcing bar remains in the elastic range. The values in columns (1) and (2) of Figure 3-30(b) are considered valid for well-confined bond regions where the clear cover is greater than $5d_b$ such that the concrete is relatively massive, or a dense arrangement of transverse reinforcement in the vicinity of the critical deformed bar. The bond stress-slip relationship for pull-out failure has not changed from earlier relationships such as in the Model Code 1990 (*CEB-FIP*, 1993 and 1996). More complex empirical expressions are found in the Model Code 2010 to account for factors such as cover dimensions and the presence of transverse reinforcement on bond splitting failure. Previous tests have indicated that the τ_{max} may be similar for splitting or for pull-out failure (Abrams, 1913) as the occurrence of these failure modes can be close together in certain conditions.

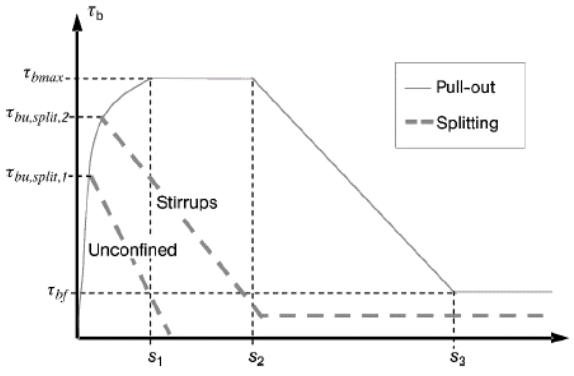

(a)

	1	2	3	4	5	6
	Pull-out (PO)		Splitting (SP)			
	$\varepsilon_s < \varepsilon_{s,y}$		$\varepsilon_s < \varepsilon_{s,y}$			
	Good bond cond.	All other bond cond.	Good bond cond.		All other bond cond.	
			Unconfined	Stirrups	Unconfined	Stirrups
τ_{bmax}	$2.5\sqrt{f_{cm}}$	$1.25\sqrt{f_{cm}}$	$2.5\sqrt{f_{cm}}$	$2.5\sqrt{f_{cm}}$	$1.25\sqrt{f_{cm}}$	$1.25\sqrt{f_{cm}}$
$\tau_{bu,split}$	–	–	$7.0\cdot\left(\frac{f_{cm}}{25}\right)^{0.25}$	$8.0\cdot\left(\frac{f_{cm}}{25}\right)^{0.25}$	$5.0\cdot\left(\frac{f_{cm}}{25}\right)^{0.25}$	$5.5\cdot\left(\frac{f_{cm}}{25}\right)^{0.25}$
s_1	1.0 mm	1.8 mm	$s(\tau_{bu,split})$	$s(\tau_{bu,split})$	$s(\tau_{bu,split})$	$s(\tau_{bu,split})$
s_2	2.0 mm	3.6 mm	s_1	s_1	s_1	s_1
s_3	c_{clear} [1)]	c_{clear} [1)]	$1.2s_1$	$0.5c_{clear}$ [1)]	$1.2s_1$	$0.5c_{clear}$ [1)]
α	0.4	0.4	0.4	0.4	0.4	0.4
τ_{bf}	$0.40\tau_{max}$	$0.40\tau_{max}$	0	$0.4\tau_{bu,split}$	0	$0.4\tau_{bu,split}$

(b)

Figure 3-30: (a) The analytical bond stress-slip relationship for monotonic loading; (b) Parameters defining the mean bond stress-slip relationship of deformed reinforcing bars according to Equations 5-6 to 5-9 (from the Model Code 2010, Chapter 6: Interface characteristics. *fib*, 2012).

Equations 5-6 to 5-9 defines the relatively simple bond stress-slip relationship for pull-out failure using the values stated in Figure 3-30(b) which depend on the quality of the bond conditions. The ascending

branch is defined by a power function α which must be representative of the effects of the relative rib area and concrete compressive stiffness on the initial bond stiffness and the slip s_1 at which the maximum bond strength τ_{max} occurs. τ_{max} is stated to be $2.5\sqrt{f'_c}$ for a plateau between slip values of 1 and 2 mm (s_1 and s_2) which is representative of severe crushing and shear cracking in the concrete between the ribs, as illustrated in Figure 3-7(c). Strength degradation due to a reduction of mechanical bearing is represented by a negative post-peak bond stiffness that linearly reduces from 2 mm slip and up until the clear rib spacing has been exceeded (expressed by s_3).

$$\tau = \tau_{max}(s/s_1)^{\alpha} \quad \text{for} \quad 0 \leq s \leq s_1 \qquad 3\text{-}14$$

$$\tau = \tau_{max} \quad \text{for} \quad s_1 \leq s \leq s_2 \qquad 3\text{-}15$$

$$\tau = \tau_{max} - \left(\tau_{max} - \tau_{bf}\right)(s - s_2)/(s_3 - s_2) \quad \text{for} \quad s_2 \leq s \leq s_3 \qquad 3\text{-}16$$

$$\tau = \tau_f \quad \text{for} \quad s_3 < s \qquad 3\text{-}17$$

A number of empirical expressions for obtaining bond response modifiers are listed in the Model Code 2010 which allows the influence of particular factors to be considered. For example, the "elastic bond response" is modified by a factor Ω_y that accounts for inelastic steel strains (discussed in Section 3.3.1.3). Supplementary discussion of some empirical expressions in the Model Code 2010 is given in *fib* (2014).

Section 3.1.4 described the relationship between bond stress and bond slip with steel strain. Strain is not explicitly considered in the Model Code 2010 bond model. Figure 3-31presents an example of how this relationship has been studied by others (Shima *et al.*, 1987; Soleymani Ashtiani, 2013). Discussion about this approach to modelling bond response is found in Maekawa *et al.* (2003). The application of any bond stress-slip-strain relationship will depend on the reliability of strain measurements.

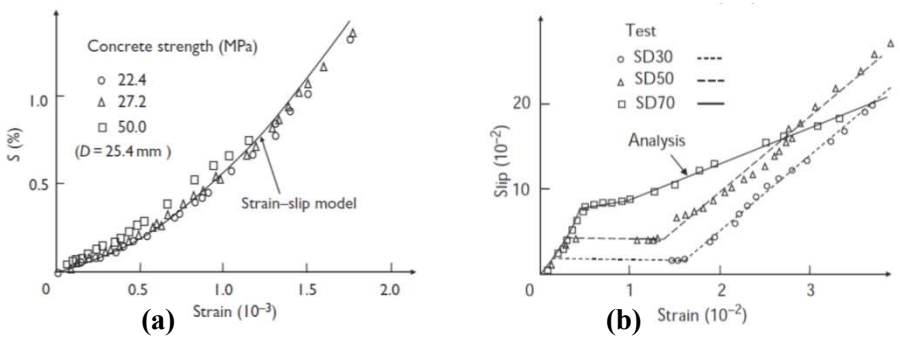

Figure 3-31: Local strain-slip relationship (a) elastic range, (b) post-yield range (Shima *et al.*, 1987).

3.5.2 Cyclic bond behaviour

Bond deterioration under cyclic loading results in a reduction in bond strength and stiffness. The physical degradation of the bond mechanism and the influence of loading history were discussed in Sections 3.2.3 and 3.3.4.1, respectively. Illustration of energy dissipated and the effects of cyclic loading on the reduced bond stress-slip relationship are qualitatively shown in Figure 3-32(a).

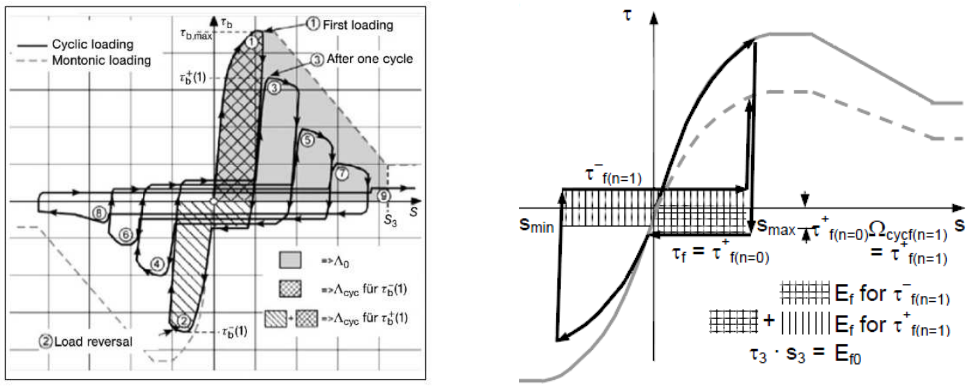

Figure 3-32: Definition of energy dissipated under monotonic and cyclic loading for (a) total bond resistance (Model Code 2010- *fib*, 2012), and; (b) frictional bond resistance (Mahrenholtz, 2012).

The Model Code 2010 uses the bond response modifier Ω_{cyc} stated in Equation 3-18 which is based on the hysteretic energy-based model for bond damage given in Eligehausen *et al.* (1983). The model parameters $a_1 = 1.2$ and $a_2 = 1.1$ are given in the Model Code 2010 from Eligehausen *et al.* (1983).

$$\Omega_{cyc} = \exp\left(-a_1 \left(\frac{E_{cyc}}{E_0} \right)^{a_2} \right) \qquad 3\text{-}18$$

where: E_{cyc} is energy dissipated during cyclic loading; and E_0 is energy dissipated during monotonic loading (note the energy parameters E are designated by Λ in Figure 3-32).

$$\Omega_{cyc,f} = \exp\left(-a_{1f} \left(\frac{E_f}{E_{0f}} \right)^{a_{2f}} \right) \qquad 3\text{-}19$$

Different levels of bond deterioration are likely to occur under different conditions. The co-efficients a_1 and a_2 can be determined from "curve fitting" with experimental data. Differences in these values may arise due to more subtle differences such as the size and geometry of the deformed bar that was tested, although more significant differences in the test conditions may lead to greater differences in the cyclic bond degradation. For example, Mahrenholtz (2012) assessed the same bond damage model in Equation 3-18 and combined the effect of crack cycling on the bond region and derived the model coefficients a_1 and a_2 as 2.5 and 1.0, respectively. Eligehausen *et al.* (1983) also presented a damage model for frictional resistance as illustrated in Figure 3-32(b). The parameter $\Omega_{cyc,f}$ shown Equation 3-18 is

presented in a similar form as before, where Eligehausen *et al.* (1983) suggested the coefficients were $a_{1f} = 1.2$ and $a_{2f} = 0.67$. The degradation of the frictional component is not separately considered in the Model Code 2010 due to a lack of interest or need to assess this compared with assessing the total bond damage based on Ω_{cyc}.

3.6 ADVANCED BOND MODELLING TECHNIQUES

A brief discussion of current bond modelling approaches is included here as this research is largely dedicated to an experimental investigation. In both research and in practice, computational models are widely used in predicting the force and deformation demands on a variety of structural systems when subjected to seismic actions. An example of the different resolution for bond modelling at macro- and micro-levels is schematically illustrated in Figure 3-33. Bond models have typically been developed assuming a pull-out failure occurs and do not account for splitting failure (Lowes, 1999).

The literature contains some earlier efforts to model bond slip behaviour in beam-column joints (Filippou *et al.*, 1983) and in ductile columns (Saatcioglu and Ozcebe, 1989). Commercial and Open Sourced software tools have become increasingly available and are continually advancing such that more complicated structural behaviour can be studied through modelling techniques. A technique that has often been used in practice for modelling RC walls is use an elastic link element between the wall base and centre-line of the foundation beam. Properties of the link element can be assigned to allow for bond slip which might occur before and after the reinforcing steel has yielded (Fenwick and Bull, 2002).

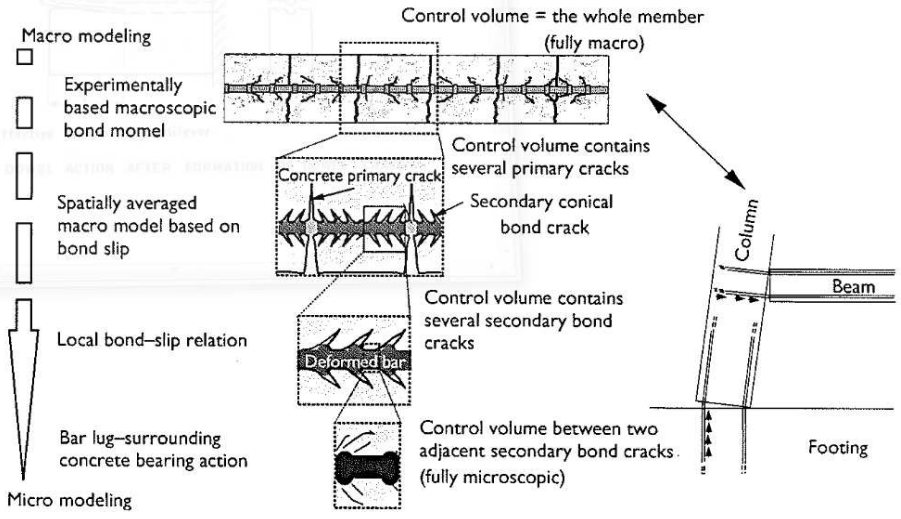

Figure 3-33: Hierarchy of bond modelling techniques (Maekawa *et al.*, 2003).

Johnson (2006) provides a comparison between different finite element modelling (FEM) approaches that can be adopted for RC structures within different software. Particular attention is given to comparing the element types and material models. Bond modelling capabilities described by Johnson (2006) are summarised in Table 3-2.

Table 3-2: Summary of bond modelling capabilities within different FEM software (Johnson, 2006).

Software:	Description:
ABAQUS	Tension stiffening along the structural component can be modelled and interfere elements can be used to model bond behaviour.
ADINA	Assumes perfect bond.
ATENA	Bond strength can be prescribed, otherwise interface elements can be used to model bond resistance. The Model Code 1990 (*CEP-FIB*, 1993) bond stress-slip relationship is available, for example.
DIANA	*Nodal*, *line* and *plane* interface elements can be used to model bond slip and discrete cracking. Bond stress-slip relationships are available.
OpenSees	Assumes perfect bond; prior to more recent work by Zhao and Sritharan (2007).
VecTor2	*Link* and *contact* elements can be used and the bond stress-slip relationship from Eligehausen *et al.* (1983) is one of the available options.
ZeusNL	Assumes perfect bond.

Some micro-modelling techniques (Lowes, 1999; Salem and Maekawa, 2004) use high resolution three-dimensional FEM to capture the material state and structural conditions that influences bond response. The complex bond model presented by Salem and Maekawa (2004) uses a very fine mesh size at the rib-concrete interface. The model can be considered to be highly accurate but also highly unpractical due to the time and complexity required in constructing the model and allowing for computational run time. For this reason, fibre-based modelling techniques are often adopted as a reasonable alternative to finite element modelling.

Zhao and Sritharan (2004, 2007) suggest a simplified fibre-based technique to account for yield penetration. A zero length fibre-section was developed for use in OpenSees (2012). This model was derived using experimental data from pull-out tests of yielding reinforcing bars in longer anchorage lengths. The application of the model is only for anchorages zones in column footings and bridge joints as the conditions in interior beam-column joints were deemed to be too complex to warrant detailed modelling based on the available experimental data. This approach might be a suitable approximation for modelling the behaviour of vertical reinforcement in walls. Further information is available at: https://pantherfile.uwm.edu/jzhao/www/Bond_SP01_pages/Bond_index.html

3.7 BOND CONSIDERATIONS IN PRACTICE

3.7.1 Maximum local bond stress

There are several reasons why values for the maximum local bond strength are not included in Parts 1 or 2 of NZS3101:2006. Some bond-related deficiencies are certainly considered in NZS3101:2006, however any reliance on τ_{max} to ensure adequate strength must be expressed with appropriate conservatism. A particular reason for omitting values for τ_{max} from NZS3101:2006 is to avoid confusion among practitioners who might attempt to design an alternative shorter anchorage/development length than is specified by existing design equations. The local bond strength should not be mistaken for average bond strength for the entire anchorage length, which may be approximately two times less (Mains, 1951; Au, 2010). The potential outcome of this misunderstanding is that the provided anchorage strength may be non-conservative.

Depending on the conditions, different standards typically state that the appropriate average bond strength along anchorages may be between 1.3 to 1.8 times $\sqrt{f'_c}$ (Paulay and Priestley, 1992; Hakuto *et al.*, 1999; Lowes, 1999).

For the purposes of assessing existing structures, probable and upper bound value for τ_{max} would be useful when assessing regions of concentrated inelastic deformations. The NZSEE (2006) seismic assessment guidelines does not currently suggest any values for the maximum local bond strength.

3.7.2 Predictions of crack width and crack spacing

The Model Code 2010 (*fib*, 2012) and other literature contain some formulae for crack width predictions which exist in design codes for practising structural engineers to use. Predictions of crack widths are usually are expressed in the form of Equation 3-20.

$$w_{crack} = k\,\frac{d_b f_{ct} \varepsilon_s}{\rho \tau} \qquad 3\text{-}20$$

where crack width is some function of:

k = a constant

f_{ct} = concrete tensile strength [MPa]

ε_s = steel strain, defined in a variety of ways.

d_b = actual bar diameter [mm] (typically 16 mm)

ρ = reinforcement ratio,

τ = either the average, or maximum, bond stress [MPa]

As discussed in Forth and Beeby (2014), expressions such as Equation 3-20 are generally based on one of three types of approaches that have different assumptions:

1. It is assumed crack width arises solely due to bond slip – the approach that was taken in the Model Code 1990 (*CEB-FIP*, 1993*)*.
2. Crack width is the assumed result of deformation of the concrete surrounding the reinforcing bar and the cracking is such that the stiffness of cover concrete is reduced. Bond slip is completely ignored
3. Crack width is assumed to be the combined result of bond slip and deformation of the surrounding cover concrete.

Forth and Beeby (2014) noted there are difficulties in determining the exact point along the reinforcing bar where the nearby crack ceases to influence the reinforcing steel strain. These difficulties would explain why the first approach, arguably the most simple of the three, has perhaps been the most widely adopted. However, Forth and Beeby (2014) note that crack width predictions have typically ignored the crack 'shape'. Their finite element analyses showed that the crack width at the bar interface is somewhat less than the crack width at the concrete surface due to shear deformation of the unrestrained cover concrete that surrounds the axially loaded reinforcing bar. If bond slip is significant, the results in Forth and Beeby (2014) suggest that the third approach is correct and crack width will predominately depend on the cover concrete thickness and the bond stress-slip behaviour. Both of these factors appear to have been considered in crack width predictions in Section 7.6.4 of the Model Code 2010 (*fib*, 2012).

One example of crack width prediction is found in Engstrom (1992) which follows the first approach stated above, using reasonably comprehensive inputs defining physical material and bond behaviour. Prior to yielding of the reinforcing bar, the crack width due to elastic bar elongation is estimated by Equation 3-21, while additional crack opening due to plastic elongation in the post-yield range is estimated by Equation 3-22. Equation 3-22 was derived from experimental tests where the deformed test bar was yielding. Therefore, the co-efficient k was derived to allow for strain hardening of the reinforcement and the effect of large inelastic strains causing bar-diameter reduction and a reduced bond strength (reduced from the maximum monotonic 'elastic bond strength', τ_{max}). If there is no strain-hardening, that is $f_{su} = f_{sy}$, then it can be seen in Equation 3-22 that there will be no additional crack opening due to bar yielding.

$$w_y = 0.576 \left(\frac{d_b \, {f_{sy}}^2}{\tau_{max} E_s} \right)^{0.714} + \frac{f_{sy}}{E_s} 4 d_b \qquad 3\text{-}21$$

$$k = \frac{f_{sy} \left({f_{su}}/{f_{sy}} - 1 \right)}{0.28 \tau_{max}} \frac{d_b}{4} \qquad 3\text{-}22$$

$$w_p = k \, \varepsilon_{su}$$

$$\therefore w_{crack} = w_y + w_p$$

where:

d_b = actual bar diameter [mm] (typically 16 mm)

E_s = the elastic modulus of the reinforcement [MPa]

ε_{su} = the ultimate tensile strain of the reinforcement (prior to fracture)

f_{sy} = the yield strength of the reinforcement [MPa]

f_{su} = the ultimate tensile strength of the reinforcement [MPa]

τ_{max} = maximum bond strength, prior to yielding of the reinforcement [MPa]

As discussed previously in Chapter 2, section 2.7.3, practising structural engineers Davey and Blaikie (2005) provided an example where the ductility of a very lightly reinforced component was assessed based on maximum crack width using Equations 3-21 and 3-22. The literature also contains some expressions for predicted minimum crack spacing s_{min}, which are generally of the form of Equation 5-1 (Kankam, 1997).

$$s_{min} = \frac{d_b f_{ct}}{4\rho\tau_{ave}} \qquad 3\text{-}23$$

where:

f_{ct} = concrete tensile strength [MPa]

d_b = actual bar diameter [mm]

ρ = the longitudinal reinforcement ratio

τ_{ave} = average bond stress [MPa]

Equation 5-1 suggests that an understanding of the bond stress distribution along the embedded reinforcing bar is required in order to predict the crack spacing. Some useful examples from the literature that attempt to link the bond stress-slip behaviour and steel stress-strain behaviour are found in Shima *et al.* (1987) and Kankam (1997).

3.7.3 Yield penetration length

In both practice and in research, the yield penetration length is often estimated as part of the effective plastic hinge length for which it is assumed the reinforcement strain distribution is uniform (discussed in Chapter 2). Estimations of the elastic strain penetration length are also prescribed in the PRESSS design guidelines (NZCS, 2010), however the physical basis for determining this is not clearly reported.

Previous quasi-static testing of RC specimens (e.g. Goodsir, 1985) has shown measured strain distributions that suggest the yield penetration length is relatively large and warrants some consideration in determining the ductility of RC components and perhaps the stiffness, depending different approaches taken by practitioners (Fenwick and Bull, 2002). Equation 3-24 illustrates the yield penetration length that is often adopted. An earlier form of the expression was $L_{yp} = 6d_b$ (Priestley and Park, 1984).

Paulay and Priestley (1992) & Priestley *et al.* (2007)	$L_{yp} = 0.022 d_b f_y$	3-24

This expression was derived from experimental measurements from quasi-static testing of RC bridge columns during the 1970s and 1980s (Priestley and Park, 1984). The reliability of these results may be comprised by disrupted bond conditions around strain gauges (discussed in Section 3.4.4). These test specimens typically had longitudinal reinforcement ratios higher than 1.5 percent and the test conditions may be such that the spread of plasticity was relative extensive (discussed previously in Chapter 2).

Section 3.2.4 discussed some previous suggestions for the length of the bond deterioration zone as being 2 to $5d_b$. The dependency of Equation 3-24 on f_y the yield stress of the reinforcing steel is somewhat contrary to the conclusions in the literature about the influence of inelastic steel strains on local bond slip (Section 3.3.1.3). The local and average bond slip will depend heavily on the steel strain demand and the redistribution of steel strains (due to bond damage) which will significantly depending on the type of loading (Section 3.3.4). Interpretations of the effect will vary depending on whether local or average bond slip is considered to be more relevant.

3.7.4 Anticipated bond deterioration in the design and detailing of anchorages

For the sake of completeness some discussion is presented here for the allowance of bond deterioration in modern design approaches for the anchorage of deformed bars. Design provisions are generally focussed on maintaining adequate strength when the structure is subjected to severe seismic actions without a significant reduction in stiffness due to bond deterioration.

Figure 3-34(b) illustrates the anchorage length required by NZS3101:2006 to account for extensive bond deterioration at exterior beam-column joints. The required development length from the design calculation is taken from the "point of commencement" at some distance, either the minimum of 0.5 times the column depth h_c or $8d_b$ from the column face back into the joint zone. Eurocode 8 (2006) makes a similar provision for the required anchorage length commencing after the maximum likely yield penetration, which is taken as $5d_b$. The anchorages design provisions stated in ACI 318 (2011) do not specify that a portion of the embedment length is disregarded to allow for bond deterioration.

Experimental research on interior beam-column joints by Hakuto *et al.* (1999) showed that small column depths or large longitudinal beam bars may result in severe bond deterioration such that tensile bar strains could penetrate through the entire joint core concrete. Figure 3-34(a) shows this behaviour in which the compression reinforcement on the other side of the joint may actually be in axial tension. Consequently, the strength and stiffness of the frame system and curvature ductility of the beams is significantly reduced. Modern design standards (e.g. NZS3101:2006, ACI 318-11) specify limiting ratios of d_b/h_c for interior beam-column joints to limit the relative amount of bond deterioration, thus mitigating undesirable structural behaviour.

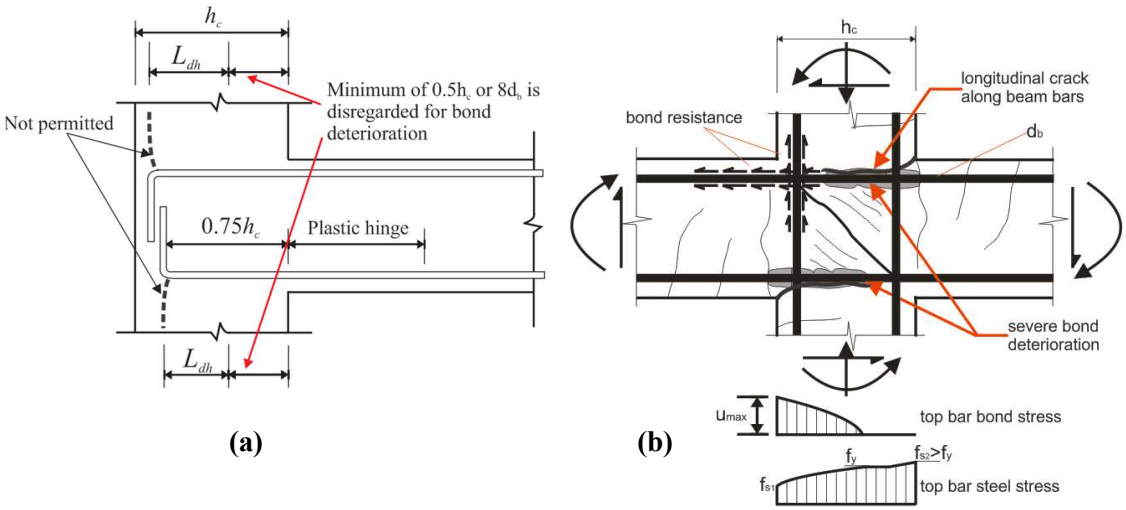

Figure 3-34: Schematic illustration of the anchorage zones of longitudinal beam bars when plastic hinge zones are permitted at the column face for: (a) exterior beam-column joints (NZS3101:2006); (b) at interior beam-column joints with severe bond deterioration (After Hakuto *et al.*, 1999).

Design provisions for anchorages and development lengths typically consider bond-related deficiencies with respect to an allowable bond stress that is conservatively taken to be somewhat less than the maximum local bond stress that has been experimentally determined from bond pull-out tests with short embedment lengths. An allowable average bond stress ranging between 60 to 80 percent of the maximum bond stress is considered to limit the deterioration of the surrounding concrete and ensure that total bond slip is minimized.

In the design of interior beam-column joints, Paulay and Priestley (1992) idealizes the likely bond stress distribution inside the joint to simplify the design approach that resulted in a reasonable yet conservative embedment length to sufficiently anchor the longitudinal beam reinforcement. The unconfined cover concrete of the column is neglected from the effective embedment length and an average bond stress of two-thirds of $2.5\sqrt{f'_c}$ is adopted, meaning that an appropriate average maximum bond stress for the beam bars over the joint depth h_c is approximately $1.35\sqrt{f'_c}$. Given the significant complexity in the structural behaviour of different configurations of beam-column joints under different stress states, Paulay and Priestley (1992) made some beneficial idealisations that result in simplified design calculation with reasonable conservatism for ensuring adequate strength capacity and that total bond slip is not excessive.

Although recent bond research by experimental testing and numerical modelling has advanced, the findings and outcomes are generally unclear or are too complex and are not readily adopted as recommendations for structural engineering practice.

3.7.5 Modern detailing of connections using debonded regions

There are modern connection details for precast RC components that are used in practice to satisfy the ULS performance criteria described previously in Section 3.1.5. SESOC (2012) recognised recent failures of precast panel splices and recommended that spliced reinforcing bars should be un-bonded over a reasonable length based on the likely elongation due to lateral displacement at ULS. A simple approach for estimating the debonded length illustrated in Figure 3-35(a) to ensure that steel strains are distributed over a reasonable length and low-cycle fatigue of the reinforcement is partially considered. Examples of some debonding the reinforcing bars at connections are schematically illustrated in Figure 3-35(b).

(a)

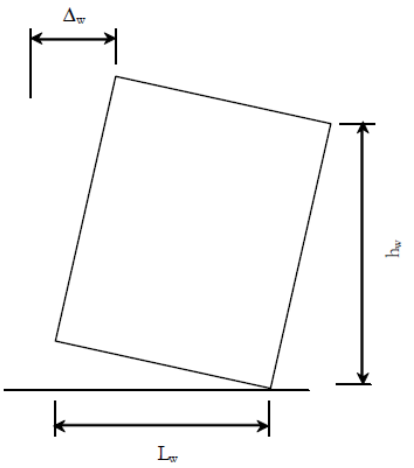

Where the debonded length is:

$$L_{dh} = \Delta_w \frac{L_w}{0.05 h_w} \qquad 3\text{-}25$$

(b)

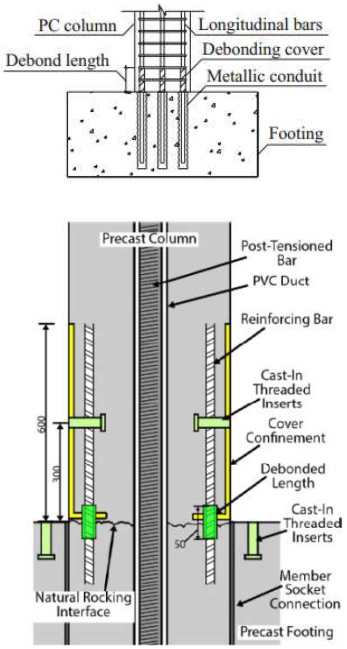

Figure 3-35: Diagrams showing debonded reinforcement in modern design: (a) example calculation used for precast concrete panels (SESOC, 2012); (b) base connections for RC bridge columns (White, 2014).

3.8 INITIAL CONCLUSIONS

Bond behaviour is fundamental for the strength and deformation capacity of RC structures, yet somewhat complex. The roles and requirements of bond in ductile RC structures were briefly introduced in this chapter and the physical mechanism of bond was described at different levels of damage under monotonic and cyclic loading. A search of the literature found that bond behaviour is influenced by a significant number of factors which subsequently affects the ductility of RC structural components. Several of the bond complexities reported in the literature are less relevant when considering the good bond conditions of the vertical reinforcement in lightly reinforced concrete walls. Summarised below are some interesting findings and decisions made for the purpose of this particular research:

- It might be reasonable to assume that the influence of rib pattern and geometry on bond behaviour is negligible due to minor variations in relative rib area and rib inclination angle between different standard reinforcing bars that are available in New Zealand. However, different international research on bond needs to consider differences in the rib geometry when attempted to compare measured bond behaviour between each particular study. Reinforcing bars conforming to standard specifications such as NZS4671:2001 generally have high initial bond stiffness, high bond strength and premature pull-out failure from excessively large relative rib areas is prohibited. For conventional grades of structural concrete, normalisation of the bond strength by $\sqrt{f'_c}$ is considered to be appropriate.
- The effect of inelastic steel strains on bond behaviour are still not clear. This is a complex phenomenon that will not be experimentally investigated in this research. Linkages between local bond behaviour and the estimated "yield penetration length" remain unclear. Practising engineers would benefit from further experimental research on this phenomenon with the appropriate test conditions and experimentation procedures.
- It is reasonable to ignore the influence of more complicated bond stress-slip behaviour in a beam column joint that is influenced by transient confining stresses and longitudinal cracking under seismic actions. Although combined axial and transverse (shear) deformation has been discussed in the literature, this is not expected to influence lightly RC walls with relatively low shear stresses.
- The effect of loading rate has been found to have some positive influence on bond behaviour, but there are no generalised values that reliably quantify the dynamic influence/enhancement of bond strength under faster loading rates. Bond behaviour under cyclic loading has been studied previously, although the cyclic loading protocols are typically fully reversed (symmetric) to either constant slip amplitudes or to gradually increasing slip amplitudes. The literature contains some gaps relating to bond behaviour under different cyclic loading histories that are reflective of seismic actions in real structures.

- The pull-out test set-up is most widely used to measure local bond behaviour due to the practicality of constructing a large number of test specimens that require a relatively simple test set-up. A major limitation of typical pull-out tests is that the concrete is confined by reaction plates such that the stress state is not representative of the behaviour in real structures. The reactions need to be spaced a sufficient distance away from the axis of the test bar to overcome this artificial test condition (discussed further in Chapter 4).
- There is some scatter in previous experimental data for the maximum local bond stress τ_{max} under very good bond conditions. τ_{max} may vary between 2.5 and 5.0 times $\sqrt{f'_c}$. The Model Code 2010 states τ_{max} of $2.5\sqrt{f'_c}$ occurs at a bond slip of an approximately 1.0 mm. Some design expressions in Paulay and Priestley (1992) referred to τ_{max} of $2.5\sqrt{f'_c}$ based on the findings of Eligehausen *et al.* (1983).
- A variety of bond modelling techniques may be adopted using different resolutions with varying complexities. The modelled behaviour significantly depends on the experimental test conditions and measurements in which the bond stress-slip (and maybe -strain) relationships and model parameters were derived. While bond models may have been verified against test results, a significantly amount of variation in bond behaviour is likely to arise due to variations in experimental procedures such as simplifications of test boundary conditions, specimen particulars and measurement techniques.
- The bond stress-slip relationship has been widely studied for confined regions away from crack planes and free surfaces; however there is little information available for the local bond strength in these regions. Maximum bond strength is not widely reporting in practice guidelines, however such values would be useful for assessing existing structures (damaged or undamaged) that may develop concentrated inelastic strains in the reinforcement at wide cracks.

3.9 REFERENCES

Abrams, D.A. (1913). Tests of bond between concrete and steel. *Bulletin 71,* University of Illinois, Urbana.

ACI Committee 408 (1992). State-of-the-art report on bond under cyclic loads: *ACI 408R-92*, American Concrete Institute, Farmington Hills, MI.

ACI Committee 408 (1998). Bond and development of reinforcement: A tribute to Peter Gergely, *Special Publication 180*. Farmington Hills, MI: ACI International. Leon, R. T: editor,

ACI Committee 408 (2003). Bond and development of straight reinforcing bars in tension: *ACI 408R-03*, American Concrete Institute, Farmington Hills, MI.

ACI Committe 318 (2011). Building code requirements of structural concrete (ACI 318-11). American Concrete Institute, Farmington Hills, MI.

Araujo, D.L., Danin, A.R., Melo, M.B, Rodrigues, P.F. (2013). Influence of steel fibres on the reinforcement bond of straight steel bars. *Ibracon Structures and Materials Jounal*. 6(2), 307-338.

ASTM A615 (2014). Standard specification for deformed and plain billet-steel bars for concrete reinforcement, *American Society for Testing and Materials.*

ASTM A944 (2010). Standard test method for comparing bond strength of steel reinforcing bars to concrete using beam-end specimens, *American Society for Testing and Materials.*

Au, E. (2010). The mechanics of a non-tearing floor connection using slotted reinforced concrete beams, *Master of Engineering Thesis*, University of Canterbury, Christchurch, New Zealand.

Balazs, G.L. (1991). Fatigue of bond. *ACI Materials Journal*, 88(6), 620-629.

Bonacci, J.F. (1994a). Bar yield penetration in monotonically loaded anchorages. *Journal of Structural Engineering*, ASCE, 120(3), 965-986.

Bonacci, J.F., and Marquez, J. (1994b). Tests of yielding anchorages under monotonic loading, *Journal of Structural Engineering*, ASCE, 120(3), 987-997.

Byrne, J. (2012). Bond and shear mechanics within reinforced concrete beam-column joints incorportating the slotted beam detail, *Master of Engineering Thesis*, University of Canterbury, Christchurch, New Zealand.

Chung, L., and Shah, S.P. (1989). Effect of loading rate on anchorage bond and beam-column joints, ACI Structural Journal, 86(2), 132-142.

Comite' Euro-Internationale du Béton (*CEB-FIP*, 1993). The Model Code 1990: *Design code*. London: T. Telford; 1993.

Comite' Euro-Internationale du Béton (*CEB-FIP*, 1996). RC elements under cyclic loading: *State-of-the-art report*. London: T. Telford; 1996.

Davey, R.A., and Blaikie, E.L. (2005). On the flexural ductility of very lightly reinforced concrete sections, C*onference proceedings of the New Zealand Society of Earthquake Engineering*, Taupo.

Davies-Colley, S., Kleinjan, B., Bull, D.K., and Morris, G.J. (2015). Review of the material and flexural overstrength factors for Grade 300E reinforcing steel used in New Zealand, *Conference proceedings of the New Zealand Society of Earthquake Engineering,* Rotorua, New Zealand.

Eligehausen, R., Popov, E.P., Bertero, V.V. (1983), Local bond stress-slip relationships of deformed bars under generalized excitations. *Report UCB/EERC-83/23,* Earthquake Engineering Research Centre, University of California, Berkeley.

Eligehausen, R., Ozbolt, J. and Mayer, U. (1998). Contribution of concrete between cracks at inelastic steel strains and conclusions for the optimisation of bond. *Symposium of the ACI Committee 408 – Bond and Development of Reinforcement* (edited by Leon, R). SP180-3: 45-80.

ETAG 001. (2006). Guideline for European technical approval of metal anchors for use in concrete, *Parts 5: Bonded anchors*. European Organization of Technical Approvals (EOTA), Brussels, Belgium.

Eurocode 2 (2005). Design of concrete structures. European Committee for Standardization; 1992-2005.

Eurocode 8 (2006). Design of structures for earthquake resistance. European Committee for Standardization; 1998-2006.

Fang, C., Gylltoft, K., Lundgren, K., and Plos, M. (2006). Effect of corrosion on bond in reinforced concrete under cyclic loading. *Cement and Concrete Research*, 36(3), 548-555.

Fédération Internationale du Béton, *fib*. (2000A), Structural concrete – Textbook on behaviour, design and performance. *State of the art report: CEB-FIB Bulletin 1*, International Federation for Structural Concrete, Lausanne, Switzerland.

Fédération Internationale du Béton, *fib*. (2000B), Bond of reinforcement in concrete. *State of the art report: CEB-FIB Bulletin 10*, International Federation for Structural Concrete, Lausanne, Switzerland.

Fédération Internationale du Béton, *fib*. (2012), Model Code 2010 – First Complete Draft, Volume 1, Lausanne, Switzerland.

Fédération Internationale du Béton, *fib*. (2014), Bond and anchorage of embedded reinforcement: Background to the fib Model Code for concrete structures, *Bulletin 72*, Lausanne, Switzerland.

Fenwick, R.C. (1966). The shear strength of reinforced concrete beams, *Doctor of Philosophy Thesis*, University of Canterbury, Christchurch, New Zealand.

Fenwick, R.C., and Sue, C.F.C. (1982). The influence of water gain upon the tensile strength of concrete, Magazine of Concrete Research, 34(120): 139-145.

Fenwick, R.C., and Bull, D.K. (2002). What is the stiffness of reinforced concrete walls? – response to the discussion from Priestley and Paulay, *SESOC Journal*, 15(1), 35-41.

Fernández Ruiz M., Muttoni A. and Gambarova P.G. (2007). Analytical Model on the Pre- and Post–Yield Behavior of Bond in Structural Concrete. *Journal of Structural Engineering*, ASCE 133(10), 1364-1372.

Filippou, F.C., Popov, E.P., Bertero, V.V. (1983). Effects of bond deterioration on hysteretic behaviour of reinforced concrete joints. *Report UCB/EERC-83/19*, Earthquake Engineering Research Centre, University of California, Berkeley.

Forth, J.P., and Beeby, A.W. (2014). Study of composite behaviour of reinforcement and concrete in tension, *ACI Structural Journal*, 111(2), 397-406.

Goodsir, J.W. (1985). The design of coupled frame-wall structures for seismic actions, *Doctor of Philosophy Thesis*, University of Canterbury, Christchurch, New Zealand.

Goto, Y. (1971). Cracks formed in concrete around deformed tension bars. *ACI Journal,* 68(26), 244-251.

Hakuto, S., Park, R., Tanaka, H. (1999). Effect of deterioration of bond of beam bars passing through interior beam-column joints on flexural strength and ductility. *ACI Structural Journal*, 96(5), 858-864.

Hare, H. J., Bull, D. K., Brown, B., Brunsdon, D. R., Jury, R., King, A., McCahon, I., Millar, P., Smith, P., and Stannard, M., (2012). Canterbury earthquake sequence: Detailed engineering evaluation of commercial buildings, *15 World Conference on Earthquake Engineering*, Lisbon.

Hawkins, N.M., Lin, I.J., and Jeang F.L. (1982). Local bond strength of concrete for cyclic reversed loadings. *Bond in concrete,* Applied Science Publishers, London, 151-161.

Hollings, J.P. (1968a). Reinforced concrete seismic design, *Bulletin of the New Zealand Society for Earthquake Engineering*. 2(3), 217-250.

Hollings, J.P. (1968a). A reinforced concrete building in Wellington, *Bulletin of the New Zealand Society for Earthquake Engineering*. 2(4), 420-442.

Huffadine, J.A., van Bysterveldt, A.G., Clifton, G.C., and Ferguson, G.W. (2015). The cracking behaviour of reinforced concrete beams under static and dynamic loading. *Conference proceedings of the New Zealand Society of Earthquake Engineering,* Rotorua.

Kankam, C.K. (1997). Relationship of bond stress, steel stress, and slip in reinforced concrete. *Journal of Structural Engineering*, ASCE, 123(1), 79-85.

Kimura, H. and Jirsa, J.O. (1992). Effects of bar deformation and concrete strength on bond on reinforcing steel to concrete. *International Conference on Bond in Concrete*, Riga, Latvia.

Kivell, A. (2011). Effects of bond deterioration due to corrosion on seismic performance of reinforced concrete structures, *Master of Engineering Thesis*, University of Canterbury, Christchurch, New Zealand.

Leon, R.T., and Deierlein, G.G. (1996). Considerations for the use of quasi-static testing. *Earthquake Spectra,* 12, 87-109.

Lowes, L.N. (1999). Finite element modelling of reinforced concrete bridge beam-column connections, *Doctor of Philosophy Thesis*, University of California, Berkeley, CA.

Lowes, L.N., Moehle, J.P., and Govindjee, S. (2004). Concrete-steel bond model for use in finite element modelling of reinforced concrete structures, *ACI Structural Journal*, 101(4), 501-511.

Mackechnie, J.R. (2003). Hardened properties of concrete containing New Zealand aggregates. *Journal of the Structural Engineering Society New Zealand Inc. (SESOC),*16(2), 20-29.

Maekawa, K., and Quereshi, J (1997). Computational model for reinforcing bar embedded in concrete under combined axial pull-out and transverse displacement. *Concrete library of the Japanese Society of Civil Engineers*, 29, 217-231.

Maekawa, K., Pimanmas, A., and Okamura, H. (2003). Nonlinear mechanics of reinforced concrete. Spon Press, New York, United States of America.

Mahin, S.A, and Bertero, V.V. (1972), Rate of loading effects on uncracked and repaired reinforced concrete members. *Report UCB/EERC-72/7,* Earthquake Engineering Research Centre, University of California, Berkeley.

Mahrenholtz, C. (2012). Seismic bond model for concrete reinforcement and the application to column-to-foundation connections, *Doctor of Philosophy Thesis,* Universität Stuttgart.

Mains, R.M.,(1951). Measurement of the distribution of tensile and bond stresses along reinforcing bars, *ACI Journal Proceedings,* 48(17): 225-252.

Mayer, U., and Eligehausen, R. (1998). Bond behaviour of ribbed bars at inelastic steel strains. *2nd International Ph.D. Symposium in Civil Engineering*, Budapest.

Michael, M., and Keuser, M. (2014). Bond of steel and concrete under high loading rates. *Proceedings of the 9th International Conference on Structural Dynamics*, Porto, Portugal.

Murcia-Delso, J., Stavridis, A., and Shing, P.B. (2013). Bond strength and cyclic bond deterioration of large-diameter bars, *ACI Structural Journal*, 110(4): 659-669.

NZCS (2010). PRESSS Design Handbook, *New Zealand Concrete Society,* Pampanin, S: Chief Editor.

NZSEE (2006). Assessment and improvement of the structural performance of buildings in earthquakes, *Recommendations of a study group of the New Zealand Society for Earthquake Engineering,* Wellington, New Zealand.

OpenSees. (2012). The Open System for Earthquake Engineering Simulation software, version 2.4.1. Pacific Earthquake Engineering Research Centre. Download available at http://opensees.berkeley.edu/

Park, R., and Paulay, T. (1975). Reinforced concrete structures, John Wiley & Son, Inc., New York, United States of America.

Park, R.J.T, (1987). Seismic performance of steel-encased concrete, *Doctor of Philosophy Thesis*, University of Canterbury, Christchurch, New Zealand.

Patel, V.J., Van, B.C., and Henry, R.S. (2014). Effect of reinforcing steel bond on the seismic performance of lightly reinforced concrete walls. *Conference proceedings of the New Zealand Society of Earthquake Engineering,* Auckland, New Zealand.

Paulay, T., and Priestley, M.J.N., (1992). Seismic design of reinforced concrete and masonry buildings. John Wiley & Son, Inc., New York, United States of America.

Priestley, M.J.N., and Park, R. (1984). Strength and Ductility of bridge substructures. *RRU Bulletin No. 71*, National Roads Board, Wellington, New Zealand.

Priestley, M.J.N., Seible, G. and Calvi, G.M. (1996). Seismic design and retrofit of bridges. John Wiley & Son, Inc., New York, United States of America.

Priestley, M.J.N., Kowalsky, M.J., and Calvi, G.M. (2007). Displacement-based seismic design of structures, IUSS PRESS, Pavia, Italy.

Raynor, D.J., Lehman, D.E. and Stanton, J.F. (2002). Bond-slip response of reinforcing bars grouted in ducts. *ACI Structural Journal*, 99(5): 568-576.

RILEM-FIP-CEB (1982). RC5 Bond test for reinforcement steel. *1. Beam test* & RC6 Bond test for reinforcement steel. *1. Pull-out test.*

Saatcioglu, M., and Ozcebe, G. (1989). Response of reinforced concrete columns to simulated seismic loading. *ACI Structural Journal*, 86(1), 3-12.

Salem, H., and Maekawa, K. (2004). Pre- and post-yield finite element method simulation of bond of Ribbed reinforcing bars. *Journal of Structural Engineering*, ASCE, 130(4), 671-680.

Scott, R.H., and Gill, P.A.T. (1987). Short-Term Distributions of Strain and Bond Stress along Tension Reinforcement," *Structural Engineer*, 65(2): 39-43, 48.

Scott, R. H., (1996). Intrinsic Mechanisms in Reinforced Concrete Beam-Column Connection Behaviour, *ACI Structural Journal*, 93(3): 1-11

Shima, H., Chou, L.L., and Okamura, H. (1987) Micro and macro models for bond in reinforced concrete. *Reprinted from Journal of the Faculty of Engineering*, The University of Tokyo, 39(2).

Skorobogatov, S. and Edwards, A. (1979). The influence of the geometry of deformed steel bars on their bond strength in concrete, *Proceedings of the Institution of Civil Engineers*, Thomas Telford, 327-339.

Soleymani Ashtiani, M. (2013). Seismic performance of high-strength self-compacting concrete in reinforced concrete structures, *Doctor of Philosophy Thesis*, University of Canterbury, Christchurch, New Zealand.

Standards New Zealand. (2006). Concrete structures standard, NZS3101, Parts 1 & 2. Standards New Zealand: Wellington, New Zealand.

Standards New Zealand. (2001). Steel reinforcing materials standard, NZS4671. Standards New Zealand, Wellington, New Zealand.

Structural Engineering Society of New Zealand, SESOC. (2012). Practice note - Design of conventional structural systems following Canterbury earthquakes. *Report prepared for the Canterbury Earthquakes Royal Commission.*

Takeda, J.I. (1984). Dynamic fracture of concrete structures due to severe earthquakes and some considerations for countermeasures. *Proceedings of the 8th World Conference on Earthquake Engineering*. 6, 299-306.

Thompson, M. K., Jirsa, J. O., Breen, J., and Klingner, R., (2002). Anchorage behaviour of headed reinforcement: literature review, *Centre for Transportation Research*, University of Texas, Austin, Texas.

Thun, H., Ohlsson, U., and Elfgren, L. (2001). Concrete strength in old Swedish concrete bridges, *Paper from Doctor of Philosophy Thesis*, Lulea University of Technology, Sweden,

Viwathanatepa, S., Popov, E. P., and Bertero, V. V. (1979). Effects of generalised loadings on bond of reinforcing bars embedded in concrete blocks, *Report UCB/EERC-79/22*, Earthquake Engineering Research Centre, University of California, Berkeley.

Vos, E., and Reinhardt, H.W. (1982). Influence of loading rate on bond behaviour of reinforcing steel and prestressing strands, *Materials and Structures*. RILEM 15(85), 3-10.

Walker, P., Batayneh, M., and Regan, P. (1997). Bond strength tests on deformed reinforcement in normal weight concrete. *Materials and Structures*, 30(7): 424-429.

Washa, G.W. and Wendt, K.F. (1975). Fifty year properties of concrete, *ACI Journal Proceedings*, 72(1), 20-28.

White, S. L. (2014). Controlled damage rocking systems for accelerated bridge construction, *Master of Engineering Thesis*, University of Canterbury, Christchurch, New Zealand.

Withey, M.O. (1961). Fifty year compression test of concrete. *ACI Journal Proceedings*, 58(12), 695-712.

Zhao, J., and Sritharan, S. (2004). Nonlinear analysis of RC structures with strain penetration effects. *Proceedings of 8th National Conference on Earthquake Engineering*.

Zhao, J., and Sritharan, S. (2007). Modelling of strain penetration effects in fibre-based analysis of reinforced concrete structures. *ACI Structural Journal*, 104(2), 133-141.

[This page is intentionally left blank]

4 EXPERIMENTAL PROGRAMME

4.1 INTRODUCTION

The structural behaviour of reinforced concrete (RC) components fundamentally depends on the mechanism of bond mechanism between deformed reinforcing steel bars and the surrounding concrete. Given the importance of this issue, bond behaviour has been the focus of many previous investigations (summarised in Chapter 3). Under certain conditions, bond behaviour may be a significant factor that influences the performance and safety of RC structures when subjected to severe earthquake-induced ground shaking. It is therefore essential that experimental measurements of bond behaviour are obtained under appropriate testing conditions (e.g. in-situ conditions and type of loading) that exist when real RC structures are subjected to severe dynamic loading.

Direct pull-out tests have been commonly used in experimental studies on bond behaviour due to the ease and repeatability of constructing and testing a large number of specimens where a range of parameters can be studied independently. One potential limitation of typical pull-out tests is that the state of stress in the specimen is not entirely consistent with those in a real RC component (Soleymani Ashtiani, 2013). This said; other bond test methods, such as beam tests, typically involve additional complexities that will often constrain the total number of tests that can be performed. Results from previous bond pull-out tests have, however, been widely used in the development in constitutive bond stress-slip relationships that have been implemented in the CEB-FIP (now *fib*) Model Codes (1993; 1996; 2012).

Although bond pull-out testing has been performed by many researchers over several decades, this type of test setup has not been effectively standardised, therefore inconsistencies between different experimental studies may be expected. Due to the apparent lack of consistent testing procedures, the ACI Committee 408 (2003) recommended a minimum amount of detail is reported by bond researchers. The sections within this chapter are dedicated to the specific details presented for the: (i) test set-up; (ii) specimen design and construction details; and (iii) an outline of the test permutations. Particular attention is given to quantifying the concrete strength that was achieved from multiple concrete pours. Concrete and steel properties are summarised and supplementary information is found in Appendix A. Sections of this chapter also provide some context to the text results and discussion presented in Chapters 5 and 6. The details in this chapter may also assist other bond-related investigations and to ensure reasonable comparison and exchange of test data between different experimental studies.

4.2 EXPERIMENTAL TEST SET-UP

4.2.1 Instron testing machine and loading frame

For this experimental programme it was important that a simple test arrangement and procedure be developed that could be repeated for 75 bond pull-out tests (the number of tests considered necessary to investigate the variables of interest in this study). An Instron loading machine at the University of Canterbury was used to apply the external load to the pull-out specimens, as shown in Figure 4-1, and has a capacity of 100 kN with displacement-controlled loading capabilities.

Figure 4-1: The 100 kN Instron machine used for monotonic and cyclic bond pull-out tests.

Figure 4-2 schematically illustrates the loading frame that was assembled to support the relatively massive concrete block as the test bars were connected at a threaded base plate. The alignment of the 32 mm reaction plates around the concrete specimen was maintained by continuous 24 mm threaded rods and M24 nuts. The threaded rods also connected to the top plate which provided fixity to the load cell and Instron machine. The nuts above the two top reaction plates were proof tightening only, as further tightening would result in additional compressive stresses in the concrete. The complete loading frame needed to have a very high stiffness and strength to support the concrete block under the applied load to the test bar. Design calculations showed that axial deformation of the threaded rods and vertical deflection due to bending of the top plate was negligible.

There was a 1.1 kN gravity load attributed to the self-weight of the entire arrangement, particularly the mass of the tests specimen (typically 32 kg) and multiple steel plates. Care was taken in the preparation of the test specimens to ensure the test bar was in a vertical plane. Adjustability of the frame was beneficial for minimizing the effect of any accidental eccentricities in the direction of loading applied to the test bar. The level of reaction plates was checked using a spirit level and a 6 mm thick rubber compound was

placed between the steel reaction plates and the concrete specimen. Tightening of the M24 nuts was done evenly to ensure there was no incidental flexure of the specimen that might induce additional stresses.

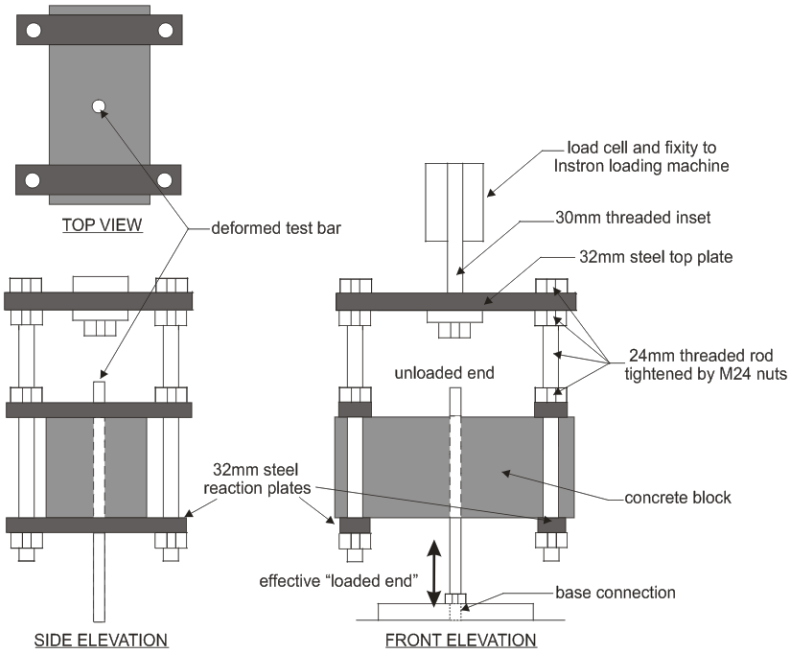

Figure 4-2: Schematic illustration of the loading frame and components used for the unconfined bond pull-out test arrangement in an Instron loading machine.

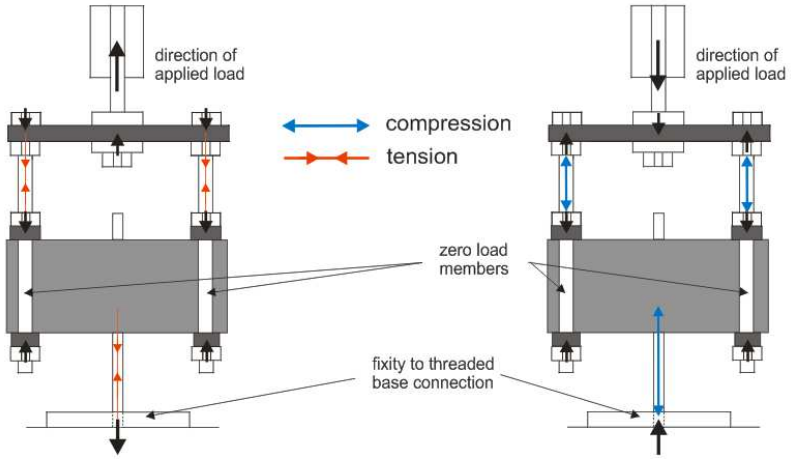

(a) test bar pulled-out **(b)** test bar pushed in out

Figure 4-3: Load paths through the loading frame due to reversing actions from the loading machine.

Figure 4-3(a) and (b) schematically illustrate how the external force is applied from the test machine and loading frame by the relative movement between the concrete block and the test bar which is fixed by a threaded base connection. Depending on the configuration of the loading frame, there are several ways in which the external forces shown in Figure 4-3(a) and (b) may be transferred as internal forces within the specimen and through to the bond mechanism.

Figure 4-4(a) illustrates how the reaction plates of a potential 'confined' pull-out test set-up would artificially restrain the radial tension field in the bond region. In this particular configuration, bond splitting forces and splitting cracks are suppressed and pull-out failure is likely to occur at relatively high bond stresses. Kivell (2011) performed monotonic and cyclic pull-out tests using a confined set-up with large reaction plates clamping the entire concrete block. A centrally drilled hole in the reaction plates only allowed for 20 mm spacing from the axis of the test bar. The monotonic bond stresses reported by Kivell (2011) were larger than 30 MPa, however, which is considerably larger than other values reported in the literature. Such high bond stresses may be attributed to bearing stresses from the reaction plates acting in the opposite direction to the mechanical bearing forces developed at the embedded ribs in the bond region.

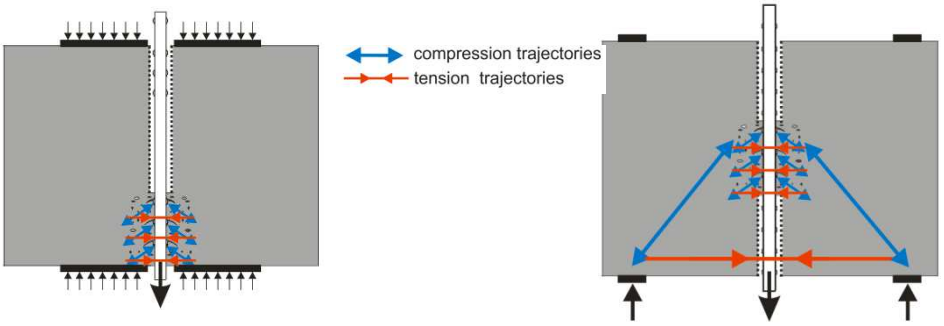

(a) Confined set-up with increased bond resistance **(b)** Unconfined set-up, specimen acts as a tied-arch.

Figure 4-4: Schematic illustration of the test specimen showing how external forces from the loading frame are transferred to the bond mechanism.

In this particular research, some tests are dedicated to investigating bond behaviour when the bond region is directly adjacent to the free surface (refer to Section 4.5.2.3). The 'confined' test set-up was therefore deemed to be inappropriate for this study due the inability to develop a realistic radial tensile stress field in the bond zone and how this may restrict potential observations of a cone break-out failure.

For this study, it was decided that an 'unconfined' set-up was most appropriate. Figure 4-4(b) illustrates how the reaction forces are spaced at a reasonable distance to minimize any interference with stresses in the bond region. The internal strut and tie is in equilibrium when the specimen behaves as a tied-arch, hence the reaction forces from the support plates of the loading frame are arching towards the bonded region of test bar. There is a trade-off between allowing these internal actions to occur in the specimen, as opposed to the alternative of using a 'confined' test set-up like that adopted by Kivell (2011).

4.2.2 Instrumentation

The instrumentation was required to measure the applied force and the relative displacement between the deformed bar and surrounding concrete. The manner in which the bond stress-slip relationship was deduced from measurements is described in Section 5.2 of Chapter 5. Set-up of the instrumentation was relatively simple with the benefit of saving time across a large number of repeated tests. The following three instruments were used:

- Figure 4-6(a) shows the 100 kN load cell that was attached to measure the external load applied to the specimen by movement of the concrete relative to the fixed test bar.
- Figure 4-6(b) shows the 30 mm spring-loaded potentiometer used to measure slip at the free-unloaded-end (see Figure 4-5). Slip measurements were approximately accurate to 0.007 mm.
- Figure 4-6(c) shows an extensometer with a 50 mm gauge length was used for estimations of the bar strain at the loaded end. The implied accuracy of 0.001 mm was achieved using a higher voltage conversion box.

Figure 4-5 schematically illustrates the deformation occurring within the specimen and how the potentiometer measures the free end slip of the test bar. Although the bar strain at the loaded end could have been measured using surface-mounted strain gauges, the additional time and labour associated with preparing the test bar and attaching the gauges was considered to be somewhat impractical.

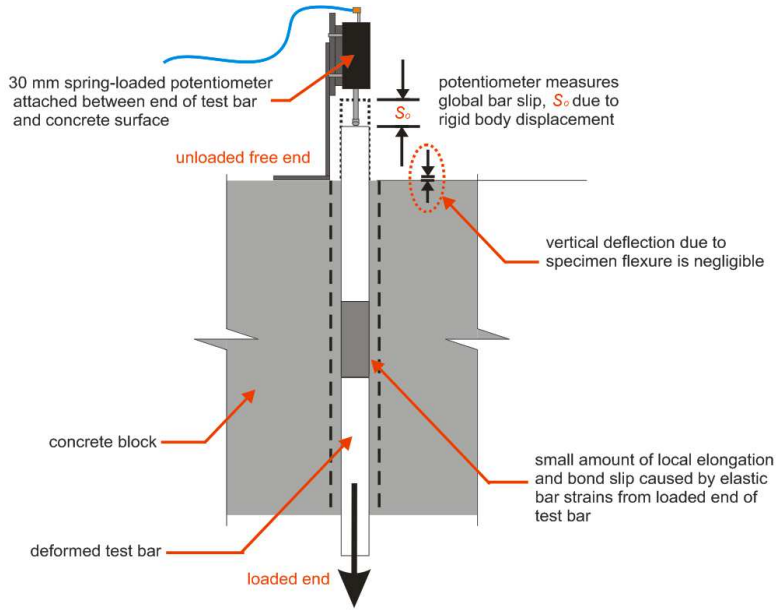

Figure 4-5: Schematic illustration of bond slip measured at the free-end of the test bar.

The instrumentation was calibrated and was checked prior to performing each test. Appendix B presents the load cell calibration that was performed prior to testing. The photograph in Figure 4-6(a) was captured during the calibration by using a 50 kN (compression) impact "proving ring".

(a) 100 kN load cell. **(b)** 30 mm potentiometer. **(c)** 50 mm gauge extensometer.

Figure 4-6: Photographs of instrumentation used in bond tests.

4.3 SPECIMEN CONSTRUCTION

4.3.1 Specimen design

Each pull-out specimen consisted of a single deformed reinforcing "test bar" that was embedded in a relatively massive volume of surrounding concrete. The specimens were designed to closely resemble the conditions found in a RC wall with a large thickness of cover concrete. Figure 4-7 shows the nominal dimensions used for the majority of specimens. Some variations included changing the specimen width from 160 mm and the position and length that is bonded to the concrete (discussed in Section 4.5.2).

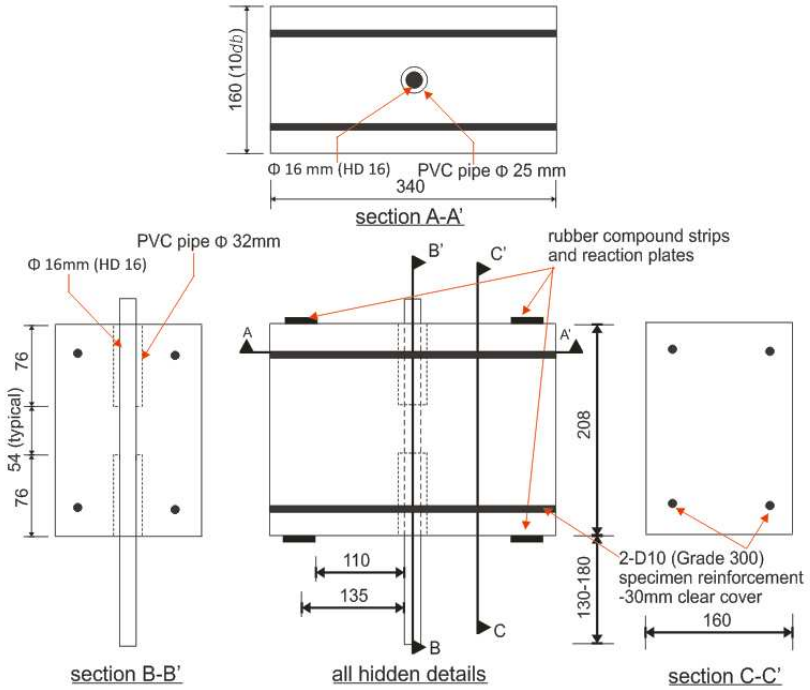

Figure 4-7: Typical details for bond pull-out specimens showing side elevation and respective cross sections.

To provide added protection against yielding of the test bar, Grade 500E reinforcing steel with a nominal yield strength of 500 MPa was chosen for the 16 mm and 20 mm tests bars (designated as HD16 and HD20). The material properties of these reinforcing bars are discussed further in Section 4.4.1.

The spacing of the reactions plates meant that the specimen would behave like a simply supported member and loading the test bar would induce some flexural tensile stresses in the concrete. Figure 4-7 shows top and bottom layers of two 10mm deformed bars (Grade 300E, designated 2-D10s) as flexural reinforcement to ensure that: (i) the likely width of any flexural crack that might develop parallel to the bar axis, would be small enough that there was negligible effect on bond behaviour; and (ii) there some factor of safety against a brittle specimen failure and protection of the loading frame and testing machine. Simple calculations indicated that the development length of the straight D10 bar was sufficient to resist the flexural induced tension force.

Figure 4-8 schematically illustrates how the short bonded length was achieved by cutting a plastic tube to match the rib inclination angle. Cutting the plastic tube in this manner enables the unbonded regions to be sealed during concrete pouring whilst the bond region contains a consistent number of ribs that are effectively embedded in concrete. There is no evidence in the literature to suggest that the same detail has been previously used in the construction of pull-out specimens.

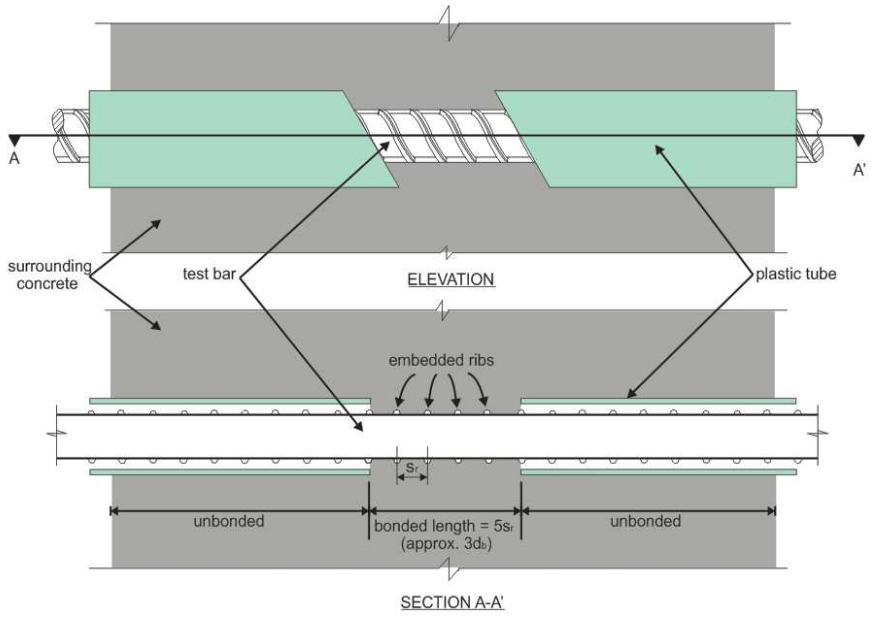

Figure 4-8: Schematic diagram showing the elevation and cross section of the bonded length achieved by embedding a short length of deformed reinforcing bar within the surrounding concrete block.

The majority of specimens had an embedded bonded length, l_e, of approximately three times the nominal bar diameter, $3d_b$. When the bond region was in the middle of the specimen, there were two unbonded lengths of approximately $5d_b$ either side. A closer examination of the geometry and rib pattern of the deformed bars found that the typical bond length could be more accurately expressed as five times the centre-to-centre rib spacing, $5s_r$, where s_r was measured to be 10.90 mm and 12.48 mm for the HD16s

and HD20s. The provision of the relatively short bond length also suggests that yielding of the test bars is unlikely to occur.

The internal diameter of the plastic tube was carefully chosen to ensure that the ribs were fully effective and to prevent localised concrete cone failures directly in front of the first rib at each end of the bonded length. Using plastic tubes with a 25 mm and 29 mm internal diameter meant there was a 3.5 to 4.0 mm gap between the outer diameter of the ribs of the HD16 and HD20 test bars, respectively.

The length of the bar between the embedded bond region and the fixed base plate was typically between 200 and 250 mm. Buckling of the bar was deemed to be unlikely to occur, even under the maximum compression load that may be applied during monotonic compression or reversed cyclic loading.

4.3.2 Formwork

Reusable formwork was constructed from 18 mm thick form-plywood which was supported by a larger frame constructed of treated clear framing timber. Figure 4-9(a) shows the entirety of the formwork placed on the vibrating table prior to concrete pouring. The formwork was fixed in place by tightening threaded steel rods passing through the plywood and timber support boards. A maximum of eight specimens could be made for each concrete mix.

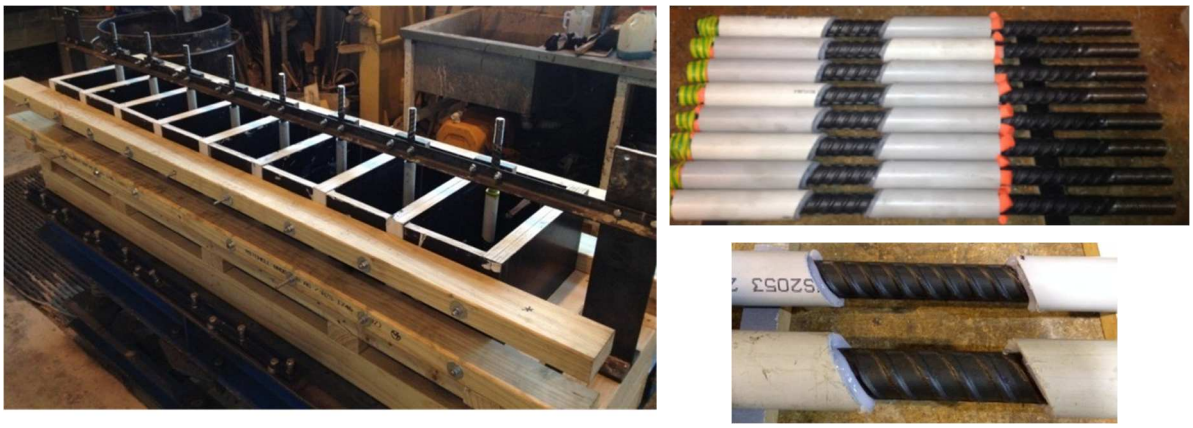

(a) **(b)**

Figure 4-9: (a) The re-usable formwork on the vibrating table prior to casting; and (b) showing how the embedded bond length was achieved when preparing the test bars.

A water-based primer was used to coat the exposed plywood and framing timber to improve the durability and integrity of the formwork which was required to withstand the moisture of about 10 pours of fresh concrete. Holes were drilled in the centre of the bottom plywood surface to allow the plastic tube (PVC) and unloaded end of the test bars to pass through.

Once the plywood moulds and framing was fixed in place, a silicon sealant was applied along corner edges and interfaces of the plywood to prevent seepage of water and fresh concrete. Sealing the formwork also

improved the durability of the formwork and made it easier to remove of the hardened specimens. Cleaning of the formwork was also required prior to re-using for subsequent pours.

4.3.3 Preparation of test bars

The deformed test bars required some preparation before placing inside the formwork prior to casting. Test bars were cut to 400 mm lengths using a cold-cut saw and care was taken to ensure that the embedded bond length did not coincide with the identification features on the bar surface (refer to Section A.1.1). A 50 mm long thread was machined at the "loaded end" of each test bar. The nominal thread size was 16 mm for the HD16s and 20 mm for HD20s, respectively.

The plastic tube (a PVC conduit) was cut to best match the rib inclination angle. Silicon was applied inside the plastic tube end and around the ribs at the end of the embedded bond region (refer to Figure 4-8 and Figure 4-9(b)) to form an effectively-sealed "O-ring" that was impervious to any water and cement paste. This process required one day for the silicon to set. Foam earplug strips and/or thin plastic rings were placed between the test bars and the plastic tube to ensure the test bar placed concentrically through the tube.

The condition of the bar surface was inspected prior to casting. Some test bars required cleaning in order to remove fine particles or oil residue.

4.3.4 Concrete mixing, placing and curing

Concrete casting was carried out after the test bars had been carefully placed and the silicon sealant had set. Prior to mixing the concrete, the formwork and accompanying cylinder moulds were coated in oil for easy removal. Figure 4-9(a) shows the formwork placed on the vibrating table ready for casting.

Concrete mixing was carried out using a 115 litre drum mixer. This volume for each mix allowed for eight pull-out specimens to be cast with at least nine test cylinder samples. Some careful preparation steps were required to ensure the mix was consistent throughout all specimens. This included pre-blending the sand from the saturated stockpile and by regularly assessing the moisture content of the sand and stone that was used.

All mixing was carried out with the help of an experienced technician. The surface of the drum mixer was saturated using a damp cloth before adding two thirds of the total water; half of the stone and sand were added before half of the cement; the remainder of the sand, cement and stone were added; then the remainder of water was added and mixing continued for three minutes until the mix was homogenous in consistency. Some mixes appeared to achieve the desired consistency and saturation before the total amount of water was added. In some instances, a small volume was held back and the amount was recorded and deducted for determining the approximate actual water-cement ratio.

Once mixing was complete, fresh concrete was poured into the formwork in three layers and the vibration table turned on between casting each layer. Similarly, the cylinders that were cast at the same time as the pull-out specimens were poured and vibrated in three layers. As the concrete was poured into the forms, the two pairs of D10s were placed at the bottom and top of the specimen. The exposed top surface was finished using a trowel within three hours after being poured.

Specimens were covered in a saturated hessian cloth about seven hours after pouring was completed and were left to harden. Stripping the specimens and corresponding cylinder samples from the formwork/moulds was usually done around 24 hours after pouring. The specimens and cylinders were then kept in a "fog room" with constant temperature (23 degrees Celsius) and moisture content (95 percent relative humidity, RH) until 28 days after casting. After curing was completed, specimens were transported and stored next to the Instron machine until the time of testing.

4.4 MATERIAL PROPERTIES

Awareness of the material and geometric properties of the reinforcing steel, and the material properties of the concrete, was critical for undertaking the experimental design (e.g. estimating the maximum expected loads and stresses). Information presented in this section (and Appendix A) is also essential for discussing the bond behaviour measured during testing (relevant to Chapters 5, 6 and 7).

4.4.1 Grade 500E reinforcing steel

Fletcher Reinforcing© was the manufacturer of the deformed reinforcing bars used in this project. The quality of the reinforcing steel used in these bond tests was of standard commercial quality and the products were compliant with the required chemical composition and mechanical properties stated in the New Zealand Standard for Steel reinforcing materials (NZS 4671:2001). The "E" designation indicates the Grade 500 reinforcing steel is a seismic (Earthquake) ductility class which must have a minimum uniform elongation of 10% at the ultimate tensile strength, f_u (NZS 4671:2001).

Direct tension tests were performed on one sample from the bundle of HD16 bars and two samples of the HD20 bar. An Avery loading machine was used for testing 500 mm long samples and an extensometer with a gauge length of 50 mm was attached to measure the elongation (and strain was inferred). Figure 4-10 shows the resulting stress-strain curves. The steel stress was derived using the external load and adopting the nominal bar diameter for calculating the approximate cross-sectional area. The steel was found to have an average yield stress (f_y) of 536 MPa and an average ultimate tensile strength of 662 MPa, which corresponds to f_u/f_y of 1.24 (sometimes denoted R_m/R_e).

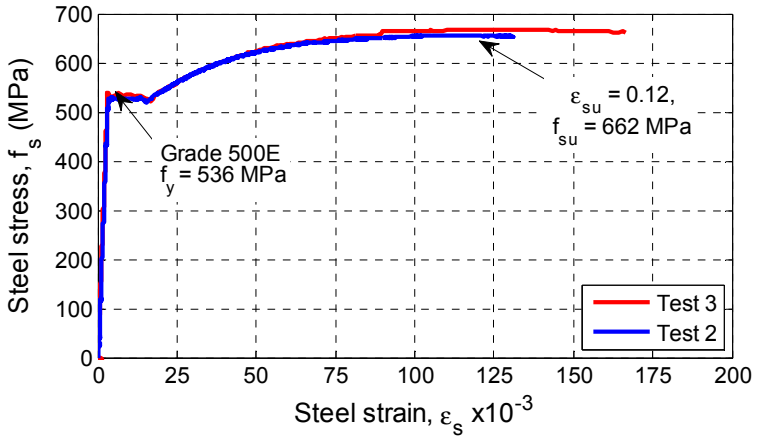

Figure 4-10: The measured stress-strain behaviour of the Grade 500E steel used for the deformed reinforcing bars in the pull-out test specimens.

Although the nonlinear stress-strain behaviour of the reinforcing steel is discussed here, information on the post-yield behaviour was not significant for this study as stresses in the test bars did not exceed the yield stress. Information obtained from the direct tension tests was useful, however, for the experimental

design, such as estimations for the maximum possible loads and stresses in the test bars. Typical values for the maximum steel stress f_s (found later during bond testing) were in the range of 0.5-0.6 f_y. Certain conditions for a particular bond test meant the externally applied load reached 94 kN, so the maximum steel may have been as high as 0.9 f_y. This case may have resulted in some stress concentration occurring at the threaded section of the bar at the loaded end; however this was considered as an exception to normal conditions. Stress concentrations at the base connection were generally unlikely to have occurred.

Table 4-1 summarises the measured rib geometry of the deformed bars. Section A.1 of Appendix A presents further details on the measured rib geometry and bar identification features. Equation 4-1 from NZS4671:2001 and ACI Committee 408 (2003) was used to calculate the relative rib areas R_r using the geometric measurements for the rib height h_r, the centre-to-centre rib spacing s_r, and the two gaps due to the longitudinal seam.

$$R_r = \frac{projected\ rib\ area\ normal\ to\ bar\ axis}{nominal\ bar\ perimeter \times centre \cdot centre\ rib\ spacing} = \frac{h_r}{s_r}\left(1 - \frac{\sum gaps}{\pi d_b}\right) \quad \text{4-1}$$

The calculated relative rib areas, R_r, were 0.11 and 0.09 for the HD16s and HD20s, respectively, which is greater than the minimum specified value in NZS4671:2001 of 0.056 for ribbed bars when d_b is between 10 mm and 40 mm. Table A-1 of Appendix A includes the calculated dimensional ratios to verify that the rib geometry of both bars conformed to NZS4671:2001.

Table 4-1: A summary of the measured rib geometry of HD16 and HD20 deformed bars.

Measures of rib geometry		
Nominal bar diameter, d_b (mm)	16.0	20.0
Rib centre-to-centre spacing, s_r (mm)	10.90	12.48
Rib height, h_r (mm)	1.34	1.23
Relative rib area, R_r (Equation 4-1)	0.11	0.09

Similar standard requirements for rib geometry are found in ASTM A615 "*Standard Specification for deformed and plain billet-steel bars for concrete reinforcement*". Two main requirements in this Standard are listed below. The minimum case of these requirements corresponds to a minimum relative rib area of 0.057, which is approximately the same as the requirements in NZS4671:2001. The rib geometry of the HD16s and HD20s also satisfy the requirements of ASTM A615.

- The average rib spacing must not exceed $0.7d_b$.
- The rib height must be greater than about 0.04 to $0.05d_b$ (depending on d_b).

4.4.2 Concrete mix design

Quality control of the concrete mix and resulting strength was required to achieve consistency between each of the test specimens. All mixes were designed to represent a typical structure concrete. Prior to constructing the pull-out specimens, three 30 L trial mixes were carried out to gain experience in mixing concrete and to assess the strength development at 7, 14 and 28 days against the predicted strength values for three specified water-cement ratios. The targeted strength values were based on 90 day specified compressive strengths $f'_{c,90days}$ of approximately 30, 45 and 60 MPa, respectively. The corresponding 28 day values were estimated using Abrams law for mixes containing 100% General Purpose (GP) cement. Appendix A presents further trial mix design details and results used to verify each of the chosen water-cement ratios.

Table 4-2 summarises the specified compressive strength targets and the mix design adopted for each of the three mixes. Products such as super plasticizers and other viscosity modifiers were not included. The aggregate was 13 mm Greywacke and the moisture content at saturated surface dry (SSD) is equal to 0.5%. The sand was taken from a saturated stockpile (covered in a container outside) with a moisture content found to range between 4 to 10% (SSD equal to 0.9%). Due to the apparent variation of the moisture content within- and between- stock piles, the sand was often blended in drum mixer prior to the time of casting.

Table 4-2: Concrete mix design for three separate mixes of concrete used in bond test specimens.

Mix number	Mix 1 (1 pour)	Mix 2 (7 pours)	Mix 3 (1 pour)
w/c ratio	0.44	0.57	0.73
$f'_{c,28days}$ [1]	51.9	37.9	25.7
$f'_{c,90days}$ [1]	60.5	44.2	30.0
Material quantity (kg per cubic metre)			
GP Cement	386	298	230
Water	170	170	170
13 mm Greywacke	1000	1000	1000
Sand	820	895	953
Theoretical density (kg/m3)	2377	2363	2352

[1] $f'_c = {}^{A}/_{B^{1.5w/c}}$; where B=5.0, and A = 150 (at 28 days) and 175 (at 90 days).

Detailed assessment of the fresh properties was a lower priority for this project. Two slump tests (for mixes used in Series 2 and Series 5/6) were prepared and completed in accordance with Part 1 of the New Zealand Standard NZS3112.2:1986. The slump test was done 3 minutes after mixing had completed as the setting time can have a significant influence on the fresh properties of concrete (Hover *et al.*, 2014). Mix 2 used for Series 2 had a slump of 100 mm and some more water was added and mixing continued

with a subsequent slump test result of 120 mm. Mix 2 for Series 5 and 6 had a slump of 120 mm and was deemed satisfactory.

There were no observed honeycombs in the hardened concrete, which was expected due to the simple specimen geometry, the materials used in each mix design and the use proper vibration. Although a slump test was not performed to quantify the fresh properties of Mix 1, at the time of placing this was found to be a relatively stiff mix, however the hardened concrete finish appeared to be adequate.

4.4.3 Hardened concrete properties

Figure 4-11 presents the cylinder compression test results for nine different concrete mixes that was used in the construction of 72 pull-out specimens. All compression tests were performed according to the New Zealand Standard NZS3112.2 (1986): *Methods of test for concrete - Part 2: Tests relating to the determination of strength of concrete.* The complete compression test results are presented in Table A-4 of Appendix A. Figure 4-11 also presents two predictive relationships for compressive strength development with time that are given in ACI 209.2 (2008) and Model Code 2010 (*fib*, 2012). Each of the curves were determined based on the water-cement ratios of the three mixes that were chosen.

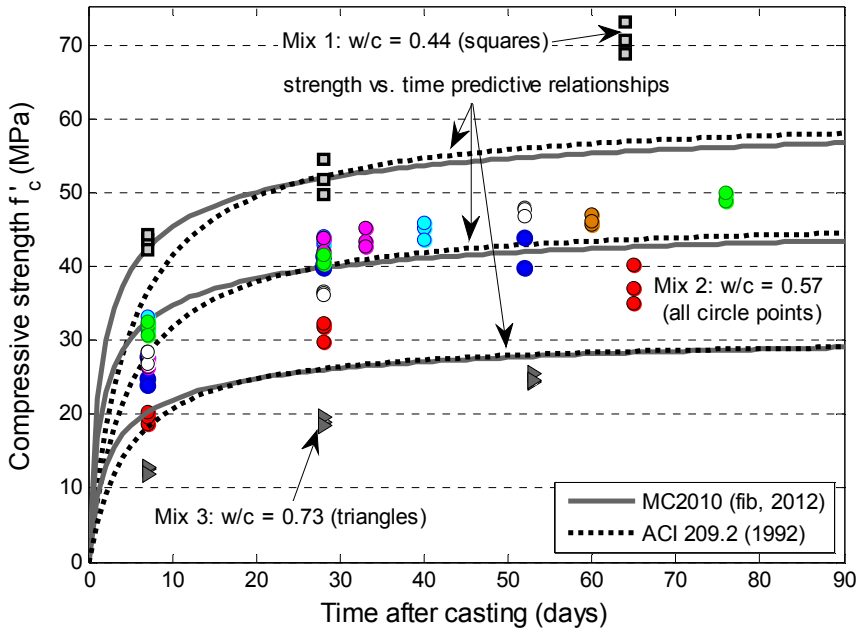

Figure 4-11: Measured concrete compressive strength development resulting from three different specified mix designs (different colours for different batches in Mix 2).

The predicted strength development shown in Figure 4-11 illustrates the results for Mix 2 compare well for the predicted values of $f'_{c,7days}$ and $f'_{c,28days}$. Although the early strength development of Mix 1 appeared reasonable, the 64 day strength increased significantly to 71 MPa.

Specimens for Series 8 were cast using mix design Mix 2, however no results were obtained at 7 or 28 days after casting as only six cylinders were prepared during casting. The average values from three

compressive tests at 60 days after casting was 46 MPa and, at 186 days, 53 MPa. An approximate strength increase of between 10 and 20% was found.

Results showed that the mix cast for Series 3-2-1/2 was greatly below the other test results. During mixing and placing the observed consistency suggested that too much water was added and post-predictions suggested the actual water-cement ratio was about 0.65. Abrams law indicates the 7 day and 28 day compressive strength may be order of 23 MPa and 31 MPa, which agrees well with the measured results. The strength of this mix is slightly lower than desired, however, and was deemed as an outlier for comparisons with other results for Mix 2.

A statistical comparison could be made for compressive tests results obtained for seven different mixes of Mix 2 that targeted 45 MPa at time of bond testing. Table 4-3 presents the average and standard deviation of the results assessed at 7 and 28 days after casting, and at the time that the pull-out specimens were tested.

Table 4-3: Measured compressive strengths for a mix with a specified water/cement ration of 0.57.

	Mean	Standard deviation	Number of mixes
$f'_{c,7days}$	28.9 MPa	2.9 MPa	5
$f'_{c,28days}$	40.9 MPa	2.7 MPa	5
f'_{c} [1]	45.8 MPa	2.5 MPa	6

[1] at time of bond testing

No splitting tensile tests or elastic modulus tests were performed. Splitting tensile tests typically have a significant amount of scatter in the results such that a large number of samples is required in order to present reliable data. Elastic modulus testing is relatively complex and time consuming. The elastic modulus was also considered to be a less significant metric that was not strictly required for interpretation of results for the measured bond behaviour.

4.5 TEST PROGRAMME

4.5.1 Loading protocols

This programme includes pull-out testing under monotonic and cyclic loading. Figure 4-3 illustrated how the test bar can be effectively pulled-out (under monotonic loading) and how reversing cycles of pull-push loading can be performed due to arrangement of the loading frame.

The loading protocols used in the test programme are listed in Table 4-4 and shown in Figure 4-12(a)-(f). The approximate test duration (or "run time") was 10 minutes for monotonic loading and 120 minutes for cyclic loading (under LH1). The run time for tests done with LH4 and LH5 was less than 40 minutes. Further discussion of the different loading protocols is given in Section 4.5.2.4.

Bond slip is the chosen engineering demand parameter for all loading protocols. 'Bond slip' refers to the slip measured by the potentiometer (refer to Section 4.2.2) at the unloaded end of the deformed test bar. Cyclic loading in the Instron machine was manually controlled, thus meaning that the potentiometer measurements displayed on the logger were observed carefully during the cyclic tests. The use of bond slip measurements are discussed further in Section 5.2 of Chapter 5, while the basis for adopting each of the cyclic loading protocols is given in Chapter 6.

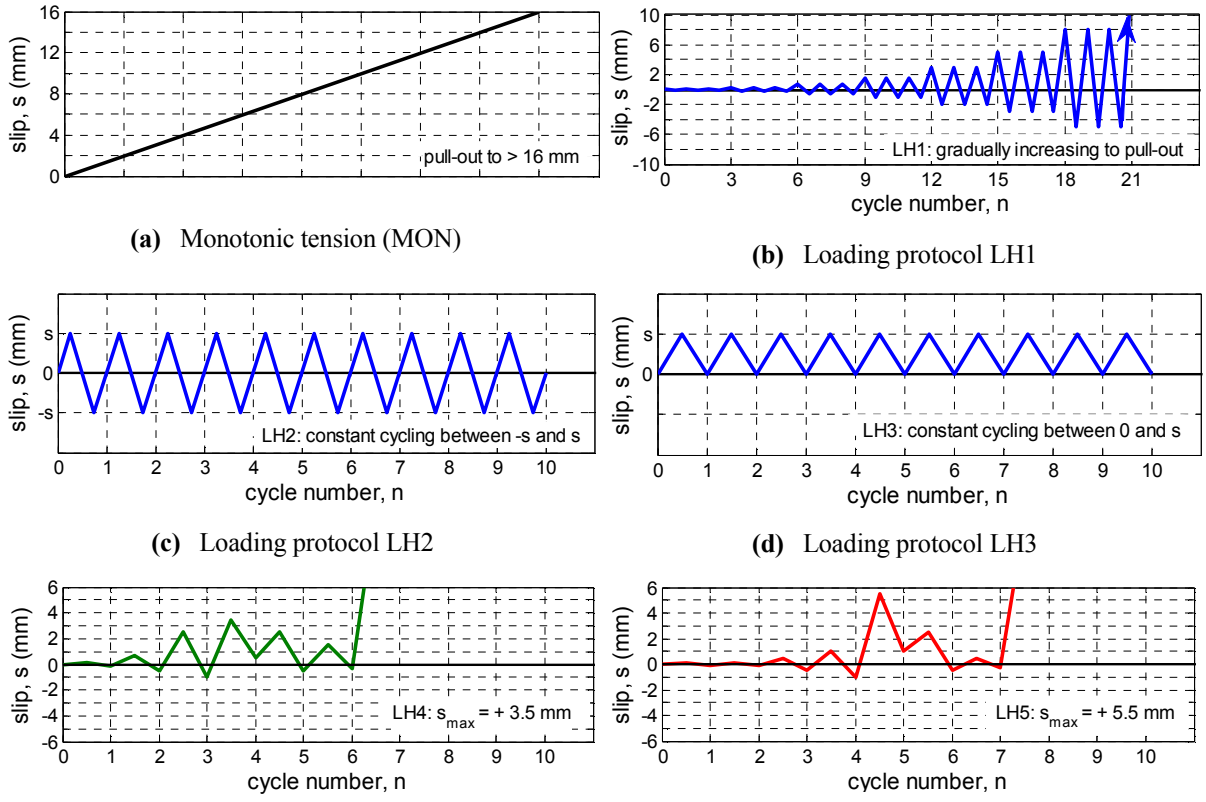

(a) Monotonic tension (MON)

(b) Loading protocol LH1

(c) Loading protocol LH2

(d) Loading protocol LH3

(e) Loading protocol LH4

(f) Loading protocol LH5

Figure 4-12: Slip-controlled loading protocols applied during some bond pull-out tests.

4.5.2 Test permutations

A large number of test permutations can be studied by using the relatively simple pull-out test set-up that was chosen. Table 4-4 provides a summary of permutations that were chosen and their relevance to this research is briefly described in the following sections. 75 specimens were tested in total; 47 of which were subjected to monotonic loading and 28 were subjected to cyclic loading. Three trial specimens were initially tested to gain experience in carrying out testing procedures and to observe the specimen behaviour.

Eight "Series" (and Rows within each Series) were established as categories for each permutation. Tests were usually repeated three times under identical parameters for each variable within a Series. Due to the large number of tests completed, some level of comparison can be made between different Series with relatively minor deviation between the test parameters. The number of specimens used in each series, or in half of that series, was generally governed by the concrete mix volume. Listed below is the typical set of "standard" parameters, and the typical specimen geometry shown in Figure 4-13.

- Concrete strength: f'_c = 46 MPa
- Cover concrete thickness: c = 72 mm
- Embedded length: l_e = 54 mm
- Nominal bar diameter: d_b = 16 mm
- Loading rate, or rate of applied slip: $\dot{s}$ = 2 mm/min
- Loading history: monotonic "tension" and cyclic LH1.

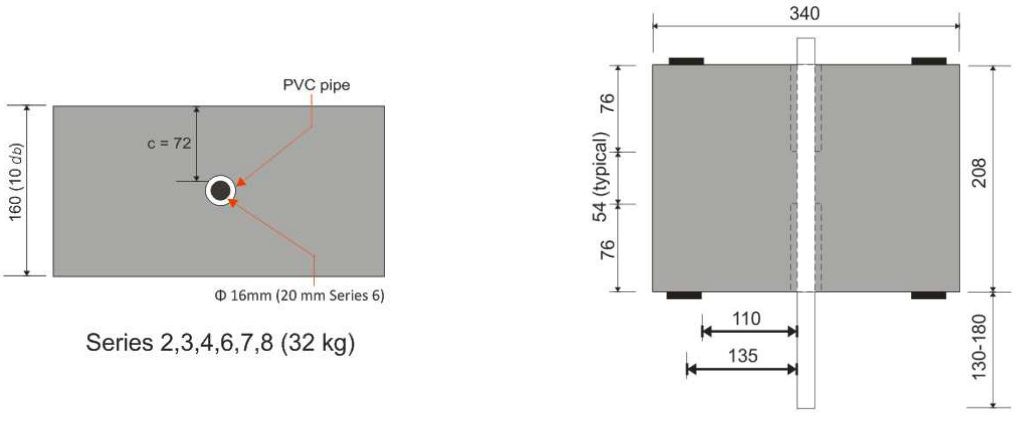

(a) Plan view **(b)** Elevation

Figure 4-13: Illustration of the generic test specimen details.

Table 4-4: Test programme for bond pull-out testing (excluding three trial tests).

Series	Row	Variable	Loading protocol	Slip rate $\dot{s}$	Bar diameter	Design w/c ratio	Bond Length, l_e	Depth from free surface	Clear cover depth	Number of tests (72)	Actual f'_c
1	1 2	Side cover	3 x MON 1 x LH1	2.0 mm/min	16 mm	0.57	54 mm	$5d_b$	48 mm 96 mm	4 4	47.5 MPa
2	1 2 3	Slip rate	MON tension	100 mm/min 2.0 mm/min 0.1 mm/min	16 mm	0.57	54 mm	$5d_b$	72 mm	3 2 3	44.9 MPa
3	1 2 3 4	Bonded depth from free surface	1 x MON tension 1 x MON compression 2 x LH1	2.0 mm/min	16 mm	0.57	54 mm	$0d_b$ $2.5d_b$ $7.5d_b$ $10d_b$	72 mm	4 4 4 4	37.4 MPa 41.8 MPa
4	1 2 3 4 5 6	Loading history	2 MON 3 LH4 3 LH5 1 LH 1 3 LH2 2 LH3	2.0 mm/min	16 mm	0.57	54 mm	$5d_b$	72 mm	2 3 3 1 3 2	49.2 MPa 24.5 MPa 70.8 MPa
5	1	Embedment length	2 x MON 1 x LH1	2.0 mm/min	16 mm	0.57	87 mm	$5d_b$	72 mm	4	43.7 MPa
6	1	Bar diameter	2 x MON 1 x LH1	2.0 mm/min	20 mm		62 mm	$5d_b$	72 mm	4	
7	1 2	Concrete strength	5 x MON 5 x MON	2.0 mm/min	16 mm	0.74 0.44	54 mm	$5d_b$	72 mm	5 5	24.5 MPa 70.8 MPa
8	1 2	Concrete maturity	1 x MON 3 x LH1	1.0- 2.0 mm/min	16 mm	0.57	54 mm	$5d_b$	72 mm	4 4	46.3 MPa 52.7 MPa

4.5.2.1 *Series 1: Cover thickness*

In RC walls, the cover thickness for the vertical reinforcement depends on the whether configuration is singly or doubly-reinforced (one or two layers along the wall length). In the end zones of walls, the cover thickness may also vary for bars positioned at corner edges. The chosen cover thickness for test specimens was mainly based on the conditions that might exist for a singly reinforced wall.

Figure 4-14 illustrates the different dimensions chosen for three different test permutations.

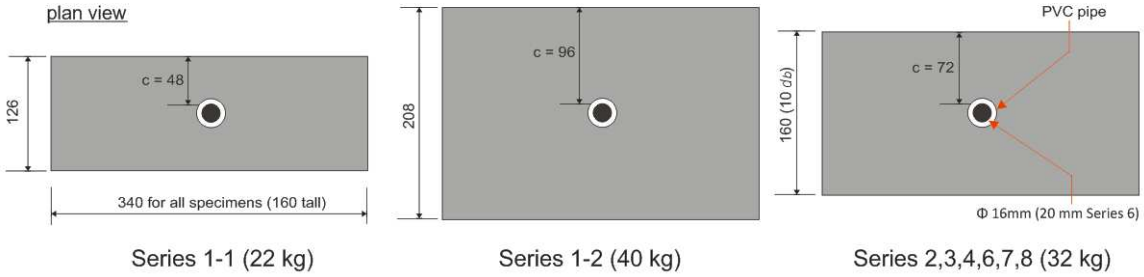

Figure 4-14: Illustration of the approximate clear concrete cover to the deformed bar in Series 1 and the typical geometry all other tests.

4.5.2.2 *Series 2: Loading rate*

The influence of loading rate on bond behaviour was studied under monotonic loading only. The benchmark loading (slip) rate $\dot{s}$ = 2 mm/min was chosen as this provides a reasonable test duration. The speed of the Instron testing machine restricted the maximum and minimum loading rate to 100 mm/min and 0.1 mm/min (50 times faster and 20 times slower than the standard rate, respectively). The fastest and slowest tests were completed within a run time of about 15 seconds and 200 minutes, respectively.

Further discussion about the chosen loading rates for testing is presented in Chapter 5.

4.5.2.3 *Series 3: Depth of bond region from free surface*

Series 3 varied the bond position relative to the free surface, which acts as an equivalent crack plane (discussed in Chapter 3). Figure 4-15 schematically illustrates the variation of the embedded length and the provision of the unbonded lengths of the test bar. The geometry of the test specimens was kept constant for two main reasons: (i) the ease of maintaining the same outer dimensions to re-use the same formwork; and (ii) the embedded length, l_e, was typically maintained to allow for reasonable comparisons between different test Series.

Figure 4-15 also illustrates that, to some extent, test series might be able to consider the influence of variable concrete strengths as a function of the casting position. It is noted however that strength gradients are expected to be reasonably uniform as the total specimen depth of 208 mm is relatively.

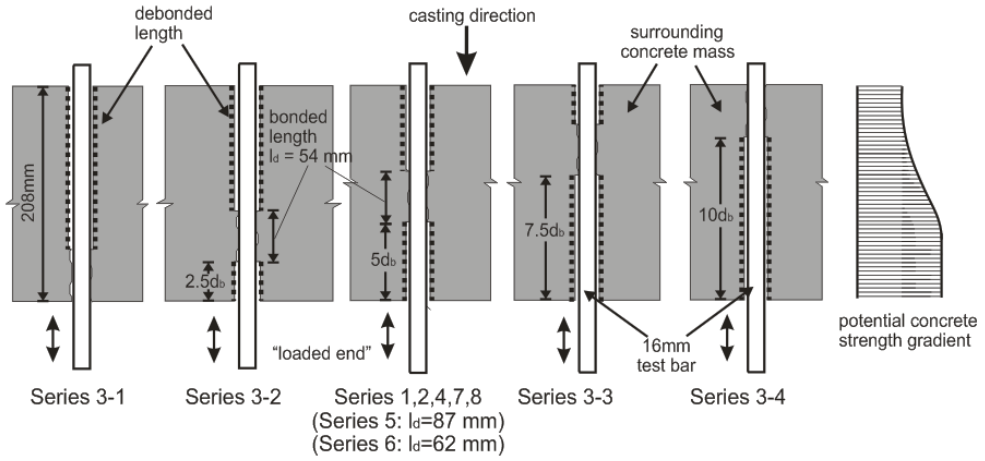

Figure 4-15: Approximate specimen dimensions for the Series 3 permutations of the position of the bond region relative to the top and bottom free surface.

4.5.2.4 *Series 4: Loading history*

The influence of loading history on bond behaviour was studied in Series 4 with five different cyclic loading histories as shown in Figure 4-12(b)-(f). Features of each loading protocol where chosen to provide a range of information about cyclic bond deterioration. Loading histories LH4 and LH5, shown in Figure 4-12(c) and (d), were chosen in attempt to represent the type of loading that a RC wall structure might experience during severe near-source ground shaking (i.e. high amplitude with low number of cycles due to short duration ground shaking and vibration period of the structure).

Further discussion on the basis for determining these cyclic loading protocols is given in Chapter 6.

4.5.2.5 *Series 5: Embedded length*

The embedment length used in Series 5 was 87 mm, larger than the length of 54 mm used in all other Series. Previous experimental research, such as Eligehausen *et al.* (1983), used an embedded length of approximately $5d_b$. The lengths used here are about 5.5 and 3.5 times the nominal bar diameter. It was not possible to reliably have an embedment length of $5d_b$ due to the manner in which the plastic tube was used to provide unbonded regions (refer to the schematic illustration in Figure 4-8). The embedment length used here depended the actual rib spacing, instead of the bar diameter d_b.

4.5.2.6 *Series 6: Bar diameter*

The nominal bar diameter in Series 6 was 20 mm, one standard size larger than the 16 mm bars that were used throughout all other Series. It is noted that the common bars sizes typically range between 20 mm and 32 mm for ductile RC beams and columns. In lightly reinforced walls, the vertical reinforcement is typically provided by 16 mm and 20 mm bars, and sometimes 12 mm bars of higher strength Grade 500 (lower characteristic yield strength of 500 MPa, e.g. in the Gallery Apartments building, described in Chapter 2).

The relative rib areas for the HD16s and HD20s used in these pull-out specimens were 0.11 and 0.09, respectively. It is reasonable to assume that, for this study, any noticeable differences in bond behaviour will be due to the variation of the bar diameter, as opposed to minor differences in the relative rib area.

4.5.2.7 *Series 7: Concrete strength*

The values of concrete strength that is widely used in laboratory testing will typically range between 25 and 40 MPa. Chapter 2 discussed some reasons for variation of the in-place concrete strength in real structures and particular attention was drawn to cases when the actual concrete compressive strength was higher than that anticipated by the structural design engineer.

Section 4.4.3 showed an upper and lower bound concrete compressive strength of 71 MPa and 25 MPa was achieved during specimen construction. This range was considered to be appropriate for a conventional structural concrete. The results showed that the mean concrete strength was about 46 MPa which means the upper and lower bound strengths are reasonably large and evenly separated. A large enough separation between different strength grades also means that results can be interpreted between tests within the bounds of other potential sources of scatter.

4.5.2.8 *Series 8: Concrete age*

Interest in the time-dependent properties of concrete has resulted in testing some nominally identical specimens at distinctly different times after casting. Eight specimens were cast simultaneously for Series 8; four of which were tested at 60 days and the remaining four were tested at 186 days.

Laboratory testing of RC components is typically carried out close to 28 days after the concrete has been poured. Across the entire testing programme, the "youngest" specimens were those tested in Series 6 where the concrete strength was about 44 MPa at 33 days. The age of the oldest specimens was governed by the constraints of completing the tests within a reasonable timeframe.

4.6 CHAPTER SUMMARY

The relevant details of the entire experimental programme for bond pull-out tests were presented in the Chapter. Design and construction of the test set-up and pull-out specimens was described within. A novel construction detail involved cutting the plastic tube to ensure the debonded lengths matched the rib inclination angle of the deformed bar. Supplementary information to this chapter was included in Appendix A. Significant care, labour and time was required to complete the pre-test preparation for 75 pull-out specimens. Results for concrete materials tests showed the majority of test specimens reached the desired strength targets at the time of testing (46 MPa) without significant variation between specimens that were cast at different times. The separation between lower and upper bound concrete strengths (25 MPa and 71 MPa, respectively) was reasonably even, albeit slightly larger than originally specified. The

typical set of test parameters and applied loading protocols were presented and the permutations of eight different "Series" of the test programme were introduced to provide context to results presented in Chapters 5 and 6.

Documentation of this experimental programme is particularly important to the field of bond-related research as testing procedures are not well-standardised. Awareness and consideration of the experimental boundary conditions used here should be maintained when explaining testing observations and interpreting the bond test results (given in Chapters 5 and 6).

4.7 ACKNOWLEDGEMENT OF EXPERIMENTAL SUPPORT

University of Canterbury technical staff provided some assistance in this phase of the research presented in this chapter and must be acknowledged. Mr. Gavin Keats is thanked for his help in assembling the formwork that was re-used throughout the specimen construction. Mr. Tim Perigo and Dr. Allan Scott are recognised for their assistance during concrete mixing and placing and Mr. Stuart Toase is recognised for threading the deformed test bars. Mr. Mosese Fifita and Mr. Alan Poynter also assisted in the preparation the test set-up. Postgraduate colleagues Samia Ali and Tushar Chaudhari must be thanked for completing some of the concrete cylinder compressive tests during my absence.

The cement used for this project was kindly supplied by Holcim Cement. Other materials used in this research were covered under the SAFER Concrete Technology funding provided by the Ministry of Business, Innovation and Employment (MBIE) via the Natural Hazards Research Platform.

4.8 REFERENCES

ACI Committee 408, (2003). Bond and development of straight reinforcing bars in tension: ACI 408R-03, American Concrete Institute, Farmington Hills, MI.

ACI Committee 209.2, (2008). Guide for modelling and calculating shrinkage and creep in hardened concrete: *ACI 209.2R-08*, American Concrete Institute, Farmington Hills, MI.

ASTM-C873/C873M-10el (2010). ASTM C873 / C873M -10el. Standard test method for compressive strength of concrete cylinders cast in place in cylindrical moulds, American Society for Testing and Materials.

ASTM A615 (2014). Standard specification for deformed and plain billet-steel bars for concrete reinforcement, *American Society for Testing and Materials.*

Comite' Euro-internationale du beton (CEB-FIP, 1993). The Model Code 1990: *Design code*. London: T. Telford; 1993.

Comite' Euro-internationale du beton (CEB-FIP, 1996) RC elements under cyclic loading: *State-of-the-art report*. London: T. Telford; 1996.

Fédération Internationale du Béton, *fib*. (2012), Model Code 2010 - Final draft, Volume 2. *fib* Bulletin No. 66, Lausanne, Switzerland.

Hover, K.C, Abel, J and Pinto, R.C.A. (2014). The exciting first day in concrete: chemical and physical processes at the micro-level drive macro-level construction operations, *Conference Proceedings of the New Zealand Concrete Industry*, Wairakei, October.

Kivell, A. (2011). Effects of bond deterioration due to corrosion on seismic performance of reinforced concrete structures, *Master of Engineering Thesis*, University of Canterbury, Christchurch, New Zealand.

Soleymani Ashtiani, M. (2013). Seismic performance of high-strength self-compacting concrete in reinforced concrete structures, *Doctor of Philosophy Thesis*, University of Canterbury, Christchurch, New Zealand.

Standards New Zealand. (2001). Steel reinforcing materials standard, NZS4671. Standards New Zealand, Wellington, New Zealand.

Standards New Zealand. (1986). Methods of test for concrete - Part 1: Tests relating to fresh concrete, NZS3112.2. Standards New Zealand, Wellington, New Zealand.

Standards New Zealand. (1986). Methods of test for concrete - Part 2: Tests relating to the determination of strength of concrete, NZS3112.2. Standards New Zealand, Wellington, New Zealand.

[This page is intentionally left blank]

5 EXPERIMENTAL RESULTS FOR MONOTONIC BOND BEHAVIOUR OF DEFORMED BARS

Morris, G.J., Bull, D.K. and Bradley, B.A., (2015) "Monotonic and cyclic bond behaviour of deformed bars in reinforced concrete structures", C*onference proceedings of the New Zealand Society of Earthquake Engineering*, April 2015, Rotorua, New Zealand.

5.1 INTRODUCTION

Extending as far back as Abrams (1913), studies on bond between deformed reinforcing bars and the surrounding concrete were initially undertaken to determine the bond strength required to prevent brittle failures from occurring at the anchorage zones and development lengths of the reinforcement in structural components. In more recent decades, bond-related studies have focussed on determining a reliable relationship between bond stress and bond slip, and to determine how this relationship is influenced by different structural conditions and different types of loading. For example, Eligehausen *et al.* (1983) completed 125 pull-out bond tests to determine a constitutive local bond stress-slip relationship which could be used in analytical and numerical predictions of the structural behaviour of beam-column joints in ductile RC frames. The findings of Eligehausen *et al.* (1983) was adopted in the Model Code 1990 (CEB-FIP, 1993) and is found in the more recent Model Code 2010 (*fib*, 2012).

Conclusions from previous research (summarised in Chapter 3) generally suggest that bond behaviour is influenced by some of the pertinent factors, or a combination of factors, that potentially contributed to the unexpected damage to some reinforced concrete (RC) buildings that was described in Chapter 2. In order to further understand bond mechanics, the experimental results that were obtained from 48 monotonic bond pull-out tests are examined in this chapter. Different specimens were used to assess how monotonic bond behaviour is influenced by: loading rate, concrete strength, concrete age, side-cover thickness, bar diameter, embedded bond length, and the position of the embedded bond region within the specimen (deep within or close to free surface). Observed failure modes are described within this chapter, while Appendix C contains supplementary observations and a full table of test results. The bond stress-slip relationships are presented for each specific test series that investigated different permutations. Lastly, the monotonic test results are generalised to allow a mean bond stress-slip relationship to be presented and compared to that implemented in the CEB-FIP (now *fib*) Model Codes (1993; 1996; 2012).

5.2 DEDUCING THE BOND STRESS-SLIP RELATIONSHIP

One approach to experimentally determine the bond stress amplitude is to follow the strict "bond concept" definition that was mentioned previously in Section 3.1.1, which would be in accordance with the expression given in Equation 3-3. This exact bond concept approach is often impractical for obtaining values of bond stress for two reasons: (i) directly utilising the stress-strain relationship of the reinforcing steel is deemed to be an unwarranted complexity; and (ii) it is extremely difficult to obtain reliable strain measurement data that would involve preparation and application of strain gauges, or relying on values measured by a clip-gauge extensometer. Eligehausen *et al.* (1983) initially attempted to use strain measurement data from bond pull-out tests to obtain the stresses in the reinforcing steel and deduce the resulting bond stress based on Equation 3-2. This approach is somewhat impractical in experiments with a large number of tests and may produce unreliable results due to the inaccuracy of measured data.

To deduce the average bond stress-slip relationship in this research, a fundamental assumption was that the applied load (measured from the load cell) was equal and opposite to the bond stress that is assumed to be uniformly distributed over the embedded bond surface area. The value of (average) bond stress, τ, that is reported in the remainder of this thesis has therefore been determined using Equation 5-1.

$$\tau = \frac{T}{\pi d_b l_e} \qquad \text{[MPa]} \qquad 5\text{-}1$$

where

T = applied force [N]

d_b = actual bar diameter [mm] (typically 16 mm)

l_e = embedment length [mm] (typically 54 mm)

The sign conventions for bond stress and bond slip are positive values when the bar is in tension. It was reasonable to assume the bond stress distribution as being uniform as the embedded bond length was relatively short (compared to long anchorage lengths with non-uniform bond stresses). The bond surface area is equal to 2714 mm^2 for the typical geometry used in the majority of these tests. Across all tests, the maximum applied load was such that steel stresses were typically between 50 to 75 percent of the nominal yield strength.

Equation 5-2 defines the incremental bond slip, ds/dx, along a particular position x of an embedded reinforcing bar. The true definition of the total local bond slip, $s(x)$, accounting for a non-uniform distribution of stresses, is given by Equation 5-3.

$$\frac{ds}{dx} = \varepsilon_s(x) - \varepsilon_c(x) \qquad 5\text{-}2$$

$$s(x) = \left(\int_{x_0}^{x} \varepsilon_s dx - \int_{x_0}^{x} \varepsilon_c dx \right) + S_0 \qquad 5\text{-}3$$

where S_0 is global slip at the unloaded free-end of the bar, and the bracketed term refers to the local slip due to relative strain incompatibility between the reinforcing steel strain, ε_s, and concrete strain, ε_c, from the free end x_0 to a particular position *x*.

Since the steel strains at the loaded end did not exceed the yield strain during testing, the additional slip due to local bar elongation along such a short embedment length was unlikely to exceed 0.1 mm. It was therefore assumed (in this thesis) that the bracketed term in Equation 5-3 could be neglected and that the local bond slip was approximately equal to the free-end slip measured by the potentiometer, i.e. $s(x) \approx S_0$.

5.3 OBSERVED FAILURE MODES

Test specimens were typically designed to promote bond pull-out failure, which was observed in 33 out of the 48 monotonic tests as summarised in Table 5-1. A description of each failure mode is presented in the following sections and supplementary information is presented in Appendix C in the form of photographs of observed damage.

Table 5-1: Quantity of different failure modes observed in monotonic bond pull-out tests

Failure mode	Quantity
Pull-out bond failure	33
Splitting bond failure	4
Cone break out failure	3
Prying failure	8
Total	48

Different bond stress-slip curves representing three failure modes are shown in Figure 5-1. Cone break-out failure was only observed in tests for Series 3-1 and the bond stress-slip curves for this behaviour are discussed in Section 5.4.4.

For two particular tests (2-2-1 and 2-2-2), Figure 5-1 shows there were separate observations of a premature specimen failure and a splitting bond failure, despite these two tests having nominally identical conditions. Along with pull-out failure, there were some instances where these failure modes occurred at similar values of maximum bond stress. Unfortunately, this suggests that the bond stress at the onset of the three different failure modes was relatively close. Table C-1 (in Appendix C) lists the observed failure mode and maximum force applied during each bond test. Some failure modes were uncertain and in some tests an apparent pull-out failure did not necessarily exhibit a typical plateau in the peak stress range of the bond stress-slip curve.

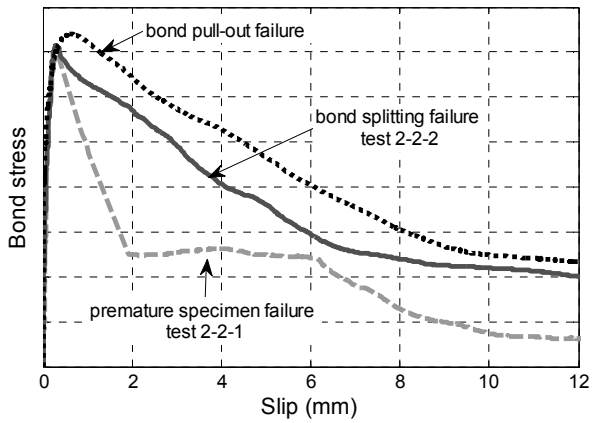

Figure 5-1: Qualitative comparison of the bond stress-slip behaviour measured for three types of failure that were observed during monotonic bond testing.

5.3.1 Trial tests and premature specimen failure

Two initial monotonic trial tests were performed to gain some experience in preparing the test set-up, calibrating the instrumentation, and observing the likely maximum applied load and behaviour of the test specimen. Both trial tests indicated that a single wide flexural crack tended to form, which then caused the specimens to burst in a brittle manner and the measured load was reduced suddenly. This type of failure is referred to herein as a 'premature specimen failure', rather than a representative bond failure. The typical bond stress-slip curve that was measured during premature specimen failure is qualitatively shown in Figure 5-1. Eight test results of this nature are included in Table C-1 of Appendix C, however these were not used to deduce information about bond behaviour. At the onset of this failure, the measured bond stress ranged between 60 to 100 percent of the maximum bond stress observed in other tests with pull-out failure. As shown in Figure 5-1, the bond stress typically reduces very suddenly after failure until the slip is equal to about 2 mm, after which there is some residual strength is provided until the slip exceeds 6 to 9 mm and the concrete key is completely destroyed.

Inspection of the damaged specimens found this failure mode may be explained by the cover thickness of 50 to 70 mm to the flexural tension reinforcement (2-D10's) being larger than intended due to construction tolerances. Figure 5-2(a) schematically illustrates how the increased cover depth allowed a large crack width of 3 to 5 mm to form before the reinforcement could provide sufficient tensile resistance. It was later found that unintentionally large cover depth was an error in the construction of some specimens where the bars had settled further downward during vibration of the fresh concrete.

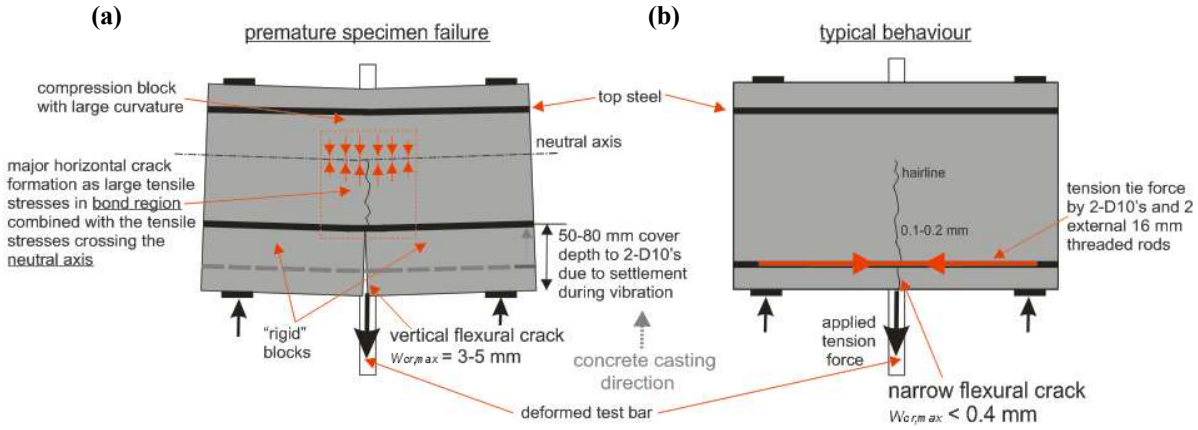

Figure 5-2: Schematic illustration of the observed specimen behaviour (a) premature specimen failure observed in 8 specimens, and; (b) typical behaviour in remainder of specimens where flexural cracking very minor or did not occur.

Considering the schematic of the test specimen shown in Figure 5-2(a), all the deformation was observed to be concentrated at crack in the mid-span, while the concrete either side of the crack moved separately as two uncracked rigid blocks. Above the neutral axis, the compression side of the specimen behaves as a continuous member where the flexural compression force induces large curvature. Incompatible deformations between the tension and compression regions within the specimen caused concrete tensile

stresses to develop in the transverse direction across the neutral axis, which ultimately led to premature specimen failure.

Figure 5-2(b) illustrates how the tension tie was modified in order to limit the width of the flexural crack and suppress the issues observed with premature specimen failure. Two external 16 mm threaded bars with end-bearing plates were snug-tightened along the flexural tension side to restrict the widening of the flexural crack and greatly reduce the total specimen deformation. It was noted that the maximum bond stress during a true pull-out or splitting failure occurred with relatively minor flexural deformation of the specimen which suggests that the presence of the external ties was unlikely to influence the maximum bond strength. Observations from bond tests typically showed that either a flexural crack did not form, or if it did then the crack width (at the soffit) ranged between 0.2 to 0.4 mm when the applied loading was at maximum. The effect of minor flexural cracking on the measured bond behaviour was deemed to be negligible and realistic pull-out and splitting bond failure modes were observed in the remaining tests.

5.3.2 Splitting bond failure

Splitting cracks were observed on the front and back faces of four test specimens, despite the clear side cover being 72 mm thick. Two or three of the splitting bond cracks were visually identified with ease and the onset of cracking could be heard during testing. Figure 5-1 indicates the general shape of the bond stress-slip curve when splitting bond failure was observed in a particular test case where relatively high bond stresses were able to develop, followed by a sudden loss in strength. The negative slope of the post-peak bond stress-slip curve shown in Figure 5-1 is similar to that for a bond pull-out failure.

Figure 5-3(a) shows a saw-cut cross section where splitting failure occurred. Adjacent to the bond region, there is a variation between the inclination angles of the three splitting cracks. Towards the loaded end, the first bond crack angle initiates at approximately 40 degrees, whilst the middle and unloaded end crack angles are approximately 30 and 15 degrees, respectively. Further outwards from the bond region the crack angles are shown to have reduced

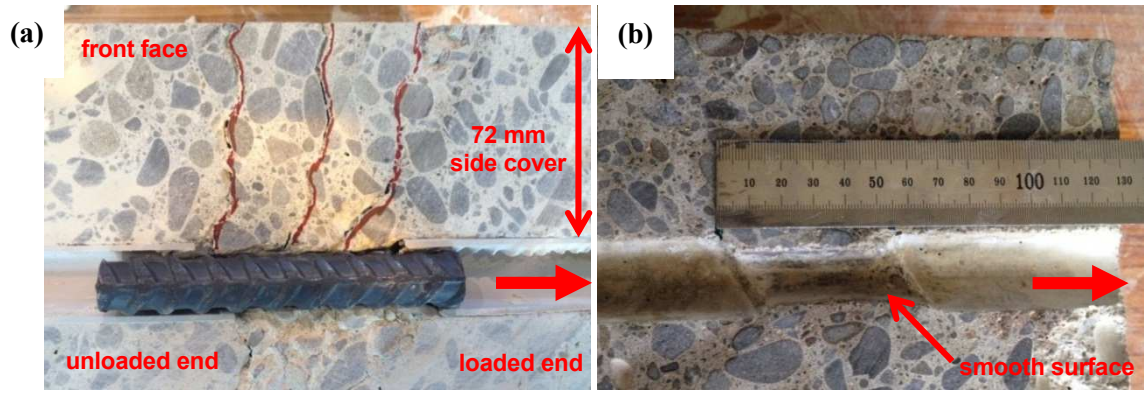

Figure 5-3: Saw-cut cross sections showing the typical damage after: (a) splitting failure, and; (b) pull-out failure.

5.3.3 Pull-out bond failure

Pull-out was observed in 32 of the 47 monotonic tests when the specimen either did not develop any flexural crack, or when single narrow flexural crack formed as illustrated in Figure 5-2(b). The occurrence of the flexural crack could be seen by a small bump in some of the measured load-slip curves at small slip values, typically when the load was between 80 and 100 percent of the measured maximum bond stress. After test completion, the bar was completely pulled out and removed from the specimen for inspection. Figure 5-4 shows the fractured 'concrete shear keys' embedded between the ribs of a HD16 deformed test bar which is the result of direct shear failure of the concrete that formed at the surface interface during casting (predominantly cement paste and sand particles). As such, Figure 5-4 shows the rib profile and crushed cement for a test were the bond length equalled 8 times the rib spacing. However, some of the concrete keys had fallen away from the deformed bar surface during handling.

Figure 5-4: Photo showing the condition of the HD16 test bar and concrete between the ribs following a pull-out failure in test 5-1-3 with a longer embedded bond length.

5.3.4 Cone break out

Cone break-out was observed in three monotonic tests conducted in Series 3-1 and Figure 5-5 shows photos of this failure (at different scales). Inspection of a portion of broken concrete in Figure 5-5(c) shows that cone failure occurred without any significant crushing of the concrete that was adjacent to the ribs. Figure 5-5(d) illustrates the average cone radius was between 100 and 110 mm, with a corresponding cone angle between 25 and 30 degrees, as labelled more closely on Figure 5-5(e).

Illustrated in Figure 5-5(e), the specific position of the bond region means that bond forces are bearing against concrete that is relatively unconfined. Figure 5-11(b), presented later in Section 5.4.4, illustrates that cone break-out failure occurred at bond stresses with the maximum value, $\tau_{max,cone}$, that are lower than a pure bond failure (generally equal to $1.4\sqrt{f'_c}$). Cone failure occurred at an average splitting stress that is approximately between 0.8 and 1.0 MPa, where these values are based upon simple hand calculations with a relatively consistent value of 25 kN for the maximum applied load (from three monotonic tests) being divided over an idealized failure surface area. The schematic diagram in Figure 5-5(e) suggests how the magnitude of the tensile stresses radially decreases away from the bond region. Local splitting stresses may have been three to four times the average value, which compares reasonably well to the predicted tensile strength of concrete which may be between 3.0 to 3.5 MPa (refer to Equation 5-4, with f'_c equal to 37 MPa at time of testing Series 3-1).

(a) (b) (c)

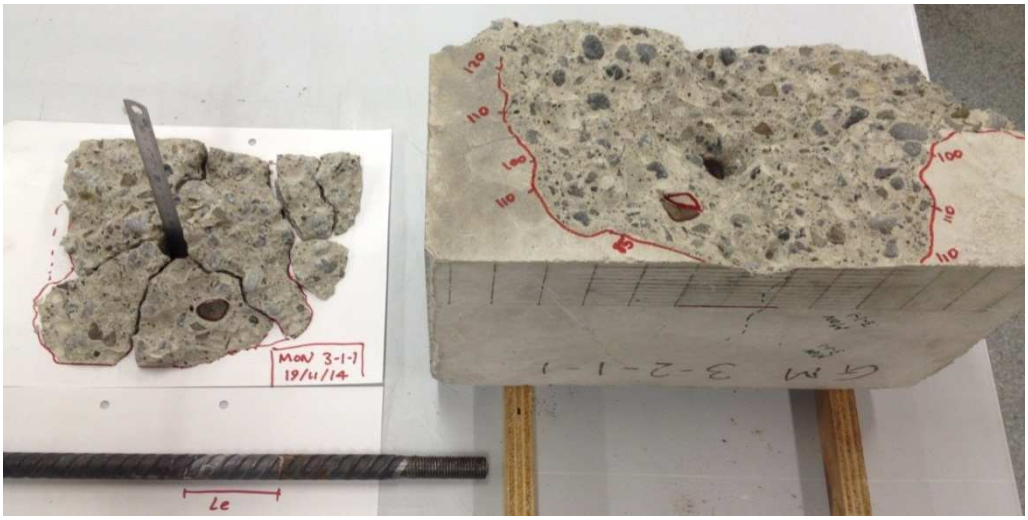

(d)

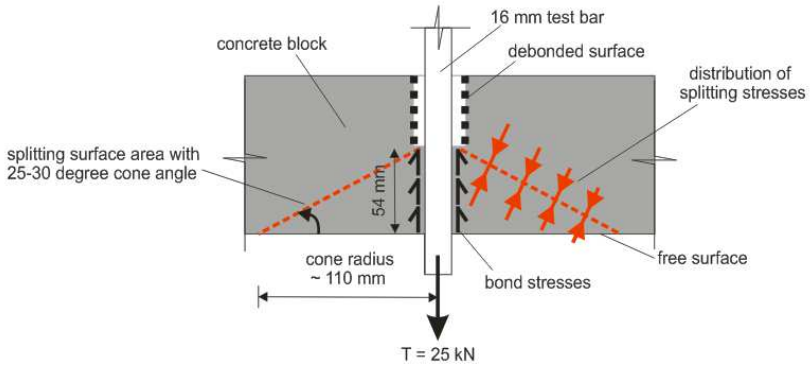

(e)

Figure 5-5: (a)-(d) Various photographs showing cone break-out failure observed during monotonic testing; (e) schematic illustration of an approximated cone failure surface used to determine the average concrete splitting stress.

5.4 RESULTS OF PARAMETRIC STUDY

This section discusses the results from monotonic bond tests performed in Series 1 to 8, with the exception of the Series 4 results for cyclic bond tests are discussed separately in Chapter 6. Results from Series 7 are presented first as the concrete strength significantly influences the amplitude of bond stress. Results for remaining Series are discussed in numerical order.

5.4.1 General bond stress-slip behaviour

As mentioned previously, 32 out of 47 monotonic bond tests exhibited bond pull-out failure. A typical bond-stress slip curve is shown for the full slip range in Figure 5-6(a) and in a smaller slip range of up to 2.0 mm in Figure 5-6(b). The inset figure on Figure 5-6(a) schematically illustrates each point at which bond slip has exceeded the physical features of the rib geometry of the 16 mm deformed bars. As discussed previously in Section 3.3.1.1, the clear spacing of the ribs, $s_{r,clear}$, determines the length of the concrete shear key (that is formed during casting) and therefore influences the bond slip range at which mechanical bearing resistance is provided. Detailed measurements of the rib geometry of 16 mm and 20 mm deformed test bars are found in Appendix A.1.2.

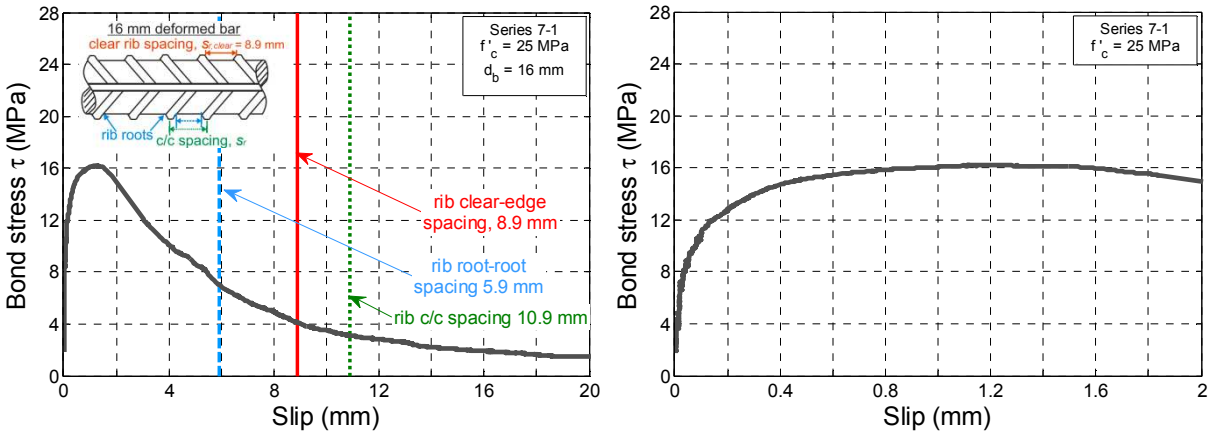

(a) typical bond stress-slip curve **(b)** initial bond stiffness

Figure 5-6: Bond stress-slip relationship in an individual test performed in Series 7-2.

For tests where pull-out failure occurred, monotonic bond behaviour was reasonably consistent with that shown in the test results of Eligehausen *et al.* (1983). The typical behaviour is described below:

- Pre-peak behaviour: Figure 5-6(b) shows the ascending branch has a very high initial stiffness that appears to be linear until the bond stress reaches approximately 50 to 60 percent of the maximum bond stress. After this linear segment, the ascending branch stiffness reduces until the slope is zero at the maximum bond stress.
- Peak behaviour: Figure 5-6(a) and (b) shows the maximum bond stress develops at a slip values of about 0.8 mm and is relatively constant until about 1.5 mm.

- Post-peak behaviour: Once slip exceeds approximately 2.0 mm, bond stress gradually decreases on a slightly curved negative slope until bond slip reaches 9.0 mm. The levelling of the bond stress-slip curve is physically caused by the bond slip exceeding the clear distance between the ribs and is labelled on Figure 5-6(a). At larger slip values, there is a residual bond stress that is approximately constant. With this in mind, the bond stress-slip curves in Figure 5-7 to Figure 5-13 are presented up to slip values of 12 mm.

Scatter between the test results was anticipated, even between specimens cast from the same batch of concrete. Figure 5-7(a) compares six individual tests results from nominally identical specimens. Four specimens had a nearly identical maximum bond stress, while the maximum bond strength in one specimen was about 15 percent lower. The scatter in these results is similar to that found by Eligehausen *et al.* (1983), where the bond stress in five nominally identical specimens was between 15 and 20 percent above or below the mean behaviour that was measured.

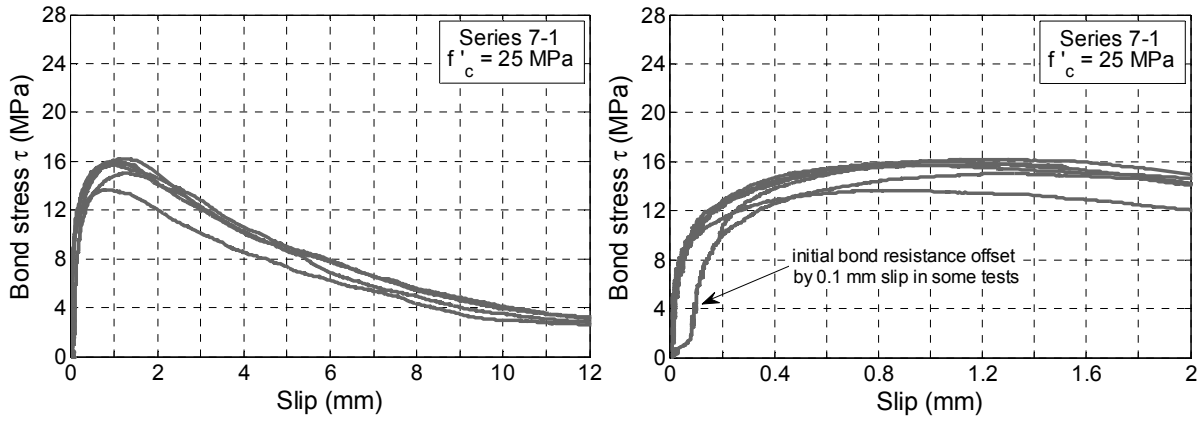

(a) bond resistance for full range of slip

(b) bond resistance for small slip values

Figure 5-7: Bond stress-slip relationship in six individual tests performed in Series 7-2.

For the same test results, Figure 5-7(b) compares the scatter in the initial stiffness. Five test results showed the bond resistance is developed with a similar initial slope, while one curve is an example showing some slip-lag in developing bond resistance. Over the entire testing programme, this initial lag was observed in about 20 percent of the total number of bond stress-slip curves that were obtained. It is unlikely that this lag is due to movement in the testing set-up, but rather due to some initial imperfection in the bond condition possibly due to the poor compaction and vibration of the fresh concrete and the effects of shrinkage. Although this initial slip is discussed here as an experimental issue, it could also apply to certain design or construction related aspects that compromise bond behaviour at initially small magnitudes of slip.

5.4.2 Series 7: Concrete strength

Specimens with three distinctly different concrete strengths resulted in the different bond stress-slip curves shown in Figure 5-8(a). For a 25 MPa concrete strength, there is a slight plateau in the maximum bond stress between slip values of 0.8 and 1.6 mm. Increasing the concrete strength (and hence increasing the concrete stiffness) has an influence on the curvature of the ascending branch in the pre-peak range and the behaviour is more "peaked" at slightly lower slip values. The trends between these three curves generally agrees with the stress-strain behaviour of plain concrete, where lower strength concrete is understood to exhibit relatively larger deformation capacity when compared to higher strength concrete that is more brittle.

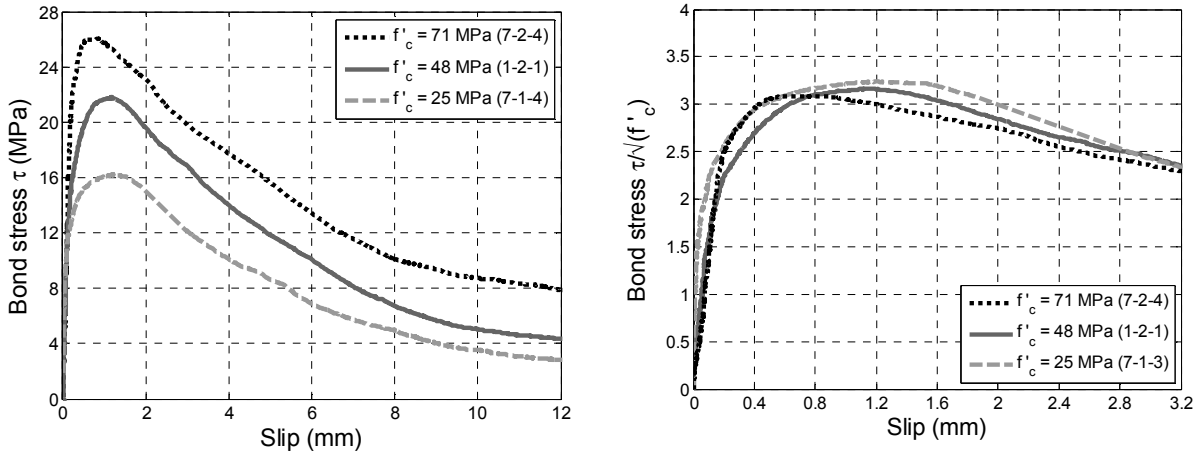

(a) Influence of concrete strength **(b)** Normalised bond strength in peak range of slip

Figure 5-8: Influence of concrete strength on measured bond stress-slip relationship

Figure 5-8(a) illustrates that bond stress is significantly influenced by the concrete strength. The difference in bond stress was expected to be similar to the respective differences in the concrete tensile strength (Eligehausen *et al.*, 1983). No splitting tension tests were performed on concrete samples in this study; however a simplified empirical prediction is made for the mean tensile strength using Equation 5-4, a proposed amendment to the New Zealand Concrete Structures Standard, NZS3101:2006.

$$f_{ct} = 0.55\sqrt{f'_c} \qquad 5\text{-}4$$

where f'_c = concrete compressive strength found from cylinder tests at the time of bond pull-out testing. Table 5-2 summarises the differences between predicted values of the mean tensile strength in comparison to differences in bond strength that were actually measured. Despite the simplicity of this comparison, the percentage differences are reasonably similar. It is noted that Equation 5-4 may not provide an accurate prediction when f'_c is as high as 71 MPa, but is within the crudeness of this quick comparison.

Table 5-2: A simple comparison between relative concrete tensile strengths and relative bond strength.

Mix	f'_c (measured)	f_{ct} (using Equation 5-4)	Δf_{ct} with Mix 2 (to within 1 %)	τ_{max} (measured)	$\Delta\tau_{max}$ (to within 1 %)
3	25 MPa	2.8 MPa	- 28 %	16 MPa	27 %
2	48 MPa	3.8 MPa		22 MPa	-
1	71 MPa	4.6 MPa	+ 22 %	26 MPa	18 %

The concrete strength variation between specimens with the same mix design was presented in Chapter 4. A normalisation of the test results is required to account for the variable concrete strengths in specimens used within different Series. Normalisation of bond stress values will also assist later with generalising these results. Previous researchers (e.g. Eligehausen *et al.*, 1983) and the Model Codes (CEP-FIB, 1993; *fib*, 2012) typically present the maximum local bond stress using a co-efficient *k* according to Equation 5-5.

$$k = \frac{\tau_{max}}{\sqrt{f'_c}} \qquad 5\text{-}5$$

Using Equation 5-5, the normalised bond stress in the "peak range" of slip is presented in Figure 5-8(b). Despite the large concrete strength variation, the normalisation of bond stress based on $\sqrt{f'_c}$ appears reasonable. Bond researchers might choose to determine relationships between the concrete strength and the gradient and curvature of the ascending branch. An insufficient number of tests were performed in this study to allow such a detailed examination of the pre-peak bond behaviour. Some minor variation between the normalised bond stress-slip curves is also expected due to inherent variability of the mechanical properties of concrete.

5.4.3 Series 1: Concrete cover thickness

Pull-out failure was observed in two monotonic tests in Series 1-1 (described previously in Section 4.5.2.1), despite the relatively small side cover thickness of 48 mm ($3d_b$) in which a splitting failure was anticipated. Three monotonic tests in Series 1-2 showed pull-out failure, which was expected due to the specimens large cover thickness of 96 mm ($6d_b$). The different sized test specimens were poured from the same concrete mix.

Figure 5-9 presents the typical bond stress-slip curves for Series 1-1 and Series 1-2. Both curves are shown to have the same initial stiffness; however the peak behaviour and maximum bond strength in Series 1-1

is 15 to 20 percent lower than Series 1-2. Figure 5-9 shows that the post-peak behaviour and residual bond stress for both curves are approximately identical.

The larger bond stresses in Series 1-2 may have been due to a larger surrounding concrete volume providing greater passive confinement to the bond zone which may delay the onset of splitting cracks and crushing of the concrete at the rib interface. Only a small number of tests were performed in this Series to identify trends between different variables; thus meaning that the influence of the side cover concrete thickness on the maximum bond strength has not been reliably quantified in this thesis.

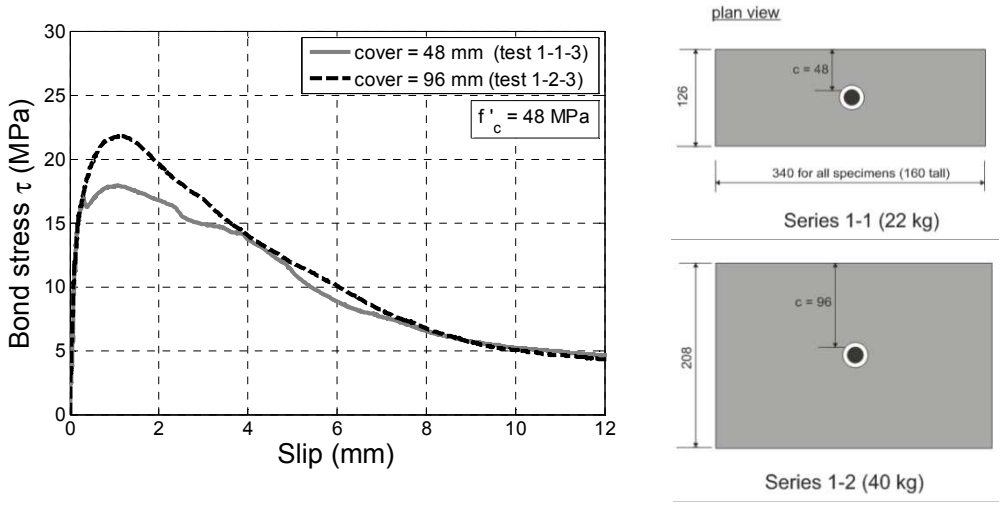

Figure 5-9: Influence of cover concrete thickness on the bond stress-slip relationship.

5.4.4 Series 2: Loading rate

The range of applied loading rates was governed by the speed of the Instron testing machine. For a slip rate of 100 mm/min, the duration of three tests completed in Series 2-1 was less than 20 seconds. The logger and computer software recorded load and end slip data at a rate of 18 samples per second, which means there is some possibility that the maximum applied load could have been slightly higher than the measured values. Series 2.3 tests were performed at a loading rate 20 times slower than all other tests and were therefore terminated at slip values just beyond 12 mm as the total test duration at this loading rate was nearly 3 hours.

Minor flexural cracking occurred during all tests in Series 2-3 and was observed to result in small peaks in the bond stress-slip curves at approximate slip values of 0.5 mm. The results from two specimens in Series 2-2 (slip rate 2 mm/min) are not presented here as severe cracking and prying of the specimen was observed in test 2-2-1 and splitting failure was observed in test 2-2-2 (two nominally identical specimens). The maximum bond strength reached in Test 2-3-3 was $2.8\sqrt{f'_c}$. However, the bond stress-slip curve did not exhibit the typical plateau seen in other pull-out failures. Due to uncertainty in the failure mode for test 2-3-3 these specific results are not presented in Figure 5-10.

The results in Figure 5-10 show that increasing the loading (slip) rate by a factor of 50 corresponds to an increased maximum bond stress of approximately 30 percent, while decreasing the loading rate by a factor of 20 suggested the 'static' bond strength may only be 10 percent less. The small difference in bond stress for 'slowest' loading rate and the 'standard' loading rate suggest that, for all other tests, it was reasonable to adopt a slip rate equal to 2 mm/min for the purpose of determining the 'static' bond behaviour. Previous attempts to quantify dynamic influence factors on bond strength have found significant scatter between test results (Michal and Keuser, 2014). Hence, given the number of tests that were performed in Series 2, it is inappropriate to adopt the results in this thesis as a statistically reliable quantification of the dynamic-bond strength enhancement.

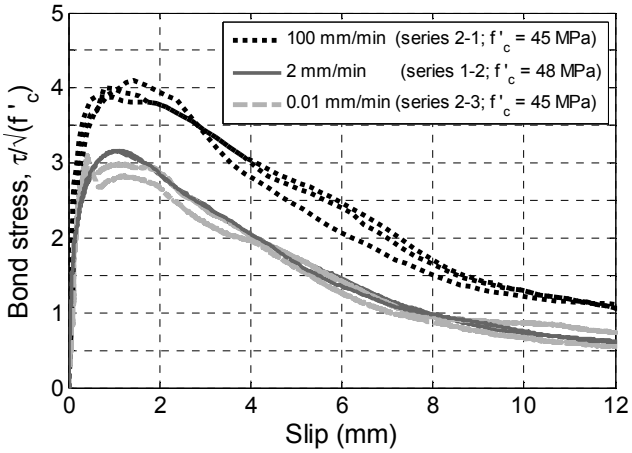

Figure 5-10: Influence of loading rate (free-end slip rate) on the bond stress-slip relationship.

5.4.5 Series 3: Position of the bond region

Sixteen specimens were tested under monotonic (and cyclic) loading with the position of the embedded bond region varied with respect to the massive block of surrounding concrete. The varied debonded lengths and bond positions are schematically illustrated in Figure 5-11(a) with labels corresponding to the individual test results that are presented in Figure 5-11(b).

Figure 5-11(b) shows that similar bond stress-slip relationships were obtained in different tests when the debonded length, L_u, was varied between 2.5, 5.0 and 7.5 times d_b. In these bond positions, the variation in the maximum bond stress is approximately 5 percent. The similarity between these results is significant for the following reasons:

- In these particular tests, bond stress-slip behaviour does not appear to be drastically influenced by flexure and/or arching action of the specimen which might have interfered with the stress state in the bond region. Any potential interference from reaction plates might have been apparent if the bond stresses in Test 3-3-1 (a compressive strut angle of 55 degrees to the reaction plates) were found to substantially higher than the bond stresses measured in Test 3-3-2 (a compressive

strut angle of 30 degrees). The similarity in these results also suggests that interference from the reaction plates was negligible for the typical specimen geometry where $L_u = 5d_b$.

- Minor variations between these three results suggest that the bond position has a relatively minor effect and is unlikely to separately influence bond behaviour when the bond length is increased in Series 5 (and the debonded length is reduced). Existing guidelines for the design of pull-out test specimens (e.g. RILEM/CEB-FIP, 1982) specify that a debonded 'pre-length' must not be less than the smaller of 200 mm, or $5d_b$. These findings suggest that a debonded length between $2.5d_b$ and $5d_b$ was reasonable for this type of unconfined pull-out test set-up.
- Beyond the distance $L_u = 2.5d_b$ from the free surface, the bond region is sufficiently confined by surrounding concrete and pull-out failure occurred at relatively high bond stresses. The local bond stress-slip relationship can therefore be considered to be independent of the position along the embedded bar, providing the considered region is $2.5d_b$ away from the free surface.

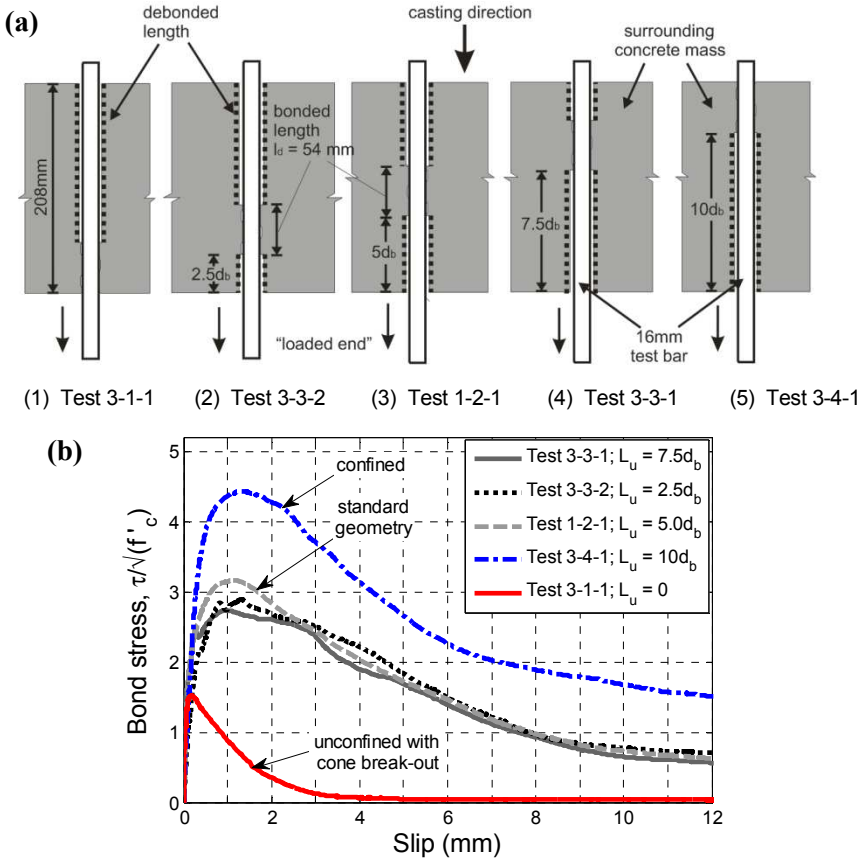

Figure 5-11: (a) Illustration of the permutations of the position of the bond region; and (b) the measured bond stress-slip relationship

The results in Test 3-4-1 shown in Figure 5-11(b) have abnormally high bond stresses that are 40 percent larger than in the other Series. This large difference in bond strength is in disagreement with the first point listed above. In this particular bond region, the enhanced bond strength is due to a second-order effect with the flexural compression forces developing transverse to the bond region, as illustrated in Figure

5-12. Transverse compressive stresses can increase the maximum bond strength by at least 30 percent (Lowes, 1999). For this particular specimen geometry, interference with the reaction plates cannot be ruled out as the angle between the centre of the bond region and the reaction plates is approximately 60 degrees.

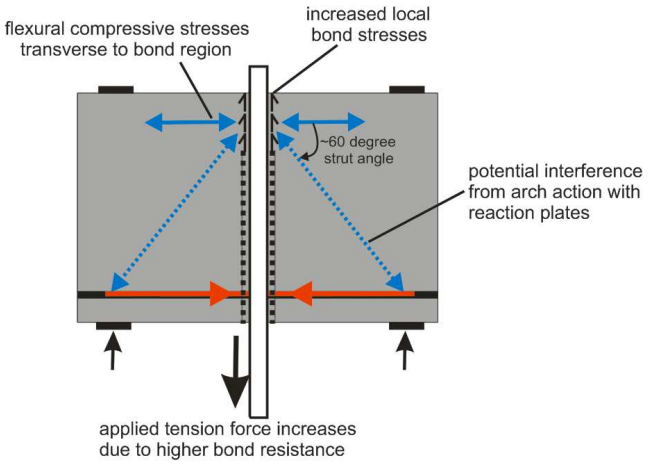

Figure 5-12: Schematic illustration of second order effect between increasing bond stresses and increasing flexural compression of the specimen.

Much larger variation between the results in Figure 5-11(b) would be expected if a 'confined' pull-out test set-up was used with the reaction plates placed close to the test bar. Under those boundary conditions, specimens with an unbonded length of $2.5d_b$, for example, may develop unrealistically high bond stresses as the bond forces have some enhanced bearing forces against the reaction plates. In these bond tests however, this problem was avoided in by using an unconfined pull-out test set up.

5.4.6 Series 5: Embedment length

The typical embedment length used in these experiments (54 mm) is shorter than $5d_b$ that was used by Eligehausen *et al.* (1983), although both their study and herein present 'local' bond behaviour. In a study by Hawkins *et al.* (1982), very short embedment lengths of $2d_b$ were used and maximum bond stresses of $5.0\sqrt{f'_c}$ were reported, which were twice that reported by Eligehausen *et al.* (1983). Series 5 was undertaken to investigate: (i) whether the local bond behaviour was affected by the specified bond length; and (ii) to confirm whether the typical bond length of 54 mm was appropriate for all other tests.

The increased bond length resulted in an approximately proportional increase in the applied loads (from typical values of 50 to 60 kN) to as high as 85 to 95 kN, the largest forces measured during all bond tests. The normalised bond stress-slip curves are presented in Figure 5-13(a). For the two bond lengths that were investigated, the normalised values of bond stress are reasonably similar. Appendix C presents the maximum loads measured in Series 5 and the values for the maximum bond stress are consistent with typical values found in other tests.

The main difference between the two curves in Figure 5-13(a) is the bond slip values at which the peak value occurs. Figure 5-13(b) shows the small slip range of the same curves to demonstrate the difference

in free-end bond slip values. For the shorter bond length, greater free-end slip is required to mobilise the maximum bond strength. As mentioned previously in Section 5.2, the values of bond slip reported here are based on measurements at the free-end. Local elongation of the test bar is not included in the bond slip values shown in Figure 5-13(a) and (b). However, using a longer bond length resulted in larger steel strains towards the loaded end of the test bar; ultimately meaning that tests performed in Series 5-1 have a slightly higher local bond slip than is shown in Figure 5-13(a) and (b). Otherwise, the bond behaviour found in this Series is not significantly affected by the bond length that was used.

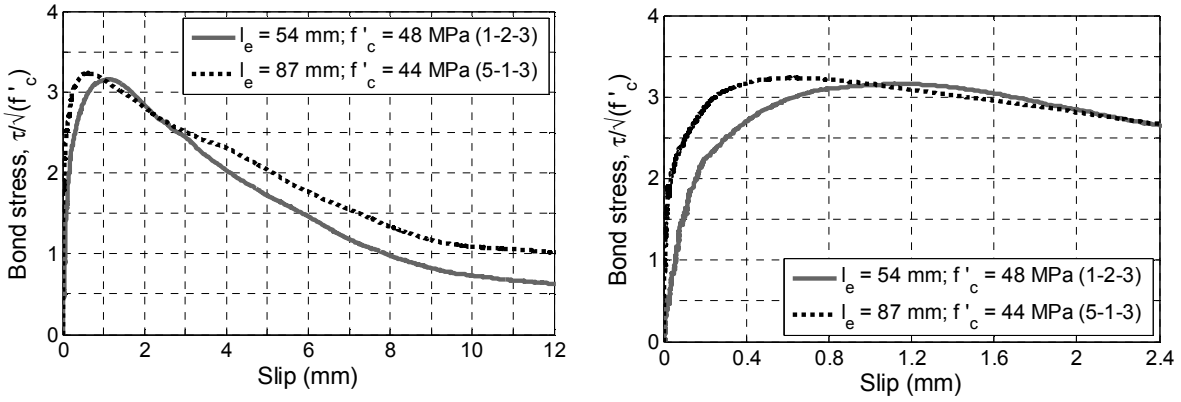

(a) Full range of bond slip

(b) Small slip range

Figure 5-13: Influence of embedment length on measured bond stress-slip relationship.

5.4.7 Series 6: Bar diameter

The typical nominal bar diameter used was 16 mm, and three monotonic tests were performed in Series 6 using 20 mm bars. A small number of tests by Eligehausen *et al.* (1983) found that the maximum bond stress of 19 mm bars may be 10 percent higher than the typical tests with a 25 mm bar, while 32 mm bars resulted in a 10 percent lower bond strength compared with 25 mm bars. Some experimental bond studies (Kivell, 2011) chose not to vary the bar diameter with the anticipation that the influence is minimal. The bond tests in Series 6 were performed in order to determine whether bond behaviour varied for 16 and 20 mm bars that had a very similar relative rib area, R_r (both $R_r \approx 0.10$). Appendix B contains further information about the measured rib geometry for these two standard bar sizes.

Although the bar diameter was increased, the same relative bond length was maintained based on embedding the same number of ribs in the concrete. As a result, the bond lengths for the 16 and 20 mm test bars were 54 and 62 mm, respectively. The differences in bar diameter and bond length are then allowed for in Equation 5-1 when deducing the bond stress-slip curve presented in Figure 5-14.

In the pre-peak and peak ranges, the bond stress-slip behaviour in both tests is shown to be good agreement and confirms that Equation 5-1 is appropriate for expressing the local average bond stress. At large slip values, towards the range of residual bond strength, Figure 5-14 illustrates that bar size has some effect on the point at which bond stress is solely attributed to friction along the bond surface. Compared with

the HD16 bars, the HD20 bar has a slightly larger rib spacing (8.9 and 10.7 mm, respectively) which means there is a longer concrete key to provide mechanical bearing resistance for slightly larger slip values.

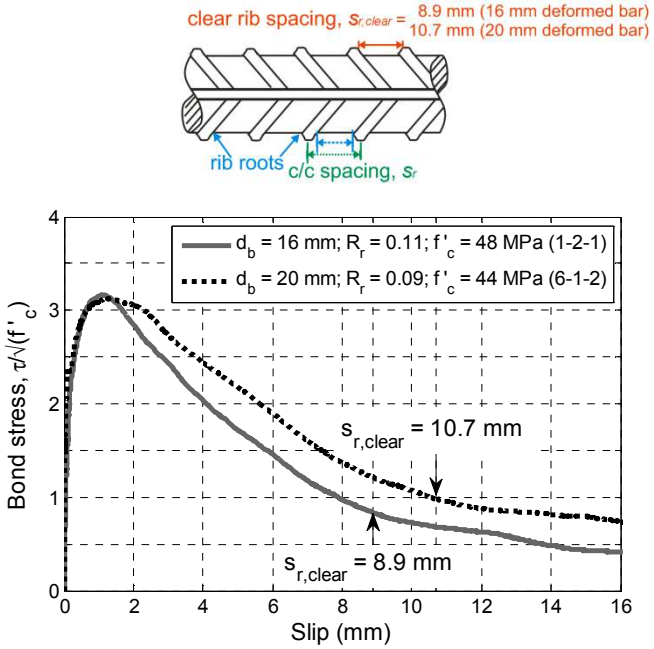

Figure 5-14: Influence of bar diameter (similar relative rib area) on bond behaviour. (Inset above shows schematic illustration of rib clear spacing).

5.4.8 Series 8: Concrete maturity

Series 8-1 comprised of testing four specimens, where three of these were some of the first to be tested under cyclic loading. Testing at 60 days after casting meant that f'_c was measured at 46 MPa. Series 8-2 comprised of another four specimens that were tested (all with monotonic loading) at 188 days after casting and f'_c was measured at 53 MPa. The specimens used in Series 8 were some of the first in the construction process. Unfortunately, three of the four specimens in Series 8-1 failed in a splitting failure mode. No reliable conclusions or outcomes can be made from this Series due to differences in the applied loading and failure modes.

5.5 INTERPRETATION OF RESULTS

Although the parametric study confirmed that bond behaviour is influenced by a number of factors, there is a need to generalise these findings to derive a bond stress-slip relationship that is readily usable without looking up specific details that influence bond behaviour. Using the monotonic test observations, the following sections provide an indication of the mean bond behaviour and distribution in the test results.

5.5.1 Distribution of maximum bond strength

For 32 monotonic tests where bond pull-out failure occurred, the distribution of the maximum bond stress is shown in Figure 5-15 in terms of the normalising co-efficient k (as per Equation 5-5). Three test observations from Series 2-1 are separated from the total test sample observations due to the large residual difference between these measurements and the predicted mean. The remaining set of 29 test observations has a mean value μ_k of 2.95 (i.e. $\tau_{max} \approx 3.0\sqrt{f'_c}$) and a standard deviation σ_k of 0.25.

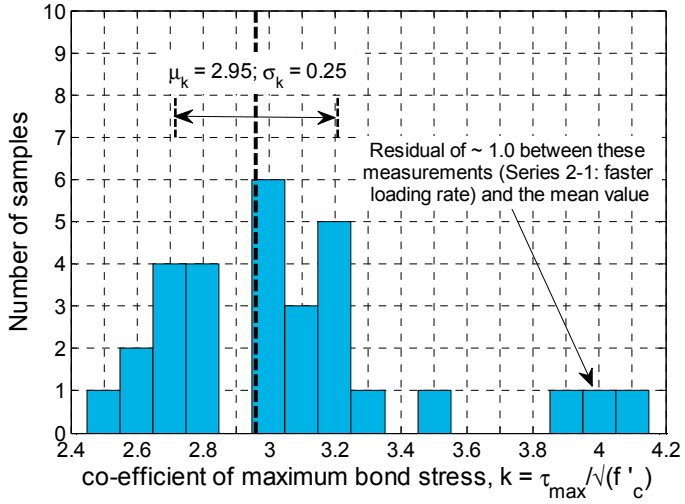

Figure 5-15: Distribution of the co-efficient of maximum bond stress observed in 32 bond tests where pull-out failure occurred.

The 5th percentile lower characteristic value for the maximum bond stress is $\tau_{max,0.05} = 2.6\sqrt{f'_c}$. It is reasonable to use this lower characteristic value for the purpose of design expressions that require some conservatism with respect to strength. Paulay and Priestley (1992) adopt a maximum bond stress of $2.5\sqrt{f'_c}$ in several design expressions (for beam-column joints), however this was based on $2.5\sqrt{f'_c}$ being the mean value of the local bond strength reported by Eligehausen *et al.* (1983).

For the purpose of assessing the maximum probable bond strength, these results suggest a 95th percentile upper characteristic value of $\tau_{max,0.95} = 3.4\sqrt{f'_c}$ may be adopted. However, this value does not make any allowance for the influence of fast dynamic loading rates, which may further increase the bond strength (possibly by 30 percent, as seen in the results from Series 2-1 shown in Figure 5-10).

5.5.2 Constitutive bond stress-slip relationship

Test results from Series 3 confirmed that there is a unique bond stress-slip relationship ($\tau - s$) that is independent of the position along the bar. In this section a bond stress-slip relationship is proposed based on the bond pull-out failures that were observed and a specific set of conditions that define this relationship is stated below. Equations 5-6 to 5-9 present the expressions used to define a mean local bond stress-slip relationship, where the mean value of maximum bond strength was discussed in the previous section. These equations take the same form as those stated in the Model Code 2010 (*fib*, 2012), however, the defining parameters have been modified based on the test results of this study.

$$\tau = \tau_{max}(s/s_1)^{\alpha} \quad \text{for} \quad 0 \le s \le s_1 \qquad 5\text{-}6$$

$$\tau = \tau_{max} \quad \text{for} \quad s_1 \le s \le s_2 \qquad 5\text{-}7$$

$$\tau = \tau_{max} - \left(\tau_{max} - \tau_f\right)\,(s - s_2)/(s_3 - s_2) \quad \text{for} \quad s_2 \le s \le s_3 \qquad 5\text{-}8$$

$$\tau = \tau_f \quad \text{for} \quad s_3 < s \qquad 5\text{-}9$$

where the parameters defining the mean bond stress-slip relationship are specified below:

- Curvature of the ascending branch: $\alpha = 0.2$
- Length of plateau: $\tau_{max} = 3.0\sqrt{f'_c}$ over the slip range s = $\begin{cases} s_1 = 0.5 \text{ mm} \\ s_2 = 1.5 \text{ mm} \end{cases}$
- Residual bond stress: $\tau_f = 0.3\,\tau_{max}$ as slip s > $s_{r,clear}$

  $s_{r,clear}$ = clear rib spacing (8.9 mm for 16 mm bars)

Listed below are the conditions to ensure the bond stress-slip relationship reflects bond pull-out failure:

- The clear cover thickness to the particular reinforcing bar must be equal to or greater than $5d_b$. The results of Series 1-1 showed that τ_{max} needs to be reduced for smaller cover thicknesses; however there is no certainty that the more brittle splitting failure mode has been suppressed. Although this condition relates to findings of the pull-out tests performed in Series 1 of this study, and was a conclusion of the study by Eligehausen *et al.* (1983), a cover thickness of is $5d_b$ is unrealistic for many regions of RC structural components, particular in beams.
- The considered bond region is a specific length (denoted L_{bu} herein) away from the crack plane, or connection interface of precast concrete components, which act as the 'effective loaded end'. In a strict sense, the length L_{bu} will physically depend on the rib spacing of the deformed bar. For example, within the finite element modelling by Fernandez Ruiz *et al.* (2007) it is stated that $L_{bu} = 3s_r$ is adopted, where s_r was shown on Figure 5-14 as the centre-to-centre spacing of the

ribs. However, it is unrealistic for structural designers to know the rib spacing for each standard deformed bar size that is used in construction. As a general rule, $2d_b \approx 3s_r$ for the 16 mm and 20 mm deformed bars used for these experiments. The Model Code 2010 (*fib*, 2012) states that $L_{bu} = 2d_b$, which is approximately the same as that stated by Fernandez Ruiz *et al.* (2007). These values are relatively short however may be reasonable as the test results from Series 3-3 confirmed that L_{bu} could be taken as $2.5d_b$.

Using the expressions given in Equations 5-6 to 5-9, the constitutive mean bond stress-slip relationship is plotted in Figure 5-16(a) and (b) (black curve). There is a reasonable agreement between the proposed relationship and the monotonic results from 29 test observations. The mean bond stress-slip relationship specified in the Model Code 2010 (*fib*, 2012) is also shown for comparison (red dashed curve). Figure 5-16(a) shows that for slip values less than 6 mm, the mean relationship in the Model Code 2010 is more conservative than the newly proposed relationship. For simplicity, both constitutive relationships use a linear slope to represent the post-peak bond behaviour. Although the test observations exhibit some curvature in the post-peak behaviour, it may be reasonable to idealize this branch using a linear slope. When using finite element modelling or empirical relationships, the shape of the post-peak branch is of relatively minor significance as the structural behaviour is more dependent on accurately defined bond behaviour in the pre-peak and peak range.

The proposed relationship specifies a residual frictional bond stress τ_f that is 0.3 times τ_{max}. Although this is slightly lower than that specified by the Model Code 2010 (*fib*, 2012), Figure 5-16(a) shows this provides a better mean value of the 29 test observations. It is unclear whether this slight difference in the amplitude of the residual bond stress is due to physical differences arising between this study and that of Eligehausen *et al.*, (1983). The residual bond stress suggested here agrees with the range of 0.3 to 0.5 times τ_{max} stated in Mahrenholtz (2012).

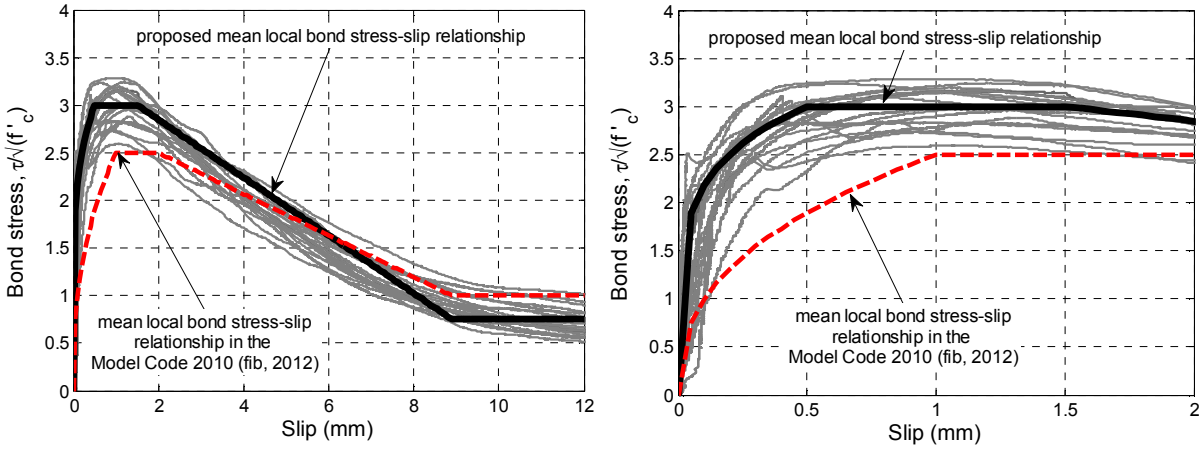

(a) Full range of bond slip

(b) Small slip range

Figure 5-16: Constitutive bond stress-slip relationship plotted against 29 monotonic test observations.

Figure 5-16(b) shows a closer examination of the pre-peak and peak behaviour and shows the Model Code 2010 relationship underestimates the initial stiffness and curvature of the ascending branch, as well as the mean value of τ_{max}. The test results suggest the length of the plateau may be the same as that in the Model Code 2010; however, the relationship proposed here specifies that the plateau begins at a smaller slip value of 0.5 mm and ends at 1.5 mm.

To some extent, the variation of the pre-peak and peak bond behaviour in these test results shown in Figure 5-16(b) and the Model Code 2010 prediction (based on test results of Eligehausen *et al.*, 1983) is partly due to differences in the rib geometry of the deformed reinforcing bars that were used in the respective tests. The relative rib area, R_r, of the 16 mm and 20 mm bars used in this study were 0.11 and 0.09 respectively, whereas the bars used by Eligehausen *et al.* (1983) were typically R_r = 0.066. Table 5-3 presents additional rib geometry measurements for deformed reinforcing bars available Germany (taken from Mahrenholtz, 2012). Also included in Table 5-3 are measurements for the 16 mm and 20 mm bars that were used in this study (underlined values) to provide comparison. There is a notable difference between the rib heights for the two different 16 mm bars that may result in rather different values for the maximum bond stress. With this notion in mind, Equation 5-10 is an expression found in Mahrenholtz (2012, from Germany) that expresses the maximum bond stress as a function of $\sqrt{f'_c}$ and R_r, as shown below:

$$\tau_{max} = 20{R_r}^{0.8}{f'_c}^{0.5} \qquad 5\text{-}10$$

The first term $20{R_r}^{0.8}$ in Equation 5-10 is the same as the co-efficient *k* that was stated earlier in Equation 5-5. The bottom line of Table 5-3 show that Equation 5-10 is very sensitive to changes in the relative rib area as it states equivalent *k* values of 3.4 and 2.9 for the 16 mm and 20 mm deformed bars used in these tests, respectively. Equation 5-10 also suggests the two different 16 mm bars have about a 20 percent difference in the maximum bond stress.

Table 5-3: Typical rib geometry for deformed reinforcing bars in Germany *[Taken from Table 5.2 of Mahrenholtz (2012)].* *Note the underlined values are measured rib geometry for the 16 and 20 mm bars used in this study (see Appendix A).

Bar diameter, d_b [mm]	10	12	16	<u>16*</u>	20	<u>20*</u>	25	32
Rib height, h_r [mm]	0.4	0.6	0.8	<u>1.3</u>	1.0	<u>1.2</u>	1.2	1.5
Rib c/c spacing, s_r [mm]	7.0	8.5	10.0	<u>10.9</u>	12.0	<u>12.5</u>	14.0	15.4
Relative rib area, R_r	0.060	0.070	0.080	<u>0.11</u>	0.085	<u>0.09</u>	0.090	0.094
$k = 20{R_r}^{0.8}$	2.1	2.4	2.7	<u>3.4</u>	2.8	<u>2.9</u>	2.9	3.0

The prediction of τ_{max} from Equation 5-10 does not compare well to the mean value of $3.0\sqrt{f'_c}$ from the 29 monotonic test results. Despite the relative rib area R_r being a reason for the notable differences between τ_{max} reported in this study and that in Eligehausen *et al.* (1983), there is an insufficient number of bond tests available for different deformed bars used in New Zealand to provide a reliable expression where τ_{max} accounts for variations of R_r. As the relative rib area of the 16 mm and 20 mm test bars used in this study is reasonably similar, it is recommended that τ_{max} depends only on $\sqrt{f'_c}$.

5.5.3 Defining concrete cone break-out failure

Three test results in Series 3 showed concrete cone break-out failure occurred at $\tau_{max,cone} = 1.4\sqrt{f'_c}$, which is 45 percent of the mean value of τ_{max} for a confined pull-out bond failure. Cone failure occurred at relatively small slip values (say 0.2 mm) and the bond stress suddenly reduced to zero. Due to the brittle nature of this failure mode (shown in Figure 5-5 and Figure 5-11(b)), some conservatism should be made when making strength-based design recommendations for concrete break-out failure. The results from Series 3 are reasonably consistent with the results from Viwathanatepa *et al.* (1979), where $\tau_{max,cone}$ was approximately 40 to 45 percent of τ_{max} measured for a local pull-out failure.

Section 17.5.7.2 of NZS3101:2006 checks the anchor strength for a potential concrete break-out failure of anchored fixings and embedded items loaded in tension. As illustrated in Figure 5-17, the projected splitting failure surface has an assumed cone angle of 35 degrees from the anchor head. The observed cone failures in Series 3-1 agree reasonable well with Figure 5-17. However, as mentioned previously in Section 5.3.4, a relatively flatter angle of between 25 and 30 degrees was observed as the concrete cone break-out surface. To some text, the splitting surface observed in Series 3 was influenced by the side cover dimension, or 'edge distance', of the test specimens. As mentioned previously in Section 3.2.4, Viwathanatepa *et al.* (1979) observed concrete break-out failure with a cone break-out angle of 35 degrees.

Plan view Section

Figure 5-17: Typical failure surface of individual anchor embedded in a massive concrete volume not limiting the edge distance (from Figure 17.1 in NZS3101:2006).

5.6 CONCLUSIONS: MONOTONIC BOND PULL-OUT TESTS

This chapter presented the results from a parametric study of 48 monotonic bond pull-out tests. The failure modes were described within and, although not all tests went as anticipated, 33 bond pull-out failures occurred. Three cone break-out failures occurred as anticipated. If the specimens were to be modified and re-designed to prevent undesired failure modes, the width of the test specimens would have been increased and the flexural reinforcement would have been placed more carefully during specimen construction.

The bond tests dedicated to studying the influence of concrete maturity did not produce any reliable outcomes, however, all other Series were deemed to be successful. Increasing the loading rate by a factor of 50 resulted in a 30 percent bond strength enhancement; the most significant influencing parameter that was found in this study. Concrete strength also had a significant effect on the maximum bond strength. Differences in the maximum bond strength were approximately proportional to differences in the concrete tensile strength and this set of results confirmed it is reasonable to express bond stress in terms of $\sqrt{f'_c}$.

Bond tests results showed the maximum local bond stress had a mean value of $3.0\sqrt{f'_c}$, a value that is higher than $2.5\sqrt{f'_c}$ stated in the Model Code 20120 (*fib*, 2012). The scatter in these test results showed that $2.5\sqrt{f'_c}$ could be adopted as a conservative value for strength-based design considerations. When assessing RC structures, the upper characteristic bond strength may be as high as $3.4\sqrt{f'_c}$ (without making an allowing for the influence of loading rate).

The bond stress-slip relationship in the Model Code 2010 (*fib*, 2012) has not changed since the Model Code 1990 (CEB-FIP, 1993), which was originally based on the findings of Eligehausen *et al.* (1983). The majority of the deformed test bars used by Eligehausen *et al.* (1983) had a relative rib area ($R_r = 0.066$) which is lower than that for the deformed bars used in this study ($R_r \approx 0.010$). Although variations in the relative rib area were not studied here, it is well known to have an influence on the slope and curvature of the ascending branch and the values at which the maximum bond stress develops. For this reason, there is good reason to re-assess the rib geometry of deformed reinforcing bars that are manufactured in the future.

5.7 REFERENCES

Abrams, D.A. (1913). Tests of bond between concrete and steel. *Bulletin 71,* University of Illinois, Urbana.

Comite' Euro-internationale du beton (CEB-FIP, 1993). The Model Code 1990: *Design code*. London: T. Telford; 1993.

Comite' Euro-Internationale du Béton (*CEB-FIP*, 1996). RC elements under cyclic loading: *State-of-the-art report*. London: T. Telford; 1996.

Eligehausen, R., Popov, E.P., Bertero, V.V. (1983), Local bond stress-slip relationships of deformed bars under generalized excitations. *Report UCB/EERC-83/23,* Earthquake Engineering Research Centre, University of California, Berkeley.

Fédération Internationale du Béton, *fib*. (2012), Model Code 2010 – First Complete Draft, Volume 1, Lausanne, Switzerland.

Fédération Internationale du Béton, *fib*. (2014), "Bond and anchorage of embedded reinforcement: Background to the *fib* Model Code for concrete structures, *Bulletin 72*, Lausanne, Switzerland.

Hawkins, N.M., Lin, I.J., and Jeang F.L. (1982). Local bond strength of concrete for cyclic reversed loadings. *Bond in concrete,* Applied Science Publishers, London, 151-161.

Lowes, L.N. (1999). Finite element modelling of reinforced concrete bridge beam-column connections, *Doctor of Philosophy Thesis*, University of California, Berkeley, CA.

Mahrenholtz, C. (2012). Seismic bond model for concrete reinforcement and the application to column-to-foundation connections, *Doctor of Philosophy Thesis,* Universität Stuttgart.

Paulay, T., and Priestley, M.J.N., (1992). Seismic design of reinforced concrete and masonry buildings. John Wiley & Son, Inc., New York, United States of America.

RILEM-FIP-CEB (1982). RC5 Bond test for reinforcement steel. *1. Beam test* & RC6 Bond test for reinforcement steel. *1. Pull-out test.*

Standards New Zealand. (2006). Concrete structures standard, NZS3101, Parts 1 & 2. Standards New Zealand: Wellington, New Zealand.

[This page is intentionally left blank]

6 EXPERIMENTAL RESULTS FOR CYCLIC BOND BEHAVIOUR OF DEFORMED BARS

Morris, G.J., Bull, D.K. and Bradley, B.A., (2015) "Monotonic and cyclic bond behaviour of deformed bars in reinforced concrete structures", C*onference proceedings of the New Zealand Society of Earthquake Engineering*, April 2015, Rotorua, New Zealand.

6.1 INTRODUCTION

Quasi-static cyclic testing of reinforced concrete (RC) structural components has long suggested there is extensive deterioration of the bond between deformed reinforcing bars and the surrounding concrete, particularly in the development zones of flexural reinforcement (Priestley and Park, 1984). However, there remains some doubt whether extensive bond deterioration can occur in 'as-built' RC structures that are subjected to dynamic near-source ground motions, such as the 22 February 2011 earthquake (Morris *et al.*, 2014). In Chapter 3, Section 3.2.3 described the physical mechanism of bond that affects the cyclic bond stress-slip relationship. Depending on the number and amplitude of the loading cycles, cyclic loading can result in significant bond deterioration (ACI Committee 408, 1992).

In order to further understand how bond behaviour is influenced by loading history, this chapter examines the experimental results from 27 cyclic bond pull-out tests. Section 3.3.4.1 listed some previous studies (Eligehausen *et al.*, 1983; Mahrenholtz, 2012, for example) where pull-out tests were completed due to the relative simplicity of the test set-up and measurement of cyclic bond behaviour. The test set-up described in Chapter 4 was specifically chosen for the ease of applying reversed cyclic loading by effectively pulling and pushing the same 'loaded end' of the deformed test bar.

The first section of this chapter discusses the rationale for selecting each of the five bond slip-controlled cyclic loading protocols. The approach used to deduce the cyclic bond stress-slip relationship from raw measurements is consistent with that stated previously in Section 5.2. Failure modes observed during the cyclic tests are described, and Appendix C contains further observations with a full table of test results. For each loading protocol that was applied, the observed cyclic bond stress-slip relationships are presented. The last section of this chapter presents some interpretation of the test results to quantify and compare the bond strength degradation and hysteretic energy dissipation (or 'bond damage') that was observed. The observed bond damage is then compared to the model prediction stated in the Model Code 2010 (*fib*, 2012).

6.1.1 Justification of cyclic loading protocols

Chapter 5 presented the results of monotonic "pull-out" tests (MON) performed as shown in Figure 6-1(a) with the bar in tension. This section describes the physical basis for the chosen loading protocols shown in Figure 6-1, Figure 6-2 and Figure 6-4. Cyclic loading was displacement controlled using measurements of bond slip at the free end of the test bar. As discussed previously in Section 5.2, it was deemed appropriate to neglect the bond slip contribution arising from strain incompatibility between the reinforcing steel in concrete. Neglecting this slip component was considered to be a reasonable simplification as the incompatible strains were not excessive, which is mainly due to pull-out specimens had a relatively short embedment length and the bar strains remained elastic range.

6.1.1.1 *Loading history LH1*

Figure 6-1(b) shows the loading protocol "LH1" that was applied in 14 out of 27 cyclic bond tests. LH1 was specifically chosen to be representative of a gradually increasing reversed cyclic loading protocol (usually fully symmetric for RC components) that is adopted in conventional quasi-static testing (see Chapter 2 for appropriate references). Other studies on cyclic bond behaviour might only study bond behaviour using a loading protocol like LH1 to be reflective of the most severe case for longitudinal beam bars passing through interior beam-column joints. These types of loading protocols typically induce significant bond stress demands along the embedded beam bars which may produce unfavourable performance of the RC frame system, particularly due to stiffness degradation (Hakuto *et al.*, 1999).

It is noted from the monotonic test results in Chapter 5 that the maximum bond strength was reached between slip values of 0.5 and 1.5 mm and the onset of strength degradation typically occurred around 2.0 mm. Several cycles below ± 2.0 mm slip were therefore chosen for protocol LH1 to measure information for bond behaviour in the pre-peak, peak and post-peak ranges. Cycles of slip in the range of ± 3.0 to ± 8.0 mm were chosen to measure information about the degradation of the concrete shear key between the ribs of the deformed bar. The 8 mm slip increment between -3 mm and +5 mm was specifically chosen as this was approximately equal to the clear rib spacing of the HD16 bars in which the concrete key is completely destroyed. A 13 mm slip increment was chosen to assess the residual bond strength purely due to frictional resistance. Tests were usually terminated once the bond slip had exceeded +12 mm, or once the potentiometer had run out of travel.

Figure 6-1(b) shows that LH1 was not completely symmetric and the initial cycles were always applied in the positive direction (bar in tension). Both of these factors are relevant for seismic-induced reversing flexural tension and compression forces in the vertical reinforcement of lightly reinforced concrete walls. For this type of RC component, it is unlikely that the first loading cycle will induce large compressive strains of the vertical reinforcement. Some physical justification of this notion is listed below Figure 6-1(b).

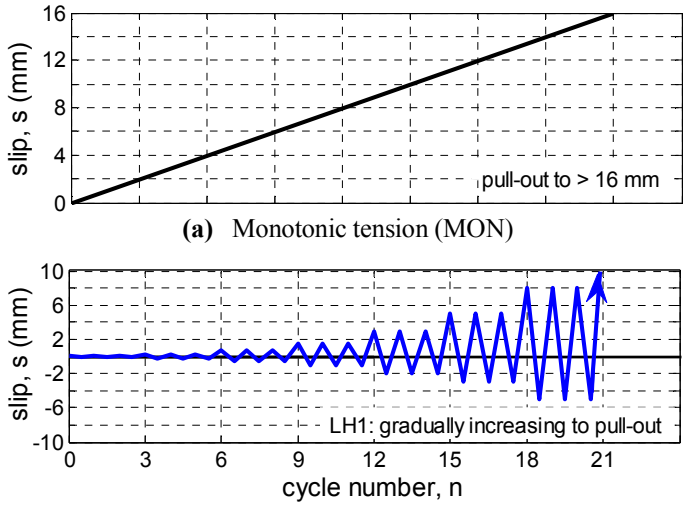

(a) Monotonic tension (MON)

(b) Loading protocol LH1

Figure 6-1: Loading protocols widely used in monotonic and cyclic bond pull-out tests.

- Once the vertical reinforcement has yielded, large curvature demands develop at the critical section of lightly reinforced walls with relatively low axial loads. While large steel strains develop in the flexural tension reinforcement, the compression reinforcement is not subjected to such large compressive strains. In this particular case, the concrete is carrying a significant portion of the compression force that balances the tension force taken by the reinforcement. Under cyclic loading, the section response is such that the reinforcement has small compressive strain demands on the compression (negative) half cycle.

- Lightly reinforced walls with a single crack/or small number of cracks will typically develop larger crack widths once the reinforcement has yielded. A large inelastic tension cycle will cause some bond slip and damage adjacent to the crack plane, causing damaged concrete in the vicinity of the crack plane to become distorted. As the crack closes under load reversal, the concrete particles become wedged in the crack and the concrete effectively expands. Compressive strains in the reinforcement cannot fully reverse and the cracked RC component tends to elongate (Fenwick and Dhakal, 2007). The elongation occurs in the direction parallel to the longitudinal axis of the component

- RC components may develop some diagonal cracking due to the combination of flexure and shear actions. Depending on the resistance of horizontal and vertical steel crossing the diagonal crack, the web region transfers the diagonal compression forces between the effective tension and compression flanges. The flexural compression force on the section, added to the longitudinal component of the diagonal compression force, must be resisted the total flexural tension force. This combined flexure-shear behaviour means the flexural tension force will be greater than the flexural compression force and, under seismic loading, the inelastic tension strains are not recovered during the compression half cycle (Fenwick and Dhakal, 2007).

Although the above points refer to the inelastic behaviour of the flexural reinforcement, it is re-emphasized that all of the bond tests completed in this research had the test bars in the elastic range. The above considerations are summarised by stating that: (i) the half cycle of the bar when subjected to compression will be somewhat less than the half cycle when the bar is in tension, and; (ii) even if the first half cycle for a particular bar is in compression, it is unlikely that this has any significance due to the concrete providing the majority of the resistance to the flexural compression force.

6.1.1.2 *Loading history 2 and 3 (LH2 and LH3)*

Figure 6-2(a) shows the fully reserved loading protocol "LH2" that was applied in three cyclic bond tests, and Figure 6-2(b) shows the half-cycle loading protocol "LH3" that was applied in two cyclic tests. The bond slip amplitudes of both loading protocols were varied to ensure that identical slip ranges were applied in some tests. These two loading protocols were chosen for the following reasons:

- To make a simple assessment of bond strength degradation and the residual bond strength on reloading to the same slip amplitude (i.e. LH2), or when loading to larger slip values (after say 10 cycles have been applied previously).
- To assess the significance of the range of bond slip that is sustained, as well as the absolute bond slip value.
- To give some further insight for cyclic bond behaviour that is useful in determining the bond slip demands and slip increments for the subsequent loading protocols, LH4 and LH5.

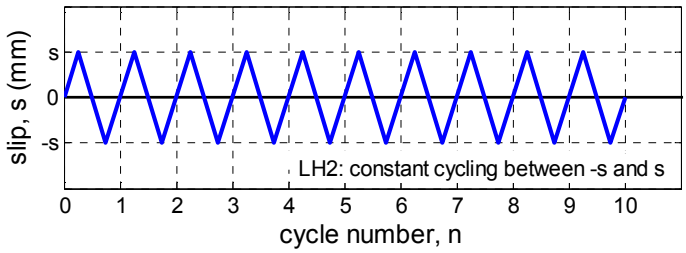

(a) Loading protocol LH2

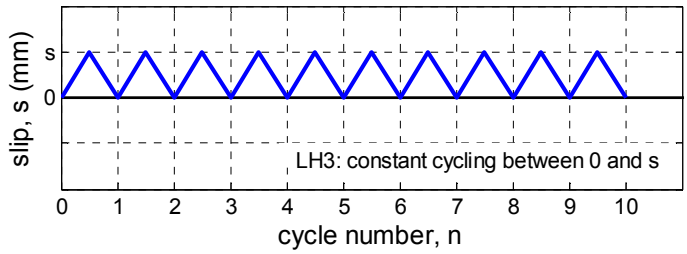

(b) Loading protocol LH3

Figure 6-2: The loading protocols used in fully-reversed and half-cycles of bond slip.

6.1.1.3 *Loading history 4 and 5 (LH4 and LH5)*

Representative loading protocols could have been determined based on the results of seismic response-history analysis of a computational model of the Gallery Apartments building (for example). However, adopting complex modelling techniques and obtaining a curvature- or strain-history implies a high level of accuracy. For this particular research project however, and in the case of the Gallery Apartments building, such detailed modelling is unwarranted due to the range of assumptions to be made and uncertainties for structural characteristics that would influence the response-history results.

A simplified alternative is shown in Figure 6-4(a) and (b) for "LH4" and "LH5", the loading protocols that were applied in a total of six cyclic bond tests (three each, respectively, out of 27 cyclic tests). LH4 and LH5 are two crude approximations of the local deformation response (bond slip) history that may have been experienced by reinforcement within the lightly reinforced concrete wall in the Gallery Apartments building during the 22 February 2011 Christchurch earthquake.

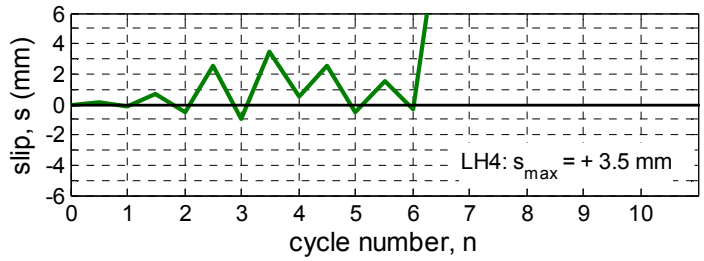

(a) Loading protocol LH4

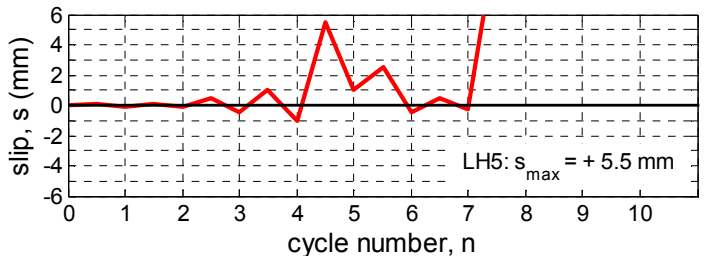

(b) Loading protocol LH5

Figure 6-4: The cyclic loading protocols used for a small number of high amplitude loading cycles.

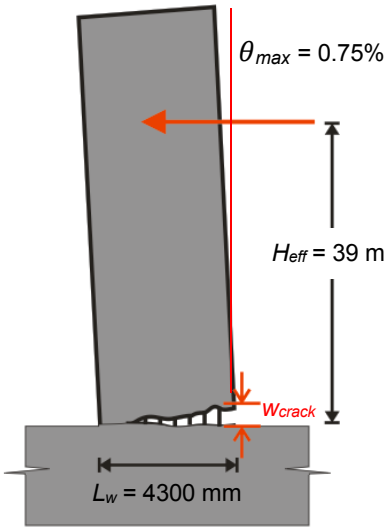

Figure 6-3: Schematic showing single-crack wall deformation with a lateral drift angle of 0.75%.

Approximately 10 seconds of strong ground shaking was recorded 400 metres away from the Gallery Apartments building at the nearest strong motion instrument 'Christchurch Hospital: CHHC'. The number of significant loading cycles was approximated by dividing the duration of strong ground motion by the first mode period of the building. Considering the effective stiffness of the critical wall (grid F) with a single-crack plastic hinge zone (PHZ), the first mode period of the building in the North-South direction may have been between 2.0 to 2.5 seconds. Estimated periods of 3.0 to 3.5 seconds determined from typical design/assessment practice accounts for a much greater reduction in the gross section stiffness with an anticipated level of well distributed cracking (CERC, 2012). The critical wall in the Gallery Apartments may have therefore sustained between three and five cycles of significant lateral displacement.

It is assumed that the global and local behaviour of the wall are linked by rotation about a single-crack that occurred at the wall base, as schematically illustrated in Figure 6-3. The amplitude of the loading cycles of the global behaviour depends on the amplitude of the ground motion and the frequency content. In the period range of 2.0 to 2.5 seconds (assumed), the spectral lateral displacement at H_{eff} (the assumed centre of mass of the building) for the CHHC ground motion is about 300 to 350 mm (Bradley and Cubrinovski, 2011). Analytical results in Sritharan *et al.*, (2014) suggest that wall failure occurred at lateral drift angle of 0.75 percent (see Figure 2-7 of Chapter 2), which agrees well with a spectral lateral displacement of 300 mm.

For the 4300 mm long wall, the lateral drift angle of 0.75 percent implies a maximum crack width, w_{crack}, of 30 to 35 mm. It should be noted however that any approaches for assessing the maximum local deformation may need to consider the onset of bar fracture that occurred. Instead of relating the crack width (or steel strain) to bond slip, which may be inappropriate at this stage in this research, the maximum bond slip demands in LH4 and LH5 are simply approximated as 3.5 mm and 5.5 mm in LH4 and LH5, respectively.

6.2 OBSERVED FAILURE MODES

Bond pull-out failure was observed in 20 out of the 28 cyclic tests. Each of the failure modes listed in Table 6-1 was described previously in Section 5.3. One trial cyclic bond test was completed to gain some experience in the set-up and instrumentation of the specimen and applying a cyclic loading protocol (LH1) for the first time. Results from the trial bond test were also deemed to be usable for this study as the observed bond behaviour was typical with that in other tests. The results for this cyclic trial bond test are shown in Figure 6-5.

Table 6-1: Quantity of different failure modes observed in cyclic bond pull-out tests

Failure mode	Quantity
Pull-out bond failure	20
Splitting bond failure	3
Partial Cone break-out failure	3
Prying failure	1
Total	27

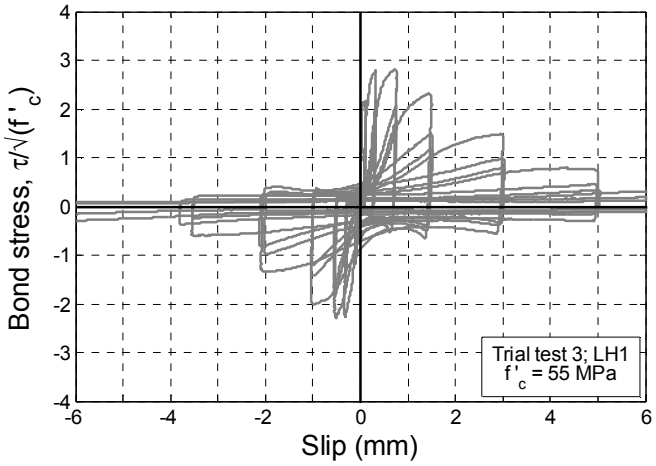

Figure 6-5: Normalised bond stress-slip relationship for a trial cyclic pull-out test (loading protocol LH1).

6.2.1 Bond pull-out and splitting failures

20 bond pull-out failures were observed, while three splitting bond failures were observed. The observations of these failure modes are consistent with those shown previously in Figure 5-3 from the monotonic testing. Figure 6-6 compares the cyclic bond stress-slip curves when pull-out failure and splitting failure occurred in two nominally identical test specimens subjected to the same loading protocol. For reference, the monotonic pull-out envelop is also shown. Splitting failure results in lower bond stresses, however the closing of cracks on unloading means there is some recoverable bond slip.

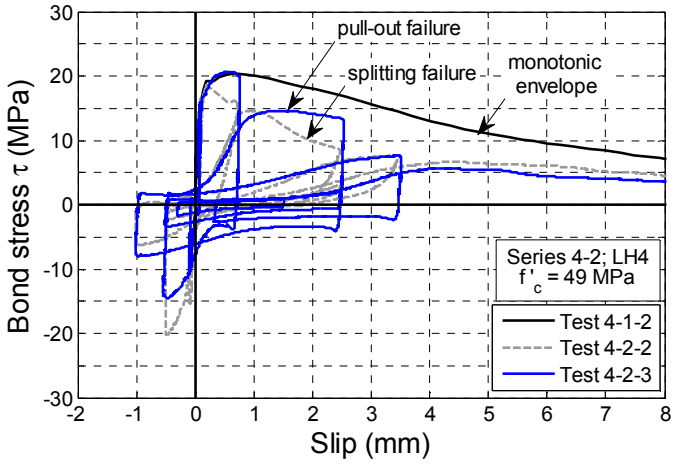

Figure 6-6: Comparison of bond stress-slip relationship when pull-out and splitting bond failure occurred during the cyclic loading protocol LH4.

6.2.2 Partial cone break-out failure

Partial cone break-out failure was observed on the compression cycles of tests in Series 3-4. A photograph looking downwards on a cracked specimen is shown in Figure 6-7. Radial cracks were observed to develop outward from the test bar, and some smaller local cone formation was observed, however a full cone failure did not occur.

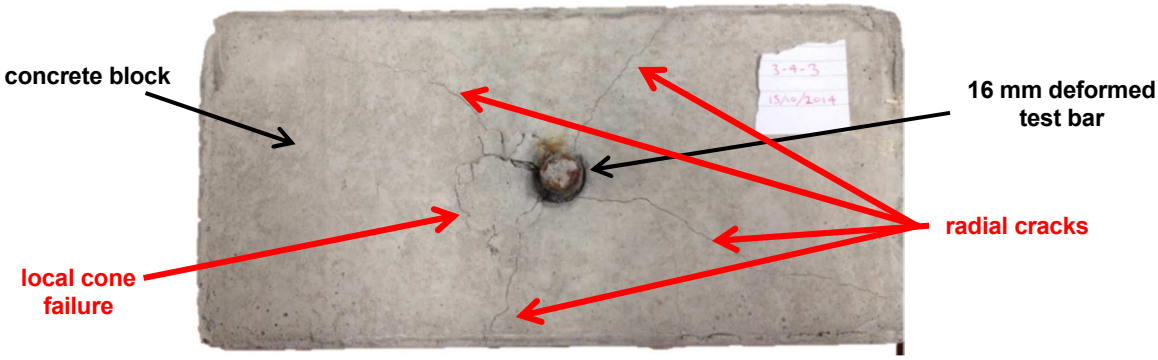

Figure 6-7: Plan view of specimen 3-4-3 showing a partial cone break-out failure and radial cracks.

Figure 6-8 shows two bond stress-slip curves obtained after three reversed loading cycles where partial cone failure occurred. It is noted that for clarity of figure presentation, the initial small loading cycles ($s \leq 0.3$ mm) in the positive direction have been removed from Figure 6-8, and should not to be mistaken for a low initial bond stiffness in these two tests.

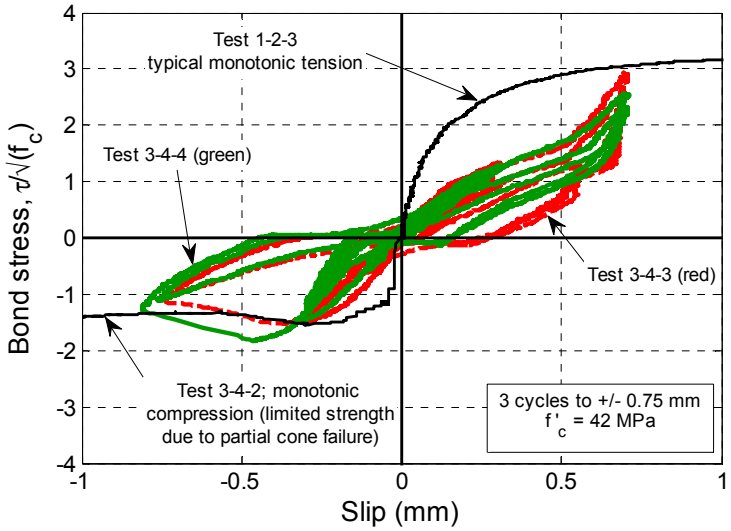

Figure 6-8: Cyclic bond behaviour (small slip range) when partial cone failure occurred.

Figure 6-8 shows that the maximum bond stress in the negative stress-slip is limited (compared to the positive stress-slip domain) due to the occurrence of partial cone failure. Opening and closing of the radial cracks leads to some pinched behaviour in the cyclic curves shown in Figure 6-8. The maximum bond stress in the negative direction was similar to the maximum value found during monotonic testing ($\tau_{max,cone} = 1.4\sqrt{f'_c}$), which was discussed previously in Section 5.5.3.

6.3 RESULTS FROM CYCLIC LOADING

The following sections present the results from cyclic bond pull-out tests conducted in Series 4 and (part of) Series 7. Values of bond stress reported in this section have been normalised by $\sqrt{f'_c}$. The appropriateness of this normalisation was previously discussed in Chapter 5. Each of the cyclic bond stress-slip curves presented in this section are compared to a monotonic envelope that was obtained within the same test series. Monotonic curves are only plotted in the positive slip domain, when pulled out in tension. A slip range of 10 or 12 mm is specifically chosen to show the residual bond strength once bond slip has exceeded the clear rib spacing of the ribs on the deformed test bars.

For all cyclic test results, Table C-1 of Appendix C presents the maximum applied loads for both tension (positive) and compression (negative) loading. Some cyclic bond tests with LH1 were performed on specimens tested in Series 3, and a single cyclic bond tests was performed in Series 5, 6, and 8. These results show the same trends described in this chapter and the results are found in Appendix D.

6.3.1 Loading protocol LH1

Figure 6-9(a) presents the typical bond stress-slip behaviour when subjected to LH1, the gradually increasing fully-reversed loading protocol shown previously in Figure 6-1(b). In general, the bond strength and stiffness on the first cycle in compression was either the same, or of lower amplitude, than the previous cycle in tension. No tests showed greater bond resistance in the negative direction, which was anticipated due to the concrete casting direction resulting in the most favourable bond resistance in the positive bond stress-slip domains (Park and Paulay, 1975).

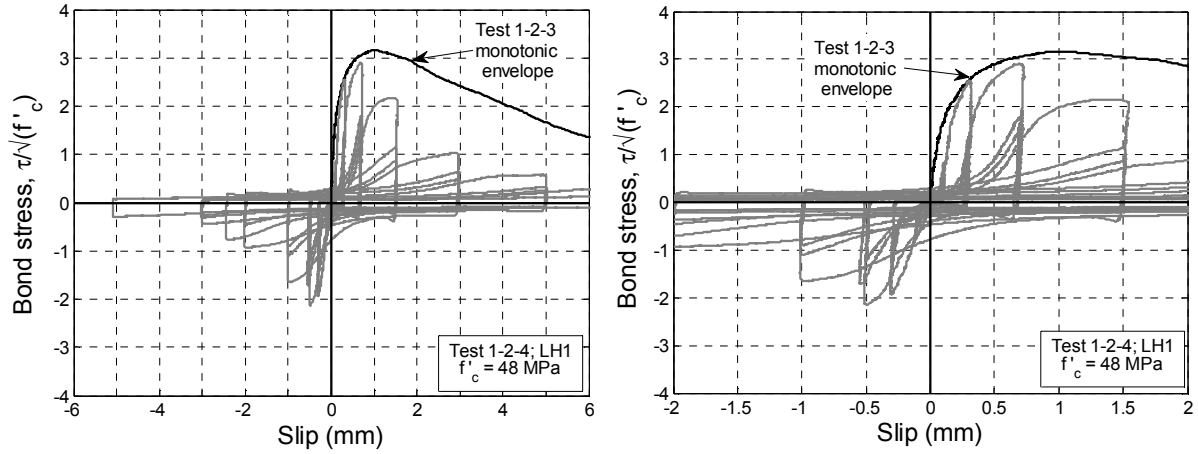

(a) typical bond stress-slip curve **(b)** small slip range

Figure 6-9: Cyclic Bond stress-slip relationship for loading protocol: LH1.

Figure 6-9(a) and (b) show that, if bond slip is greater than previously sustained, the bond-stress slip curves are concave on the first cycle, and re-loading cycles to the same slip do not mobilise any additional bearing resistance. Instead, the damaged concrete in the vicinity of the ribs is crushed and bond slip is irrecoverable on unloading. Reloading to the onset of newly mobilised mechanical bearing is shown by a point of inflexion in the bond stress-slip curve. Mechanical bearing is destroyed once the slip range is equal to the clear rib spacing, which is shown by the cycles between -3.0 mm and 5.0 mm on Figure 6-9(a).

Slip cycling to smaller slip amplitudes than those specified here may not cause significant bond deterioration to occur. This was observed in Eligehausen *et al.* (1983), where cycling below about 70 to 80 percent of the maximum bond stress meant that the cyclic path could still return to the monotonic envelope on larger subsequent slip cycles. The results shown in Figure 6-9(b) generally agree with this notion as slip cycles to + 0.3 mm typically do not reach 80 percent of the maximum bond stress, however the first cycles up to + 0.7 mm slip shows that the cyclic path is reasonably close to returning to the monotonic envelop.

Three loading cycles were repeated for each of the specified slip amplitudes in LH1. Figure 6-9(b) shows that the majority of bond damage generally occurs on the first loading cycle and there is a smaller difference between the bond strength on the second and third loading cycles. Increasing the bond slip demand to a new relative maximum causes the bond stress-slip curve in Figure 6-9(b) to almost follow the path that was taken on the third cycle at the previous slip amplitude. The cyclic bond behaviour under LH1 is representative of severe bond deterioration compared to that under loading protocols LH4 and LH5 (discussed in Section 6.3.4 and 6.3.5).

6.3.2 Loading protocol LH2

The constant-slip fully-reversed loading protocol shown in Figure 6-2(a) was used for three slip amplitudes with 10 cycles between: ± 0.75 mm, ± 1.5 mm, and ± 3.0 mm. The bond stress-slip curves corresponding to each test is shown in Figure 6-10(a)-(c).

The path of the first positive loading cycles shown in Figure 6-10(a) and (b) are both up to the peak range of the monotonic envelope. Damage to the concrete on the first cycle is significant as the bond stress on the second positive cycle is shown to be approximately half of the maximum bond stress. For the first 10 cycles, Figure 6-10(a) and (b) both show the majority of bond damage occurs in the first five loading cycles (i.e. the next five loading cycles are insignificant).

Figure 6-10(a) and (b) also shows some secondary bond stress-slip curves that indicate the residual bond resistance during some additional loading cycles to the higher slip amplitudes. Figure 6-10(a) shows the cyclic path does not from return to the monotonic envelope when increasing the slip amplitude to ± 1.5 mm. Instead, there is a significant reduction in bond stress shown on the first cycle to + 1.5 mm (the 11th

loading cycle). Figure 6-10(b) shows a similar level of residual bond stress on the first cycle to + 3.0 mm slip.

The cyclic path shown in Figure 6-10(c) extends to + 3.0 mm slip, which is beyond the slip range for the peak behaviour of the monotonic curve. As a result, the second positive loading cycle shows that bond stress has decreased significantly. Section 6.4.1 continues to quantify and compares the amount of bond strength degradation shown in Figure 6-10(a)-(c).

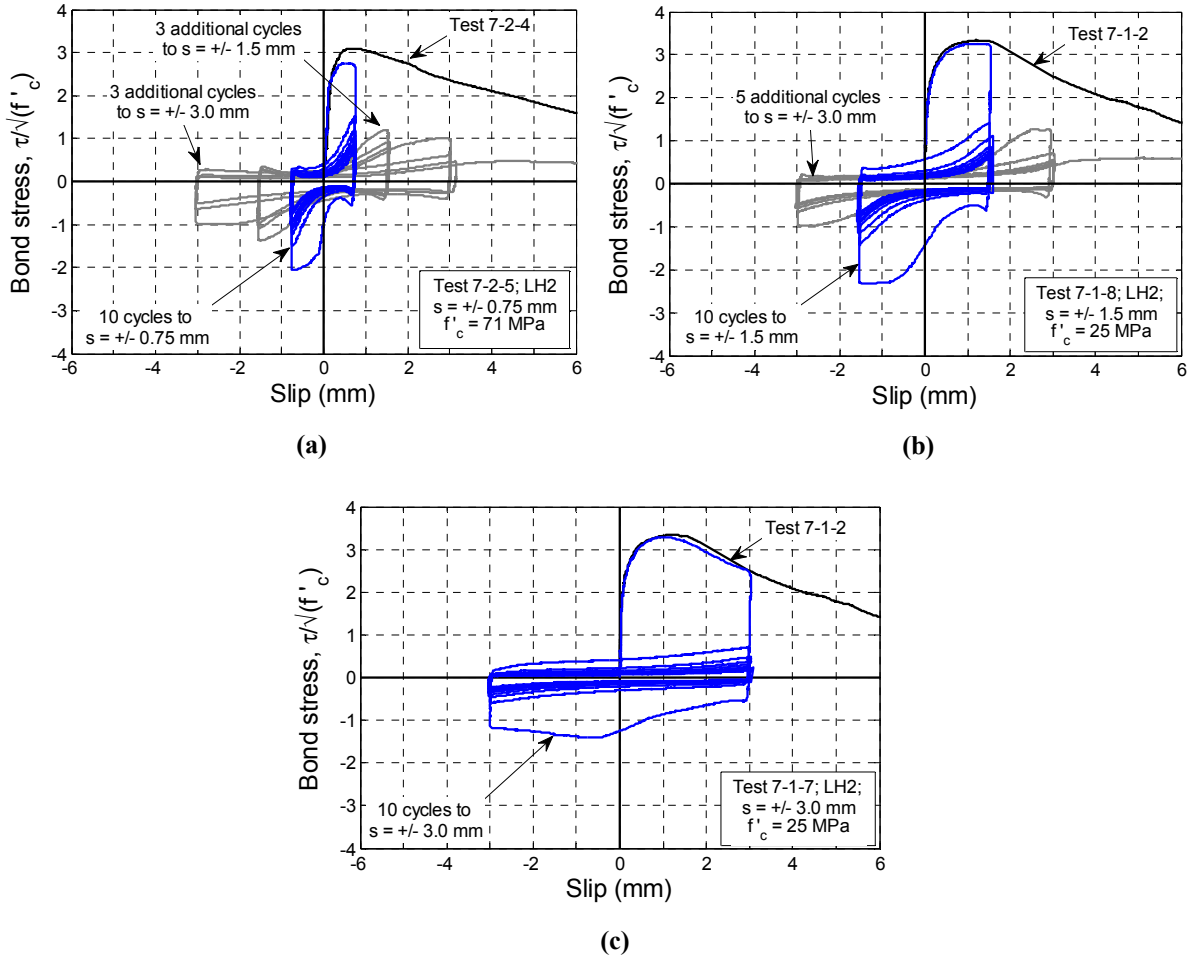

Figure 6-10: Bond stress-slip behaviour for loading protocol LH2; 10 cycles of fully-reversed constant-slip.

6.3.3 Loading protocol LH3

The unidirectional loading protocol LH3 shown in Figure 6-2(b) was used for two slip ranges with 10 cycles from 0 mm up to + 1.5 mm, and + 3.0 mm, respectively. The bond stress-slip curves corresponding to each test is shown in Figure 6-11(a) and (b).

Figure 6-11(a) and (b) both show that two or three half cycles cause the cyclic bond stress-slip path to become centred about the point $(\delta s/2, 0)$, i.e. a new datum away from the origin by an offset equal to half of the incremental slip. By comparing the same incremental slip, the cyclic path in Figure 6-11(a) is

re-produced in Figure 6-11(c) with a comparison to the fully reversed path during LH2. In Figure 6-11(c), the rate of bond strength degradation for these two particular tests appears to be very similar, and likewise with the results in Figure 6-11(d). These results suggest that the bond slip range has a significant influence on deterioration of bond under cyclic loading, and is discussed further in Section 6.4.1.

For the same incremental slip range shown in Figure 6-11(c), the reloading of the cyclic path of Test 7-2-8 (shown in red) appears that it would tend towards the same path of Test 7-2-5 (shown in blue) if first time loading into the negative slip domain was to occur (i.e. monotonically increasing the bar compression force). The results in Figure 6-11(d) also appear to support this notion, however as the + 3.0 mm slip range is relatively large, greater damage to the concrete between the ribs may mean that there is a reduced envelope for the first time loading in the negative slip domain.

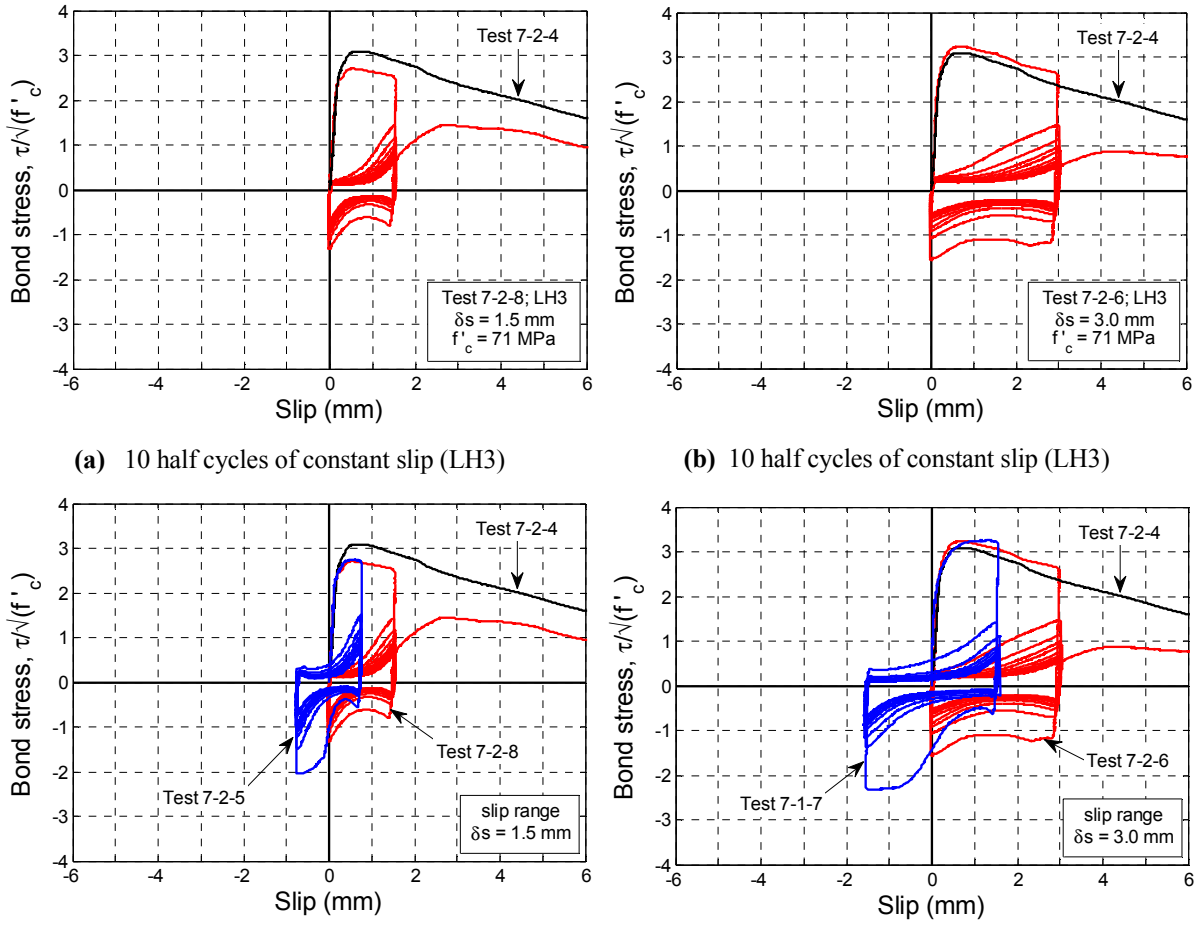

(a) 10 half cycles of constant slip (LH3)

(b) 10 half cycles of constant slip (LH3)

(c) comparison from LH2 and LH3

(d) comparison from LH2 and LH3

Figure 6-11: Bond stress-slip behaviour for constant slip cycling.

6.3.4 Loading protocol LH4

The LH4 loading protocol shown in Figure 6-3(a) corresponds to the cyclic bond stress-slip curve shown in Figure 6-12. For reference, the cyclic bond stress-slip curve obtained during LH1 is also presented in Figure 6-12. The green curve for Test 4-2-3 shows that one loading cycle through s = ±0.1 mm has no effect on the peak bond behaviour and the cyclic path to $s = +0.75$ mm follows the monotonic envelop. Subsequent loading cycles show some bond strength degradation. At s = +3.0 mm the cyclic path of Test 4-2-3 and Test 1-2-4 have approximately the same bond stress of $1.0\sqrt{f'_c}$.

When s = +8.0 mm, the residual bond stress is about half of the monotonic envelope, and approximately the same as Test 1-2-4 at s = +5.0 mm, which is after a slip of −3.0 mm on the previously cycle, meaning the slip increment is also equal to 8.0 mm and hence the residual bond stress is shown to be approximately similar.

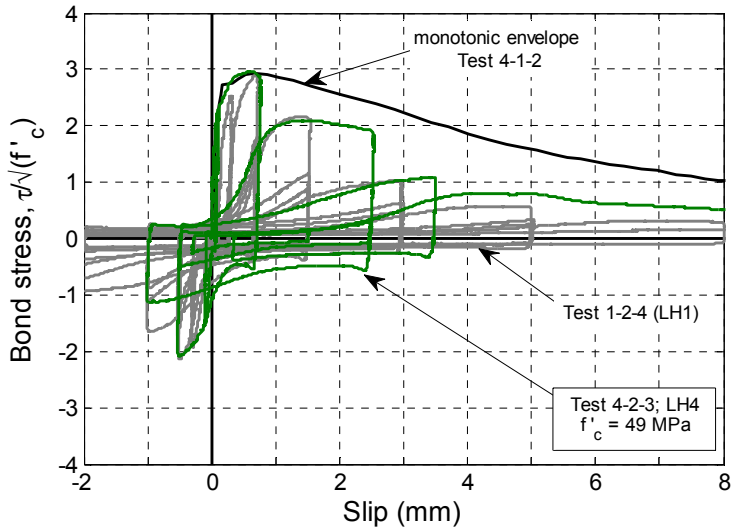

Figure 6-12: Bond stress-slip behaviour for a small number of high amplitude cycles; loading protocol LH4.

6.3.5 Loading protocol LH5

The loading protocol LH4 shown in Figure 6-1(f) corresponds to the cyclic bond stress-slip curve shown in Figure 6-13(a). Although the maximum slip increment of in LH5 was larger than in LH4, a slightly larger number of small and moderate slip cycles were applied. Test 4-3-1 shows the cyclic path to s = +0.5 mm follows the monotonic envelope; however, the following cycle to s = +1.0 mm does not regain the same peak bond stress. As largest cycle reaches s = +5.5 mm the cyclic path appears to be returning towards the monotonic envelope.

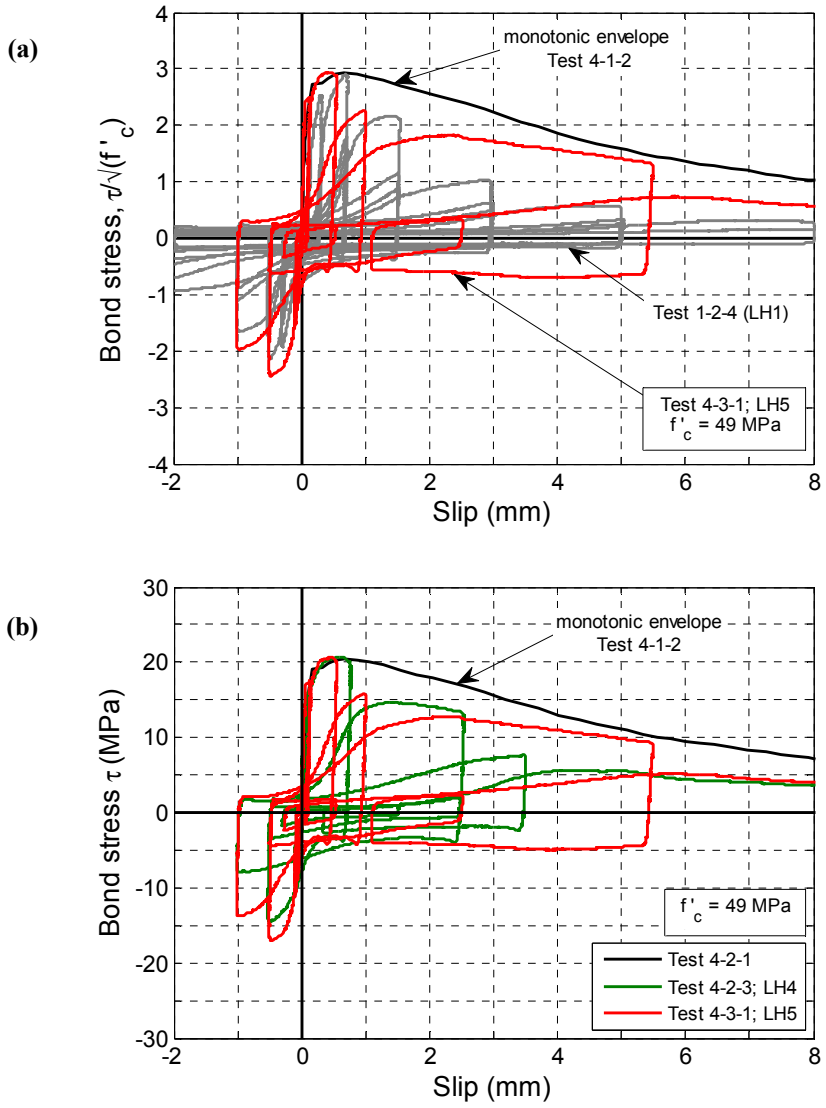

Figure 6-13: (a) Bond stress-slip behaviour for loading protocol LH5 compared to LH1, and (b) comparison between cyclic bond behaviour for LH4 and LH5.

Figure 6-13(b) compares the cyclic response to LH4 and LH5 (using the actual bond stress values, not normalised). Prior to the final pull-out of the test bar, the cumulative energy dissipated in the LH4 and LH5 tests are approximately 15 percent less and 10 percent more, respectively, than the energy dissipated during a typical monotonic test. However, Figure 6-13(b) shows that the residual bond stress is approximately identical in both tests when the slip value has exceeded +6.0 mm. The mechanical bearing resistance has been largely destroyed in both tests, and only frictional resistance remains in bond cases. Further discussion of cumulative energy dissipation in these tests is presented in Section 6.4.2 and Appendix D compares the cyclic bond deterioration and energy dissipated with each loading cycle of these two particular loading protocols.

6.4 INTERPRETATION OF RESULTS

6.4.1 Peak bond strength degradation

Visual inspection of the bond stress-slip behaviour during the LH2 and LH3 test series indicated the extent of bond strength degradation was similar if the bond slip increment (or slip range) was the same. Closer examination of the bond response history allowed for the peak amplitudes on each loading cycle to be compared as a ratio of the maximum bond strength that developed on the first cycle. The outcomes of this examination are shown in Figure 6-14(a).

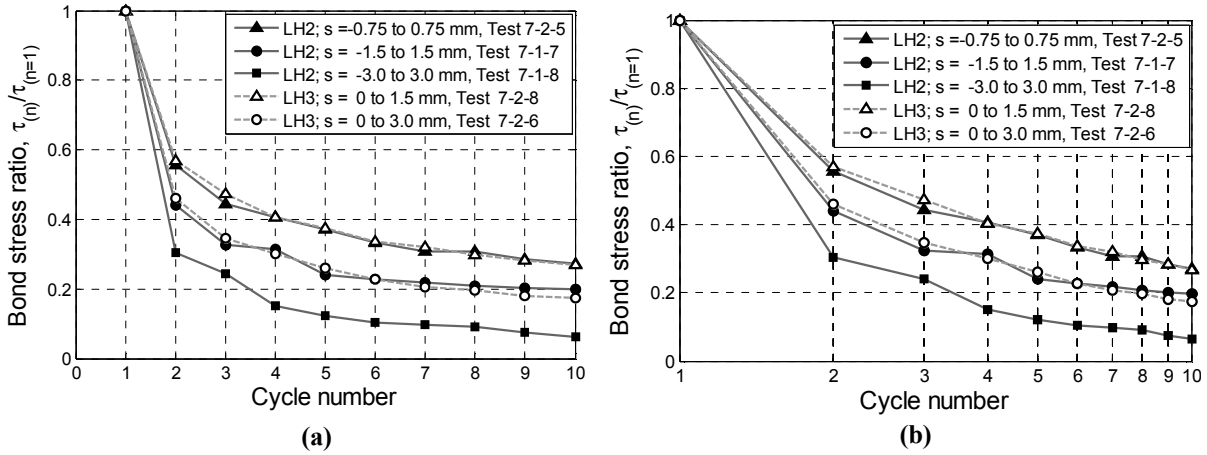

Figure 6-14: Cyclic bond strength degradation for fully reversed and half cycles of slip plotted in both linear (a) and logarithmic (b) x axes.

As described previously in Section 6.3.2, Figure 6-14(a) shows that a significant amount of bond damage occurs on the first loading cycle. Figure 6-14(a) confirms that the two curves shown in Figure 6-11(c) for tests 7-2-5 and 7-2-8 have reasonably identical bond strength degradation for the same bond slip range of 1.5 mm. Similarly, when the bond slip range was 3.0 mm the bond strength degradation in tests 7-1-7 and 7-2-6 follows the same trend, regardless of the whether the loading was fully-reversed cycles or half-cycles.

Other researchers (Balazs, 1991) have previously presented models for fatigue of bond behaviour based on logarithmic relationships between the number of loading cycles and the reduction in bond stress with each loading cycle. Figure 6-14(b) is re-produced so the cycle number is in log scale, which illustrates a bilinear relationship between the bond strength degradation and the log of the number of cycles.

6.4.2 Hysteretic energy dissipation

Section 6.3 showed that bond deterioration was predominantly observed once the cyclic path entered the peak range of the monotonic envelope, between the slip range of about 0.5 and 1.5 mm, which results in the cyclic path having reduced bond stresses during subsequent loading cycles. The aim of this section is to consider the previously sustained bond damage in attempt to predict the bond stress-slip path that is

taken during subsequent loading. To achieve this prediction, this section outlines the method stated in the Model Code 2010 (*fib*, 2012) which is based on a hysteretic energy-based model that was proposed much earlier by Eligehausen *et al.* (1983).

The method states that Equation 6-1 can be used to predict the cyclic bond stress, τ_m, for the cyclic path on the next loading cycle, *n*+1. However, the cyclic bond response parameter, Ω_{cyc} must first be determined using Equation 6-2 to quantify how much the cyclic path is reduced from the monotonic bond stress, τ_0, along the monotonic envelope curve that was defined previously in Section 5.5.

$$\tau_{m(n+1)} = \Omega_{cyc}\, \tau_{o(n)} \tag{6-1}$$

where:

$$\Omega_{cyc} = \exp\left(-a_1 \left(\frac{E_{cyc}}{E_0}\right)^{a_2} \right) \tag{6-2}$$

Determining Ω_{cyc} is based on quantifying the cumulative hysteretic energy dissipated, which simply refers to the area bound by the cyclic bond stress-slip curve, E_{cyc}, as a ratio of the area under the monotonic bond stress-slip curve, E_0. Further details on quantifying E_0 and E_{cyc} is outlined in the following two sections. The prediction made by Equation 6-2 also requires bond damage model parameters a_1 and a_2, to ensure E_{cyc}/E_0 is related to Ω_{cyc} with reasonable accuracy. These model parameters are discussed further in Section 6.4.2.2.

6.4.2.1 *Monotonic energy dissipation, E_0*

Equation 6-2 shows that a ratio between cyclic and monotonic energy dissipated (i.e. E_{cyc}/E_0) is needed to determine the bond response parameter Ω_{cyc}. The values of E_0 assessed in this section refers to the damage that occurs during the engagement and loss of mechanical bearing resistance up until bond slip has exceeded the clear spacing, $s_{r,clear}$, between the ribs on the deformed bar. For the purpose of this thesis, the frictional bond resistance at larger slip values (beyond the clear rib spacing) has been ignored from the model prediction. Equation 6-3 defines how values of E_0 can be determined from the area under the monotonic bond stress-slip curve, $\tau_0(s)$, for a bond slip domain that extends up to the clear spacing of the ribs, $s_{r,clear}$.

$$E_0 = \int_{s=0}^{s=s_{r,clear}} \tau_0(s)ds \tag{6-3}$$

$$E_0 \cong \sum_{n=0}^{n=i} (s_{n+1} - s_n) \times \frac{(\tau(s_n) + \tau(s_{n+1}))}{2} \tag{6-4}$$

Values of E_0 could either be assessed from individual monotonic test results, or based on the constitutive bond stress-relationship that was defined in Section 5.5.2 to represent the mean monotonic bond

behaviour. In either case, the trapezium rule is used to estimate E_0 and hence the bond slip domain was discretised as stated in Equation 6-4 in order to simplify the calculations.

Figure 6-15(a) shows some example calculations of $E_0/\sqrt{f'_c}$ for two particular monotonic tests. The bond slip domain was divided into approximately 300 strips, where the incremental slip values (as shown in Equation 6-3, $ds = s_{n+1} - s_n$) typically ranged between 0.007 and 0.08 mm. For test 1-2-3, the normalised value of E_0 was found to be approximately equal to 17.0. There is more energy dissipated ($E_0 \approx 21.1$) in test 6-1-2 because the 20 mm deformed bar has a larger rib clear spacing of 10.7 mm which means that mechanical bearing resistance is sustained over a larger slip domain (shown previously in the monotonic test results in Section 5.4.7).

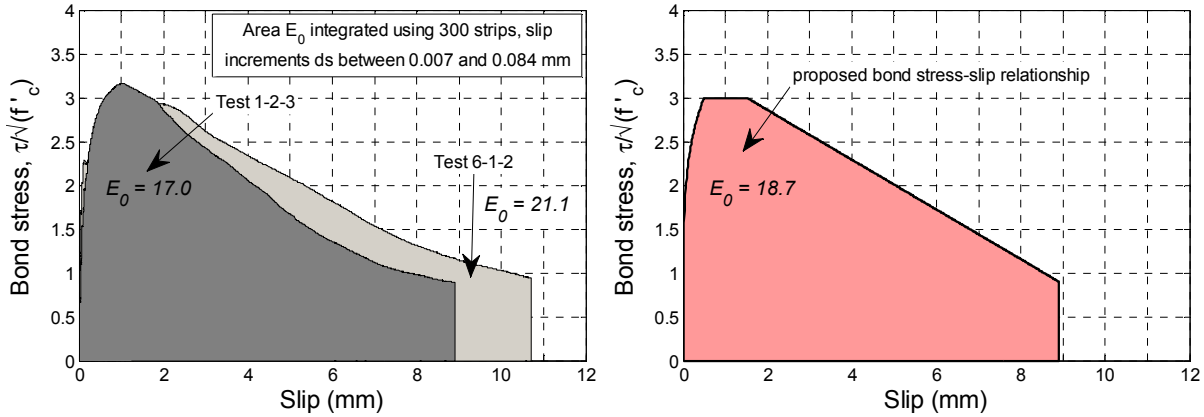

(a) Calculation of E_0 two monotonic bond tests with 16 mm and 20 mm deformed bars.

(b) Calculation of E_0 for the proposed bond stress-slip relationship (from Chapter 5).

Figure 6-15: Examples of the energy dissipated during monotonic bond tests.

The values of E_0 determined from a select number of experimental test results show that E_0 typically ranges between 15 and 21. Figure 6-15(b) illustrates that E_0 for the mean monotonic bond stress-slip ($\tau_0 - s$) relationship was found to be 18.7. For the calculations presented in the following section, the value of E_0 = 18.7 is used as this is representative of the mean monotonic bond behaviour.

6.4.2.2 *Cyclic energy dissipation, E_{cyc}*

Reliable quantification of E_{cyc} requires careful consideration of the number of loading cycles and the slip range of each cycle that has occurred previously. To help in understanding the cumulative calculations that were undertaken, Figure 6-16 provides a simple illustration showing how E_{cyc} is assessed for each loading cycle and labels the values of τ_m that need to be extracted from the cyclic test results.

Once values of $\tau_{m(s,n+1)}$ have been extracted from the test results for the number of loading cycles that is of interest, the observed values of Ω_{cyc} come from a re-arrangement of Equation 6-1, where $\tau_{m(n+1)}$ is expressed as a ratio with the monotonic bond stress at the same slip value, $\tau_{o(s,n)}$. For example, Table 6-2 presents observed values of Ω_{cyc} against the calculated values of the cumulative energy dissipated

during cyclic loading during test 7-1-7 and 7-1-8. Note that observed cyclic bond stresses are only been presented for the first few loading cycles. Appendix D contains record of the cyclic bond deterioration in three tests subjected to loading protocols LH2, LH4 and LH5, respectively.

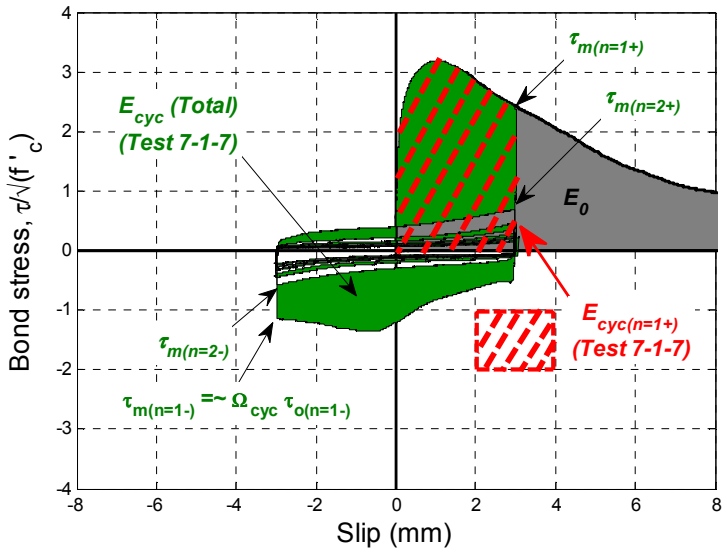

Figure 6-16: Qualitative illustration of measured cyclic bond stresses $\tau_{m(n+1)}$ and how energy dissipated during cyclic loading E_{cyc} is defined.

Table 6-2: Energy dissipated during the first loading cycles in test 7-1-7 and 7-1-8.

Test	Loading cycle, n	Slip domain, s_0 to s_{max}	Bond stress values[1]			Energy dissipated[1,2]		
			Model[2] $\tau_{o(s_{max},n=1)}$	Measured $\tau_{m(n)}$	$\Omega_{cyc} = \tau_{m(n)}/\tau_{o(s)}$	From previous loading cycle $E_{cyc(n-1)}$	Cumulative $\sum_n E_{cyc}$	$\frac{\sum E_{cyc}}{E_0}$
7-1-8 (LH2)	1+	0 to 1.5 mm	3.0	- [3]	1.00	-	0	0
	1-	-1.5 to 1.5 mm		-2.2	0.73	4.47	4.47	0.24
	2+			1.4	0.47	4.29	8.76	0.47
	2-			-1.3	0.43	2.01	10.8	0.58
	3+			1.2	0.40	1.25	12.1	0.65
7-1-7 (LH2)	1+	0 to 3.0 mm	2.6	- [3]	1.00	-	0	0
	1-	-3.0 to 3.0 mm		-1.2	0.46	8.45	8.45	0.45
	2+			0.7	0.27	5.96	14.4	0.77
	2-			-0.6	0.23	2.52	16.9	0.90
	3+			0.5	0.18	1.90	18.8	1.00

[1] all values of bond stress τ and energy dissipated E_{cyc} are normalised by $1/\sqrt{f'_c}$

[2] based on mean local bond stress-slip relationship for monotonic loading, where E_0 = 18.7

[3] first time loading follows monotonic backbone

The measured values of Ω_{cyc} from select bond tests are plotted against the ratio of E_{cyc}/E_0 in Figure 6-17. Test observations are compared in order to represent a range of the different loading protocols that were applied. Figure 6-17 also presents a grey dashed curve showing the prediction when the damage model parameters in Equation 6-2 are set to: $a_1 = 1.2$ and; $a_2 = 1.1$ as stated in the Model Code 2010 (based on the earlier findings of Eligehausen *et al.* (1983). More recent experimental measurements from Mahrenholtz (2012) did not compare well with the Model Code 2010 and a new set of damage model parameters of $a_1 = 2.5$, and; $a_2 = 1.0$ were recommended (shown by the black curve). When comparing the two models against one another, Figure 6-17 shows the Mode Code 2010 predicts relatively higher values of Ω_{cyc}, which therefore means the predicted bond damage is less than that stated by Mahrenholtz (2012).

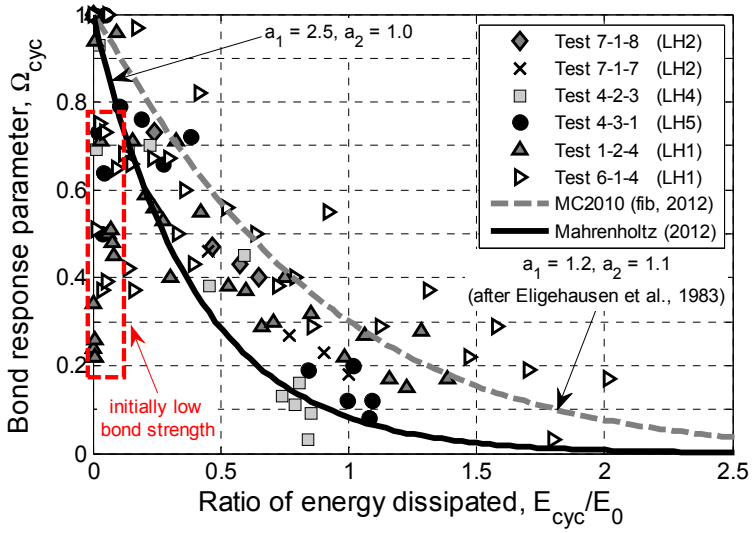

Figure 6-17: Bond response parameter Ω_{cyc} plotted against normalised energy dissipation during cyclic loading (data points only shown for the first four half cycles in test's 7-1-7 and 7-1-8).

Figure 6-17 consistently shows there is a large amount of scatter in nearly half of the observed values of Ω_{cyc} when E_{cyc}/E_0 is less than 0.2. The initially small loading cycles in the negative direction ($s \leq 0.3$ mm, indicated by the red box in Figure 6-17) typically reached lower bond stresses compared with the behaviour in the positive direction. As discussed previously in Section 6.3.1, this behaviour occurs when the test bar was loaded in tension and pulled out against the casting direction of the concrete. That is, the bond stiffness and strength was lower, or apparently 'softer', when the test bar was pushed in the same direction as the concrete was cast. With this in mind, Figure 6-18 re-produces the measured values of Ω_{cyc} and the data points from the initial loading cycles in the negative direction are removed.

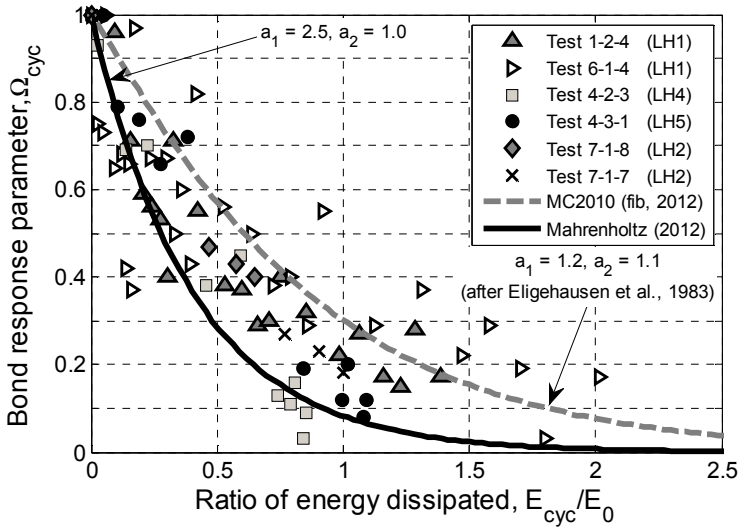

Figure 6-18: Reproduced from Figure 6-17 with data points removed at initially small values of bond slip.

Figure 6-18 illustrates the exponential reduction in Ω_{cyc} when E_{cyc}/E_0 increases. When the ratio of E_{cyc}/E_0 tends towards 1.0, the test observations and model predictions suggest that values of Ω_{cyc} is between 0.1-0.3. In general, Figure 6-18 illustrates that majority of the test observations generally fit between the predictions of the two models. It can be concluded that the hysteretic energy model that was proposed (after Eligehausen *et al.*, 1983) gives a reasonable method for predicting bond deterioration that was observed in some cyclic bond tests. Figure 6-18 shows an offset between the test observations and the predictions from both models which indicates a potential need to revise the values for the damage model parameters a_1 and a_2. However, it is also clear from Figure 6-18 that there is significant scatter between the five test observations to allow any new and reliable values for a_1 and a_2 to be specified.

As the model defined by Equation 6-2 normalises the energy dissipated during cyclic loading by the energy dissipated from the monotonic test, the parameter Ω_{cyc} is independent of the surrounding concrete strength. Providing that the monotonic bond stress-slip envelope that is used for the normalisation is correct, then the model is not influenced by different concrete strengths between different test specimens. Using the same values for a_1 and a_2, Mahrenholtz (2012) was able to match the model prediction to the test observations when the concrete specimens were either cracked and uncracked (like in these tests and in those by Eligehausen *et al.*, 1983), and when the test bars were either those originally cast in-place or post-installed bars embedded in epoxy mortar. In the case of the cracked concrete, for example, a reduced monotonic envelop curve was used by Mahrenholtz (2012) for the normalisation to correctly determine the values of the parameter Ω_{cyc}.

Since the predicted bond deterioration is not influenced by the quality of the surrounding concrete, the differences between model predictions and test observations shown in Figure 6-18 could alternatively be due to: (1) varying properties of the deformed tests bars, and (2) differences in specimen designs. Addressing the first point, and as mentioned previously in Section 5.5.2, the 16 mm deformed test bars

used in this study had a relative ribs areas of R_r equal to 0.11. Mahrenholtz (2012) mainly used 16 mm bars too. However, those 16 mm bars had a R_r equal to 0.07, which is about the same as R_r equal to 0.066 for the 20 mm bars that were used in the majority of tests by Eligehausen *et al.* (1983). Although the values of R_r are similar in Eligehausen *et al.* (1983) and in Mahrenholtz (2012), Figure 6-18 illustrates that these two model predictions lay either side of the test observations obtained in this study. Similarly to the previous discussion for the concrete strength, the parameter Ω_{cyc} should be relatively independent of the rib geometry. The significance of rib geometry on cyclic bond deterioration may be better understood if the bond stress-slip relationship was assessed in a more complex approach with two separate components of: (1) mechanical bearing resistance and (2) frictional resistance. Mahrenholtz (2012) provides a recent example where cyclic energy dissipation was calculated separately for the mechanical and frictional components and therefore two bond deterioration models are required. However, the additional complexity in having two separate bond deterioration models offers a relatively minor improvement in the accuracy of the overall prediction.

Considering the second point above, the pull-out specimens tested by Eligehausen *et al.* (1983) are different to those tested in this research. The Eligehausen specimens were specifically designed to be representative of the longitudinal beam bars anchored inside beam-column joints, therefore meaning that additional vertical and transverse reinforcement surrounded the test bar (i.e. to represent the column reinforcement in close proximity to an anchored beam bar). It is plausible that the additional specimen reinforcement led to greater passive confining pressures that enabled higher post-peak and residual bond stresses to occur the cyclic tests (relative to the test observations from this research). There are several other factors that may have resulted in some scatter between different test observations, including the test set-up and boundary conditions, and the different approaches for obtaining measurements and reporting the bond stress-slip relationships.

6.5 CONCLUSIONS: CYCLIC BOND PULL-OUT TESTS

This chapter presented the results from 27 cyclic pull-out tests where five different slip-controlled loading protocols were applied. The first section of this chapter described the reasons and physical features of each loading protocol. The observed failure modes were described within and, overall, 21 bond pull-out failures occurred. Some partial cone failure was observed in Series 3 when the bond region was directly adjacent to the free surface of the test specimen.

In general, the cyclic behaviour during loading protocol LH1 showed that small loading cycles (less than 0.3 mm bond slip) were able to mobilised bond stresses of up to 80 percent of the maximum bond stress. However, these initial pre-peak cycles typically do not cause any notable bond damage. Using test 1-2-4 as a specific example, three fully reversed cycles to $\pm$0.1 mm slip and a further three cycles to $\pm$0.3 mm caused a cumulative energy dissipation that was less than 10 percent of the total energy dissipated during

monotonic loading (E_0). Relatively minor bond damage during these initially small cycles generally meant that the next loading cycle in the peak-range was able to develop bond stresses between 90 and 100 percent of the maximum bond stress on the monotonic backbone envelope. Initially small load cycles also indicated lower values of bond stiffness and bond stress developed when the test bar was pushed in compression. This apparent softness in the negative bond stress-slip domain is probably due to a lower quality bond condition in the loading direction that is the same as the concrete casting direction which leads to local water gain under the ribs of the deformed bar.

Loading protocols LH2 and LH3 cycled between constant-slip values and confirmed that the same extent of bond strength degradation occurs for the same bond slip increment (or slip range), despite LH2 comprising fully-reserved slip cycles and LH3 comprising of half-reversed cycles. These tests showed a significant proportion of total bond damage occurs on the first loading cycle into the peak range.

Cumulative energy dissipation was assessed for monotonic and cyclic bond tests based on the area under the bond stress-slip curve. Extensive bond deterioration occurred loading protocol LH1 as an energy dissipation ratio E_{cyc}/E_0 of 1.0 had already been reached half way through the loading sequence, on first cycle when the slip range had reached 5.0 mm. Reducing the number of cycles applied in loading protocols LH4 and LH5 allowed for much greater post-peak bond resistance. Despite the main loading cycle having an incremental bond slip as large as 4.5 mm (in LH4) and 6.5 mm (in LH5), both of these cyclic paths were not significantly less than the monotonic backbone envelope. For the slip range equal to clear rib spacing of 8.9 mm, where mechanical bearing was fully consumed, the cumulative energy dissipation, E_{cyc}, during LH4 was found to be 15 percent less than the energy dissipated during a monotonic test E_0, whereas LH5 was 15 percent greater energy dissipation. However, final pull-out of the test bar showed both tests had the same residual bond stress at large slip values (beyond $+6.0$ mm).

Cyclic bond deterioration observed in these cyclic bond tests compared reasonably well with model predictions found in the Model Code 2010 (*fib*, 2012) and in Mahrenholtz (2012). Both models predict that the bond stress at a particular slip value along on the path of the upcoming loading cycle depends on the accumulative hysteretic energy dissipation. From the cyclic bond tests the observed bond deterioration was found to fit between the two model predictions, where the Model Code 2010 relationship provides a slight under-estimate of the bond stress reduction, whereas the model by Mahrenholtz (2012) provides an over-estimate, or an upper bound. The level of error between the cyclic test observations from this research and the two previously proposed models is not overly significant and therefore a new equation has not been proposed in this thesis. If lightly reinforced RC structures are being modelled for the purpose of detailed seismic response history analysis, then using the equations in the Model Code 2010 (*fib*, 2012) would be more appropriate for a lower bound on the ductility capacity. At the present time, researchers in New Zealand (such as Cuevas, 2015) are conducting detailed analysis of RC structures that could incorporate these constitutive bond models.

6.6 REFERENCES

ACI Committee 408 (1992). State-of-the-art report on bond under cyclic loads: *ACI 408R-92*, American Concrete Institute, Farmington Hills, MI.

Balazs, G.L. (1991). Fatigue of bond. *ACI Materials Journal*, 88(6), 620-629.

Bradley, B. A. and Cubrinovski, M. (2011). Near-source strong ground motions observed in the 22 February 2011 Christchurch earthquake. Bulletin of the New Zealand Society of Earthquake Engineering, 44(4): 181-194.

Cuevas, A. and Pampanin, S. (2015). Effect of strain-rate and material characteristics on the seismic residual capacity of reinforced concrete plastic hinges: numerical investigation. Conference proceedings of the New Zealand Society of Earthquake Engineering, Rotorua.

Eligehausen, R., Popov, E.P., Bertero, V.V. (1983), Local bond stress-slip relationships of deformed bars under generalized excitations. *Report UCB/EERC-83/23*, University of California, Berkeley.

Fédération Internationale du Béton, *fib*. (2012), Model Code 2010 - Final draft, Volume 2. *fib* Bulletin No. 66, Lausanne, Switzerland.

Fenwick, R.C. and Dhakal, R.P. (2007). Material strains and relevance to seismic design. SESOC Journal, 20(1): 5-12.

Hakuto, S., Park, R., Tanaka, H. (1999). Effect of deterioration of bond of beam bars passing through interior beam-column joints on flexural strength and ductility. *ACI Structural Journal*, 96(5), 858-864.

Kivell, A. (2011). Effects of bond deterioration due to corrosion on seismic performance of reinforced concrete structures, *Master of Engineering Thesis*, University of Canterbury, Christchurch, New Zealand.

Lu, Y., Henry, R.S., and Ma, Q.T. (2014). Numerical modelling and testing of concrete walls with minimum vertical reinforcement. C*onference proceedings of the New Zealand Society of Earthquake Engineering*, Auckland.

Mahrenholtz, C. (2012). Seismic bond model for concrete reinforcement and the application to column-to-foundation connections, *Doctor of Philosophy Thesis,* Universität Stuttgart.

Morris, G.J., Bull, D.K. and Bradley, B.A. (2014). Reviewing uncertainties in seismic experimentation following the unexpected performance of RC structures in the 2010-2011 Canterbury earthquakes. C*onference proceedings of the New Zealand Society of Earthquake Engineering*, Auckland.

Park, R., and Paulay, T. (1975). Reinforced concrete structures, John Wiley & Son, Inc., New York, United States of America.

Priestley, M.J.N., and Park, R. (1984). Strength and Ductility of bridge substructures. *RRU Bulletin No. 71*, National Roads Board, Wellington, New Zealand.

Sritharan, S., Beyer, K., Henry, R.S., Chai, Y.H., Kowalsky, M.J., and Bull, D.K (2014). Understanding poor seismic performance of concrete walls and design implications. *Earthquake Spectra,* 30(1), 307-334.

[This page is intentionally left blank]

7 CONCLUSIONS AND IMPLICATIONS FOR BOND BEHAVIOUR IN RC STRUCTURES

7.1 SUMMARY

The research presented in this thesis examined the local bond behaviour of deformed reinforcing bars embedded in typical structural concrete. When a RC component has an insufficient quantity of longitudinal reinforcement, a single-crack plastic hinge zone is expected to develop under severe seismic actions. In this particular case, it is beneficial for extensive local bond deterioration in the vicinity of the crack plane to occur such that inelastic steel strains can distribute over a longer length of the reinforcement. Despite bond mechanics being so fundamental to the structural design and assessment of RC structures, the linkages between bond behaviour and the overall structural behaviour of RC components remains somewhat unclear. As a result, bond mechanics continues to be an area of open research due to limited understanding of bond mechanics that has been demonstrated by the empirical nature of prediction models in the CEB-FIP (now *fib*) Model Codes (1993; 1996; 2012).

Within this particular research, bond behaviour was experimentally investigated using the method of pull-out tests. A particular test set-up and experimental programme was developed with the advantages of relative ease and repeatability for constructing and testing 75 pull-out specimens. In order to obtain measurements of local bond stress-slip behaviour, 48 monotonic tests and 27 cyclic tests were completed where each specimen contained a deformed reinforcing bar that was embedded (or 'bonded') over a short length. Chapter 4 described the test set-up, details of the specimen design and construction, and the experimental programme that was followed during the research.

The results obtained from both monotonic tests (Chapter 5) and cyclic tests (Chapter 6) allowed for parametric comparisons to be made between several factors. A sufficient number of tests were also performed and repeated to allow the typical bond behaviour to be presented in a generalised form. In Chapter 5, a constitutive bond stress-slip relationship was proposed, based on the mean (average) behaviour of the test results, as a monotonic backbone curve to represent the local bond behaviour. In Chapter 6, the observed bond deterioration during cyclic tests was compared to existing model predictions. The monotonic bond stress-slip relationship and the model prediction for cyclic bond deterioration are both presented in a reasonably simple manner for the ease of implementation in finite element modelling (FEM) and analysis to study the significance of bond behaviour on the overall structural behaviour of RC components. FEM implementation was not undertaken within this research, but may be adopted within current studies such as Lu *et al.* (2014) and Cuevas (2015), for example.

7.2 CONCLUSIONS AND RECOMMENDATIONS

This section summarises the main outcomes and conclusions followed by brief discussion of the implications for structural behaviour. The conclusions presented below are somewhat repeated and/or abbreviated from the separate conclusion sections that were presented within Chapters 3, 4, 5 and 6. Each of those chapters contained a separate list of references that are also relevant to the conclusions listed in this section.

From an extensive literature review on bond mechanics, the following conclusions can be made:

- Previous experimental studies have shown that bond behaviour is significantly influenced by the strength of the surrounding concrete and the rib geometry of the deformed reinforcing bars. Previous studies have also shown that loading rate can significantly enhance the maximum bond strength, τ_{max}, however there is appreciable scatter between different studies and it is difficult to use a single parameter to quantify this dynamic influence.
- For several practical reasons, the majority of the previous experimental studies used the pull-out test set-up for measuring local bond behaviour. The test set-up is relatively simple and allows for a large number of test specimens to be constructed and different test permutations can be easily studied independently.
- The literature contains some scatter in the reported values of τ_{max} for deformed bars in good bond conditions. The mean value of τ_{max} in different studies varies between 2.5 and 5.0 times $\sqrt{f'_c}$, whilst the Model Code 2010 (*fib*, 2012) states the mean value of τ_{max} should be taken as $2.5\sqrt{f'_c}$ based on the findings of Eligehausen *et al.* (1983). A number of design expressions in Paulay and Priestley (1992) reference τ_{max} of $2.5\sqrt{f'_c}$ from the study by Eligehausen *et al.* (1983).
- The literature agrees that the magnitude of the inelastic steel strain has a significant influence on local bond behaviour as the bar cross-section area changes due to the Poisson effect. As the bar cross-section reduces at large axial tensile strains, the effective rib height that is able to provide mechanical bearing resistance is also reduced. However, the influence of inelastic steel strains appears to be less extensive for higher grades of reinforcing steel.
- The literature also agrees that the ratio of the ultimate to yield strength of the steel (f_u/f_y) has a significant influence on the distribution of bond stress-slip along an embedded reinforcing bar. For deformed reinforcing bars used in New Zealand construction, the f_u/f_y ratio for Grade 500E reinforcing steel is on the order of 1.25, which is somewhat less than the Grade 300E steel where f_u/f_y is on the order of 1.43 (Davies-Colley *et al.*, 2015).

From the experimental investigation of 48 monotonic and 27 cyclic bond pull-out tests (undertaken for this thesis), the following conclusions can be made:

- The observed failure modes in some tests indicated that the side cover dimension of the test specimens should have been larger in order to avoid these types of bond splitting failures through the concrete side cover. However, the weight of the typical test specimens was 22 kg and increasing the outer dimensions would have the disadvantage of increased difficulty when handling the specimens.
- During the monotonic bond tests, the parametric study showed that the maximum local bond strength, τ_{max}, was not significantly influenced by the variations of deformed bar size and embedded bond length that was used. However, only 16 mm and 20 mm deformed bars were used and similar relative rib areas, R_r, were found for the rib geometry. Other bond researchers should be mindful of the rib geometry of deformed bars used in their own individual studies, but also when comparing test results with other research and with existing prediction models for bond behaviour.
- The parametric study showed that the concrete strength and loading rate had a significant influence on bond behaviour. Results showed that bond stress is proportional to the square-root of the concrete compressive strength, $\sqrt{f'_c}$. Therefore the measured bond stresses were normalised by $\sqrt{f'_c}$ for reporting in Chapter 5 and 6. Increasing the loading rate (bond slip rate) by a factor of 50 resulted in a 30 percent bond strength enhancement. These results support the discussion presented in Chapter 2, confirming that the structural behaviour of some RC buildings was influenced by a particular combination of moderate to high concrete strengths and relatively fast, dynamic loading rates.
- From a sample of 29 monotonic tests, a mean bond stress-slip constitutive relationship was proposed in Chapter 5. The relationship proposed in this study was found to have several differences with the same relationship given in the Model Code 20120 (*fib*, 2012). The Model Code relationship states a lower initial bond stiffness where 1.0 mm of bond slip is required to mobilise a maximum bond stress of $\tau_{max(MC,2010)} = 2.5\sqrt{f'_c}$, before a post-peak reduction in bond stress occurs at 2.0 mm of bond slip. In contrast, this study found that 0.5 mm of bond slip mobilised a maximum bond stress of $\tau_{max} = 3.0\sqrt{f'_c}$, which can be sustained until 1.5 mm of bond slip before loss of bond strength. In this study, the 5th percentile lower characteristic value was $\tau_{max,0.05} = 2.6\sqrt{f'_c}$ and the 95th percentile upper characteristic value was $\tau_{max,0.95} = 3.4\sqrt{f'_c}$.

- A small number of tests demonstrated a brittle failure due to concrete cone break-out. The onset of cone failure was found to occur when average splitting stress over the cone surface area was between 0.8 and 1.0 MPa, and the maximum bond stress was $\tau_{max,cone} = 1.4\sqrt{f'_c}$. The geometry of the cone failure surface compared well with observations from previous tests by Viwathanatepa *et al.* (1979) on fully-anchored deformed bars. The angle of cone break-out observed in these tests was approximately 30 degrees, which is reasonably consistent with Section 17.5.7.2 of NZS3101:2006 which assumed failure surface at a cone angle of 35 degrees.

- Cyclic bond tests showed that bond deterioration predominantly occurs once the loading cycles have gone into the peak stress range, where bond slip exceeds 0.5 mm. Tests showed that bond deterioration depended mostly on the bond slip range, regardless of whether the load cycling is half- or fully-reversed. The physical reason is due to the mechanical bearing forces causing an equal amount of damage (for the same bond slip) at one or at both ends of the concrete shear key that is between the ribs. Further cyclic tests showed that the post-peak residual bond stress was significantly larger when the loading protocols comprised of a relatively small number of loading cycles.

- There appears to be a valid exponential relationship between the cumulative hysteretic energy dissipated and the extent of bond deterioration that occurs. The Model Code 2010 (*fib*, 2012) contains a bond deterioration (or damage) model that computes the cumulative hysteretic energy under the bond stress-slip curve and is then able to predict the bond stress that the next cyclic path will follow. Observed bond deterioration from five cyclic bond tests, each with different loading protocols, provided a reasonable fit between the predicted bond deterioration defined by the Model Code 2010 and a more recent model found in Mahrenholtz (2012).

- In practice, structural engineers often use probable values for material and/or for assessing the capacity and potential vulnerabilities of existing structural members. The use of probable strength values deviates from common design practice where lower characteristic 5th percentile values are used to determine the nominal capacity for newly designed structures. With this practice approach in mind, a recommendation of this research is to use probable values for τ_{max} for deformed reinforcing bars in existing RC structures that are being assessed for structural capacity and. To do so, the concrete compressive strength f'_c should be determined using reliable test methods and reinforcing bar samples that are extracted from undamaged regions of the structure should be inspected to determine the relative rib area, R_r. If there is substantial variation between R_r for the samples and that for the bars used in this study ($R_r \approx 0.10$), then the predicted values τ_{max} may need to account for the variation in R_r.

- It is NOT recommended that the mean local bond stress of $\tau_{max} = 3.0\sqrt{f'_c}$ is adopted as a 'design bond strength' in the design calculations for anchorage and development lengths of reinforcement (or other embedded items). This is strongly advised against. The bond tests conducted in this research used short embedment lengths where the local bond stress was uniform. Given the need to develop much larger forces (and to limit associated bond slip), typical anchorage and development lengths need to be much longer. As the embedded length increases (beyond say $5d_b$), the distribution of bond stresses along the reinforcement is highly non-uniform (and generally much less than $3.0\sqrt{f'_c}$ at most locations).

Listed below is a generalised summary of advantages and disadvantages of the bond stress-slip response on the seismic performance of RC structures:

Advantages:

- At the serviceability limit state (SLS), the relatively high initial bond stiffness and bond strength means that there is unlikely to be any significant bond slip that will contribute to deformations such as crack widening and the total deflections of cracked RC components.
- At the ultimate limit state (ULS), high bond stiffness and strength means that tensile stresses in the reinforcement are transferred to the surrounding concrete reasonably effectively, which will therefore promote the formation of secondary cracks. Additional secondary cracking means the reinforcement develops a more even strain distribution such that the strain capacity is well-utilized and ductile regions can develop the required plastic deformations (such as plastic elongations and plastic hinges rotations).
- The design provisions in NZS3101:2006 ensure there is adequate strength and minimal bond slip occurring in anchorage zones and development lengths of the reinforcement. In modern well designed RC structures, the occurrence of any local bond deterioration is unlikely to result in significant strength and stiffness degradation.
- Relatively simple model predictions and relationships are capable of representing physical bond behaviour that occurs during monotonic and cyclic loading. The bond stress-slip response can easily be defined and implemented within modelling software such as MASA and VecTor2.

Disadvantages:

- Relatively high bond strength may mean that a bond pull-out failure is less likely to occur and, instead, brittle fractures may be observed for the reinforcement that is used.
- At the ultimate limit state (ULS), when secondary cracking cannot occur, the limited extent of bond slip means that inelastic steel strains may be restricted to a very short 'bond deterioration length'. The lack of bond slip may mean the maximum crack width is greatly restricted which means that RC structural components may unexpectedly brittle.

In New Zealand practice, there are several applications where bond behaviour has concerning implications for the ductility capacity of certain structural components. These applications may include, but are not limited to, those listed below.

1. The use of epoxy mortars/grout around deformed reinforcing bars in ducts construction joints and in post-installed bars.

   The literature review found very high bond strengths for deformed bars embedded in grouted ducts (Raynor *et al*., 2002) which provide additional confining behaviour to the deformed bar. While this is a research finding, structural engineers should consider that the ducts may not have been completely filled in during construction. As another example, bond tests by Mahrenholtz (2012) showed $\tau_{max} = 28$ MPa for post-installed bars bonded to epoxy mortar.

2. Precast concrete panels that are lightly reinforced with mesh.

   In such cases, the area of reinforcing steel is often lower than the requirements of NZS3101:2006 and the ultimate moment capacity of the panel is less than the cracking moment capacity. A published example of this issue by practising structural engineers in New Zealand is found in Batchelor *et al.* (2014), who made a structural engineering assessment and consideration of the repair required for under reinforced panels that were damaged following the Canterbury earthquake sequence. The fabrication of lightly reinforced precast panels is a current concern within New Zealand practice.

As noted above, high bond strengths combined with insufficient reinforcement may be problematic for the limited ductility capacity of reinforcement in various types of concrete structures, or structural components, which have been constructed in New Zealand.

7.3 CLOSING REMARKS

Overall, the research presented in this thesis concludes that the deformed reinforcing bars used in NZ, embedded in moderate to high strength concrete, are able to develop high local bond stresses that are mobilised by a small amount of local bond slip. Under dynamic loading rates the bond resistance was found to be further enhanced. Such a small amount of local bond slip means that limited bond deterioration can occur. Within lightly reinforced structural components, governed by yielding of the reinforcement at a single-crack plane, high bond stresses and a lack of bond deterioration means that inelastic steel strains are unable to spread along the longitudinal reinforcement. In this particular case, the strain capacity of the reinforcement is poorly utilized, thus meaning that the limited extent of bond deterioration has ultimately limited the ductility capacity of the structural component. These findings means there is less confidence for the ability of lightly reinforced ductile concrete structures to achieve the life-safety performance objective during severe seismic events. Consequently, it is possible that structural engineers could make non-conservative assumptions or predictions of the maximum crack width and/or length that the vertical reinforcement has yielded over, thus leading to over-estimates in the potential ductility of lightly reinforced structural components.

7.4 REFERENCES

Batchelar, W., Mashal, M, and Southwick, D. (2014). Time history analysis correlation between observed and predicted response of typical industrial buildings with steel portal frame and concrete tilt panel cladding during Christchurch earthquake. C*onference proceedings of the New Zealand Society of Earthquake Engineering*, Auckland.

Comite' Euro-internationale du beton (*CEB-FIP*, 1993). The Model Code 1990: *Design code*. London: T. Telford; 1993.

Comite' Euro-Internationale du Béton (*CEB-FIP*, 1996). RC elements under cyclic loading: *State-of-the-art report*. London: T. Telford; 1996.

Cuevas, A. and Pampanin, S. (2015). Effect of strain-rate and material characteristics on the seismic residual capacity of reinforced concrete plastic hinges: numerical investigation. Conference proceedings of the New Zealand Society of Earthquake Engineering, Rotorua.

Davies-Colley, S., Kleinjan, B., Bull, D.K., and Morris, G.J. (2015). Review of the material and flexural overstrength factors for Grade 300E reinforcing steel used in New Zealand, *Conference proceedings of the New Zealand Society of Earthquake Engineering,* Rotorua, New Zealand.

Engstrom B. (1992). Anchorage of ribbed bars in the post-yield stage. *International conference – Bond in Concrete*: Riga, Latvia.

Fédération Internationale du Béton, *fib*. (2012), Model Code 2010 – First Complete Draft, Volume 1, Lausanne, Switzerland.

Holmes Solutions. (2011). Materials testing in buildings of interest: *Prepared for the Canterbury Earthquakes Royal Commission*, November 2011, Christchurch, New Zealand.

Lu, Y., Henry, R.S., and Ma, Q.T. (2014). Numerical modelling and testing of concrete walls with minimum vertical reinforcement. C*onference proceedings of the New Zealand Society of Earthquake Engineering*, Auckland.

Mahrenholtz, C. (2012). Seismic bond model for concrete reinforcement and the application to column-to-foundation connections, *Doctor of Philosophy Thesis,* Universität Stuttgart.

Priestley, M.J.N., Kowalsky, M.J., and Calvi, G.M. (2007). Displacement-based seismic design of structures, IUSS PRESS, Pavia, Italy.

Raynor, D.J., Lehman, D.E. and Stanton, J.F. (2002). Bond-slip response of reinforcing bars grouted in ducts. *ACI Structural Journal*, 99(5): 568-576.

Sritharan, S., Beyer, K., Henry, R.S., Chai, Y.H., Kowalsky, M.J., and Bull, D.K (2014). Understanding poor seismic performance of concrete walls and design implications. *Earthquake Spectra,* 30(1), 307-334.

Shima, H., Chou, L.L., and Okamura, H. (1987) Micro and macro models for bond in reinforced concrete. *Journal of the Faculty of Engineering*, The University of Tokyo, 39(2).

Standards New Zealand. (2006). Concrete structures standard, NZS3101, Parts 1 & 2. Standards New Zealand: Wellington, New Zealand.

APPENDICES

A PROPERTIES OF THE REINFORCING STEEL AND CONCRETE

A.1 REINFORCING STEEL

A.1.1 Identification features of Grade 500E deformed bars

Reinforcing steel manufacturers are required by the identification rules of the New Zealand Standard for Steel reinforcing materials (NZS 4671:2001) to provide distinct surface features to indicate different strength grades, ductility classes and producer specific markings. These rules ensure clear differentiation between reinforcing bars on construction sites. Two missing ribs can be seen Figure A-1 which is to identify the strength grade is Grade 500. The manufacture process can often influence the material or strength characteristics.

Fletcher Reinforcing© was the manufacturer of the deformed reinforcing bars used in this project. The bars used for in these experiments are a micro-alloy (MA) bar. These complete identification stamps are spaced at approximately 1.0 metre on a standard 6 m length. Segments of the HD16 and HD20 reinforcing bars used for these experiments are shown in Figure A-2

Figure A-1: identification features for grade and manufacture

A.1.2 Rib pattern and geometry

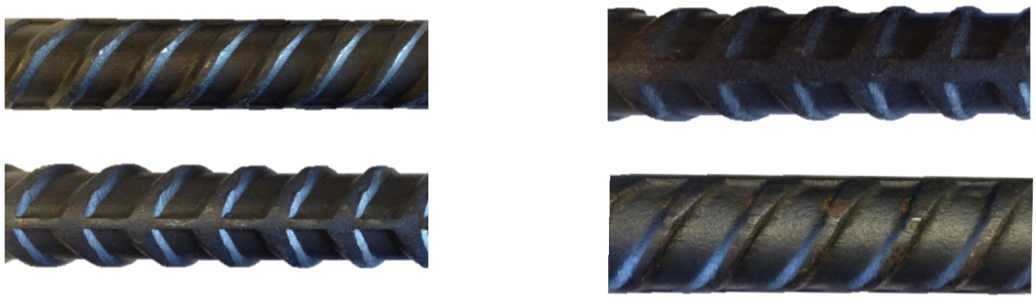

(a) HD16 **(b)** HD20

Figure A-2: Photos showing the rib pattern of the Grade 500 deformed reinforcing bars used in this research.

Figure A-2 illustrates the rib pattern on segments of the deformed reinforcing bars that were used. The different dimensions shown in Figure A-3 for bar and rib geometry were obtained. Deformed bars used in New Zealand construction have ribs that are inclined at approximately 30 to 35 degrees.

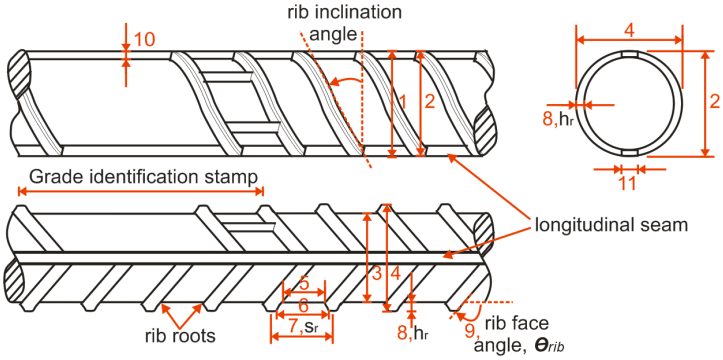

Figure A-3: Two elevations and a cross section labelling the features and measured geometry of the deformed reinforcing bars used for the bond tests.

Values for the dimensions on Figure A-3 are listed in Table A-1. These measurements were obtained using digital veneer callipers of 0.01 mm accuracy. Table A-1 presents the average rib geometry that was determined from five measurements taken along a 500 mm sample. The rib face angle θ_{rib}, was calculated based on the average values for the rib height and spacing to be 45° for the HD16s and 45° for the HD20 bars, respectively. Most researchers that are inspecting the geometry of the deformed bar are typically interested in the rib height h_r, and the centre-to-centre rib spacing.

Table A-1: Measured and calculated geometry of HD16 and HD20 deformed reinforcing bars.

Tag (Figure A-4)	**Measured dimensions and geometric ratios**		
	Nominal bar diameter, d_b (mm)	16.0	20.0
	Actual bar diameter (average, mm) [1]	15.85	19.89
1	seam diameter (midway between ribs, mm)	17.31	20.84
2	seam-seam diameter (at ribs, mm)	16.95	20.64
3	core diameter (midway between ribs, mm)	14.92	19.00
	→ seam height, h_s/d_b	0.07	0.06
4	rib-rib diameter (othorgonal to seam, mm)	17.60	21.46
5	rib spacing root-root (mm)	5.88	6.90
6	clear rib spacing, top edge-edge (mm)	8.90	10.71
7	rib spacing rib centre-centre, s_r (mm)	10.90	12.48
	→ s_r/d_b	0.68	0.62
	→ rib crest width ratio w_c/s_r	0.18	0.14
8	rib height, h_r calculated (mm)	1.34	1.23
	→ h_r/d_b	0.08	0.06
9	rib face angle, θ_{rib} (degrees)	45	
10	seam height, calculated (mm)	1.19	0.92
	→ initial bond angle, θ_{bond} (degrees)	45	

11	seam width (mid-height mm)	1.59	3.93
	→ calculated relative rib area, R_r	0.11	0.09

[1] Calculated using a measured sample length l_s (in mm) and mass m_s (in grams) divided by known value for the average density of reinforcing steel 7850kg/m³. Therefore $d_{b(actual)} = 12.736\sqrt{m_s/l_s}$.

A.2 CONCRETE MIX DESIGN AND PROPERTIES

A.2.1 Trial mix designs

Table A-2 summarises the specified 90 day and estimated 28 day compressive strength values with the corresponding water-binder ratios to be specified for each trial mix; TM1, TM2 and TM3. Table A-2 shows the material composition terms of the bulk volume (amount by mass per cubic metre, kg/m³).

Table A-2: Concrete mix design for three separate trial mixes.

Trial mix number	TM1	TM2	TM3
w/c ratio	0.44	0.57	0.73
$f'_{c,28days}$ [1]	51.9	37.9	25.7
$f'_{c,90days}$ [1]	60.5	44.2	30.0
Material quantity (kg per cubic metre)			
GP Cement	386	298	230
Water	170	170	170
13 mm Greywacke	1000	1000	1000
Sand	820	895	953
Theoretical density (kg/m3)	2377	2363	2352

[1] $f'_c = A/B^{1.5w/c}$; where B=5.0, and A = 150 (at 28 days) and 175 (at 90 days).

Table A-3 contains compression strength test results for mixes TM1, TM2 and TM3 at 7, 14 and 28 days. Figure A-5 illustrates a reasonable comparison between the observed strength development and predictive relationships found in ACI Committee 209.2 (2008) and Model Code 2010 (fib, 2012).

Table A-3: Summary of concrete compression strengths from cylinder testing on three trial mixes.

Trial mix number	Number of days after casting	Concrete compressive strength, f'_c (MPa)		
		Cylinder 1	Cylinder 2	Cylinder 3
TM1	7 days	39.5	39.3	39.8
	14 days	46.6	47.7	47.5
	28 days	55.1	53.4	53.1
TM2	7 days	23.9	26.9	24.8
	14 days	36.1	35.1	36.1
	28 days	41.5	45.3	46.4
TM3	7 days	20.6	20.3	20.6

	14 days	24.4	25.9	27.0
	28 days	32.2	32.2	31.9

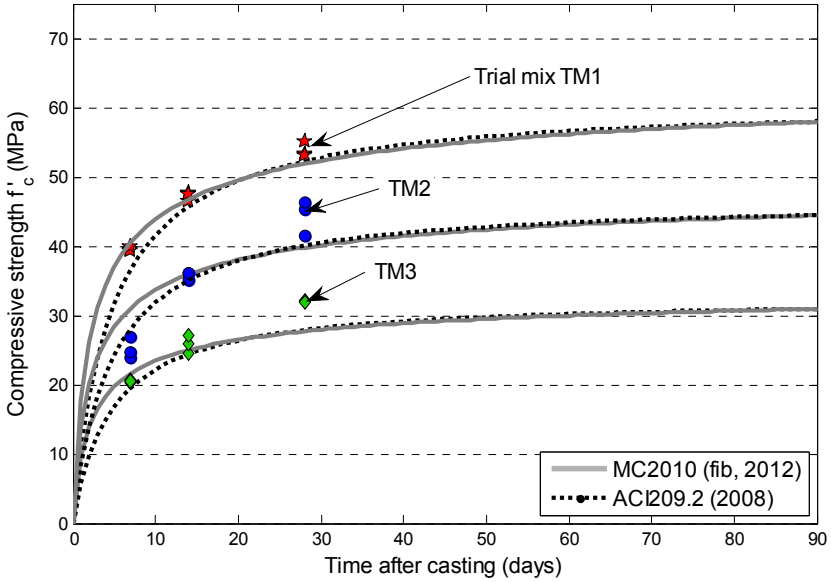

Figure A-5: Measured compressive strength of three concrete trial mixes assessed at 7, 14 and 28 days.

A.2.2 Test results for actual concrete mixes

Section 4.4.3 of Chapter 4 discussed the concrete strength development and statistical comparisons between different mixes. The complete record of compression test results are presented in Table A-4.

Table A-4: Summary of concrete compression strengths from cylinder testing.

Concrete mix	Series - Row(s)	Number of days after casting	Concrete compressive strength, f'_c (MPa)			
			Cylinder 1	Cylinder 2	Cylinder 3	Mean value
2	1-1, 1-2	7 days	28.5	26.9	28.5	28.0
		28 days	36.5	36.4	35.2	36.4
		52 days[1]	48.0	47.6	46.9	47.5
	2-1, 2-2, 2-3	7 days	32.3	33.3	31.5	32.4
		28 days	43.0	43.4	44.1	43.5
		40 days[1]	45.2	43.5	45.9	44.9
	3-1, 3-2	7 days	18.8	19.7	20.3	19.6
		28 days	29.7	31.9	32.3	31.3
		65 days[1]	40.2	37.0	35.0	37.4
	3-3, 3-4	7 days	24.8	23.8	27.9	25.5
		28 days	39.7	41.4	40.3	40.5
		52 days[1]	35.9[2]	39.7	43.9	41.8
	4-1, 4-2, 4-3	7 days	31.8	30.6	32.5	31.6
		28 days	40.5	40.4	41.5	40.8
		76 days[1]	49.0	48.7	50.0	49.2
	5-1, 6-1	7 days	26.3	27.1	27.6	27.0
		28 days	43.9	42.1	43.9	43.3
		33 days[1]	43.5	45.1	42.6	43.7
	8-1, 8-2	60 days	47.0	45.6	46.2	46.3
		186 days[1]	53.0	49.0	55.3	52.7
1	7-1	7 days	12.5	12.7	11.9	12.4
		28 days	19.0	19.5	18.5	19.0
		53 days[1]	25.5	24.4	24.6	24.6
3	7-2	7 days	43.6	44.3	42.3	43.4
		28 days	49.7	51.9	54.5	52.0
		64 days[1]	68.8	73.0	70.5	70.8

[1] time of commencing bond pull-out tests

[2] test result ignored due to premature failure of cylinder in combined compression/shear

A.3 REFERENCES

ACI Committee 209.2, (2008). Guide for modelling and calculating shrinkage and creep in hardened concrete: *ACI 209.2R-08*, American Concrete Institute, Farmington Hills, MI.

Fédération Internationale du Béton, fib. (2012), Model Code 2010 - Final draft, Volume 2. *fib Bulletin* No. 66, Lausanne, Switzerland

B LOAD CELL CALIBRATION

Prior to undertaking the bond tests, the calibration found an appropriate scale factor was 0.051029 counts/kN (where the logger input is limited to 7 decimal places). The load cell was calibrated using an "Impact ring" with a 50 kN capacity. This calibration technique could only be conducted for compression loading (hence the measurements presented in Table B-1 are negative). It was assumed that the compression and tension loads produce the same linear scale factor between the true load and the measured AD count.

The AD count is plotted in Figure B-1 for increments of -5.0 kN. Linear regression suggests that scale factor, after all bond tests were completed, was 0.0512813 counts/kN. The percentage error between the calibration before and after testing was found to be 0.5 percent. This amount of error was acceptable for these tests.

Table B-1: Force increments used for calibration of a 100 kN load cell.

Ring vertical deflection [mm]	**"True" Load** [kN]	**Measured AD Count**	**Recorded load on logger** [kN]
0.0	0	0	0
120.0	-5	-97	-4.950
244.0	-10	-196	-10.002
365.0	-15	-292	-14.901
488.0	-20	-390	-19.901
612.1	-25	-486	-24.800
735.0	-30	-585	-29.852
861.8	-35	-683	-34.853
986.5	-40	-780	-39.803
1113.0	-45	-878	-44.804
1238.0	-50	-975	-49.754

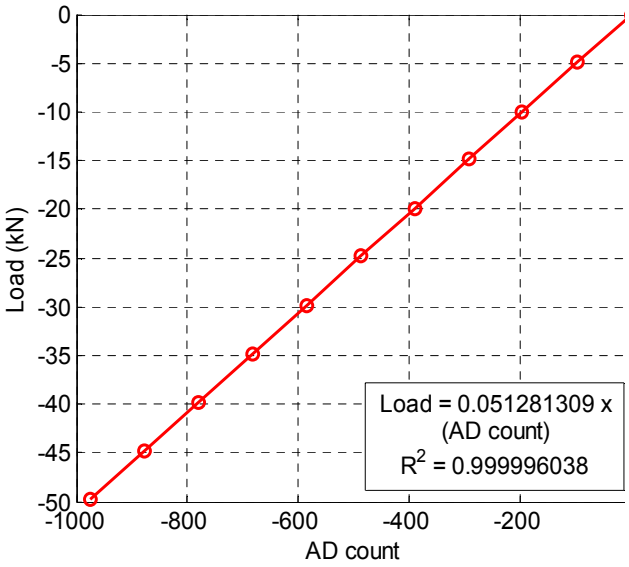

Figure B-1: Linear relationship used for load cell calibration

C FAILURE MODES AND OBSERVATIONS FROM EXPERIMENTAL TESTING

C.1 ADDITIONAL TESTING OBSERVATIONS

Chapters 5 and 6 contain sections physically describing the observed specimen damage and types of failure modes observed. This appendix provides supplementary information to those previously descriptions, which is recommended reading.

C.1.1 Premature specimen failure

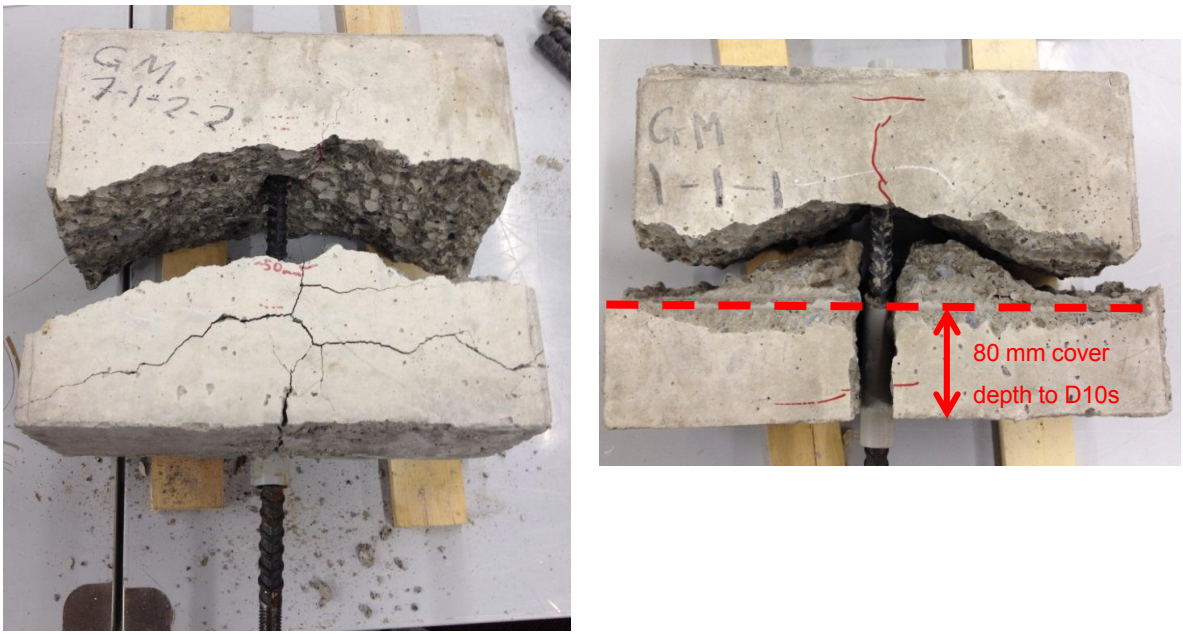

Figure C 1: Photos showing the typical damage caused by premature failure of 9 test specimens (8 monotonic, 1 cyclic).

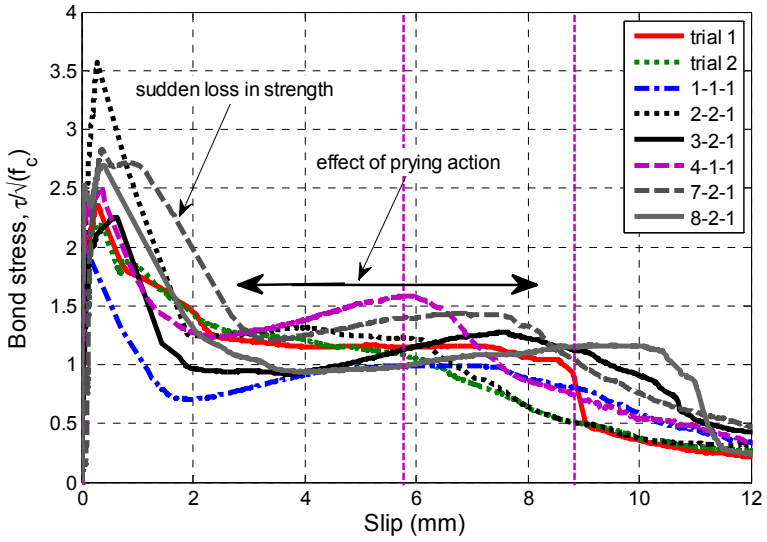

(a) Premature failure occurred during 8 monotonic tests.

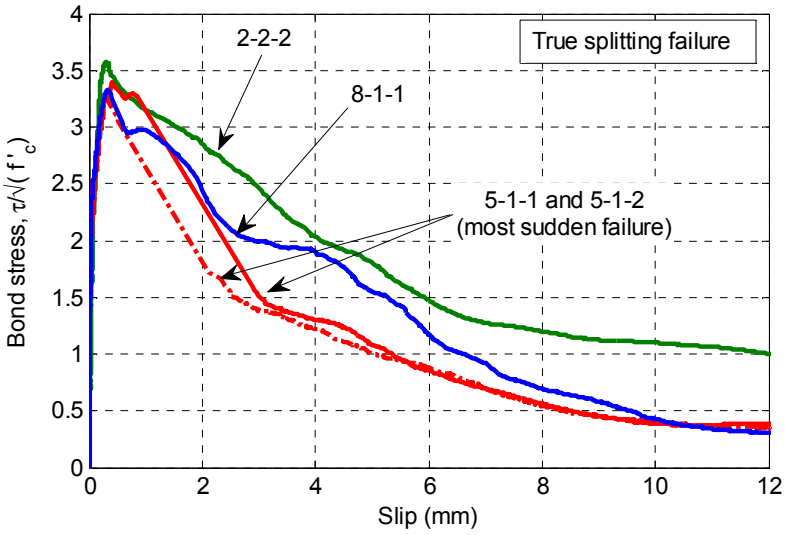

(b) Splitting failure occurred during 4 monotonic tests.

Figure C-1: Test results showing the bond stress-slip behaviour that was obtained when pull-out failure did not occur.

C.1.2 Splitting failure

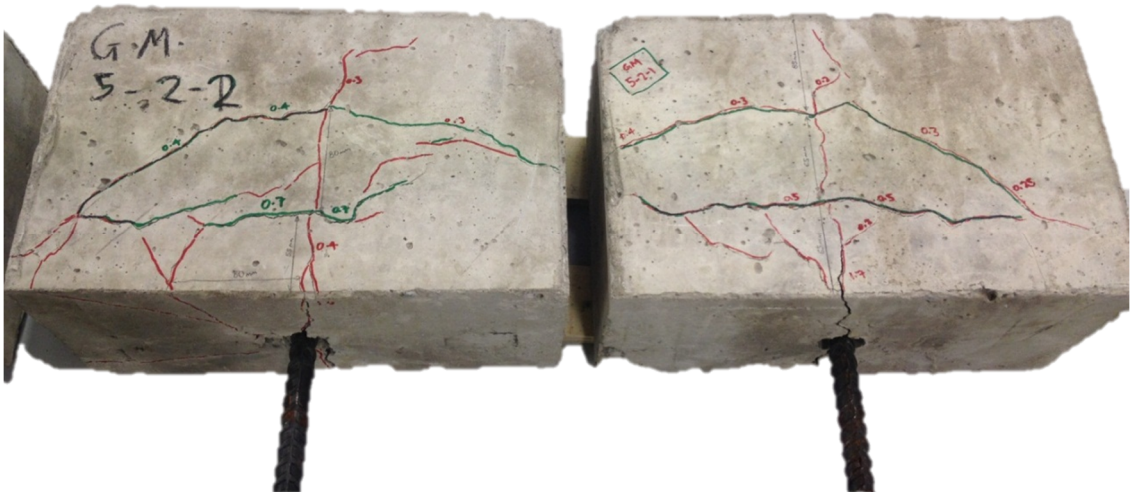

Figure C-2: Photos showing the typical damage sustained during a bond splitting failure in 7 tests (4 monotonic, 3 cyclic).

C.1.3 Pull-out failure

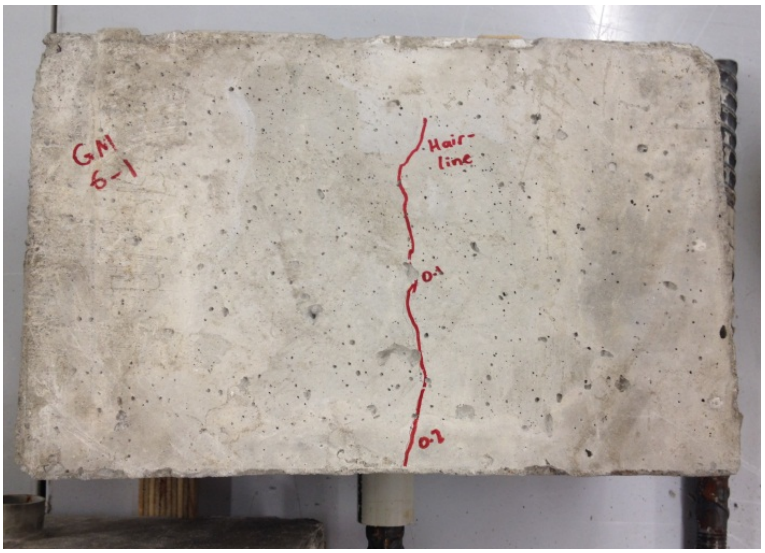

Figure C-3: Photo showing typical specimen damage of a narrow flexural crack where crack width did not exceeded 0.2 mm under the maximum applied pull-out force.

(a) Test specimen cut open to assess the pull-out failure surface.

(b) Crushed concrete between the ribs of the deformed bar.

Figure C-4: Photo showing typical damage at the interface of the deformed bar following a bond pull-out failure.

C.2 RECORD OF BOND TEST FORCES AND FAILURE MODES

Table C-1: Recorded maximum load and mode of failure mode for each bond test performed.

Series-Row-Test			**Loading type**	**Maximum applied force, T (negative = compression)** (to nearest 1.0 kN)	**Bond stress at failure τ_{max}** (to nearest 0.5 MPa)	$\frac{\tau_{max}}{\sqrt{f'_c}}$ (to nearest 0.01)	**Failure mode**
Trial	-	1	Monotonic tension	47	17.5	2.3	Splitting & prying action
		2		44	16.0	2.2	
		3	Cyclic LH1	51, -41	19.0	2.5	Pull-out
1	1	1	Monotonic tension	37	13.5	2.0	Splitting & prying action
		2	Monotonic compression	-51	18.5	2.7	Pull-out
		3	Monotonic tension	49	18.0	2.6	Pull-out
		4	Cyclic LH1	50, -44	18.5	2.7	Pull-out
	2	1	Monotonic tension	59	22.0	3.2	Pull-out
		2		56	20.5	3.0	Pull-out
		3		59	22.0	3.2	Pull-out
		4	Cyclic LH1	54, -40	20.0	2.9	Pull-out
2	1	1	Monotonic tension	73	27.0	4.0	Pull-out
		2		75	27.5	4.1	Pull-out
		3		71	26.0	3.9	Pull-out
	2	1		65	24.0	3.5	Splitting & prying action
		2		65	24.0	3.5	Splitting
	3	1		57	21.0	3.1	Pull-out
		2		56	20.5	3.0	Pull-out
		3		51	18.5	2.8	Pull-out/splitting

Series-Row-Test			Loading type	**Maximum load, T** (negative = compression) (to nearest 1.0 kN)	**Bond stress at failure τ_{max}** (to nearest 0.5 MPa)	$\frac{\tau_{max}}{\sqrt{f'_c}}$ (to nearest 0.01)	Failure mode
3	1	1	Monotonic tension	25	9.5	1.4	Cone break out
		2	Monotonic tension	25	9.5	1.4	Severe splitting
		3	Cyclic	27, -38	10.0	1.5	Severe splitting
		4	Cyclic	24, -28	8.5	1.4	Splitting & prying action
	2	1	Monotonic tension	37	13.5	2.1	Splitting & prying action
		2	Monotonic compression	-46	17.0	2.6	Pull-out
		3	Cyclic LH1	41, -38	15.5	2.4	Pull-out
		4	Cyclic LH1	34, -37	12.5	2.0	Pull-out/splitting
	3	1	Monotonic tension	48	17.5	2.9	Pull-out
		2	Monotonic compression	-51	19	2.9	Pull-out
		3	Cyclic LH1	52, -44	19.0	3.1	Pull-out/splitting
		4	Cyclic LH1	48, -38	18.0	2.9	Pull-out/splitting
	4	1	Monotonic tension	78	28.7	4.4	Pull-out
		2	Monotonic compression	-27	10.0	1.6	Cone break out
		3	Cyclic LH1	66, -27	24.5	4.0	Pull-out/ cone splitting
		4	Monotonic tension	58,-32	21.0	3.5	Pull-out/cone splitting

Series-Row-Test			**Loading type**	**Maximum load, T (negative = compression)** (to nearest 1.0 kN)	**Bond stress at failure τ_{max}** (to nearest 0.5 MPa)	$\frac{\tau_{max}}{\sqrt{f'_c}}$ (to nearest 0.01)	**Failure mode**
4	1	1	Monotonic tension	48	17.5	2.5	Splitting & prying action
		2	Monotonic tension	56	20.5	2.9	Pull-out
	2	1	Cyclic LH4	50	18.5	2.7	Splitting
		2		56	20.5	3.0	Pull-out
		3		56	20.5	3.0	Pull-out
	3	1	Cyclic LH5	56	20.5	3.0	Pull-out
		2		62	23.0	3.3	Pull-out
		3		52	19.0	2.7	Pull-out
5	1	1	Monotonic tension	86	19.5	3.0	Splitting
		2		83	19.0	2.9	Splitting
		3		94	21.5	3.2	Pull-out
		4	Cyclic LH1	85, -57	19.5	2.9	Pull-out
6	1	1	Monotonic tension	70	18.0	2.7	Pull-out
		2		77	20.0	3.0	Pull-out
		3		64	16.0	2.5	Pull-out
		4	Cyclic LH1	75, -52	19.0	2.9	Pull-out

Series-Row-Test			Loading type	**Maximum load, T** **(negative = compression)** (nearest 1.0 kN)	**Bond stress at failure τ_{max}** (nearest 0.5 MPa)	$\frac{\tau_{max}}{\sqrt{f'_c}}$ (nearest 0.1)	Failure mode
7	1	1	Monotonic tension	41	15.0	3.0	Pull-out
		2		43	16.0	3.2	Pull-out
		3		37	14.0	2.8	Pull-out
		4		44	16.0	3.2	Pull-out
		5		48	17.5	3.5	Pull-out
		6	Cyclic LH1	34, -33	12.5	2.6	Pull-out
		7	Cyclic LH2	43, -18	16.0	3.2	Pull-out
		8	Cyclic LH2	43, -31	16.0	3.3	Pull-out
	2	1	Monotonic tension	65	24.0	2.8	Splitting & prying action
		2	Monotonic tension	66	24.5	2.9	Splitting failure
		3	Monotonic tension	69	25.5	3.0	Pull-out
		4	Monotonic tension	71	26.0	3.1	Pull-out
		5	Cyclic LH2	81, -63	23.0	2.7	Pull-out
		6	Cyclic LH3	74	627.5	3.2	Pull-out
		7	Monotonic tension	69	25.0	3.0	Pull-out
		8	Cyclic LH3	62	23.0	2.7	Pull-out
8	1	1	Monotonic tension	55	20.0	2.9	Pull-out/splitting
		2	Cyclic LH1	50, -41	18.5	2.7	Pull-out
		3		49, -48	18.0	2.7	Splitting
		4		53, -41	19.5	2.9	Splitting
	2	1	Monotonic tension	53	19.5	2.7	Splitting & prying action
		2		65	24.0	3.3	Pull-out
		3		56	20.5	2.8	Pull-out
		4		56	20.5	2.8	Pull-out

D SUPPLEMENTARY CYCLIC TEST RESULTS

D.2 CYCLIC BOND TESTS

The following figures are the measured bond stress-slip relationships for different bond test permutations. Each figure has a label showing the test number, loading protocol and the concrete compressive strength (presented earlier in Section A.2) at the time of testing.

The typical cyclic bond behaviour observed in these tests were described in Chapter 6 and therefore the following figures are considered to be supplementary.

D.2.1 Loading history 1 (LH1)

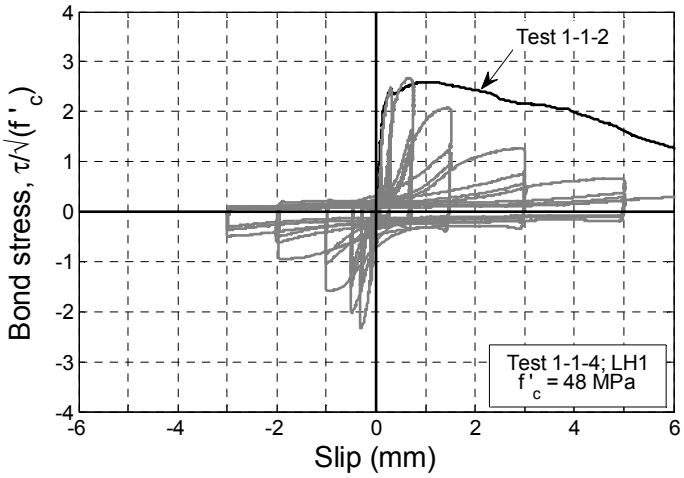

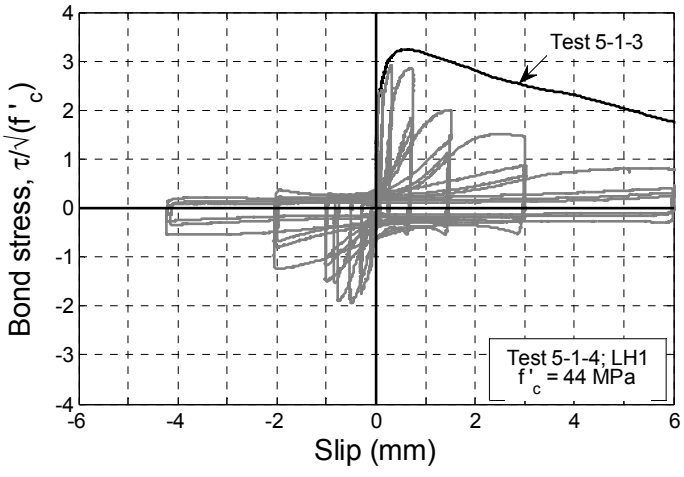

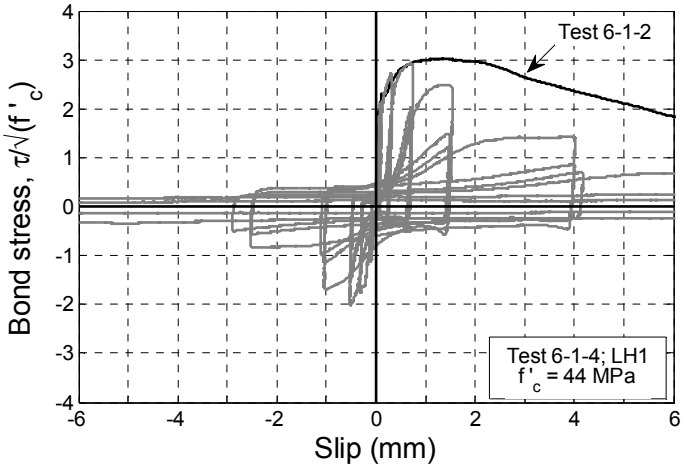
Test 6-1-2
Test 6-1-4; LH1
f'c = 44 MPa
Bond stress, τ/√(f'c)
Slip (mm)

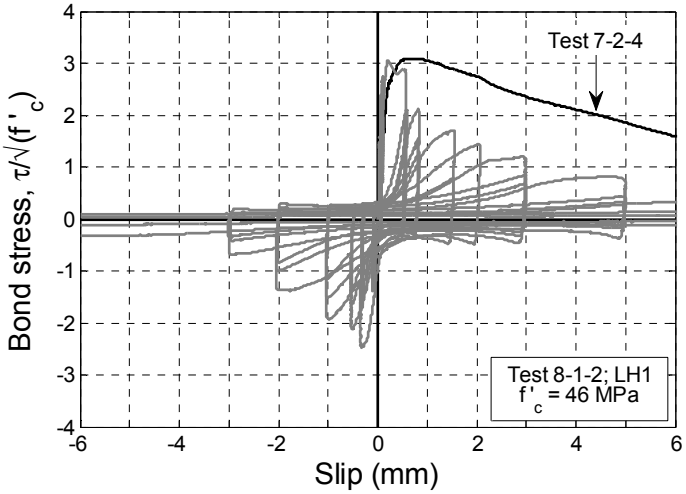
Test 7-2-4
Test 8-1-2; LH1
f'c = 46 MPa
Bond stress, τ/√(f'c)
Slip (mm)

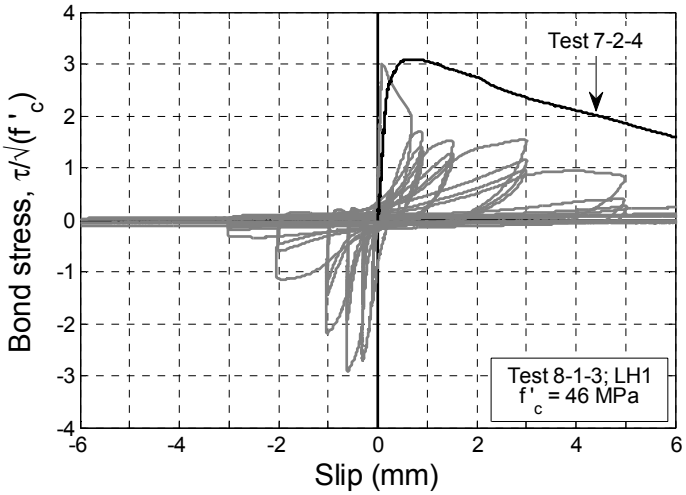
Test 7-2-4
Test 8-1-3; LH1
f'c = 46 MPa
Bond stress, τ/√(f'c)
Slip (mm)

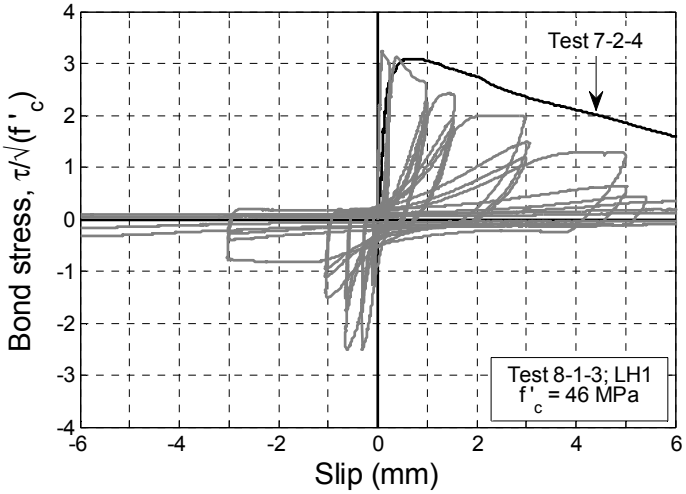
Test 7-2-4
Test 8-1-3; LH1
f'c = 46 MPa
Bond stress, τ/√(f'c)
Slip (mm)

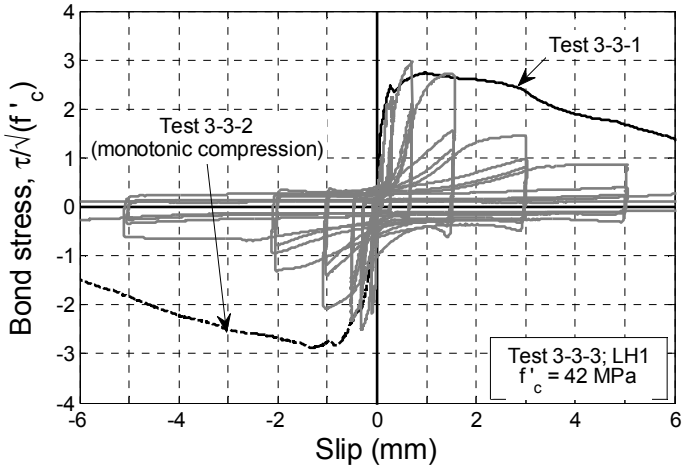
Test 3-3-1
Test 3-3-2
(monotonic compression)
Test 3-3-3; LH1
f'c = 42 MPa
Bond stress, τ/√(f'c)
Slip (mm)

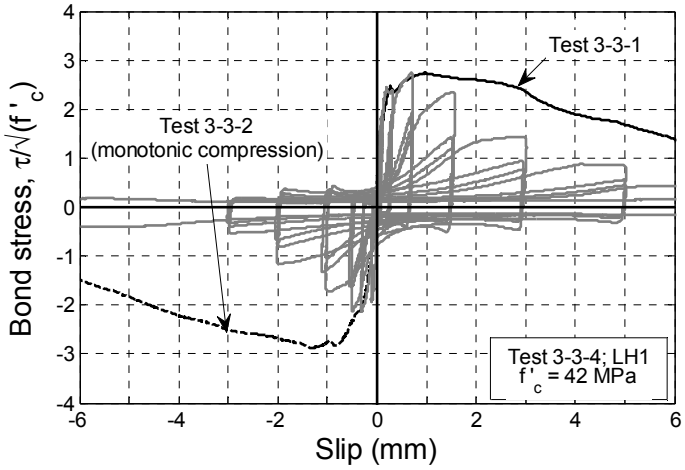
Test 3-3-1
Test 3-3-2
(monotonic compression)
Test 3-3-4; LH1
f'c = 42 MPa
Bond stress, τ/√(f'c)
Slip (mm)

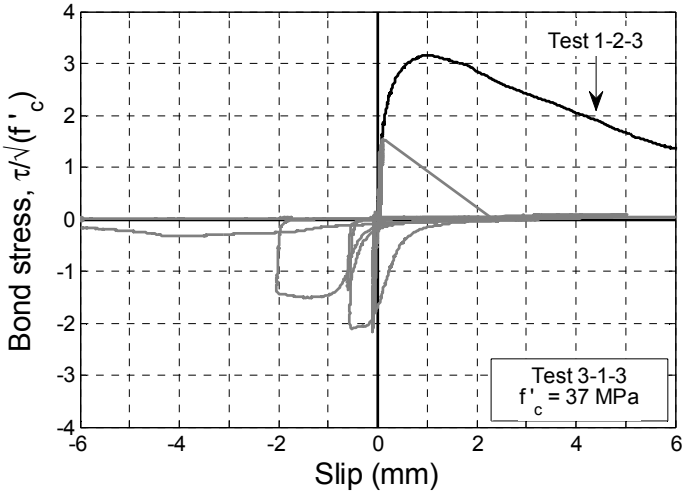
Test 1-2-3
Test 3-1-3
f'c = 37 MPa
Bond stress, τ/√(f'c)
Slip (mm)

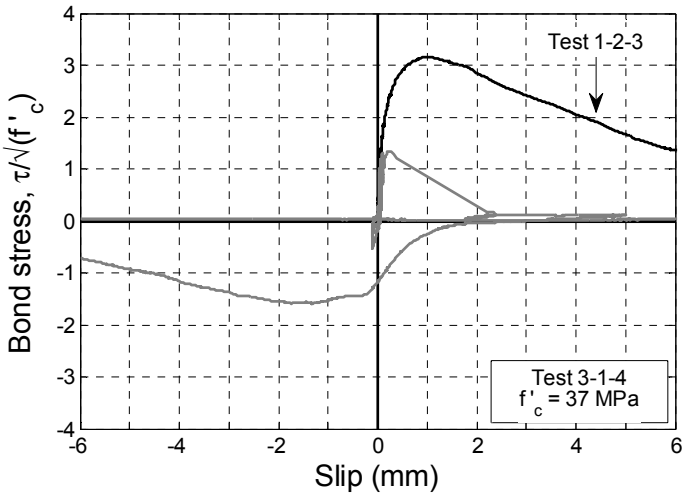
Test 1-2-3
Test 3-1-4
f'c = 37 MPa
Bond stress, τ/√(f'c)
Slip (mm)

D.2.2 Loading history 4 (LH1)

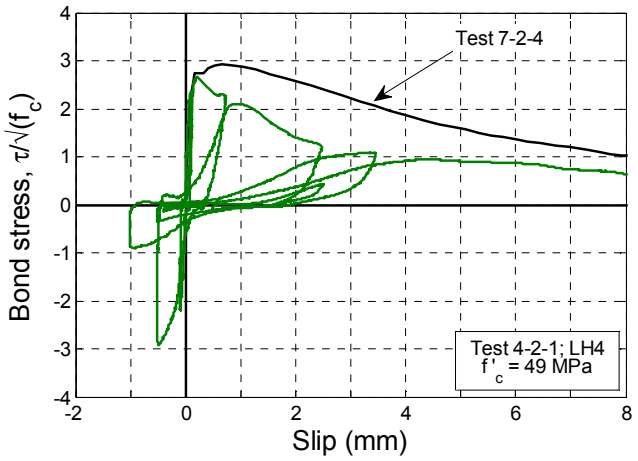

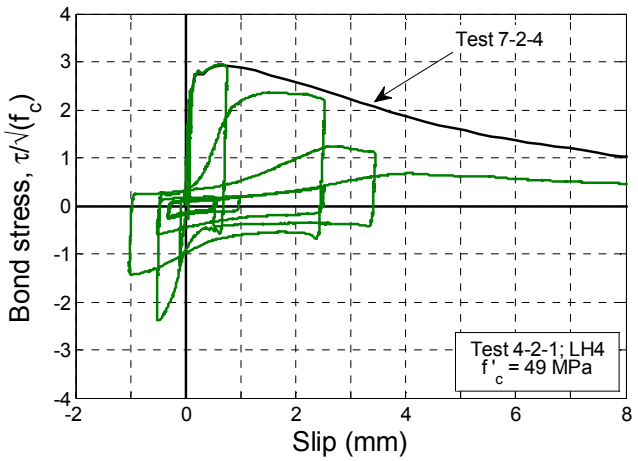

D.2.3 Loading history 5 (LH1)

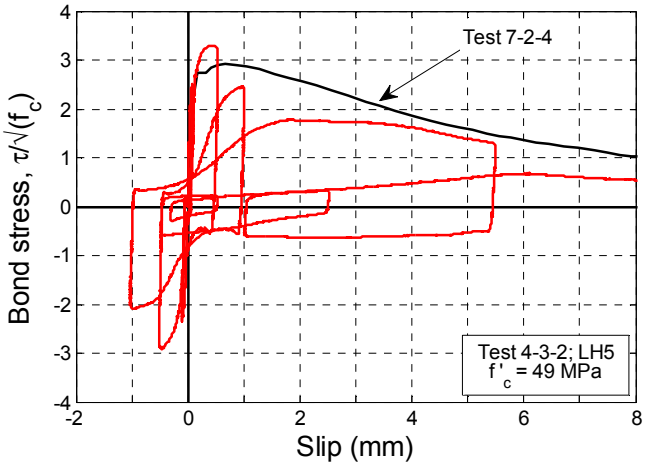

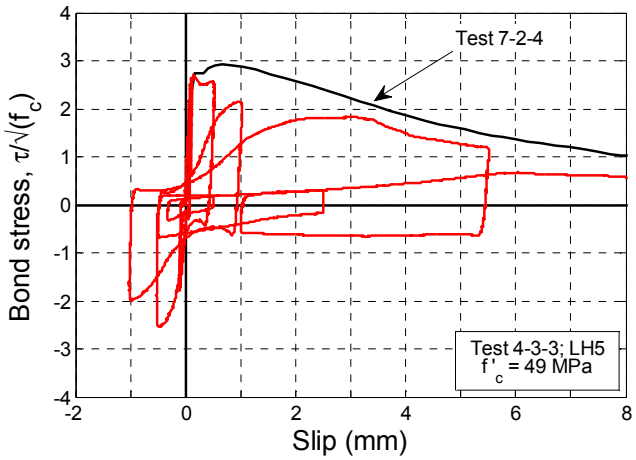

D.3 CYCLIC ENERGY DISSIPATED VS. OBSERVED BOND DEGRADATION

Table D-1: Energy dissipated during the first 16 loading cycles in test 1-2-4.

Test	Loading cycle, n	Slip domain, s_0 to s_{max}	Bond stress values[1]			Energy dissipated[1,2]		
			Model[2] $\tau_{o(s_{max,n-1})}$	Measured $\tau_{m(n)}$	$\Omega_{cyc} = \tau_{m(n)}/\tau_{o(s)}$	From previous loading cycle $E_{cyc(n-1)}$	Cumulative $\sum_n E_{cyc}$	$\frac{\sum E_{cyc}}{E_0}$
1-2-4 (LH1)	1^+	0 to 0.1 mm	2.2	- [3]	1.00	0	-	
	1^-	0.1 to -0.1 mm		-0.8	0.34	0.03	0.03	0.002
	2^+			0.5	0.24	0.06	0.09	0.005
	2^-			-0.5	0.22	0.03	0.12	0.006
	3^+			0.6	0.26	0.04	0.16	0.008
	3^-			-0.5	0.22	0.03	0.19	0.010
	4^+	-0.1 to 0.3 mm	2.7	2.5	0.94	0.02	0.21	0.011
	4^-	0.3 to -0.3 mm		-1.9	0.71	0.41	0.62	0.033
	5^+			1.4	0.50	0.51	1.13	0.060
	5^-			-1.4	0.51	0.19	1.31	0.070
	6^+			1.3	0.48	0.17	1.48	0.079
	6^-			-1.2	0.45	0.10	1.58	0.084
	7^+	-0.3 to 0.7 mm	3.0	2.9	0.96	0.16	1.74	0.093
	7^-	0.7 to -0.5 mm		-2.1	0.71	1.17	2.91	0.16
	8^+			1.8	0.59	0.98	3.89	0.21
	8^-			-1.7	0.56	0.62	4.51	0.24
	9^+			1.6	0.53	0.62	5.13	0.27
	9^-			-1.2	0.40	0.51	5.64	0.30
	10^+	-0.5 to 1.5 mm		2.1	0.71	0.43	6.08	0.32
	10^-	1.5 to -1.0 mm		-1.6	0.55	1.86	7.93	0.42
	11^+			1.1	0.38	1.98	9.91	0.53
	11^-			-1.1	0.37	1.33	11.2	0.60
	12^+			0.9	0.29	1.09	12.3	0.66
	12^-			-0.9	0.30	0.86	13.2	0.71
	13^+	-1.0 to 3.0 mm	2.6	1.0	0.40	0.83	14.0	0.75
	13^-	3.0 to -2.0 mm	2.8	-0.9	0.32	1.95	16.0	0.85
	14^+			0.6	0.22	2.44	18.4	0.99
	14^-			-0.8	0.27	1.52	19.9	1.07

	15^+			0.5	0.17	1.78	21.7	1.16
	15^-			-0.4	0.15	1.24	23.0	1.23
	16^+	-2.0 to 5.0 mm	1.95	0.6	0.28	1.04	24.0	1.28
	16^-	5.0 to -3.0 mm	2.6	-0.4	0.17	1.87	25.9	1.38

[1] all values of bond stress τ and energy dissipated E_{cyc} are normalised by $1/\sqrt{f'_c}$

[2] based on mean local bond stress-slip relationship for monotonic loading, where E_0 = 18.7

[3] first time loading theoretically follows monotonic backbone

Table D-2: Energy dissipated during the first 12 loading cycles in test 6-1-4.

Test	Loading cycle, n	Slip domain, s_0 to s_{max}	Bond stress values[1]			Energy dissipated[1,2]		
			Model[2] $\tau_{o(s_{max,n=1})}$	Measured $\tau_{m(n)}$	$\Omega_{cyc} = \tau_{m(n)}/\tau_{o(s)}$	From previous loading cycle $E_{cyc(n-1)}$	Cumulative $\sum_n E_{cyc}$	$\frac{\sum E_{cyc}}{E_0}$
6-1-4 (LH1)	1^+	0 to 0.1 mm	2.2	- [3]	1.00	0	-	0
	1^-	0.1 to -0.1 mm		-1.1	0.51	0.28	0.28	0.013
	2^+			1.7	0.75	0.26	0.54	0.026
	2^-			-0.8	0.37	0.26	0.80	0.038
	3^+			1.6	0.73	0.17	0.96	0.046
	3^-			-0.9	0.39	0.14	1.10	0.052
	4^+	-0.1 to 0.3 mm	2.7	2.7	1.00	0.16	1.26	0.060
	4^-	0.3 to -0.3 mm		-1.7	0.65	0.71	1.97	0.093
	5^+			1.8	0.68	0.59	2.56	0.12
	5^-			-1.2	0.42	0.33	2.89	0.14
	6^+			1.8	0.66	0.24	3.14	0.15
	6^-			-1.0	0.37	0.28	3.42	0.16
	7^+	-0.3 to 0.7 mm	3.0	2.9	0.97	0.20	3.62	0.17
	7^-	0.7 to -0.5 mm		-2.0	0.67	1.36	4.98	0.24
	8^+			2.0	0.67	1.25	6.22	0.30
	8^-			-1.5	0.50	0.81	7.03	0.33
	9^+			1.8	0.60	0.61	7.64	0.36
	9^-			-1.3	0.43	0.61	8.26	0.39
	10^+	-0.5 to 1.5 mm		2.5	0.82	0.49	8.74	0.41
	10^-	1.5 to -1.0 mm		-1.7	0.56	2.36	11.1	0.53
	11^+			1.5	0.50	2.37	13.5	0.64
	11^-			-1.1	0.38	1.78	15.3	0.72

	12^+			1.2	0.40	1.39	16.6	0.79
	12^-			-0.9	0.29	1.48	18.1	0.86
	13^+	-1.0 to 4.0 mm	2.5	1.4	0.55	1.29	19.4	0.92
	13^-	4.0 to -2.5 mm	2.5 to -2.8	-0.8	0.29	4.37	23.8	1.13
	14^+			0.9	0.37	3.95	27.7	1.31
	14^-			-0.6	0.22	3.30	31.0	1.47
	15^+			0.7	0.29	2.32	33.3	1.58
	15^-	4.0 to -3.0 mm	2.7	-0.5	0.19	2.57	35.9	1.70
	16^+	-3.0 to 8.0 mm	1.5	0.05	0.03	2.04	38.0	1.80
	16^-	8.0 to -7.0 mm	1.7	-0.3	0.17	4.59	42.5	2.02

[1] all values of bond stress τ and energy dissipated E_{cyc} are normalised by $1/\sqrt{f'_c}$

[2] based on mean local bond stress-slip relationship for monotonic loading, where E_0 = 21.1 (for the 20 mm deformed bar)

[3] first time loading theoretically follows monotonic backbone

Table D-3: Energy dissipated during the first loading cycles in test 7-1-7 and 7-1-8.

Test	Loading cycle, n	Slip domain, s_0 *to* s_{max}	Bond stress values[1]			Energy dissipated[1,2]		
			Model[2] $\tau_{o(s_{max},n=1)}$	Measured $\tau_{m(n)}$	$\Omega_{cyc} = \tau_{m(n)}/\tau_{o(s)}$	From previous loading cycle $E_{cyc(n-1)}$	Cumulative $\sum_n E_{cyc}$	$\frac{\sum E_{cyc}}{E_0}$
7-1-8 (LH2)	1^+	0 to 1.5 mm	3.0	- [3]	1.00	-	0	0
	1^-	-1.5 to 1.5 mm		-2.2	0.73	4.47	4.47	0.24
	2^+			1.4	0.47	4.29	8.76	0.47
	2^-			-1.3	0.43	2.01	10.8	0.58
	3^+			1.2	0.40	1.25	12.1	0.65
7-1-7 (LH2)	1^+	0 to 3.0 mm	2.6	- [3]	1.00	-	0	0
	1^-	-3.0 to 3.0 mm		-1.2	0.46	8.45	8.45	0.45
	2^+			0.7	0.27	5.96	14.4	0.77
	2^-			-0.6	0.23	2.52	16.9	0.90
	3^+			0.5	0.18	1.90	18.8	1.00

[1] all values of bond stress τ and energy dissipated E_{cyc} are normalised by $1/\sqrt{f'_c}$

[2] based on mean local bond stress-slip relationship for monotonic loading, where E_0 = 18.7

[3] first time loading follows monotonic backbone

Table D-4: Energy dissipated during Test 4-2-3 and 4-3-1.

Test	Loading cycle, n	Slip domain, s_0 *to* s_{max}	Bond stress values[1]			Energy dissipated[1,2]		
			Model[2] $\tau_{o(s_{max,n=1})}$	Measured $\tau_{m(n)}$	$\Omega_{cyc} = \tau_{m(n)}/\tau_{o(s)}$	From previous loading cycle $E_{cyc(n-1)}$	Cumulative $\sum_n E_{cyc}$	$\frac{\sum E_{cyc}}{E_0}$
4-2-3 (LH4)	1^+	0 to 0.1 mm	2.2	- [3]	1.00	-	0	0
	1^-	0.1 to -0.1 mm		-1.5	0.69	0.24	0.24	0.01
	2^+	-0.1 to 0.8 mm	3.0	2.8	0.93	0.24	0.48	0.03
	2^-	0.8 to -0.5 mm		-2.1	0.69	2.10	2.58	0.14
	3^+	-0.5 to 2.5 mm	2.7	1.9	0.70	1.57	4.15	0.22
	3^-	2.5 to -1.0 mm	3.0	-1.1	0.38	4.36	8.51	0.44
	4^+	-1.0 to 3.5 mm	2.4	1.1	0.45	2.60	11.1	0.59
	4^-	3.5 to 0.3 mm	3.0	-0.4	0.13	2.65	13.8	0.74
	5^+	0.3 to 2.5 mm	2.7	0.3	0.11	0.99	14.8	0.79
	5^-	2.5 to -0.5 mm	3.0	-0.5	0.16	0.34	15.1	0.81
	6^+	-0.5 to 1.5 mm		0.1	0.03	0.64	15.7	0.84
	6^-	1.5 to -0.3 mm	2.7	-0.3	0.09	0.24	16.0	0.86
4-3-1 (LH5)	1^+	0 to 0.1 mm	2.2	- [3]	1.00	-	0	0
	1^-	0.1 to -0.1 mm		-1.6	0.73	0.34	0.34	0.02
	2^+	-0.1 to 0.1 mm		1.1	0.50	0.31	0.65	0.03
	2^-	0.1 to -0.1 mm		-1.4	0.64	0.12	0.77	0.04
	3^+	-0.1 to 0.5 mm	3.0	3.0	1.00	0.09	0.86	0.05
	3^-	0.5 to -0.5 mm		-2.4	0.79	1.10	1.96	0.10
	4^+	-0.5 to 1.0 mm		2.3	0.76	1.54	3.50	0.19
	4^-	1.0 to -1.0 mm		-2.0	0.66	1.68	5.18	0.28
	5^+	-1.0 to 5.5 mm	1.8	1.3	0.72	2.01	7.19	0.38
	5^-	5.5 to 1.0 mm	3.0	0.6	0.19	8.54	15.7	0.84
	6^+	1.0 to 2.5 mm	2.7	0.3	0.12	2.85	18.6	0.99
	6^-	2.5 to -0.5 mm	3.0	-0.6	0.20	0.40	19.0	1.01
	7^+	-0.5 to 0.5 mm		0.2	0.08	1.21	20.2	1.08
	7^-	0.5 to -0.3 mm	2.7	0.3	0.12	0.22	20.4	1.09

[1] all values of bond stress τ and energy dissipated E_{cyc} are normalised by $1/\sqrt{f'_c}$

[2] based on mean local bond stress-slip relationship for monotonic loading, where E_0 = 18.7